



HAL
open science

Relations entre systèmes tectoniques et sédimentaires à la limite Nord de la plaque Caraïbe (Cuba-Hispaniola) : implications géodynamiques

Alana Oliveira de Sa

► To cite this version:

Alana Oliveira de Sa. Relations entre systèmes tectoniques et sédimentaires à la limite Nord de la plaque Caraïbe (Cuba-Hispaniola) : implications géodynamiques. Géophysique [physics.geo-ph]. Sorbonne Université, 2023. Français. NNT : 2023SORUS625 . tel-04504931

HAL Id: tel-04504931

<https://theses.hal.science/tel-04504931>

Submitted on 14 Mar 2024

HAL is a multi-disciplinary open access archive for the deposit and dissemination of scientific research documents, whether they are published or not. The documents may come from teaching and research institutions in France or abroad, or from public or private research centers.

L'archive ouverte pluridisciplinaire **HAL**, est destinée au dépôt et à la diffusion de documents scientifiques de niveau recherche, publiés ou non, émanant des établissements d'enseignement et de recherche français ou étrangers, des laboratoires publics ou privés.



**THÈSE POUR OBTENIR LE GRADE DE DOCTEUR DE SORBONNE
UNIVERSITÉ**

ED 398 - Géosciences, Ressources Naturelles et Environnement

**Relations entre systèmes tectoniques et sédimentaires
à la limite Nord de la plaque Caraïbe (Cuba-Hispaniola).
Implications géodynamiques**

Par Alana OLIVEIRA DE SA

Sous la direction de Dr. Sylvie LEROY, Dr. Elia D'ACREMONT et de Dr. Sara LAFUERZA

21 novembre 2023

Devant le jury composé de :

| | |
|-------------------------------------------------------------------------------------------------------------|---------------------|
| Dr Serge Lallemand, Directeur de Recherche CNRS, Géosciences Montpellier, Université de Montpellier | Rapporteur |
| Dr Aurélien Gay, Maître de Conférence, Géosciences Montpellier, Université de Montpellier | Rapporteur |
| Dr Mélody Philippon, Maître de Conférence, Géosciences Montpellier, Université des Antilles et de la Guyane | Examinatrice |
| Dr Rémy Deschamps, Ingénieur de Recherche, IFP Energies nouvelles (IFPEN) | Examineur |
| Dr Claudio Rosenberg, Professeur, Institut des Sciences de la Terre de Paris (ISTeP) | Examineur |
| Elia d'Acremont, Professeur, Institut des Sciences de la Terre de Paris (ISTeP) | Directrice de thèse |
| Sylvie Leroy, Directrice de Recherche, Institut des Sciences de la Terre de Paris (ISTeP) | Directrice de thèse |
| Sara Lafuerza, Maître de Conférence, Institut des Sciences de la Terre de Paris (ISTeP) | Directrice de thèse |

Président du jury: Dr Claudio Rosenberg

Remerciements

La réalisation de cette thèse n'aurait pas été possible sans l'intervention de nombreuses personnes que je tiens à remercier.

Tout d'abord, je souhaite exprimer ma profonde gratitude à mes directrices Sylvie LEROY, Elia d'ACREMONT et Sara LAFUERZA. Merci pour toutes les opportunités offertes, la confiance sans faille, et votre patience inébranlable. Votre soutien constant, vos précieux conseils, et l'attention portée à mon travail ont nourri mes réflexions. Je suis très reconnaissante envers elles de m'avoir procuré tous les moyens nécessaires au bon déroulement de mon travail, de m'avoir reçu à chaque fois que j'avais besoin d'elles et d'être là jusqu'au tout dernier moment. Je vous remercie pour le savoir que vous m'avez transmis et pour votre soutien à chaque étape.

Je tiens également à adresser mes remerciements à l'ensemble du jury. Serge LALLEMAND et Aurélien GAY, mes rapporteurs, je vous suis reconnaissante de m'avoir fait l'honneur d'évaluer mon manuscrit de thèse. Merci à Mélody PHILIPPON et Rémy DESCHAMPS pour avoir accepté d'examiner mon travail. Mes remerciements s'étendent également à Claudio ROSENBERG pour ses retours constructifs lors de mes comités de suivi et pour avoir accepté l'invitation de présider le jury.

Ma reconnaissance va à mes amis et collègues pour leur soutien moral et intellectuel tout au long de cette aventure. Je remercie en particulier Alain RABAUTE pour ses conseils précieux concernant le logiciel ArcGIS. Mes pensées vont également aux doctorants, post-docs et stagiaires qui ont contribué à l'ambiance conviviale et dynamique pendant ces années de thèse. Un merci tout spécial à Agathe, Jean-Baptiste, Vincent, Marilou, Boubacar, Aniès et Victor pour tous ces moments partagés au bureau.

Du fond du cœur, je souhaite remercier Benjamin SÉGUIER. Ton encouragement constant et ta foi en moi m'ont été précieux. Les mots me manquent pour exprimer toute ma gratitude.

Enfin, je tiens à exprimer ma gratitude envers moi-même pour avoir eu le courage d'affronter l'inconnu, de croire en la possibilité de réaliser ce que beaucoup considéraient comme impossible pour moi, et d'avoir maintenu ma détermination à avancer.

Resumé

La limite entre la plaque tectonique Nord-Américaine et la plaque Caraïbes constitue une frontière de plaque complexe, principalement située en mer. Cette frontière est marquée par un système de failles décrochantes senestres, connu sous le nom de Système de failles Septentrionale-Orientale (SOFZ), qui permet à la plaque Caraïbe de se déplacer à une vitesse d'environ 20 mm/an vers l'est de manière oblique par rapport à la plaque Nord-Américaine. Au niveau de la plaque Nord-Américaine, la plate-forme carbonatée des Bahamas agit comme un butoir, empêchant l'échappement vers l'est de la plaque Caraïbe. Selon cette configuration, la frontière nord de la plaque Caraïbe est qualifiée de frontière en collision oblique. En conséquence, la déformation qui se produit le long de cette frontière se divise en deux types : d'un côté, des déformations décrochantes, et de l'autre, des déformations compressives qui ont un impact particulièrement marqué sur les îles d'Hispaniola et de Cuba. Le partitionnement de la déformation dans cette région forme par conséquent une grande variété des structures tectoniques. L'héritage structural de ces déformations a aussi une forte influence sur le remplissage sédimentaire et sur l'évolution des caractéristiques morphologiques de ces zones tectoniquement actives.

L'histoire géologique de la frontière actuelle au nord de la plaque Caraïbe a été largement étudiée à terre, notamment à Cuba et à Hispaniola. Toutefois, bien que des aspects clés de cette histoire soient bien documentés, une grande partie de cette histoire a été enregistrée par les séries sédimentaires en mer et reste encore inexplorée. De nombreuses interrogations persistent concernant la position, la configuration et la chronologie des différents segments de failles situés en mer, ainsi que la relation du fonctionnement de ces failles avec la distribution des éléments morphologiques du fond marin. Le principal objectif de ce travail est d'étudier les déformations, passées et présentes, du système de failles décrochantes et du prisme d'accrétion en mer qui marque la frontière entre la plaque Caraïbe et la plaque Nord-Américaine. En étudiant les déformations des séries sédimentaires marines, nous cherchons à détailler l'évolution de cette frontière, en définissant les phases majeures de déformation et leur influence sur le contexte régional. De plus, ce travail vise à explorer la relation entre la dynamique sédimentaire et la tectonique, en intégrant à la fois l'histoire de la déformation et les processus sédimentaires actuels.

Pour atteindre ces objectifs, cette étude combine des données géologiques et des observations de terrain issues de la littérature concernant Cuba, la région nord d'Haïti et de la République Dominicaine, avec des données de géophysique et des carottes sédimentaires superficielles recueillies lors de diverses campagnes océanographiques.

Les données de sismique réflexion sont utilisées pour effectuer l'analyse stratigraphique et structurale de la couverture sédimentaire en mer. Les données de bathymétrie multifaisceaux ont servi à élaborer les cartes bathymétriques de la région étudiée, permettant ainsi de mettre en évidence les éléments morphologiques du fond marin. Les données bathymétriques et de sismique réflexion sont combinées pour déterminer l'activité sur les segments de failles cartographiés. Les carottes sédimentaires ont fait l'objet d'une description détaillée et d'un échantillonnage permettant une série d'analyses telles que l'analyse granulométrique, la radioscopie RX, la spectrométrie par fluorescence des rayons X (XRF). Ces analyses ont été intégrées dans le but de décrypter et de comprendre les processus sédimentaires dominants affectant les unités sédimentaires en surface.

Les résultats de cette étude dévoilent que les phases majeures de déformation identifiées à terre ont des correspondances tectoniques et stratigraphiques dans les unités sédimentaires marines, s'étendant de la côte nord-est de Cuba jusqu'à la côte nord d'Haïti. L'histoire géologique présente dans ces séries marines ne se limite pas à la période récente de la frontière nord de la plaque Caraïbe. Elle nous révèle une histoire géologique bien plus lointaine, remontant à la formation du domaine caraïbéen qui s'initie avec le rifting de la Pangée et la mise en place de la grande province des Bahamas, et se poursuit avec l'ouverture et la fermeture de l'ancien domaine océanique de la Proto-Caraïbe, aboutissant à la collision du bloc cubain avec la plateforme des Bahamas. Cette collision a engendré la création d'une succession de systèmes de failles décrochantes, permettant la migration vers l'est de la plaque Caraïbe malgré le butoir de la province carbonatée des Bahamas. Ces sauts de décrochements vers le sud ont transféré peu à peu le bloc Cubain vers la Plaque Nord-Américaine. Ceci jusqu'à la formation de l'actuelle limite de plaque représentée par la mise en place du Système de failles décrochantes sénestres Septentrionale-Oriente (SOFZ).

La dynamique récente et les relations entre les événements tectoniques et sédimentaires ont été mis en évidence au nord de la côte d'Haïti. Des dépôts d'instabilité Pliocène inférieur semble influencer la déformation des unités sédimentaires récentes, engendrant une morphologie de fond marin irrégulière. Les dépôts de transport en masse anciens interagissent avec les courants de fond, générant des dépôts et des structures contouritiques. Ces processus cumulés à un étalement gravitaire en raison de la forte accumulation sédimentaire sur un niveau de décollement donnent forme à l'actuelle morphologie du fond marin au Nord d'Haïti. De plus, les chenaux des canyons sous-marins sont perturbés latéralement par l'activité des failles, montrant que les éléments géomorphologiques sont également impactés par la tectonique décrochante de la région.

Cette étude offre une analyse intégrative des relations entre les processus tectoniques et sédimentaires à la frontière nord de la plaque Caraïbe, mettant en lumière des aspects cruciaux de l'évolution géodynamique et des dynamiques sédimentaires contemporaines en contexte de convergence oblique.

Abstract

The boundary between the North American tectonic and Caribbean plates represents a complex plate boundary, mainly located at sea. This boundary is characterized by a sinistral strike-slip fault system, known as the Septentrional-Oriente Fault Zone (SOFZ), which allows the Caribbean plate to move at a speed of approximately 20 mm/year towards the east in an oblique manner relative to the North American plate. At the North American plate, the Bahamian carbonate platform is located, which acts as a kind of buttress to the eastward escape of the Caribbean plate. Based on this configuration, the northern boundary of the Caribbean plate is thus described as an oblique collision boundary. Consequently, the deformation occurring along this boundary splits into two types: on one hand, strike-slip deformations, and on the other, compressive deformations, which notably impact the islands of Hispaniola and Cuba. Therefore, the partitioning of deformation in this region forms a wide variety of tectonic structures. The structural heritage of these deformations also greatly influences sedimentary filling and the evolution of morphological features in these tectonically active areas.

The geological history of the current northern boundary of the Caribbean plate has been extensively studied on land, especially in Cuba and Hispaniola. However, while key aspects of this history are well-documented, much of this history is recorded in the marine sedimentary sequences and remains unexplored. Numerous questions persist about the position, configuration, and chronology of the various fault segments at sea, as well as the relationship between the functioning of these faults and the distribution of the marine seabed's morphological elements. The main objective of this work is to study past and present deformations of the strike-slip fault system that marks the boundary between the Caribbean and North American plates. By examining marine sedimentary sequence deformations, we aim to detail the evolution of this boundary, defining the major phases of deformation and their influence on the regional context. Additionally, this study explores the relationship between sedimentary dynamics and tectonics, integrating the history of deformation and current sedimentary processes.

To achieve these goals, this study combines geological data and terrestrial observations from the literature concerning Cuba, northern Haiti, and the Dominican Republic with geophysical data and superficial sedimentary cores collected during various oceanographic campaigns. Reflection seismic data is used to perform the stratigraphic and structural analysis of the marine sedimentary cover. Multibeam bathymetry data has been used to develop bathymetric maps of the study area, highlighting the morphological features of the seabed. Bathymetric and reflection seismic data were combined to determine activity on the mapped fault segments. Sedimentary cores underwent detailed description and sampling, followed by a series of analyses such as granulometry, X-ray radiography and X-ray fluorescence spectrometry (XRF). These analyses were integrated with the aim of decrypting and understanding the dominant sedimentary processes affecting the surface sedimentary units.

The results of this study reveal that the major phases of deformation identified on land have tectonic and stratigraphic correspondences in the marine sedimentary units, extending from the northeast coast of Cuba to the north coast of Haiti. The geological history present in these marine series is not limited to the recent period of the northern boundary of the Caribbean plate. It unveils a much more distant geological history, dating back to the formation of the Caribbean domain, which began with the rifting of Pangea and the establishment of the great province of the Bahamas and continued with the opening and closing of the ancient oceanic domain of the Proto-Caribbean, leading to the collision of the Cuban block with the Bahamas platform. This collision created several strike-slip fault systems, allowing the eastward migration of the Caribbean plate and gradually transferring the Cuban block to the North American Plate. This continued until the formation of the current plate boundary marked by the establishment of the Septentrional-Oriente Fault Zone (SOFZ).

The recent dynamics between tectonic and sedimentary phenomena have been highlighted north of the Haitian coast. Lower Pliocene mass transport deposits seem to influence the deformation of recent sedimentary units, generating an irregular seabed morphology which interacts with bottom currents, producing deposits and contouritic structures shaping the current seabed morphology in the region. Furthermore, submarine canyons are laterally displaced by fault activity, showing that geomorphological elements are also impacted by the region's strike-slip tectonics.

This study offers an integrative analysis of the relationships between tectonic and sedimentary processes within the northern Caribbean area, highlighting crucial aspects of geodynamic evolution and contemporary sedimentary dynamics at the northern boundary of the Caribbean plate.

TABLE DES MATIÈRES

| | |
|-------------------------------------------------------------------------------------------------------------------------------|----|
| CHAPITRE I : Introduction générale et problématique..... | 1 |
| PREMIÈRE PARTIE..... | 4 |
| CHAPITRE II : Présentation de la zone d'étude et état de l'art | 5 |
| II.1 La Plaque Caraïbe | 5 |
| II.2 Origine de la plaque Caraïbe | 7 |
| II.2.1 Modèle inter-américain..... | 8 |
| II.2.2 Modèle pacifique..... | 8 |
| II.3 Structure de la croûte caribéenne..... | 10 |
| II.4 Structure et dynamique de la Frontière Nord Caraïbe..... | 12 |
| II.5 Contexte sismotectonique de la Frontière Nord de la Plaque Caraïbe | 13 |
| II.5.1 La sismicité sur Frontière Nord de la Plaque Caraïbe..... | 15 |
| II.6 La province Carbonatée des Bahamas (Le Great Bahama Bank) | 16 |
| II.6.1 Hypothèse de la croûte continentale amincie sous-jacente à la Province Carbonatée des Bahamas | 17 |
| II.6.2 Hypothèse d'une croûte océanique sous-jacente à la Province Carbonatée des Bahamas | 18 |
| II.6.3 Hypothèse d'une grande province ignée sous la Province Carbonatée des Bahamas..... | 19 |
| II.7 Évolution du Domaine Nord Caraïbe..... | 19 |
| II.7.1 Crétacé : Mise en place de la Plaque Caraïbe | 19 |
| II.7.2 Cénozoïque : Collision Ouest-Est de la Plaque Caraïbe avec la Plateforme des Bahamas..... | 20 |
| II.8 Phases de Déformation à Cuba et Hispaniola | 23 |
| II.8.1 Les phases de déformation à Cuba : un enregistrement géologique de l'évolution du domaine Caraïbe..... | 23 |
| II.8.2 Les phases de déformation à Hispaniola : un enregistrement géologique de l'évolution de la Frontière Nord Caraïbe..... | 24 |
| DEUXIÈME PARTIE | 30 |
| CHAPITRE III : Données et méthodologie | 31 |
| III.1 Données..... | 31 |
| III.1.1 Les données bathymétriques multifaisceaux..... | 32 |
| III.1.1.1 Acquisition..... | 32 |
| III.1.1.2 Principe de la méthode | 33 |
| III.1.2 Données sismiques | 34 |
| III.1.2.1 Acquisition..... | 34 |
| III.1.2.2 Principe de la méthode | 34 |
| III.1.3 Carottes Sédimentaires | 35 |

| | |
|---------------------------------------------------------------------------------------------------|----|
| III.1.3.1 Technique de Carottage par Carottier Kullenberg | 35 |
| III.2 METHODOLOGIE..... | 36 |
| III.2.1. Analyse des données acoustiques..... | 36 |
| III.2.2. Interprétation sismique..... | 36 |
| III.2.3. Analyses sur carottes..... | 37 |
| TROISIÈME PARTIE..... | 38 |
| CHAPITRE IV : Evolution long-terme d'une limite de plaques - Cuba oriental..... | 39 |
| IV. The Protracted Evolution of a Plate Boundary: Eastern Cuba Block and Old Bahamas Channel | 39 |
| Abstract | 40 |
| IV.1. Introduction | 40 |
| IV.2. Geological setting: a synthesis | 42 |
| IV.2.1 Northern Proto-Caribbean Passive margin | 43 |
| IV.2.2 Bahamas domain..... | 45 |
| IV.2.3 The Proto-Caribbean Seaway..... | 46 |
| IV.2.4 Cretaceous Caribbean plate | 49 |
| IV.2.5 Cuban Arc..... | 49 |
| IV.3. Data and methods..... | 50 |
| IV.4. Results | 53 |
| IV.4.1 Morphology of the study area | 53 |
| IV.4.2 Seismic Stratigraphy..... | 53 |
| IV.4.2.1 Basement | 53 |
| IV.4.2.2 Unit A..... | 54 |
| IV.4.2.3 Unit B..... | 55 |
| IV.4.2.4 Unit C..... | 55 |
| IV.4.2.5 Unit D | 55 |
| IV.4.2.6 Unit E..... | 56 |
| IV.4.2.7 Other Seismic Features – Bahamian Highs and chaotic bodies | 58 |
| IV.4.3 Structural analysis | 58 |
| IV.4.3.1 Tilted Basement blocks | 58 |
| IV.4.3.2 Thrust faults | 62 |
| IV.4.3.3 Growth faults | 62 |
| IV.5. Discussion..... | 65 |
| IV.5.1 Age of Seismic Units | 65 |
| IV.5.1.1 Unit A..... | 65 |
| IV.5.1.2 Unit B..... | 67 |
| IV.5.1.3 Units C, D, and E..... | 68 |

| | |
|--------------------------------------------------------------------------------------------------------------------------------------------------------|-----|
| IV.5.2 Main structural and geological features | 68 |
| IV.5.2.1 Rifting of the Eastern Cuban Block..... | 68 |
| IV.5.2.2 Reef related to basement features and sea-level rises..... | 68 |
| IV.5.2.3 Evidence of salt | 69 |
| IV.5.2.4 Structure and Deformation in Insular Slope: strike-slip, compression, reactivation..... | 70 |
| IV.5.3 Geological evolution of the Old Bahamas Channel, Eastern Cuba Block..... | 71 |
| IV.5.3.1 Post-rift phase | 71 |
| IV.5.3.2 Orogenic phase | 72 |
| IV.5.3.3 Post-Orogenic phase and shear zone jumps..... | 74 |
| IV.6. Summary and conclusions..... | 74 |
| Acknowledgments: | 76 |
| IV.7 References..... | 76 |
| CHAPITRE V : Déformation polyphasée et migration de la déformation le long du Système de failles décrochantes sénestres Septentrionale-Oriente | 83 |
| V. Polyphase deformation and strain migration on the Septentrional-Oriente Fault Zone in the Windward Passage, Northern Caribbean Plate boundary | 83 |
| Abstract | 84 |
| V.1 Introduction | 84 |
| V.2 Tectonic Settings | 86 |
| V.3 Data and Methods..... | 89 |
| V.4 Results | 92 |
| V.4.1 Seismic stratigraphy | 92 |
| V.4.1.1 Windward Passage Sill | 92 |
| V.4.1.2 Windward Passage Deep..... | 93 |
| V.4.2. Structural Analysis..... | 96 |
| V.4.2.1. Windward Passage Sill structural features..... | 96 |
| V.4.2.2 The Windward Passage Deep structural features..... | 98 |
| V.5. Discussion..... | 101 |
| V.5.1 Deformation events in the Windward Passage..... | 103 |
| V.5.1.1 Windward Passage Sill | 103 |
| V.5.1.2 Windward Passage Deep..... | 103 |
| V.5.2 Tectonic interpretation of deformation events and onshore correlations..... | 104 |
| V.5.2.1 Eocene Deformation: Piggyback basins phase..... | 105 |
| V.5.2.2 Late-Oligocene: Extensional Phase | 106 |
| V.5.2.3 Middle Miocene Deformation: Compressional phase | 107 |
| V.5.2.4 Pliocene to Present Deformation: Transpressional phase..... | 107 |

| | |
|----------------------------------------------------------------------------------------------------------------------------------------|-----|
| V.5 Conclusions | 111 |
| Acknowledgments | 112 |
| V.6 References..... | 112 |
| CHAPITRE VI : Évolution de la limite de plaque Nord Caraïbe au Nord d’Haïti | 118 |
| VI. Dynamic Evolution of the Northern Caribbean Plate Boundary: Impact on Seabed and Tectonics from Miocene to Present | 118 |
| Abstract | 118 |
| VI.1 Introduction | 119 |
| V.I.2.1 Regional Tectonic Setting..... | 122 |
| VI.2.2 Morpho-structural settings | 123 |
| VI.2 Data and Methodology | 125 |
| VI.3. Results | 126 |
| VI.3.1 Submarine canyons and channels..... | 126 |
| VI.3.2 Seafloor Depressions..... | 128 |
| VI.3.3 Seismic stratigraphy | 128 |
| VI.3.4 Deformation front | 133 |
| VI.3.5. Morpho-structural domains..... | 134 |
| VI.4. Discussion..... | 137 |
| VI.4 Stratigraphic record and seafloor morphology variability | 138 |
| VI.4.1 Evidence of post-depositional remobilisation within Unit U4 | 139 |
| VI.4.2 Significance of the MTD in the Eastern Domain | 140 |
| VI.4.3 Wave-like pattern of the Subunit U4b | 141 |
| VI.5. Tectonic Influences on the Submarine Canyons of the Eastern Domain..... | 143 |
| VI.5.1 Influence of Deep Faults on Canyon Paths | 143 |
| VI.5.2 Influence of deformation Front on Canyons morphology | 145 |
| VI.6 Deformation partitioning and distribution of the morphological features | 145 |
| VI.7. Timing Constraints for the Deformation along the Northern Hispaniola Margin..... | 147 |
| VI.7.1 From Oligocene to Early Pliocene (Unit 1 to 3; U4; onset of U4a) | 147 |
| VI.7.2 Pliocene (Further Unit U4a) | 148 |
| VI.7.3 From Pliocene to present-day (Unit U4b) | 149 |
| VI.8 Conclusion | 150 |
| VI.9 References..... | 150 |
| CHAPITRE VII : Interactions entre les processus tectoniques profonds et processus sédimentaires au large de la côte nord d'Haïti | 157 |
| VII. Enigmatic deep-water seafloor depressions east of Tortue Island, Northern Haiti margin | 157 |
| Abstract | 157 |

| | |
|------------------------------------------------------------------------------------------------------|-----|
| VII.1. Introduction | 158 |
| VII.2. Geological and oceanographic settings | 160 |
| VII.2.1 Geological Setting | 160 |
| VII.2.2 Oceanographic Setting | 161 |
| VII.3. Data and Methodology | 162 |
| VII.3.1 Geophysical data | 164 |
| VII.3.2 Sedimentological data | 164 |
| VII.3.3. Geochemical data | 164 |
| VII.4 Results | 165 |
| VII.4.1 Seafloor geomorphology | 165 |
| VII.4.1.1 Depressions | 165 |
| VII.4.1.2 Backscatter | 165 |
| VII.4.2. Seismic facies | 166 |
| VII.4.3. Sediment facies | 170 |
| VII.4.3.1 Facies F1 | 170 |
| VII.4.3.2 Facies F2 | 170 |
| VII.4.3.3 Facies F3 | 173 |
| VII.4.3.4 Facies F4 | 173 |
| VII.4.3.5 Facies F5 | 173 |
| VII.5. Discussion | 175 |
| VII.5.1 Synthesis and interpretation of the main sedimentary facies | 175 |
| VII.5.2 Possible Origins of the seafloor depressions | 179 |
| VII.5.2.1 Pockmarks | 180 |
| VII.5.2.2 Submarine karstification | 180 |
| VII.5.2.3 Differential compaction and post-MTD sediment distribution | 181 |
| VII.5.2.4 Erosional features related to irregular seafloor in a contouritic system | 182 |
| VII.5.3 A model for the formation of the seafloor depressions along the northern Haitian coast | 183 |
| VII.6 Conclusion | 186 |
| VII.7 References | 187 |
| QUATRIÈME PARTIE | 194 |
| CHAPITRE VIII : Conclusions et Perspectives | 195 |
| VIII.1. Conclusions | 195 |
| VIII.2. Les perspectives | 203 |
| REFERENCES BIBLIOGRAPHIQUES | 205 |

CHAPITRE I : Introduction générale et problématique

La plaque Caraïbe est limitée par quatre plaques tectoniques différentes, les plaques tectoniques Nord-Américaine, Sud-Américaine, de Nazca et de Cocos. La frontière Nord de la Plaque Caraïbe correspond à un système de failles décrochantes senestres, qui s'étend principalement à travers des domaines océaniques situés à des profondeurs variant entre 600 et 7000 mètres. Ce système de failles, connu sous le nom de Système de failles décrochantes senestres Septentrionale-Orientale (SOFZ), est globalement orienté Est-Ouest. Le mouvement NE de la plaque Caraïbe par rapport à la plaque Nord-Américaine s'effectue de manière oblique par rapport à la frontière de plaque. On parle alors d'une frontière en transpression ou en collision oblique. Cela se traduit par un partitionnement de la déformation entre, d'une part, des déformations décrochantes et, d'autre part, des déformations compressives.

A ce scénario géologique complexe, s'ajoute un risque sismique élevé, comme attesté par les séismes dévastateurs survenus en Haïti durant les années 2010, 2018 et 2021. Ces événements ont catalysé une intensification des recherches géologiques dans la région, mettant en évidence le besoin urgent de mieux comprendre les mécanismes sous-jacents à ces phénomènes destructeurs. Une bonne compréhension de ce système transpressif semble donc nécessaire. Cette compréhension passe par une description précise de la géométrie de la frontière nord de la plaque Caraïbe, de son évolution géodynamique dans le temps, de la localisation des structures le long desquelles a lieu la déformation ainsi que son partitionnement sur ces structures.

Avec cette thèse, nous souhaitons apporter de nouvelles contraintes sur la mise en place de l'actuelle frontière nord de la Plaque Caraïbe, à partir de l'étude des déformations des séries sédimentaires en mer (jusqu'alors très peu étudiées). En effet, la mise en place de l'actuelle frontière au nord de la plaque Caraïbe, y compris les épisodes de déformation associés ont largement été étudiés sur les affleurements à Cuba et à Hispaniola, et sont aujourd'hui relativement bien contraints. Cependant, une grande partie de cette histoire a été enregistrée par les séries sédimentaires en mer et reste encore inexplorée. Des questions demeurent encore ouvertes concernant l'emplacement, la géométrie et le calendrier de mise en place des différents segments localisés en mer, ainsi que la relation entre le fonctionnement de ces failles avec la distribution des éléments morphologiques du fond marin.

Nous souhaitons ainsi comprendre l'implication de ces différentes phases de déformation sur la morphologie du fond marin de part et d'autre des segments actifs de la SOFZ, mises en jeu au travers de la frontière nord de la Plaque Caraïbe, et de répondre aux questions suivantes : Quelle est la géométrie précise de la SOFZ ? Sur quelles structures sont accommodées la composante compressive de la déformation et quelle sédimentation y est associée ? Quel est le calendrier de la migration de ces différents segments actifs ? Quels sont les conséquences de cette migration et ses implications sur les éléments morphologiques du fond marin ? A quels types de sédimentation et de systèmes sédimentaires sont associés ce système de faille ? Existe-t-il un lien entre les processus tectoniques profonds et l'actuel morphologie du fond marin ? Quelles sont les implications géodynamiques de nos résultats sur le fonctionnement dans le temps de la frontière Nord de la plaque Caraïbe ?

Cette thèse comporte trois objectifs principaux :

- 1) identifier les phases de déformation qui affectent la couverture sédimentaire en mer, leur impact régional, leur style structural et leur évolution ;
- 2) contraindre l'histoire de la déformation de la limite nord de la plaque caraïbe, en prenant en compte le domaine marin et ;
- 3) caractériser l'interaction entre la dynamique sédimentaire et la déformation en examinant la tectonique régionale et les processus sédimentaires actifs.

Pour atteindre ces objectifs, cette étude intègre des données géologiques et des observations à terre issues de plusieurs travaux menés sur Hispaniola (Calais & Mercier De Lépinay, 1992; de Zoeten & Mann, 1991, 1999; Escuder-Viruete, Valverde-Vaquero, Rojas-Agramonte, Jabites, et al., 2013; Escuder-Viruete & Pérez, 2020; Mann, 1999; Mauffret & Leroy, 1999a) et sur Cuba (Calais and Mercier De Lépinay, 1992; de Zoeten and Mann, 1999; Iturralde-Vinent and Macphee, 1999; Rojas-Agramonte et al., 2008; Zoeten and Mann, Paul, 1991). Ceci ont été combinées à l'étude des profils sismiques, des cartes bathymétriques et des carottes sédimentaires acquises durant différentes campagnes en mer (HAITI-SIS 1 et 2, NORCARIBE, Haïti BGF) (Ellouz-Zimmermann & Beaufort, 2015; Leroy, 2012; Leroy & Ellouz-Zimmermann, 2013; Rodríguez-Zurrunero et al., 2019, 2020).

Nous avons effectué une interprétation des lignes sismiques disponibles en la combinant à une étude morpho bathymétrique détaillée, ainsi qu'à des analyses sédimentologiques réalisées sur des carottes sédimentaires prélevées dans la région d'étude. Ces données et méthodes nous ont permis de caractériser les différents styles de déformation des séries sédimentaires en mer associées aux différents segments actifs et inactifs des failles et, ainsi de reconstituer l'histoire de la migration de la frontière nord de la Plaque de Caraïbe. Cette étude nous a aussi permis de démontrer qu'il existe un lien intrinsèque entre la mise en place de ces segments avec la distribution des éléments morphologiques des fonds marins.

Ainsi, ce manuscrit s'organise en quatre parties. La première partie est consacrée à la présentation de la zone d'étude au sein du chapitre II. Celle-ci présente une contextualisation exhaustive de l'actuelle configuration de la plaque Caraïbe (section II.1) et son origine (II.2), sa structure (II.3), la structure et la dynamique de la frontière nord Caraïbe (II.4), son contexte sismotectonique (II.5) et sa limite au nord avec la plateforme des Bahamas (II.6). Dans cette partie, nous présentons le modèle d'évolution du domaine Nord Caraïbe depuis le Jurassique (II.7.1) jusqu'à la fin du Cénozoïque (II.7.2) et les différentes phases de déformation enregistrées à Cuba (II.8.1) et à Hispaniola (II.8.2). A la fin de cette partie, nous mettons en relief les questions non résolues relatives à l'évolution de cette frontière.

Dans la deuxième partie, nous présentons les types de données utilisées dans cette étude. Au sein du Chapitre III, les différentes campagnes en mer pendant lesquelles ces données ont été acquises sont présentées. Les principes d'acquisition sont décrits (III.1), ainsi que la méthodologie adoptée pour l'analyse et l'interprétation de ces données (III.2).

Les résultats sont ensuite présentés sous la forme de quatre articles en anglais, dans la troisième partie. Ces articles sont présentés dans différents chapitres selon une structure méthodique, qui divise la zone d'étude en trois sous-régions : la région au large du Nord-est de Cuba, la région du détroit du Passage du vent et la région au large du Nord d'Haïti. Chacune de ces études correspond à des axes thématiques spécifiques explorés, en vue de parvenir à une compréhension régionale intégrée des problématiques adressées dans ce travail de recherche.

Le premier article soumis à G-cubed (CHAPITRE IV) présente les résultats de l'étude menée sur la région offshore Nord-est de Cuba. Dans cette étude, nous dévoilons la dynamique long terme de la frontière de plaque et proposons une chronologie des phases de déformation qui ont influencé les dépôts sédimentaires marins, tout en les intégrant aux événements géologiques majeurs enregistrés à Cuba depuis le Jurassique jusqu'à l'Éocène.

Le deuxième article publié à Tectonics (CHAPITRE V) présente les résultats de l'étude menée dans la région du détroit du Passage du Vent. Dans cette étude, nous démontrons les phases de déformation associées à l'abandon de l'ancienne frontière de plaques au nord de Cuba et à la formation des segments actifs actuellement localisés entre le sud-est de Cuba, dans le Bassin du Passage du vent.

Le troisième article en préparation pour Tectonophysics (CHAPITRE VI) présente les résultats de l'étude menée dans la région située au large de la Côte Nord d'Haïti. Dans cette étude, nous éclaircissons le processus non linéaire de la progression vers l'est des segments de SOFZ. Les résultats révèlent la dynamique complexe de la mise en place et d'abandon des failles décrochantes et leurs interactions avec les processus sédimentaires qui influencent la distribution des éléments morphologiques sur le fond marin. Le partitionnement de la déformation en réponse à la cinématique des plaques apparaît majeur.

Le quatrième article en préparation pour EPSL (CHAPITRE VII) présente les résultats obtenus à partir de l'étude sédimentologique réalisée sur les carottes sédimentaires prélevées sur la marge au Nord d'Haïti. Dans celui-ci, nous décrivons les types de dépôts sédimentaires présents actuels, en mettant un accent particulier sur l'origine des dépressions énigmatiques qui façonnent le fond marin. Nous examinons comment les processus tectoniques profonds ont influencé l'actuelle dynamique du fond marin, les courants marins et ses conséquences sur l'environnement de dépôt et l'actuelle morphologie du fond.

Enfin, en conclusion, dans la quatrième partie, nous synthétisons les résultats majeurs et les idées principales issues des travaux réalisés. Cette conclusion et perspective offre un récapitulatif des découvertes clés et des implications importantes de cette thèse.

PREMIÈRE PARTIE

— *Présentation de la zone d'étude et état de l'art* —

CHAPITRE II : Présentation de la zone d'étude et état de l'art

II.1 La Plaque Caraïbe

Géographiquement centré autour de la mer des Caraïbes (Figure II.1) et englobant les Antilles, les Caraïbes sont une sous-région des Amériques qui s'étend d'est en ouest, depuis les Petites Antilles jusqu'à l'Amérique centrale, et du nord au sud, couvrant la zone allant du Golfe du Mexique, incluant Cuba, jusqu'à la Colombie et le Venezuela.

Il convient de noter que si la région des Caraïbes est située sur la plaque lithosphérique Caraïbe en grande partie, ses frontières géographiques ne se superposent pas aux frontières de cette plaque. Ainsi, au nord, l'île de Cuba, le bassin du Yucatán et le Golfe du Mexique font partie de la plaque Amérique du Nord, mais sont dans la région Caraïbe. Et au sud-ouest, l'extension du Bloc de Chortís jusqu'à la limite sud du Panama est rattachée à la plaque Caraïbe, alors que géographiquement elle fait partie de l'Amérique Centrale.

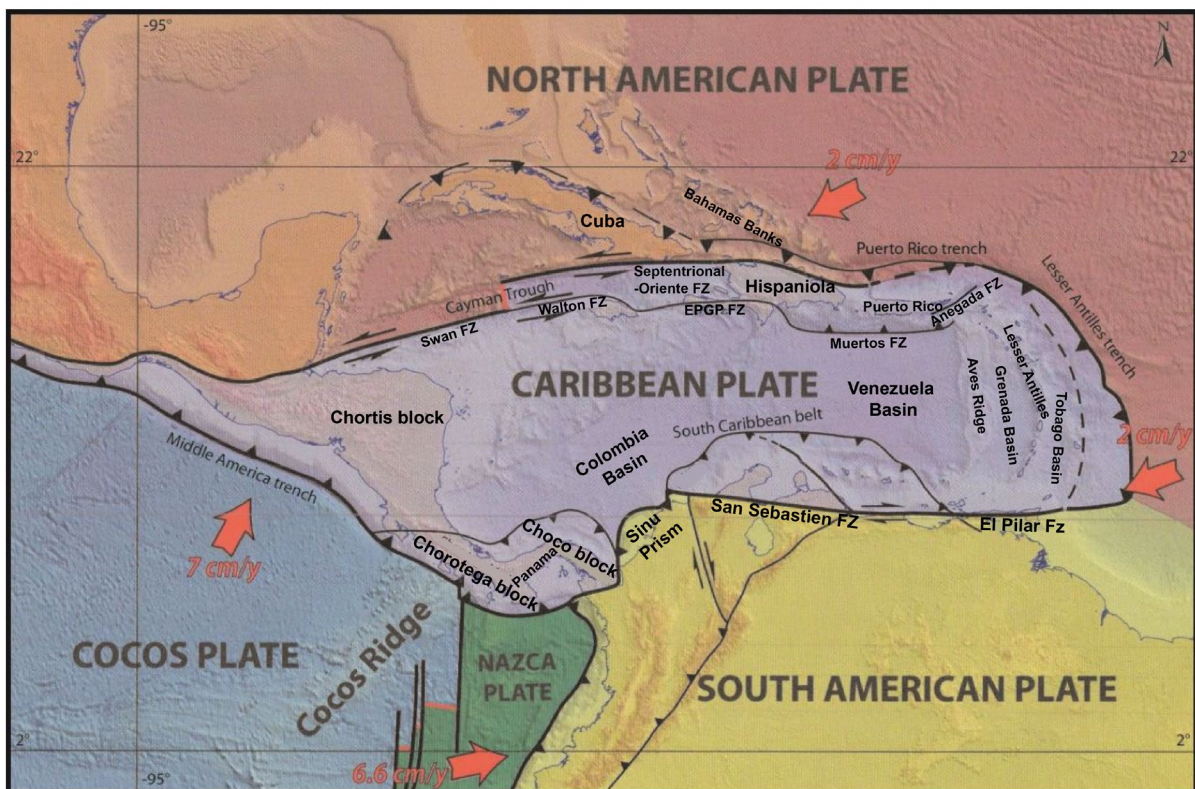


Figure II.1: Carte structurale simplifiée de la plaque Caraïbe et des plaques Nord et Sud Américaines, Cocos et Nazca. Les flèches rouges représentent les vitesses relatives à la plaque Caraïbe fixe. EPG : Enriquillo Plantain Garden ; Fz : Fault Zone. Modifié d'après Bouysse et al., 2020 (Source : Montheil, 2023).

Dans sa configuration actuelle, la plaque Caraïbe se trouve à l'intersection de quatre plaques lithosphériques : les plaques Amérique du Nord, Amérique du Sud, Cocos, et de Nazca (Figure II.1).

La plaque Caraïbe constitue un petit fragment lithosphérique qui mesure environ 2500 km d'Est en Ouest et 1000 km du Nord au Sud encastré entre les blocs continentaux nord et sud-américains (Figure II.1). Sa délimitation, basée sur des caractéristiques sismotectoniques, a été établie par Molnar and Sykes en 1969.

Au sud, la frontière est caractérisée par des décrochements dextres. De l'est à l'ouest, cette frontière est marquée par les failles d'El Pilar et San Sébastien (Figure II.1), qui évoluent en un système en compression le long du front de la cordillère orientale de Colombie se connectant à la zone de subduction de la plaque Nazca (Figure II.1).

À l'ouest, la subduction de la lithosphère océanique Pacifique sous l'Amérique centrale crée une limite de plaques convergente, qui accommode la convergence des plaques Cocos et Nazca avec la plaque Caraïbe (7 cm/an, Demets, 1992) (Figure II.1).

À l'est, la bordure orientale de la plaque caraïbe est délimitée par une subduction active, où la lithosphère océanique atlantique plonge sous les Petites Antilles (Macdonald et al., 2000) (Figure II.1).

Au nord, la limite de la plaque Caraïbe est caractérisée par un vaste système de décrochements senestres. De l'ouest à l'est, ce système est constitué par la zone de failles de Polochic-Motagua (au Guatemala), qui se prolonge en mer par les failles de Swan et d'Enriquillo Plantain Garden, puis est relayée par un axe d'accrétion océanique orienté nord-sud, situé au cœur du fossé Cayman (Figure II.1) (Leroy et al., 2000). La délimitation entre les plaques Caraïbes et Nord-Américaine continue vers l'est par la faille Septentrionale-Orientale, pour se connecter à la subduction oblique au nord de Porto Rico.

Les zones de décrochements dans le sud et le nord des Caraïbes, ainsi que la subduction des Petites Antilles, accommodent un déplacement relatif de 2 cm/an selon une direction est-nord-est à ouest-sud-ouest entre les plaques Nord-Américaine, Sud-américaine et la plaque Caraïbe (Demets, 1992) (Figure II.1).

II.2 Origine de la plaque Caraïbe

L'origine de la plaque Caraïbe a suscité des débats hautement controversés depuis de nombreuses années. Deux groupes de modèles opposés tentent d'expliquer cette origine : le modèle inter-américain (James, 2009) et le modèle pacifique (Mann, 1999; Mann et al., 2006; Pindell et al., 2006a; Pindell et al., 2012).

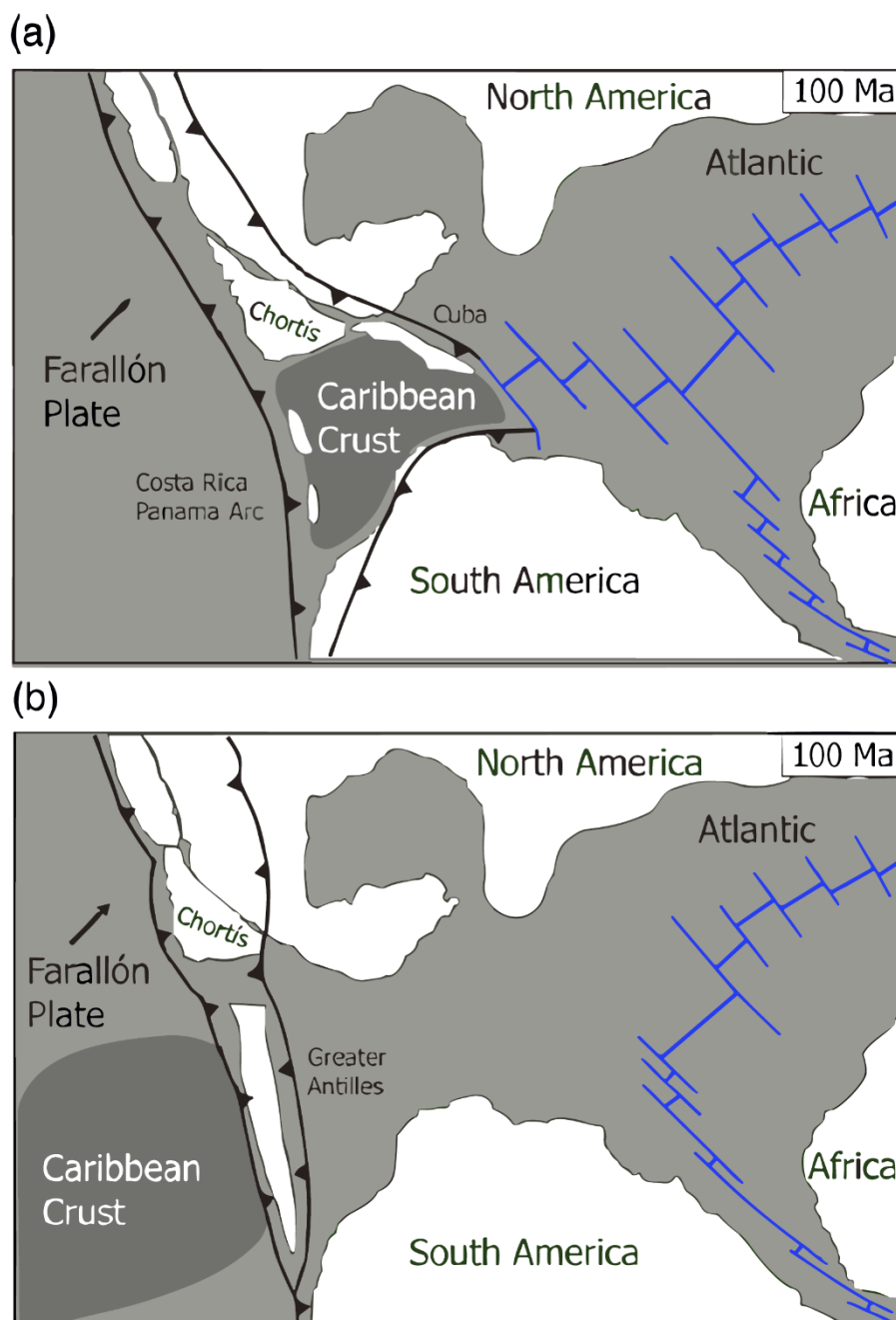


Figure II.2 : Modèles proposés dans la littérature pour l'origine de la plaque Caraïbe. (a) Modèle d'origine in situ pour la plaque Caraïbe. Selon cette théorie, la plaque Caraïbe aurait évolué sur place pendant la période de séparation entre l'Amérique du Nord et l'Amérique du Sud. (b) Modèle d'évolution pacifique de la plaque des Caraïbes. Selon cette hypothèse, la plaque Caraïbe s'est formée à l'origine dans la région du Pacifique oriental, puis a migré vers la zone entre l'Amérique du Nord et l'Amérique du Sud au fil du temps (Pindell et al., 1988, 2006a). Adapté de Brandes and Winsemann (2018).

II.2.1 Modèle inter-américain

Ce modèle implique que la plaque Caraïbe a évolué près de sa position actuelle entre les plaques Nord-Américaine et Sud-américaine (Figure II.2a) (Frisch et al., 1992; James, 2009; Meschede, 1998; Meschede & Frisch, 1998). Lors de la séparation de la Pangée, les plaques Nord-Américaine et Sud-Américaine ont été séparées par un système de rift orienté nord-ouest - sud-est qui incluait à la fois le golfe du Mexique et les Caraïbes. Au Jurassique supérieur, ce rift a évolué en un centre de propagation formant la croûte océanique de la plaque proto-Caraïbe. Au Crétacé, un panache mantellique s'est formé et a induit un volcanisme basaltique répandu, qui a affecté toute la région (Denyer & Gazel, 2009; Diebold et al., 1999; Kroehler et al., 2011). Pendant cette phase volcanique, la Province Ignée des Caraïbes (CLIP) s'est mis en place ce qui a conduit à une augmentation significative de l'épaisseur de la croûte de la plaque Caraïbe (Burke et al., 1978).

Ce modèle inter-américain repose principalement sur des données paléomagnétiques, indiquant une formation de la plaque des Caraïbes près de l'équateur (Acton et al., 2000; Frisch et al., 1992). De plus, aucun changement significatif de latitude depuis le Jurassique n'a pu être observé et tous les mouvements documentés de la plaque correspondent aux mouvements de l'Amérique du Sud. Par conséquent, une juxtaposition de la plaque Caraïbe avec la plaque sud-américaine est probable. Un lien avec la plaque Farallon ou avec d'autres plaques du Pacifique n'est pas étayé par les données paléomagnétiques (Frisch et al., 1992).

Les incertitudes majeures de ce modèle découlent essentiellement de l'absence d'anomalies magnétiques nettes au sein de la majeure partie de la plaque Caraïbe. Ce phénomène s'explique en partie par la position géographique à basse latitude de cette plaque, mais également par le fait qu'elle aurait très probablement émergé durant le Superchron normal du Crétacé (CNS) (García-Reyes & Dymant, 2021). Le CNS correspond à une période de polarité géomagnétique normale relativement stable s'étendant entre 83 et environ 120 millions d'années (Helsley & Steiner, 1968). L'absence d'inversions magnétiques pendant cette période explique l'absence des anomalies caractéristiques qui sont habituellement utilisées pour dater le plancher océanique.

Mis à part la série d'anomalies bien établies, s'étendant de l'anomalie 22 à 0 (46-0 Ma), identifiée de part et d'autre de l'axe d'accrétion océanique du fossé Cayman (Leroy et al., 2000), de nombreuses tentatives visant à déceler des anomalies magnétiques sur la plaque Caraïbe (dans les bassins de Colombie et du Venezuela) ont abouti à des interprétations divergentes. Cette situation découle principalement de la faible amplitude du signal magnétique observé et de la rareté des données disponibles (García-Reyes & Dymant, 2021; Ghosh et al., 1984; Guevara et al., 2013).

II.2.2 Modèle pacifique

Le modèle pacifique (Figure II.2b) suggère une origine de la plaque des Caraïbes dans la région du Pacifique et suppose qu'elle aurait migré vers sa position actuelle (Pindell et al., 1988, p. 198, 2006a, 2012; Ross and Scotese, 1988; Kerr et al., 1999; Mann, 1999; Pindell and Kennan, 2001; Hoernle et al., 2002; Mann et al., 2006, Garcia-Reyes and Dymant 2021). Dans ce modèle, la plaque Caraïbe constituée d'un plateau océanique (A. C. Kerr, Tarney, Marriner, Klaver, et al., 1996; A. C. Kerr, Tarney, Marriner, Nivia, et al., 1996), a été transportée vers le nord-est avec la plaque Farallon bordé au nord-est par le Grand Arc des Caraïbes (Figure II.2b) (Burke et al., 1984 ; Burke, 1988). Les bases de cette hypothèse sont les similarités pétrologiques et géochimiques entre les basaltes de la croûte des Caraïbes et les plateaux océaniques bien connus dans le Pacifique occidental. Une similarité dans la structure crustale et dans les caractéristiques acoustiques de la croûte des Caraïbes et des

plateaux océaniques a également été trouvée (Bowland & Rosencrantz, 1988; Diebold et al., 1981; Mauffret & Leroy, 1999a).

Les reconstructions cinématiques les plus récentes de la région Caraïbe depuis le Jurassique inférieur tendent à soutenir une variante du modèle pacifique (Boschman et al., 2014; Mann, 2021; Pindell et al., 2006a). Les principaux arguments sont les suivants :

- (1) L'âge de la croûte océanique au large de Porto Rico (195 Ma) est antérieur à la séparation des Amériques d'environ 30 millions d'années (Pindell & Kennan, 2001) ainsi qu'à l'expansion océanique dans l'Atlantique d'environ 25 millions d'années (Bird et al., 2007).
- (2) L'assemblage faunique des cherts du Jurassique supérieur sur l'île de La Désirade est typique des radiolarites d'origine pacifique (Mattinson et al., 2008; Montgomery & Kerr, 2009).

Un autre argument souvent utilisé se base sur l'origine des basaltes du CLIP (Caribbean Large Igneous Province) du Crétacé supérieur, celle-ci est associée à ceux provenant d'un panache dans l'océan Pacifique (Boschman et al., 2014). Ceci indiquerait que la plaque des Caraïbes a migré depuis cette période (Geldmacher et al., 2008).

L'initiation du volcanisme d'arc vers environ 75-70 Ma et le début du dépôt volcanoclastique d'arc marquent la mise en place d'une nouvelle zone de subduction à l'ouest du bloc Chortís (Figure II.1). En outre, la subduction d'une portion d'au moins 1100 km (selon van Benthem et al., 2014), de la lithosphère atlantique sous la Ride d'Aves et sous l'arc des Petites Antilles, en conjonction avec la présence de marges passives le long des plaques orientales Nord-Américaine et Sud-Américaine, suggère un mouvement relatif vers l'est de la plaque Caraïbe. Ceci contredit l'idée d'une plaque qui aurait largement stagné dans le temps et l'espace, mettant en évidence plutôt une dynamique d'échappement vers l'est de la Plaque Caraïbe.

II.3 Structure de la croûte caribéenne

La structure crustale de la Plaque Caraïbe est le résultat d'une amalgamation tectonique impliquant une hétérogénéité de types de croûtes, allant de la croûte continentale, la croûte d'arc insulaire, la croûte de plateau océanique et la croûte océanique classique (Figure II.3)(Mann, 2021).

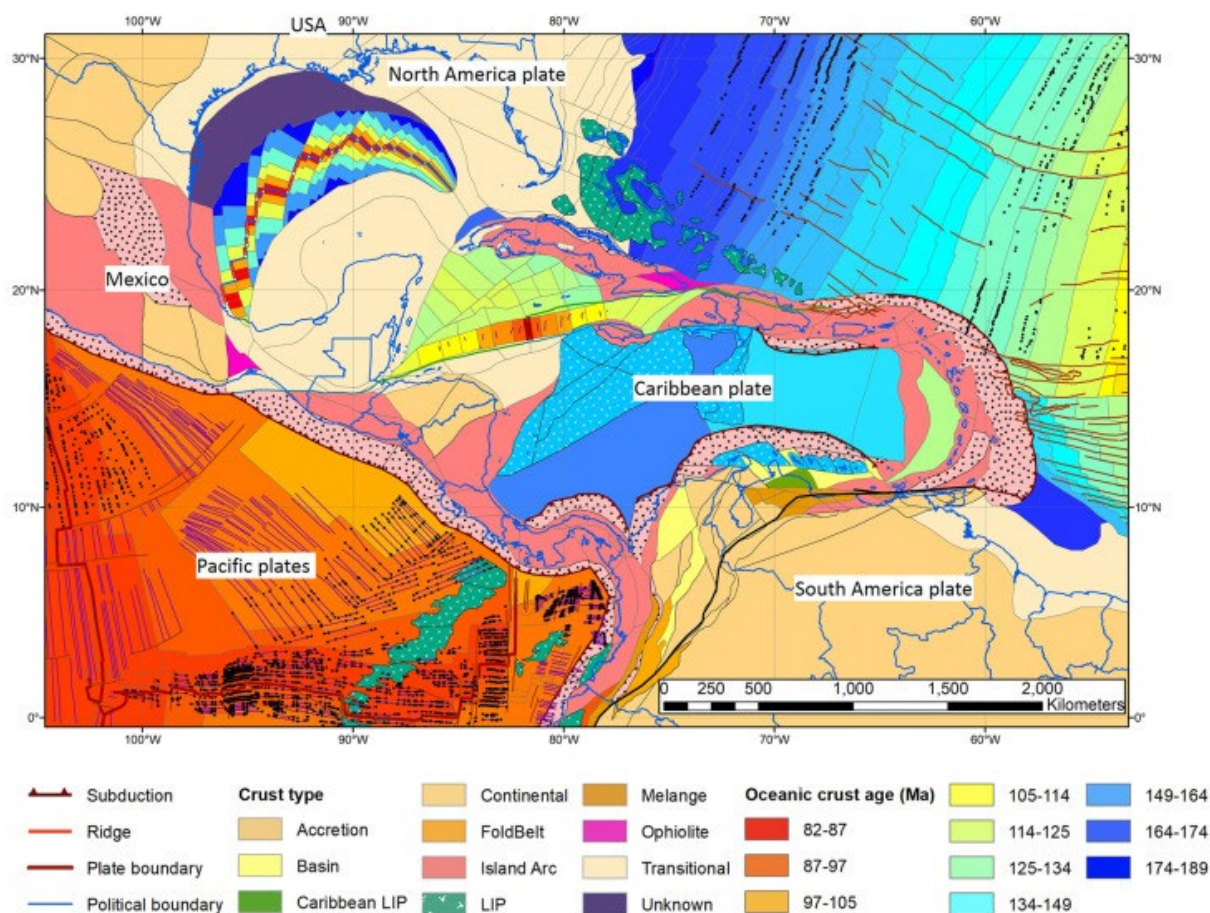


Figure II.3. Types de croûtes et structure actuelle des Caraïbes. Une grande variété de types de croûtes est présente dans la région des Caraïbes, allant de la croûte continentale épaisse non-étendue à la croûte continentale riftée, jusqu'à la croûte d'arc insulaire, croûte océanique et de plateau océanique épaissi. D'après Mann (2021).

L'essentiel de la plaque est dominé par une croûte océanique d'âge Jurassique épaissie par du matériel volcanique (basaltes) du Crétacé supérieur (Figure II.3) (Sigurdsson et al., 1997), mais surtout par des cumulats ultra-mafiques et picrites à sa base (Mauffret & Leroy 1999, Revillon et al 2000; Mauffret et al 2001). Ces basaltes font partie intégrante de la Province Magmatique des Caraïbes (CLIP) (Figure II.3) (*Caribbean Large Igneous Province*, e.g. Burke, 1988; Mauffret and Leroy 1999, Hauff et al., 2000). Des échantillons prélevés en submersible sur la ride de Beata (centre de la CLIP) possèdent un âge de 88 Ma et une géochimie typique de LIP (Mauffret et al 2001).

La structure de la croûte océanique (en dehors de la CLIP), révélée par son épaisseur (5 km), sa profondeur actuelle et sa couche sédimentaire, suggère un âge Jurassique (Mauffret & Leroy, 1997). Des échantillons prélevés sur l'île de La Désirade, datés entre 195 et 145 Ma, montrent un ensemble faunique rappelant les radiolarites du Pacifique (Mattinson et al., 2008; Montgomery & Kerr, 2009). Leurs analyses suggèrent qu'ils ont une origine liée à la plaque Farallon (A. C. Kerr et al., 1999; Mattinson et al., 2008; Montgomery et al., 1994; Montgomery & Kerr, 2009). Des anomalies

magnétiques identifiées dans le bassin du Venezuela, ainsi que sur les rides d'Aves et de Beata, suggèrent que cette croûte océanique s'est formée au sein d'une dorsale océanique d'accrétion lente du Pacifique (Guevara et al., 2013).

Des affleurements dans diverses régions des Caraïbes dévoilent que plusieurs complexes ignés ont été accrétés sur les continents, dont l'âge, entre 92 et 74 Ma, coïncide avec celui de la CLIP au centre de la plaque (Alvarado et al., 1997; A. C. Kerr, Tarney, Marriner, Nivia, et al., 1996; Lapierre et al., 2000; Sinton et al., 1998). Des forages profonds ont mis en lumière des basaltes et dolérites du Turonien au Santonien, entre 94 et 84 Ma, coïncidant avec l'évènement d'extrusion de la CLIP (Bader et al., 1970; Boschman et al., 2014; Duncan & Hargraves, 1984; Edgar et al., 1973; Geldmacher et al., 2008; A. Kerr et al., 2003; Révillon et al., 2000; Sinton et al., 1998). Bien que l'origine de la CLIP ait été très souvent associée à une phase en tête de panache au-dessus du point chaud des Galápagos (Duncan & Hargraves, 1984; Geldmacher et al., 2003; Révillon et al., 2000), une étude récente de Boschman et al. (2014) conteste cette hypothèse car la localisation des Galapagos était trop lointaine, ils proposent que les basaltes proviennent probablement d'un panache mantellique distinct, situé à 2 000-3 000 km plus à l'est du point chaud moderne des Galápagos.

Mis à part l'accrétion océanique dans le fossé Cayman et dans le bassin du Yucatan, aucune preuve d'accrétion n'a été relevée postérieurement à la formation de la CLIP. L'accrétion océanique du bassin du Yucatan s'est produite dans un bassin décrochant, dit en « pull-apart », flanqué par de failles décrochantes senestres, entre Cuba et la marge du Belize (Rosencrantz et al., 1988; Gordon et al., 1997; Leroy et al., 2000; Cruz-Orosa et al., 2012; Ramos and Mann, 2023). L'accrétion océanique dans le fossé Caïman débute il y a environ 49 Ma, et la propagation vers le Sud de son axe d'accrétion au Miocène inférieur (20 Ma) est contemporaine de la formation de la faille Walton (trace initialement inactive de la faille transformante de Swan (Leroy et al., 1996, 2000).

Tandis que l'intérieur de la plaque Caraïbe est dominé par une croûte océanique épaissie, ses bordures sont caractérisées par la présence d'arcs volcaniques (Figure II.3). Le terme "Grand Arc des Caraïbes" désigne cette série de roches d'arc, s'étalant depuis le début du Crétacé jusqu'à l'actuel, délimitant les frontières nord, est et sud de la plaque caribéenne contemporaine (Figure II.3) (Mann, 2021).

À l'ouest, la plaque est marquée par des blocs continentaux Paléozoïques (Chortis, Chorotega et Choco, Figure II.1) superposés de roches d'arc insulaire liée à la subduction des plaques Cocos et Nazca (Denyer et al., 2006; Denyer & Gazel, 2009; Gazel et al., 2021). À l'est, la ride d'Aves marque sur son flanc ouest, les contours du bassin du Venezuela, s'étendant de la marge Sud-Américaine jusqu'aux Grandes Antilles. À l'est de cette ride, les Petites Antilles affichent une croûte d'arc remarquablement épaissie à l'exception du bassin de Grenade qui présente un croûte de type océanique (Figure II.1)(Garroq et al., 2021; Melekhova et al., 2019; Padron et al., 2021).

Le sud de la plaque est caractérisé par les prismes de Panama et de Sinu et la ceinture Sud-Caribéenne, formés par la subduction et l'accrétion entre les plaques Caraïbe et Sud-Américaine (Gorney et al., 2007; Kroehler et al., 2011; Montes et al., 2019; van der Lelij et al., 2010).

Et, enfin, le nord de la plaque expose des roches issues de l'accrétion successive de marges continentales, observables sur des îles telles que Cuba, la Jamaïque et Hispaniola (Bouysse et al., 2020; García-Casco et al., 2008; Laó-Dávila, 2014).

II.4 Structure et dynamique de la Frontière Nord Caraïbe

La partie nord-ouest de la plaque Caraïbe se distingue par la présence d'une mosaïque de blocs structuraux délimités par des failles d'échelle crustale.

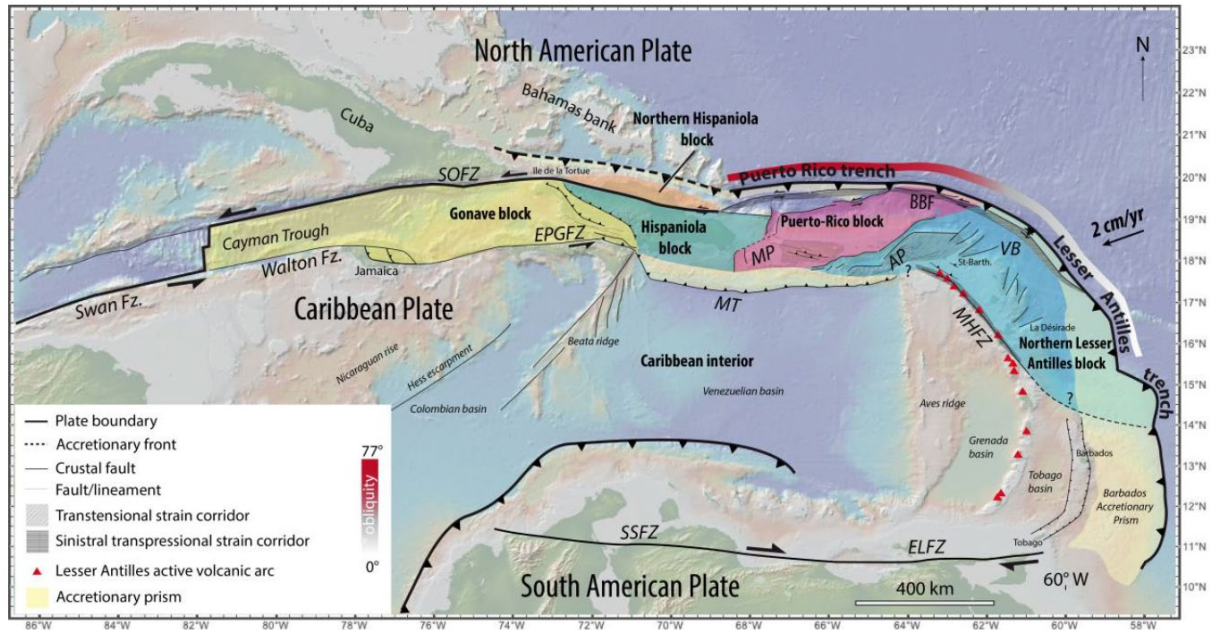


Figure II.4 : Carte structurale de la plaque Caraïbe et des blocs tectoniques de la Frontière Nord Caraïbe. Les blocs sont délimités d'après Symithe et al., (2015) et Bouysse et al., (2020). Flèches noires: vitesse de convergence d'après DeMets et al., (2000). AP : Passage d'Anegada ; BF : Faille de Bunce ; ELPZ : Zone de Faille El Pilar ; EPGFZ : Zone de Faille Enriquillo-Plantain ; MHFZ : Zone de Faille Montserrat-Harvers ; MT : Fosse des Muertos ; MP : Passage de Mona ; SOFZ : Zone de Faille Septentrional-Orientale ; SSFZ : Zone de Faille San Sebastian. D'après Montheil (2023).

Le bloc Gonave (Mann et al., 1995) est limité à l'ouest par la dorsale océanique du fossé Cayman (Figure II.4). Deux systèmes de failles décrochantes senestres délimitent les bordures nord et sud de ce bloc : la zone de faille Septentrionale-Orientale (SOFZ) au nord (Calais and Mercier De Lépinay, 1995; Leroy et al., 2015), et les failles Enriquillo-Plantain Garden et Walton (EPGFZ) au sud (Leroy et al., 2000; 2015). Vers l'est, sa frontière est caractérisée par une zone de plis et de chevauchements, qui marquent la limite ouest du bloc Hispaniola (Pubellier et al., 2000). Le bloc Hispaniola (Benford et al., 2012; Manaker et al., 2008), est lui-même encadré au nord par la SOFZ, isolant ainsi le bloc Nord Hispaniola (Smith et al. 2015) ou Bloc Septentrional (Escuder-Viruete et al., 2023) qui s'étend jusqu'au front de déformation.

À l'Est, le bloc Hispaniola est limité par le rift Mona (van Gestel et al., 1998), qui le sépare du bloc Porto Rico – Iles Vierges (Figure II.4). Ce dernier est limité par la fosse de subduction de Porto Rico au Nord, par le chevauchement de Muertos au Sud et par le couloir transtensif d'Anegada (Jany et al., 1990; Laurencin et al., 2017) à l'Est qui le sépare du bloc Nord des Petites Antilles.

II.5 Contexte sismotectonique de la Frontière Nord de la Plaque Caraïbe

Les données GPS révèlent que la plaque Caraïbe se déplace à une vitesse d'environ 20 mm/an vers l'est par rapport à la plaque nord-américaine, suivant un vecteur de déplacement orienté à environ 70°N (Mann et al., 2002a) (Figure II.5). Les zones de décrochement au sud et au nord des Caraïbes, ainsi que la subduction aux Petites Antilles, permettent d'accommoder la convergence oblique entre la plaque des Caraïbes et la plaque nord-américaine (Demets, 1992) (Figure II.5).

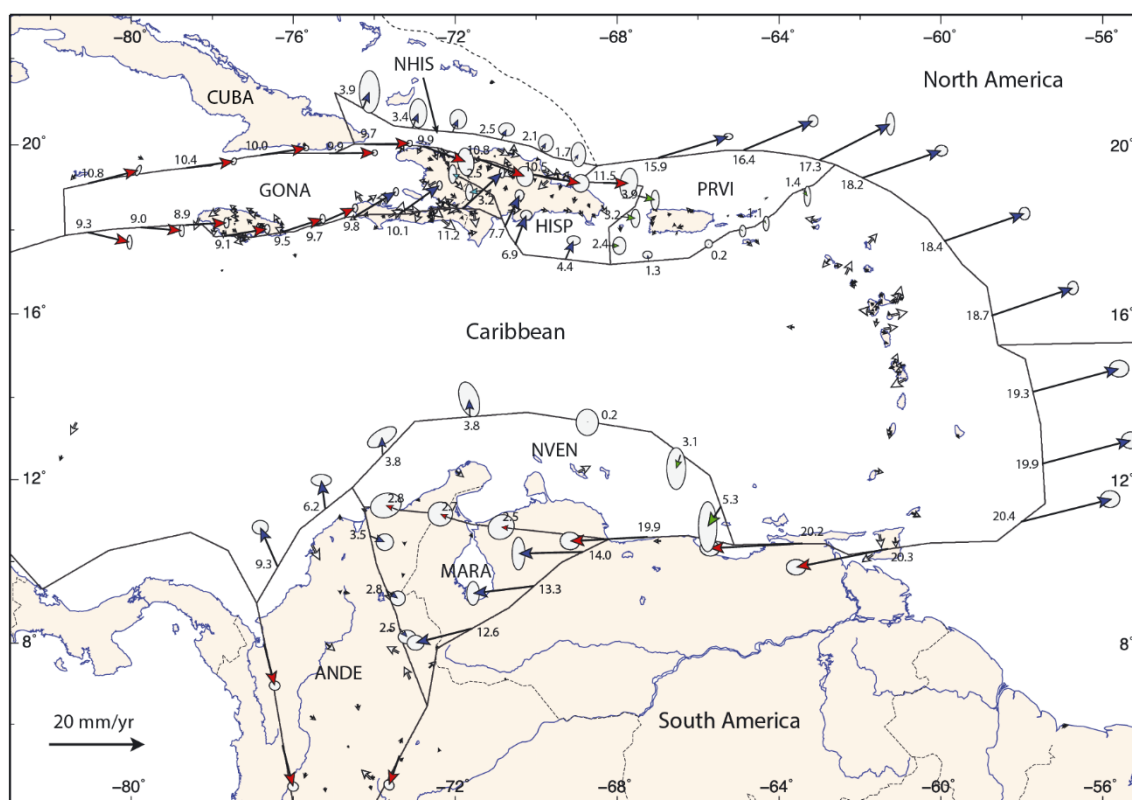


Figure II.5 : Estimations des vitesses le long des frontières de blocs à partir des mesures GPS (adapté de Symithe et al., 2015). Les flèches rouges représentent un mouvement décrochant (environ à 30° des failles), les flèches bleues symbolisent un mouvement inverse ou transpressif, et les flèches vertes indiquent un mouvement normal ou transtensionnel.

Au nord de la Plaque Caraïbe la composante décrochante est principalement accommodée le long de SOFZ, au Nord, et le long des failles de Swan et EPGFZ au Sud (Figure II.5 et II.6a). La SOFZ s'étend depuis l'extrémité nord du fossé des Caïmans, longe la bordure orientale de Cuba au sud, puis se prolonge vers l'est à travers le Passage du Vent, le long de la côte nord d'Haïti et dans la vallée du Cibao au nord de la République dominicaine (Figure II.5) (Calais & Mercier De Lépinay, 1991; Mann et al., 1995). Les estimations des vitesses le long des frontières de blocs à partir des mesures GPS dans les Caraïbes (Symithe et al., 2015), ainsi que des investigations paléo-sismiques dans la vallée du Cibao (Prentice et al., 1993), montrent que la SOFZ présente un taux de glissement de 9 à 11 mm/an.

L'EPGF s'étend depuis l'extrémité sud du fossé Cayman dans le prolongement du système de failles Swan (Corbeau et al., 2016; Mann et al., 1991), et se prolonge au travers de la Jamaïque, puis se poursuit vers l'est en mer par le Passage de la Jamaïque avant d'atteindre la péninsule sud d'Haïti

(Leroy et al., 2015). Ce système de failles, accommode environ 10 mm/an du mouvement vers l'est de la plaque de Caraïbe (E. Calais et al., 2022).

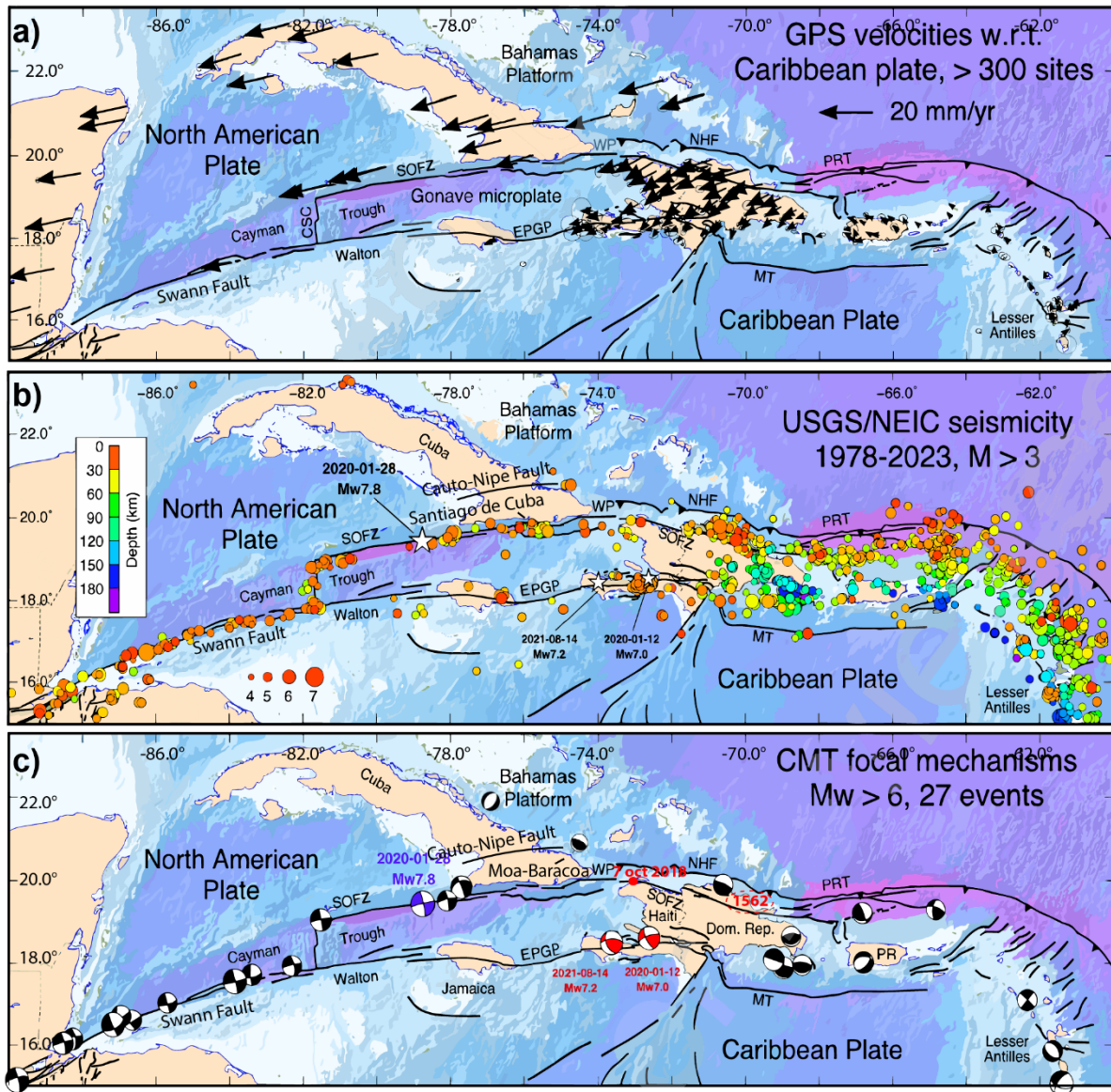


Figure II.6: Sismotectonique et configuration cinématique des plaques à la frontière au nord de la plaque des Caraïbes. A : Vitesses déduites par GNSS par rapport à la plaque des Caraïbes. Remarquez la transition des séismes en décrochement peu profonds et de la cinématique de la frontière de plaque à l'ouest d'environ 74°O, vers une combinaison de décrochement et de raccourcissement de la frontière de plaque à l'est de cette longitude. B : Sismicité de 1978 à 2023 le long de la frontière de la plaque des Caraïbes septentrionales selon le catalogue USGS/NEIC, avec une magnitude $M > 3$. C : Mécanismes au foyer pour les séismes ayant une M_w supérieure à 6, selon le catalogue gCMT (à l'exception des séismes au nord de Cuba et du séisme de 2018 en Haïti). SOFZ : Système de failles décrochante Septentrional-Oriente, WP : Passage du Vent, EPGF : Faille Enriquillo-Plantain Garden, NHF : Faille Nord Hispaniola, PRT : Fosse de Porto Rico, MT : Fosse des Muertos, CSC : Fossé des Caimans, PR : Porto Rico. Modifié d'après Calais et al. (2023).

Ces systèmes de failles décrochantes sont connectés vers l'est par les failles inverses de la Faille Nord d'Hispaniola et le fossé de Muertos. Au niveau d'Hispaniola, la limite entre les plaques est marquée par une collision oblique entre le plateau des Bahamas et Hispaniola (Dolan et al., 1998; Mann et al., 2002a). Les mesures GPS montrent que la faille Nord d'Hispaniola accommode un

raccourcissement d'environ 2-4 mm/an (Manaker et al., 2008; Symithe et al., 2015), évoluant ensuite vers l'est en une composante de glissement fortement oblique d'environ 15-18 mm/an sur la subduction de Porto Rico.

II.5.1 La sismicité sur Frontière Nord de la Plaque Caraïbe

Les failles SOFZ et de Swan concentrent le plus grand nombre des séismes recensés au Nord de la plaque Caraïbe, en particulier les séismes de grande magnitude, délimitant clairement sa frontière nord (Figure II.6b).

Le 28 janvier 2020, un séisme d'une magnitude de 7,8 a été enregistré sur la SOFZ, à une latitude de 79° (Figure II.6c), soulignant ainsi le fort potentiel sismogène de ce système de failles (Tadapansawut et al., 2021). Le long de la bordure orientale de Cuba, la majeure partie de la déformation actuelle semble se concentrer au large de Santiago de Cuba, avec des hypocentres peu profonds, situés le long de la SOFZ (Figure II.7). Dans la région au sud de Santiago de Cuba, la SOFZ présentent une sismicité plus élevée, tandis que au large de Guantanamo les segments de la faille présentent une faible sismicité (Figure II.6b)(Cotilla-Rodríguez, 2021).

Vers l'est de la frontière, l'activité sismique sur la SOFZ est plus importante sur île d'Hispaniola (Figure II.6b), avec des séismes de magnitude supérieure à 7. La SOFZ et la faille Nord Hispaniola sont les sources sismiques potentielles dans cette région nord. Bien que la sismicité attribuée à la SOFZ peut être confondue avec celle de la faille Nord-Hispaniola, la sismicité instrumentale montre une activité plus soutenue pour les segments plus à Est de ce système de failles. Parmi les séismes majeurs, on peut mentionner celui du 2 décembre 1562, avec une magnitude estimée à 7,7 selon ten Brink et al. (2011). L'épicentre de ce séisme aurait été localisé au nord de la République dominicaine (Figure II.6c). Cependant, son lien avec SOFZ suscite des débats, notamment à la lumière des études paléoséismologiques qui indiquent qu'aucune rupture de surface n'a été observée dans la partie terrestre de cette faille, située en République dominicaine, au cours des 800 dernières années (Prentice et al., 1993).

En plus des données paléoséismologiques de la région, deux séismes survenus le 7 octobre 2018, de magnitudes respectives 5,9 et 5,4, avec un épicentre situé dans la partie sous-marine de la SOFZ au nord d'Haïti, nous rappellent le potentiel sismogénique élevé de cette faille.

Contrairement à la côte nord d'Hispaniola, l'intérieur du bloc de Cuba oriental et sa côte nord ne présentent pas une sismicité importante. Des structures potentiellement actives ont été repérées à l'intérieur de Cuba Oriental (Alvarez et al., 1985), parmi lesquelles se distinguent la Faille de Cauto-Nipe (Figure II.7) (Calais et al., 2023; Cotilla-Rodríguez, 2021; Garcia Pelaez et al., 2003). Cependant, la compilation récente de données géophysiques réalisée par Arango-Arias and Escobar-Pérez (2021), a conduit ces chercheurs à conclure que la faille Cauto-Nipe ne montre pas de signes récents de déplacement en surface, suggérant ainsi qu'elle n'est pas active et ne représente donc pas une menace sismogène pour Cuba.

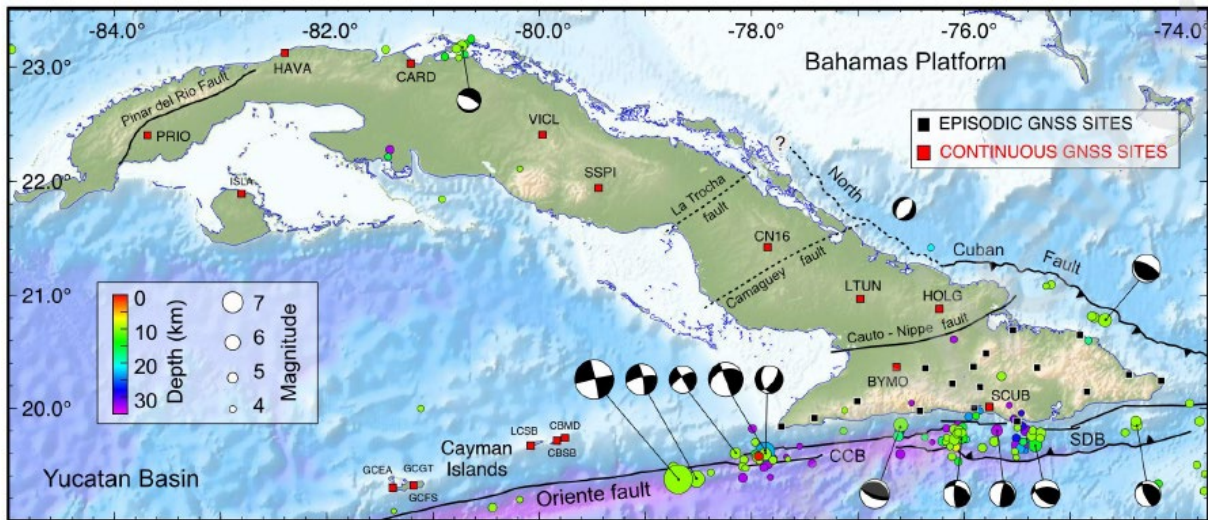


Figure II.7: Carte sismotectonique de Cuba et de ses environs montrant les principales failles actives et potentiellement actives (discutées dans le texte), l'emplacement des stations GNSS (permanentes et temporaires) utilisées dans cette étude, la sismicité $M > 3$ de 1978 à 2023 issue du catalogue USGS/NEIC, ainsi que les mécanismes au foyer des séismes $M > 5$ provenant de la base de données CMT. Une exception dans ce contexte décrochant et compressif, est le séisme de magnitude $M_w 4,7$ du 17 décembre 2022, présentant un mécanisme de faille normale sur un plan de faille orienté NE-SW au large de la faille du Nord de Cuba, à la base du plateau des Bahamas. CCB : bassin de Cabo Cruz, SDB : ceinture déformée de Santiago. D'après Calais et al. (2023).

Le long de la marge nord-est de Cuba, la "faille du Nord de Cuba" (Calais et al., 2023) constitue le prolongement occidental du système de failles actif de Puerto Rico et de la faille Nord Hispaniola (Figures II.6 PRT et NHF respectivement ; II.7). Il semble que la faille du Nord de Cuba soit active en tant que faille inverse jusqu'à une longitude d'environ 75° Ouest, comme le démontrent les données de réflexion sismique en mer (Rodríguez-Zurrunero et al., 2020), et cela est corroboré par un séisme en mer au large du Massif Ophiolitique de Moa-Baracoa (Figure II.7). Cependant, au-delà de cette longitude, il demeure une énigme de savoir si cette faille inverse est toujours active. Braunmiller et al. (2017) ont décrit un séisme d'une magnitude de $M_w 5,1$ avec un mécanisme de faille normale le long de la suture Bahamas-Cuba au nord de Cuba (Figure II.7). Un autre événement de faille normale, de magnitude $M_w 4,7$, s'est produit plus au sud de la faille du Nord de Cuba, avec un plan de faille orienté NE-SW (Calais et al., 2023). En tenant compte de son emplacement et de son mécanisme de source (Figure II.7), il est probablement associé à l'effondrement gravitationnel ou à la flexion extensionnelle du plateau des Bahamas, plutôt qu'à une activité de la faille du Nord de Cuba (Calais et al., 2023).

II.6 La province Carbonatée des Bahamas (Le Great Bahama Bank)

L'archipel des Bahamas, et en particulier le *Great Bahama Bank*, représente une vaste province carbonatée contemporaine située au sud-est du continent nord-américain (Figure II.8) (Anselmetti et al., 2000; Meyerhoff & Hatten, 1968). La Province Carbonatée des Bahamas s'étend sur une superficie d'environ 170 000 km² (Meyerhoff & Hatten, 1974).

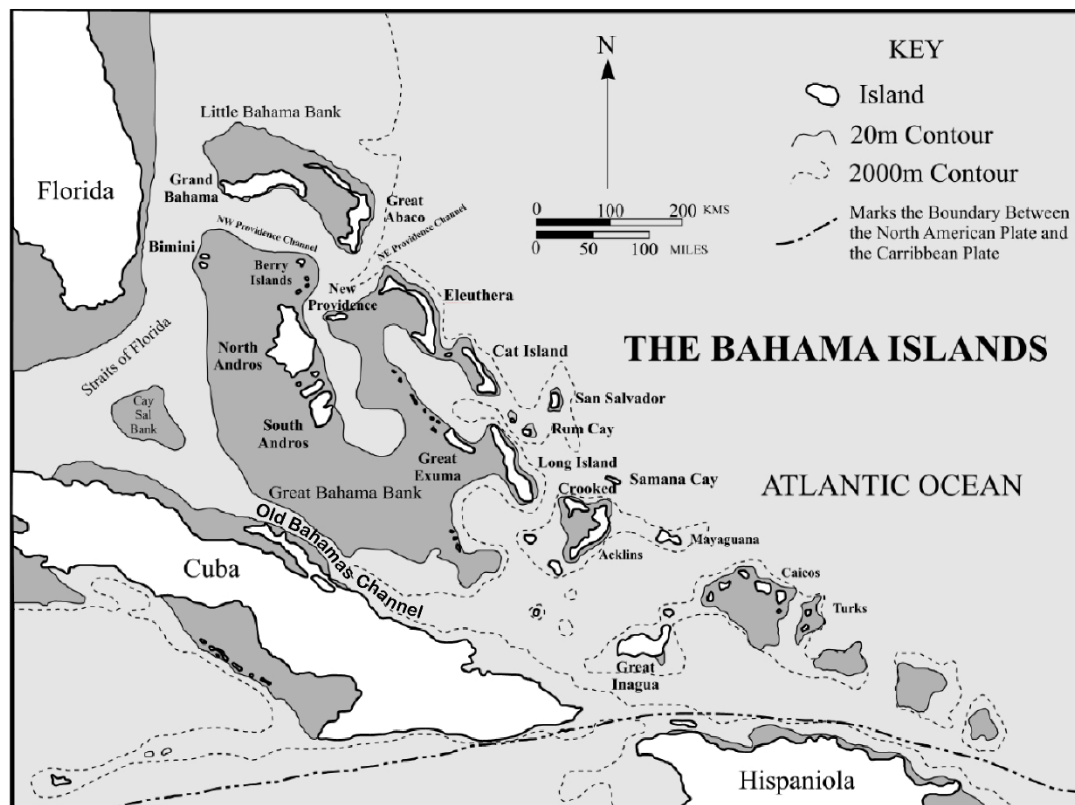


Figure II.8. Carte de l'archipel des Bahamas, indiquant l'emplacement du Grand Banc des Bahamas (nord-ouest) et le Petit Banc des Bahamas (Sud-est), ainsi que l'ensemble des bancs formant cet archipel. Modifié de Walker et al. (2008).

Les origines de l'archipel des Bahamas demeurent un sujet de débat en raison du manque de données géologiques et géophysiques. Trois origines tectoniques ont été envisagées pour expliquer la nature de la croûte cristalline sous-jacente aux bancs carbonatés de la Province Carbonatée des Bahamas. Ces trois modèles proposent des origines distinctes pour la croûte sous-jacente, à savoir une croûte continentale amincie, une croûte océanique, ou une croûte océanique épaissie par l'activité volcanique associée à la grande province ignée située sous les Bahamas.

II.6.1 Hypothèse de la croûte continentale amincie sous-jacente à la Province Carbonatée des Bahamas

Cette hypothèse a été avancée pour la première fois par Field et al. (1931) en se basant sur les premières mesures gravimétriques. Les auteurs suggèrent que la Province Carbonatée des Bahamas n'est pas supporté par des roches ignées et qu'il n'a probablement pas été formé en raison d'une activité volcanique. Selon leur point de vue, la croûte sous-jacente aux Bahamas possède des caractéristiques continentales, et les anomalies gravimétriques observées à plusieurs stations sont vraisemblablement attribuables à la présence de matériaux anormalement légers à proximité de ces stations.

Ball (1967) a également proposé la présence d'une croûte continentale amincie sous les Bahamas en utilisant les résultats des données de sismique réflexion des zones offshore et des corrélations stratigraphiques avec les roches continentales du Paléogène qui affleurent à Cuba. Dans les années 1960 et 1970, une cartographie améliorée de la géologie de Cuba et des acquisitions de profils de sismique réflexion et de réfraction dans le Old Bahamas Channel (Figure II.8), qui sépare Cuba de la plateforme carbonatée des Bahamas, ont montré que la partie au sud de la plateforme carbonatée des Bahamas a été accrétée le long de la côte Nord de Cuba lors de la collision Paléogène.

La plupart de ces chercheurs ont adopté l'origine continentale des Bahamas pour expliquer son rôle tectonique en tant que "butoir résistant" pour la collision paléogène du segment cubain du Grand Arc des Caraïbes (Mattson, 1972). Cette hypothèse est également renforcée par la présence d'affleurements localisés de roches cristallines Paléozoïque et Précambrienne plissées et chevauchées, preuve d'un socle continental du même âge s'étendant vers le nord-est sous le plateau carbonaté des Bahamas (Furrazola-Bermúdez, 1964; Khudoley, 1967; Meyerhoff & Hatten, 1968, 1974).

Mullins & Lynts (1977) ont entrepris d'élucider la controverse concernant la nature crustale des Bahamas en utilisant des données de sismique réflexion, de sismique réfraction, de gravimétrie et de magnétisme. Les données de gravimétrie et de magnétisme ont permis de proposer que les Bahamas sont constitués de croûte continentale qui a été largement intrudée et sous-plaquée par des roches ultramafiques allant du Trias inférieur au Jurassique inférieur, en relation avec un processus de rifting. Cette intrusion a entraîné une augmentation de la densité de la croûte continentale, générant ainsi des anomalies gravimétriques et magnétiques distinctes par rapport à celles observées dans une croûte continentale normale.

Selon cette hypothèse d'une croûte continentale amincie, deux hypothèses sont proposées pour expliquer la morphologie actuelle du *Great Bahama Bank* :

(1) La première hypothèse, appelée "hypothèse du Graben" (Mullins & Lynts, 1977), suggère que la physiographie moderne des Bahamas découle de la configuration des marges continentales riftées (Horst et grabens) formées lors de la séparation de l'Amérique du Nord et de l'Afrique, il y a environ 200 Ma. Selon cette hypothèse, le dépôt des bancs carbonatés en eau peu profonde était limité aux horsts/paléo-rides, tandis que les grabens étaient remplis de sédiments d'eau plus profonde.

(2) La deuxième hypothèse, connue sous le nom d'Hypothèse du Mégabanc (Bryant et al., 1969; Meyerhoff & Hatten, 1968; Schlager & Ginsburg, 1981), suggère qu'au cours du Jurassique supérieur jusqu'au Crétacé moyen, une vaste plateforme carbonatée d'eau peu profonde s'est développée depuis la plateforme ouest-floridienne jusqu'aux Bahamas. Eberli and Ginsburg (1987) ont suggéré que les plateformes bahamiennes n'ont pas seulement connu des événements de submersion ou de rifting, mais que les activités tectoniques relatives à sa collision avec la Plaque Caraïbe, ainsi que la coalescence des plateformes jouent également un rôle crucial dans la configuration actuelle des plateformes.

II.6.2 Hypothèse d'une croûte océanique sous-jacente à la Province Carbonatée des Bahamas

En utilisant des données dispersées de sismique réflexion et réfraction, Uchupi et al.(1971) ont proposé que le nord-ouest des Bahamas était une croûte continentale, comme l'avaient déjà postulé Dietz et al. (1970), mais que la croûte plus mince du sud-est des Bahamas aurait une autre origine. Selon Uchupi et al. (1971), l'existence d'une croûte mince (~20 km) suggère la présence d'une croûte océanique dans le sud-est des Bahamas qui a commencé à se développer le long d'une zone de fracture transtensive lorsque la propagation du plancher océanique a commencé à séparer l'Amérique du Nord et l'Afrique.

Klitgord et al. (1984) ont avancé l'hypothèse que la croûte sous-jacente à la Floride et à la région des Bahamas est exclusivement composée de croûte océanique, entrecoupée de zones de fractures océaniques linéaires. Ces caractéristiques linéaires pouvaient être suivies sur les cartes gravimétriques et magnétiques régionales, s'étendant de manière ininterrompue depuis la croûte

océanique indéniable de l'océan Atlantique occidental, traversant ensuite la région des Bahamas et de la Floride, pour finalement se prolonger dans le golfe du Mexique.

II.6.3 Hypothèse d'une grande province ignée sous la Province Carbonatée des Bahamas

Newell (1955) suggère que l'ensemble de la Province Carbonatée des Bahamas s'est construite sur une croûte océanique caractérisée par de grands volcans ou monts sous-marins, et que le plateau carbonaté actuel s'est développé sous la forme d'atolls carbonatés individuels entourant les volcans, s'élevant et s'étendant progressivement, puis fusionnant à mesure que les volcans devenaient inactifs et s'enfonçaient.

Par la suite, Drake et al. (1963) ont contesté l'idée que les Bahamas soient édifiées sur une croûte océanique comportant des volcans sous-marins, en se basant sur des données magnétiques, à l'exception de la région située au sud-est des Bahamas, comprenant les îles Turks et Caïcos (voir Figure II.8), où une structure volcanique a été déduites par l'existence d'anomalies magnétiques fortes et localisées. Dans d'autres régions des Bahamas, ces chercheurs ont conclu à la présence d'un socle continental en se basant sur un champ magnétique relativement uniforme sur de vastes zones et sur l'absence totale d'anomalies qui sont généralement associées à la présence de matériaux volcaniques.

Des modèles récents tels que le modèles de Pindell & Kennan (2009), reprennent l'hypothèse d'un volcanisme associé à la présence du « Hotspot des Bahamas » qui aurait épaissi la croute de la région sud-est des Bahamas

Pour expliquer l'origine d'un socle océanique épaissi sous les Bahamas, Dietz (1973) a avancé l'idée que les Bahamas se soient formées au-dessus d'un point chaud lors de son déplacement, potentiellement associé à ce que l'on connaît maintenant sous le nom de panache magmatique de la Province de l'Atlantique central (CAMP) (Schlische et al., 2002). Selon le modèle de Dietz (1973), les monts sous-marins correspondent à des sommets de volcans moins profonds que le plancher océanique environnant. Par la suite, des récifs coralliens s'y sont développés et ont progressivement agradée en suivant le rythme de subsidence des monts sous-marins et de la croûte océanique environnante due au refroidissement thermique.

II.7 Évolution du Domaine Nord Caraïbe

II.7.1 Crétacé : Mise en place de la Plaque Caraïbe

Durant le Crétacé moyen, des modifications significatives des mouvements relatifs des plaques tectoniques se sont produites, et ce, non seulement dans la région des Caraïbes, mais également à une échelle globale (Burke et al., 1984; Frisch et al., 1992; Meschede, 1998; Ross & Scotese, 1988). Un changement dans la polarité de vergence de la zone de subduction, passant d'un plongement nord-est à un plongement sud-ouest, a induit une migration du Grand Arc des Caraïbes (GAC) vers le nord-est (Ross & Scotese, 1988). La plaque dite Caraïbe a migré vers le nord-est avec le GAC. Le mouvement de cet arc, transitant depuis la zone du Pacifique oriental vers sa position actuelle dans la région des Caraïbes, a permis la subduction vers le sud-est de la croûte océanique préexistante formant la "Proto-Mer des Caraïbes" ou Proto-Caraïbe (Figure II.9) (Mann et al., 1995; Pindell et al., 2006b; Pindell & Kennan, 2001; Ross & Scotese, 1988).

À la fin du Crétacé, la collision entre la portion occidentale cubaine du GAC et la péninsule du Yucatan a conduit à la formation d'une faille transformante senestre (voir Figures II.9, II.10 et II.12A) (Pindell et al., 2005, 2006b).

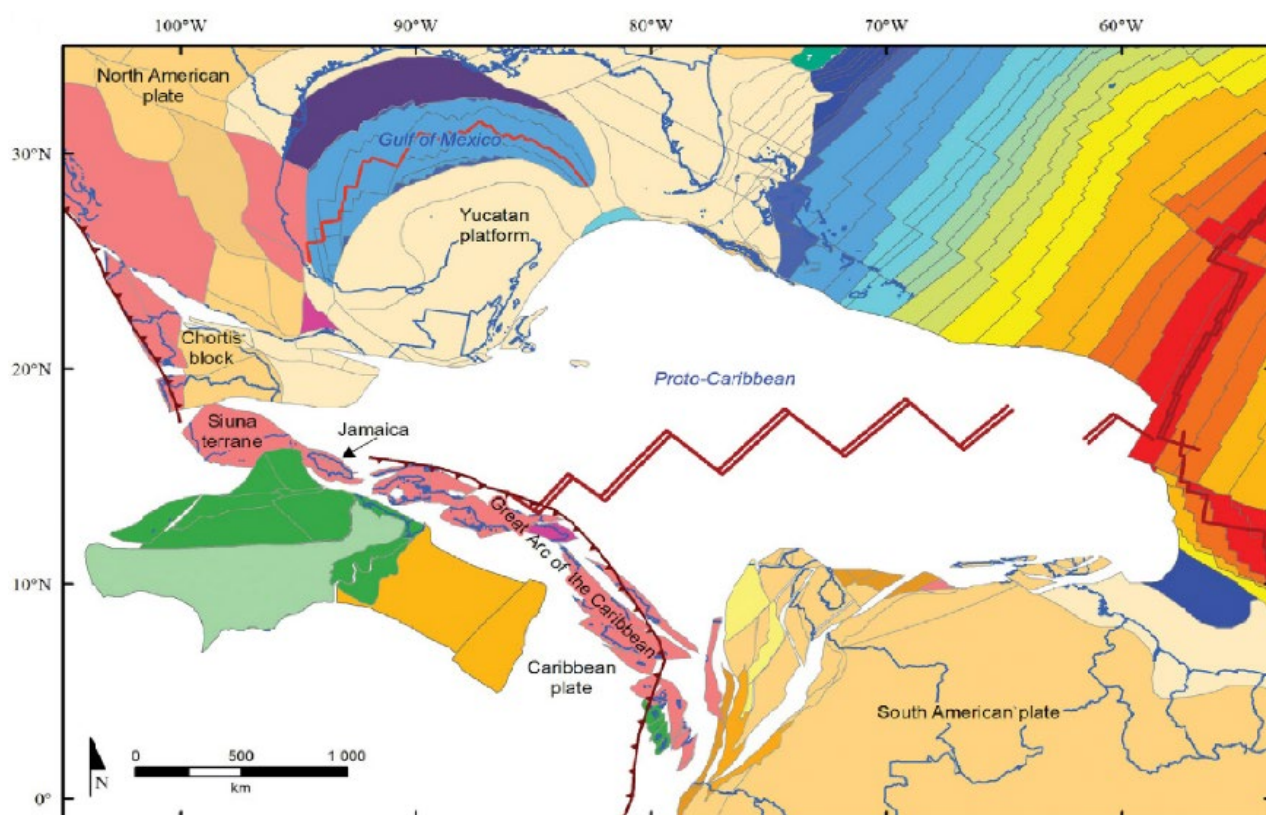


Figure II.9. Reconstruction du Golfe du Mexique et des Caraïbes à la fin du Crétacé (83 Ma), montrant l'entrée du Grand Arc dans la zone de la Proto-Mer des Caraïbes, avec une convergence initiale entre le Grand Arc et le bloc continental de Chortis. D'après Mann (2021).

II.7.2 Cénozoïque : Collision Ouest-Est de la Plaque Caraïbe avec la Plateforme des Bahamas

La progression nord-est du segment cubain du GAC, engage sa collision avec la plateforme des Bahamas au cours du Paléogène (Figure II.12B). Cette collision entre les plaques Caraïbes et Nord-Américaine entraîne la formation d'une ceinture orogénique dans la région Cuba-Bahamas, la région des Bahamas s'est alors transformée en bassin d'avant-pays (Cruz-Orosa et al., 2012; Masaferrro & Eberli, 1999).

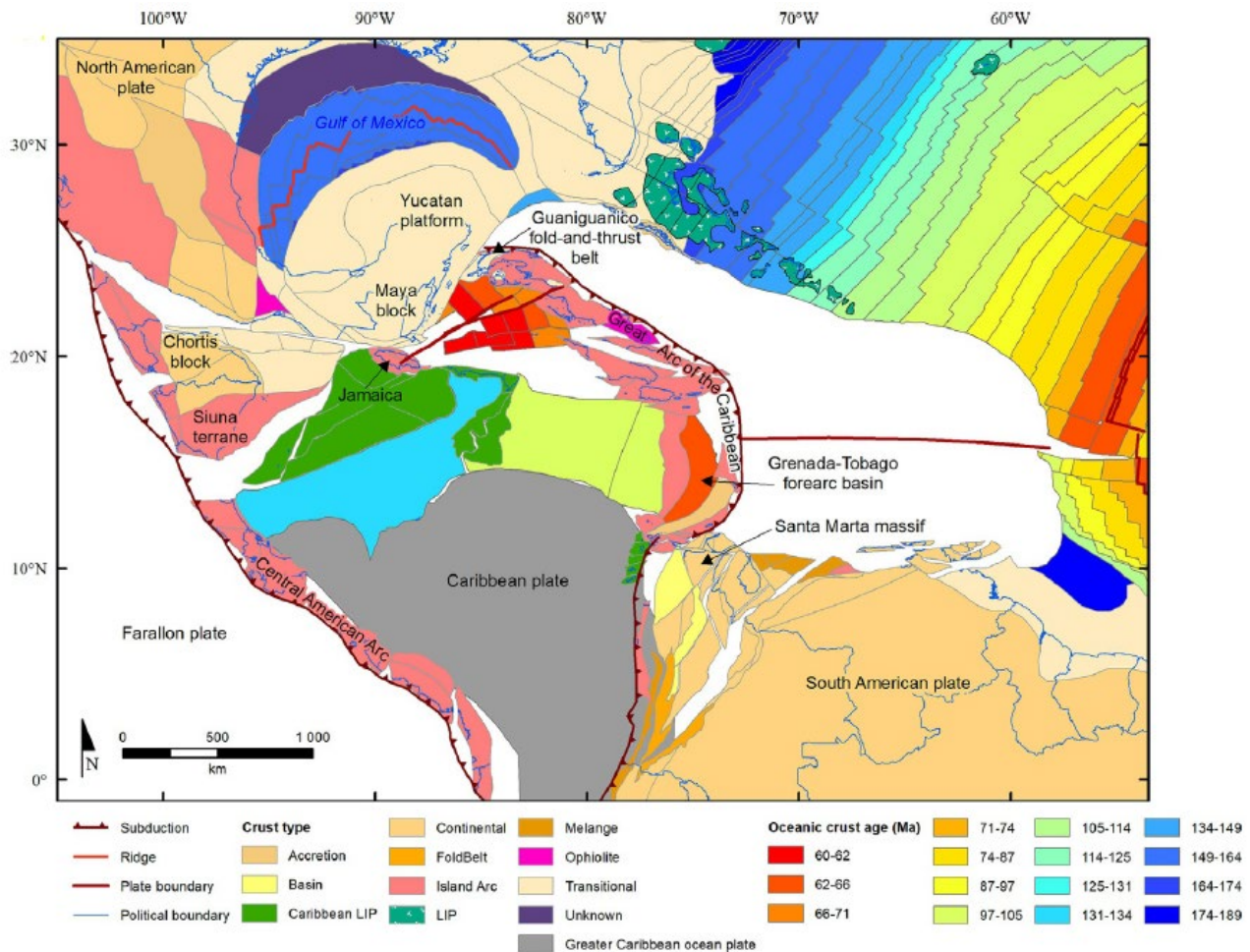


Figure II.10. Reconstruction des plaques à la fin du Crétacé supérieur (67 Ma), caractérisée par la formation du bassin arrière-arc du Yucatan au sud-ouest et le segment cubain du Grand Arc des Caraïbes. D'après Mann (2021).

La collision progressive entre l'arc cubain et la plate-forme des Bahamas a conduit à la fragmentation de la bordure nord de la plaque Caraïbe le long d'une série de failles décrochantes senestres en lien avec un processus de tectonique d'échappement (Figure II.11) (Mann et al., 1995). Ceci inclut la faille de Pinar-Varadero (Paléocène), La Trocha (Éocène inférieur), ainsi que Cauto-Nipe (Éocène moyen/tardif) et la Faille Oriente (Éocène inférieur de l'Oligocène) du Nord au Sud de Cuba. La localisation d'une zone de faille décrochante senestre au sud de Cuba est suivie de l'ouverture du système du fossé Cayman (Figure II.11) pendant l'Eocène (Figure II.12C-D)(Leroy et al., 2000; Mann, 1997). L'apparition de la croûte océanique au pied de la marge est datée à environ 49 Ma

(Anomalie magnétique 22, Yprésien, Éocène inférieur)(Figures II.11 et II.12C-D) (Leroy et al., 2000; Hayman et al., 2011).

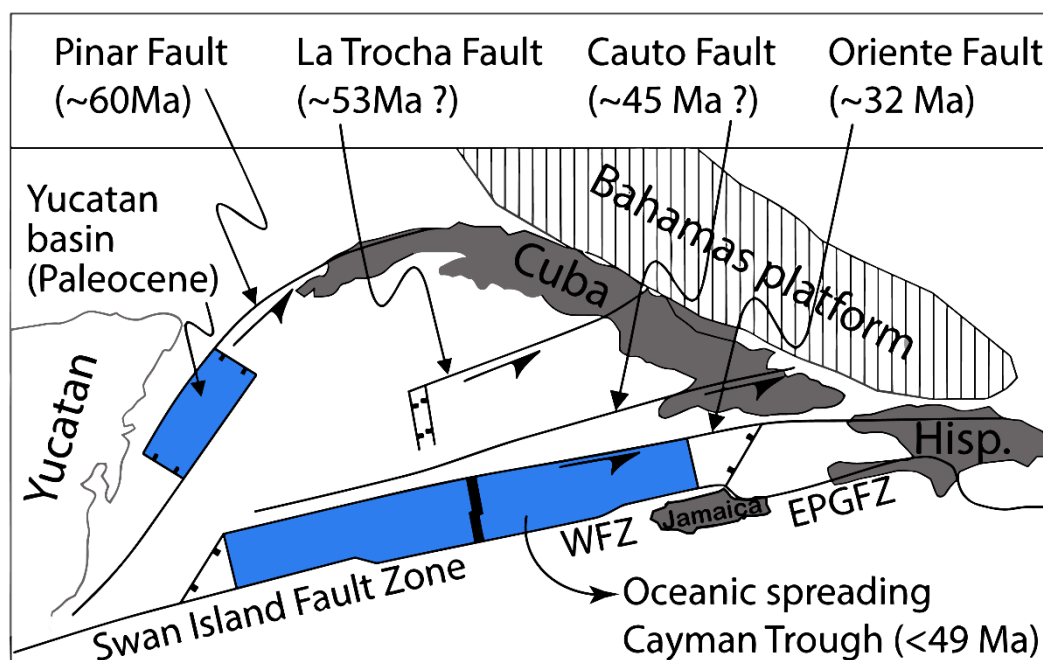


Figure II.11 : Reconstruction schématique du Nord-Ouest de la plaque Caraïbe et calendrier d'activation des failles de Cuba et du bassin de Cayman. WFZ : Walton Fault Zone, EPGFZ : Enriquillo Plantain Garden Fault Zone. D'après Wessels, 2019a, modifié d'après Leroy et al., 2000.

La formation du fossé Cayman, orientée globalement est-ouest, témoigne du changement de direction du mouvement de la plaque Caraïbe, passant d'une direction NNE (Maastrichtien) à une direction E (Éocène moyen) (Pindell et al., 2005). Cette tendance est en cohérence avec sa direction actuelle de mouvement, telle qu'observée par des études GPS (Calais et al., 2016; DeMets et al., 2000; Mann, 2007; Smithe et al., 2015) (Figures II.12 F-G).

Le fossé Cayman permet de retracer environ 1100 km de déplacement senestre de la plaque caribéenne. La majorité des études reconnaissent l'existence de ce déplacement de grande ampleur (voir Figure I-8).

L'évolution Cénozoïque de la Plaque Caraïbe est donc caractérisée par l'activité de failles décrochantes senestres qui ont progressivement segmenté l'Arc de Cuba en diverses microplaques. Ces fragments, initialement attachés à la plaque Caraïbe, ont été progressivement transférés vers la plaque Amérique du Nord (Leroy et al., 2000; Pindell et al., 2006b). Cette dynamique de fragmentation et de

transition de microplaques perdue, comme en témoigne la formation plus récente de la microplaque Gonâve au sein des Grandes Antilles (Mann et al., 1995; Symithe et al., 2015) (Figures II.4 et II.12).

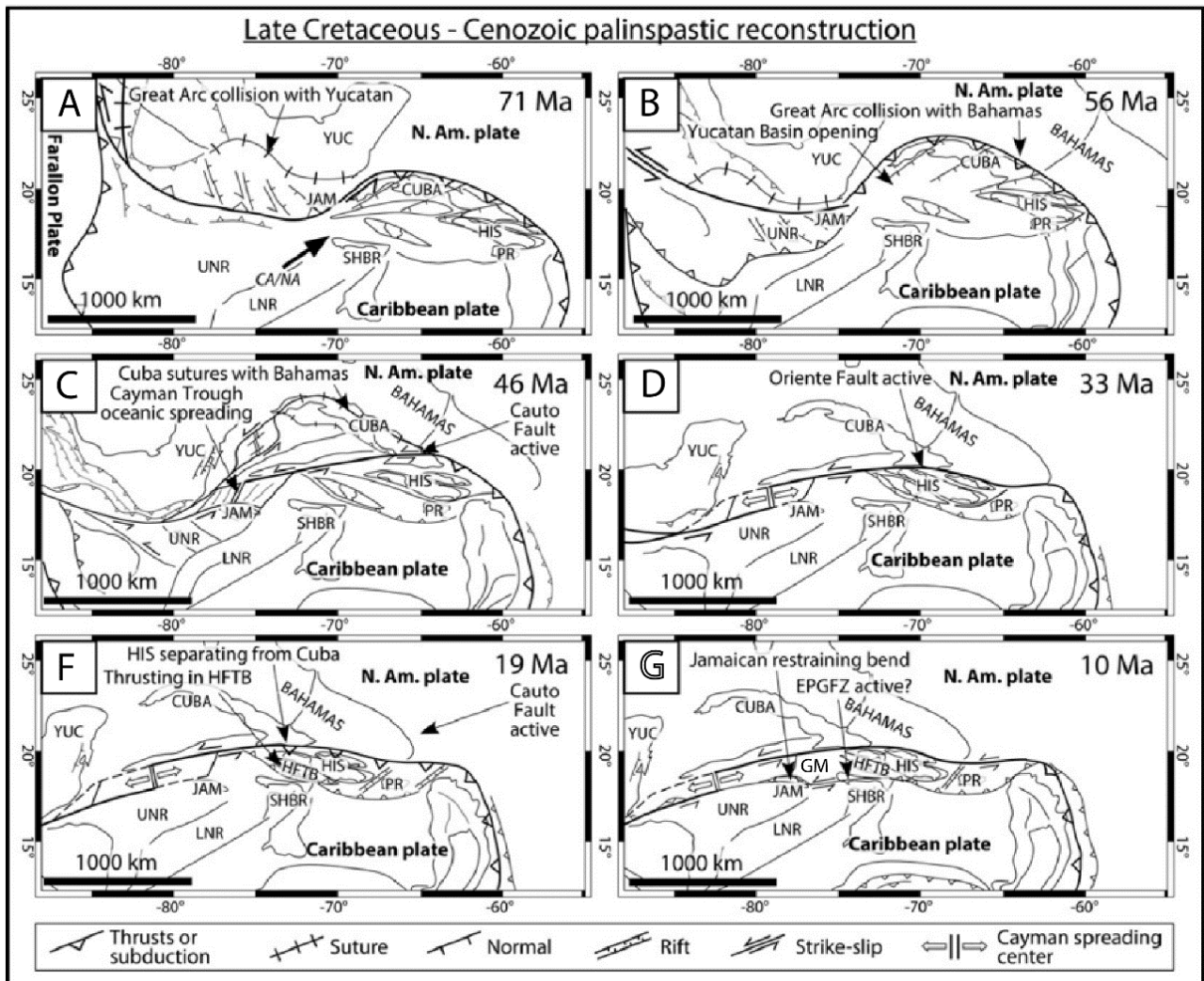


Figure II.12. (A) Collision du Grand Arc des Caraïbes avec la péninsule du Yucatan. (B) Chronologie de l'activation des failles entre le Yucatan et le fossé Cayman. (C–G) Reconstruction de la frontière nord des Caraïbes entre 71 à 10 Ma. CA, Caraïbes ; HFTB, ceinture de plis et chevauchements haïtienne ; HIS, Hispaniola ; JAM, Jamaïque ; LNR, Ride inférieure du Nicaragua ; NA, Nord-américain ; PR, Porto Rico ; SHBR, Bassin Sud Haïti—ride de Beata ; UNR, Ride supérieure du Nicaragua ; YUC, Péninsule du Yucatan ; GM, Microplaque Gonâve. D'après Wessels (2019)

II.8 Phases de Déformation à Cuba et Hispaniola

II.8.1 Les phases de déformation à Cuba : un enregistrement géologique de l'évolution du domaine Caraïbe

L'évolution du domaine Caraïbes, depuis les premières étapes jusqu'à sa configuration actuelle, est bien documentée dans la géologie de Cuba. Les formations géologiques qui affleurent aujourd'hui sur l'île, témoignent des phases tectoniques qui ont eu lieu depuis la fragmentation de la Pangée et la formation de la Proto-Caraïbe, jusqu'à la migration vers le nord-est de la plaque caraïbe entre les plaques nord et sud-américaines.

Plusieurs études ont décrit la géologie de Cuba (par exemple, Khudoley, 1967; Rosencrantz et al., 1988; Iturralde-Vinent, 1998; Moretti et al., 2003; Gaumet et al., 2004; Iturralde-Vinent et al., 2008, 2016; Pardo, 2009). L'île de Cuba constitue un archipel orogénique du Crétacé tardif à l'Éocène, caractérisé par des sédiments de marges métamorphisés, des ophiolites obductées, des carbonates de plateformes imbriqués, des mélanges et des roches volcaniques d'arc (Masafarro, 1997).

Deux principales unités structurales sont définies à Cuba : la ceinture plissée et le « néo-autochtone » (Iturralde-Vinent, 1994). Les unités de la ceinture plissée sont principalement subdivisées en unités continentales (plateformes des Bahamas et du Yucatan) et océaniques (arcs volcaniques et ophiolites). La plateforme des Bahamas et les terrains du sud-ouest forment l'unité continentale. En revanche, l'unité océanique est composée d'arcs volcaniques du Crétacé, d'une ceinture ophiolitique nord et d'un arc insulaire du Paléocène. L'élément le plus ancien de la ceinture ophiolitique nord est considéré comme étant du Jurassique tardif (Saura et al., 2008). Les unités de la ceinture plissée sont recouvertes par l'unité néo-autochtone, qui est composée de roches sédimentaires datant de l'Éocène tardif à l'actuel.

La région située le long de la côte nord-ouest de Cuba suit le front de déformation. Celui-ci sépare les unités accrétées à la marge continentale, du bassin flexural *offshore* au nord. Ce dernier s'est formé lors de la collision entre la partie nord-ouest du Grand Arc des Caraïbes et les bancs des Bahamas. Cette phase de collision a débuté au Crétacé Supérieur et s'est terminée à l'Éocène moyen (Echevarria-Rodriguez et al., 1991; Malfait & Dinkelman, 1972; Pindell & Barrett, 1991). Ainsi, l'histoire géologique de Cuba a enregistré trois principales phases tectoniques :

- Une phase pré-orogénique avec l'évolution sédimentaire de la marge passive nord de la proto-Caraïbes du Jurassique au Santonien.
- Une phase orogénique due au déplacement vers le nord-est du Grand Arc des Caraïbes, de la subduction de la croûte proto-Caraïbe, puis de la collision avec la marge sud de la plaque Nord-Américaine.
- Une phase post-orogénique (de l'Éocène tardif à l'actuel), marquée par la fin de la collision à la suite de la migration vers l'est de la frontière nord de plaque Caraïbe.

II.8.2 Les phases de déformation à Hispaniola : un enregistrement géologique de l'évolution de la Frontière Nord Caraïbe

Des études sur le terrain à Cuba et à Hispaniola (Calais & Mercier De Lépinay, 1992; de Zoeten & Mann, 1999; Erikson et al., 1998; Escuder-Viruete et al., 2015; Escuder-Viruete & Pérez, 2020; M. Iturralde-Vinent & Macphée, 1999; Rojas-Agramonte et al., 2008; Zoeten, 1991) montrent que l'évolution tectonique de l'actuelle frontière nord de la plaque Caraïbe est marquée par des épisodes majeurs survenus notamment à l'Éocène, Miocène Moyen et Pliocène supérieur, en lien avec un processus de tectonique d'échappement associée à la collision avec les bancs des Bahamas (Figures II.9 à II.12).

Les séries sédimentaires de Hispaniola et Cuba enregistrent une histoire commune jusqu'au Miocène Inf. d'après Calais et Mercier De Lépinay (1992), ces deux blocs forment une seule et même entité structurale jusqu'à ce que le régime décrochant de OFZ (Oriente Fault zone, Figure II.12D) se mettent en place pendant le l'Oligocène (~ 32 Ma) et commence à séparer ces 2 blocs.

L'Éocène est décrit par plusieurs auteurs comme une période d'intense déformation compressive au nord de la plaque Caraïbe (Calais & Mercier De Lépinay, 1992; Leroy et al., 2000; Mann et al., 2002b; Pubellier et al., 2000). L'arc insulaire constituant la partie centrale de Cuba se retrouve bloqué

dans sa propagation vers l'est par la collision avec la plateforme des Bahamas (M. Iturralde-Vinent & Macphee, 1999). La faille Trocha est alors abandonnée au profit d'une nouvelle faille décrochante située plus au Sud (Figure II.11), qui permet l'échappement de la plaque Caraïbe vers l'est et la formation du fossé Cayman (Leroy et al. 2000 ; Oliveira de Sa et al 2021 ; Figure 3a de l'article 1, section III). Il s'agit de la faille décrochante sénestre de Cauto qui se met en place dans un contexte de raccourcissement SO-NE à partir de l'Yprésien (49 Ma) (Figure 3b de l'article 1, section III) (Cruz-Orosa et al., 2012). Cette faille est contemporaine de l'océanisation du fossé Cayman (Figure II.11, Hayman et al., 2011; Leroy et al., 2000). La frontière nord de la plaque Caraïbe migre alors vers la faille de Cauto et le bloc cubain est en partie transféré vers la plaque Nord Amérique (Boschman et al., 2014; Leroy et al., 2000). Au SE de Cuba, la chaîne montagneuse de La Sierra Maestra est formée par des roches pré-néogènes déformées par des plis ayant une orientation presque E-W et des chevauchements à vergence vers le nord (Calais & Mercier De Lépinay, 1991; Rojas-Agramonte et al., 2005).

Au nord d'Hispaniola, les roches d'âge Paléocène-Eocène Moyen de la Formation de los Hidalgos sont recoupées par de nombreux dykes et sills de la formation de Palma Picada, de même âge (Figures II.13 et II.14)(de Zoeten & Mann, 1999; Zoeten, 1991). Ces deux formations apparaissent fortement plissées sur les affleurements à Hispaniola (Zoeten and Mann, 1991). Concrètement, les séquences turbiditiques d'âge Éocène Supérieur-Oligocène de la formation d'Altamira recouvrent les Formations de los Hidalgos, de nature pélagique, et de Palma Picada d'origine volcanique, avec une discordance angulaire basale, mettant en évidence un épisode compressif majeur d'âge Éocène Moyen (Figure II.14). Cet épisode compressif marque la fin de l'activité volcanique au nord d'Hispaniola (la formation de Palma Picada), ainsi que le soulèvement du bassin avant-arc dans lequel les carbonates pélagiques de la formation de los Hidalgos s'étaient déposés.

Dans la région de Puerto de la Plata (République Dominicaine) (Figure II.13a), la mise en place de séquences inverses (grano-croissantes) constituées de fragments de roches ophiolitiques dans la Formation d'Imbert, contemporaine de la Formation de los Hidalgos (Upper Paleocene to Lower/Middle Eocene; Escuder-Viruete et al., 2015), laisse supposer un changement de morphologie du bassin avant-arc. Ce changement pourrait être induit par son soulèvement lors de la collision, et par la mise en place d'un complexe ophiolitique (de Zoeten & Mann, 1999; Escuder-Viruete et al., 2015). D'après Escudier-Viruete et al (2015), l'évolution des dépôts de la formation d'Imbert souligne deux périodes importantes dans l'évolution du prisme d'accrétion au nord d'Hispaniola : une période caractérisée par le dépôt de turbidites distales et mudstones hémipélagiques, radiolarites et par un volcanisme lié à l'arc contemporain, suivie d'une autre période enregistrant des séquences turbiditiques plus proximales avec des brèches et conglomérats dérivés des ophiolites. Ces changements prouvent ainsi la mise en place d'un paléoenvironnement marin progressivement moins profond. La formation d'Imbert enregistrerait donc l'évolution d'une sédimentation de bassin avant-arc vers une sédimentation de bassin en piggy-back durant le Paléocène supérieur à l'Éocène moyen, en conséquence de la collision avec la plateforme des Bahamas, située au Nord. Cette période de tectonique intense est suivie d'une phase de subsidence enregistrée par le dépôt des séries turbiditiques

de la formation d'El Mamey Group (Figures II.13 et II.14) (De Zoeten & Mann, 1991; de Zoeten & Mann, 1999).

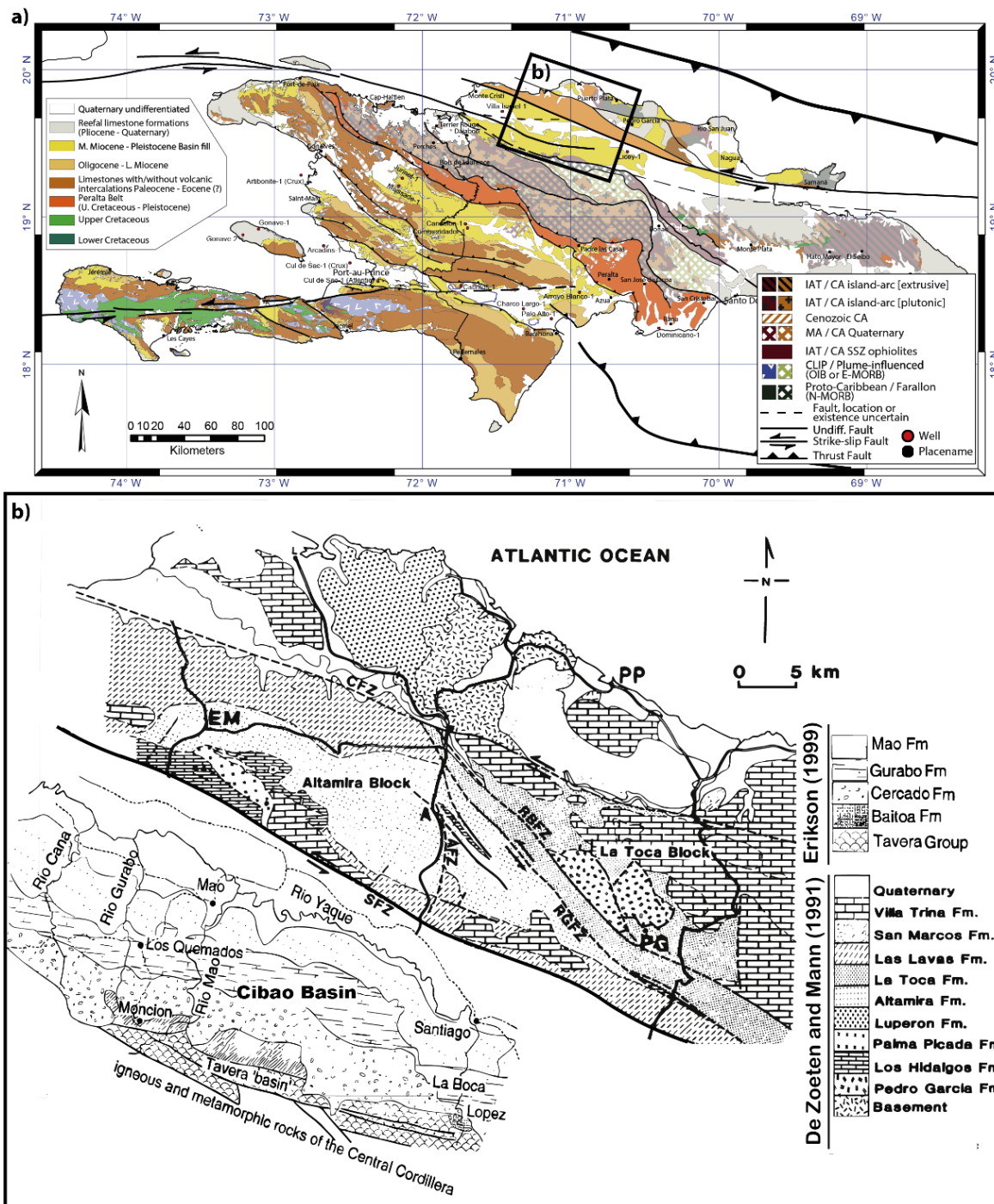


Figure II.13: a) Carte géologique simplifiée d'Hispaniola d'après Wessel (2019). La carte géologique d'Haïti été modifiée d'après Boisson et Pubellier (1987, 1988), Boisson et al. (1989), et Bien-Aimé Momplaisir et al. (1988). La carte géologique de la République Dominicaine modifiée d'après Hernaiz Huerta et al. (2007). b) Carte géologique et structurale de la Cordillère Septentrionale centrale (D'après Zoeten & Mann, 1991) et du Bassin de Cibao (d'après Erikson (1999)). Cinq grandes failles traversent la Cordillère Septentrionale centrale : la zone de faille Septentrional (SFZ) ; la zone de faille Rio Grande (RGFZ) ; la zone de faille Rio Bajabonico (RBFZ) ; la zone de faille Camú (CFZ) ; et la zone de faille Altamira (AFZ). La RGFZ sépare des lithologies de socle distinctes des blocs d'Altamira et de La Toca. EM = El Mamey ; PP = Puerto Plata ; A = Altamira ; PG = Pedro Garcia. Modifié d'après (De Zoeten & Mann, 1991; Erikson et al., 1998).

L'intervalle de l'Éocène supérieur au Miocène inférieur, d'après de Zoeten et Mann (1991), semble ne pas avoir de composante compressive importante en raison du manque de discordances angulaires dans les formations du *El Mamey Group*. D'après ces auteurs, cette période serait caractérisée par un mouvement purement décrochant au nord d'Hispaniola mis en évidence par l'accrétion océanique dans le fossé Cayman depuis l'Éocène (Leroy et al., 2000; Rosencrantz et al., 1988). Calais (1992) décrit aussi cet intervalle comme une période de relative quiescence tectonique liée à l'absence de déformations compressives sur la bordure nord de la plaque Caraïbe.

| Chronostratigraphy | | CIBAO BASIN | | | CORDILLERA SEPTENTRIONAL | | | |
|--------------------|-----------------|---------------------------|---------------------------------|---------------------------|--------------------------|----------------------------------------|------------------------------------------------------------------|--------------------------------------------|
| Ma | AGE | Vaughan and others (1921) | Dohm (1943) | Bermudez (1949) | Eberli et al. (1949) | Redmond (1982) | De Zoeten and Mann (1991) | |
| 5.3 | PLIOCENE | | | Mao Fm. | SFZ | Villa Trina Fm. | Villa Trina Fm. | Villa Trina Fm. |
| 11.2 | MIOCENE | U | Mao Fm. | Gurabo Fm. | | Villa Trina Fm. | El Mamey Group | La Toca Fm. |
| 16.2 | | M | Mao Fm. Gurabo Fm. | Gurabo Fm. | | | | |
| 25.2 | | L | Cercado Fm. Bulla Fm. | Gurabo Fm. Cercado Fm. | Cercado Fm. | | | |
| 30 | OLIGOCENE | U | Cercado Fm. | | El Mamey Fm. | | | |
| 36 | | L | Cevicos Limestone Tabera Fm. | Tabera Fm. | Tabera Fm. | Luperon Facies Altamira Facies | Las Laves Fm. El Limon Canada Bonita Mbr. Ranchete Mbr. | RGFZ FAULT |
| 39.4 | EOCENE | U | Limestone at Damajagua | | | Altamira Fm. | | |
| 48 | | M | | Plaisance Fm. | Hidalgo Limestone | | | |
| 54 | | L | | | Abullot Fm. | Palma Picada Fm. | | |
| 66.5 | PALEO. | | ? ? ? | ? ? ? | | | Los Hldalgos Fm. | |
| | LATE CRETACEOUS | | Basement | Basement | Pedro García Fm. | Pedro García Fm. (Palma Picada Fm.) | Palma Picada Intrusives | Pedro García Fm. (Rio San Juan Complex) |

Figure II.14: Comparaison des colonnes stratigraphiques de la Cordillère Septentrionale centrale. Le légendé ondulé rouge correspond à la discordance majeure Miocène. Le noir a la phase d'érosion Eocène sup. Modifié d'après de Zoeten & Mann (1991)

Pendant l'Oligocène, par l'effet de la collision diachrone entre l'Arc cubano-hispaniolien et les Bahamas, la faille Cauto est abandonnée par la mise en place de la faille Oriente plus au sud (Figures II.11 ; 3c de l'article 1, section III). Cuba est alors complètement transféré vers le domaine de la plaque Nord-Américaine (Iturralde-Vinent & Gahagan, 2002). Le bloc de Cuba et Hispaniola qui formaient une seule et même entité structurale commence à s'écarter par l'activité de la faille Oriente permettant l'échappement de la plaque Caraïbe vers l'est (Figure II.12D; Calais and Mercier De Lépinay, 1992; Leroy et al 2000; Boschman et al., 2014; Oliveira de Sa, 2021).

L'oligocène tardif est décrit par plusieurs auteurs comme une période de réorganisation paléogéographique des contraintes à la limite nord de la plaque Caraïbes due au développement de la faille d'Oriente (Calais & Mercier De Lépinay, 1992; Iturralde-Vinent, 1998; Rojas-Agramonte et al., 2008). Les observations à terre de Rojas-Agramonte et al (2008) dans la région de la Sierra Maestra (Sud Cuba) suggèrent que les structures compressives rémanentes de la phase compressive éocène sont décalées par des failles normales à la fin de l'Oligocène. Calais et Mercier De Lépinay (1991) suggèrent aussi qu'une phase transtensive est liée à la mise en place du Fossé Oriente au large de la côte SE de Cuba.

Le Miocène (~ 23 Ma) est marqué par un nouvel épisode compressif au nord d'Hispaniola.

Dubreuilh (1982) et Desreumaux (1987) relatent qu'une forte phase d'érosion a lieu entre le Miocène inf. et le Miocène moyen au nord d'Haïti. Sur la Sierra Maestra à Cuba, les unités du Miocène sont discordantes sur les séries pré-néogènes déformées lors de l'épisode compressif de l'Éocène. Des plis au sein des unités ont une longueur d'onde inférieure à celle de la première phase de compression (Rojas-Agramonte et al, 2005). Cette nouvelle phase de plissement au cours du Miocène a été moins importante que la phase de déformation Éocène (De Zoeten & Mann, 1991; Pindell & Draper, 1991). Les formations du *El Mamey Group* d'âge Éocène Sup.-Miocène Inf. à Hispaniola (Altamira, Las Lavas et La Toca Formations ; De Zoeten et Mann, 1999) sont ainsi plissées au cours d'un épisode de compression d'âge Miocène moyen (Calais & Mercier De Lépinay, 1995; De Zoeten & Mann, 1991; Erikson et al., 1998; Escuder-Viruete & Pérez, 2020; Pindell & Draper, 1991).

Pendant cette phase de compression des dépôts de la région de la Cordillère Septentrionale ont été soulevées et exposées, comme l'indique une discordance angulaire du Miocène moyen à supérieur (surface ondulée rouge, Figure II.14) (de Zoeten & Mann, 1991; Erikson et al., 1998; Pindell & Draper, 1991). Cependant, les dépôts des grès et des conglomérats mélangés (Formation Cercado), suivi d'accumulations de siltstone/argilites (Formation Gurabo), et de siltstone calcaire à son sommet (Formation Mao) indique une période de transgression dans le bassin du Cibao au sud de la Cordillère (Figures II.14 et II.15a)(Erikson et al., 1998). Le dépôt de la plateforme carbonatée de la Formation de Villa Trina par-dessus les séries turbiditiques de l'El Mamey Group, pendant la fin du Miocène supérieur-Pliocène inférieur (Escudier-Viruete et Perez, 2020) marque aussi la subsidence plus tardive de la région de la Cordillera Septentrional. Cependant, la destruction de cette plateforme carbonatée indique le changement vers une sédimentation dans un environnement marin peu profond, mettant en évidence une nouvelle période de soulèvement au nord d'Hispaniola au Miocène moyen (Figure II.15b) (de Zoeten & Mann, 1999; Escuder-Viruete & Pérez, 2020).

Le *Pliocène* (~5 Ma) est marqué par la collision oblique de la partie orientale du bloc d'Hispaniola avec le banc des Bahamas (Calais et al., 2016; Escuder-Viruete & Pérez, 2020). La frontière nord de la plaque Caraïbe (CAR) subit alors une réorganisation paléogéographique drastique (Calais et al., 2016; Calais & Mercier De Lépinay, 1995). L'obliquité de la collision génère une composante transpressive entre Hispaniola et les Bahamas (Pindell & Draper, 1991). Celle-ci, à son tour, permet l'activation de failles décrochantes sénestres, tel que le système de failles Septentrionale (SFZ) également initiées à l'époque du Pliocène (Leroy et al., 2015; Calais et al., 2016). Ces failles accommodent en partie la convergence oblique entre les plaques Caraïbe et Nord Amérique (Calais et al., 2016; Escuder-Viruete & Pérez, 2020). La composante de compression qui accompagne le mouvement est à l'origine du soulèvement de la Cordillère Septentrionale à sa position actuelle à 1250 m au-dessus du niveau de la mer (De Zoeten and Mann, 1999 ; Calais et al, 2016).

Au début du Pléistocène (2 Ma), la Presqu'île du Sud d'Haïti et la Ride de Beata composées de séries volcaniques épaisses de 20 km sont entrées en collision avec Hispaniola (Figure II.12, Mauffret & Leroy, 1999b; Pubellier et al., 2000). Cette compression active est probablement responsable du soulèvement des terrasses marines constituées de récifs quaternaires le long de la côte nord-ouest haïtienne et de la côte sud-est de Cuba (môle de Saint-Nicolas; Sorel et al., 1991; Calais & Mercier De Lépinay (1992); Authemayou et al. (2023). À Hispaniola, les récifs coralliens de la Formation de Isabella constituent des terrasses marines au nord de la Cordillera Septentrional (Figure II.15c) (République Dominicaine ; Escudier-Viruet and Perez, 2020). En Haïti, d'après Sorel et al. (1991), la plus récente terrasse marine du Môle de Saint-Nicolas date de 80Ka. À Cuba, les terrasses marines de Guantanamo sont plus élevées (jusqu'à 400 m, Muhs et al., 2017; Peñalver et al., 2021; Authemayou et al. 2023) que celles décrites le long de la côte cubaine, supportant un soulèvement fort et rapide en

raison de la néotectonique transpressive régionale (Iturralde-Vinent, 2003; Rojas-Agramonte et al., 2008; Authemayou et al. 2023).

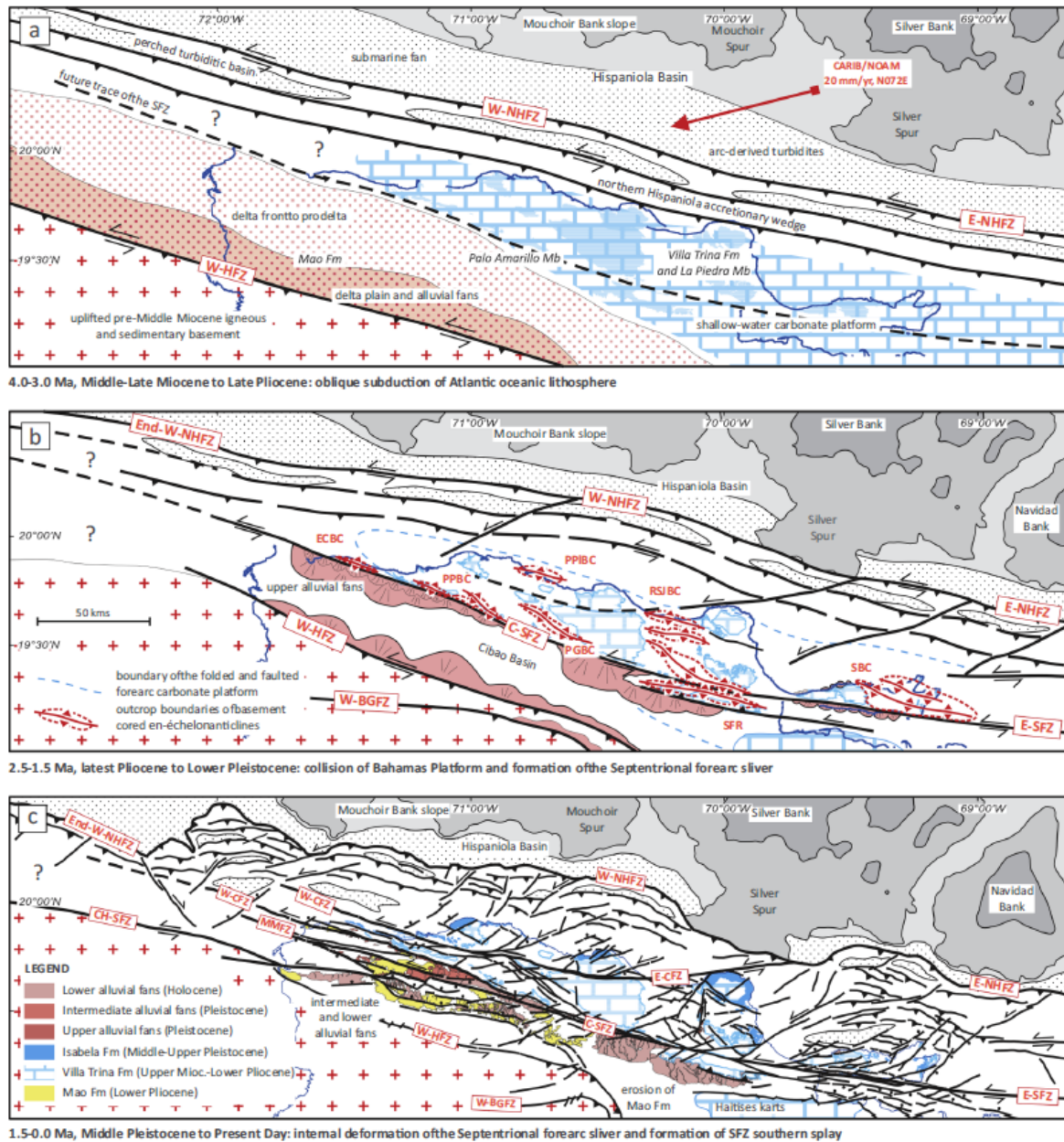


Figure II.15. Évolution néotectonique du nord d'Hispaniola d'après Escuder-Viruete & Pérez (2020). Trois phases de déformation de la région de la Cordillera Septentrional sont distinguées : (a) pré-collisionnelle au Pliocène moyen à tardif ; (b) syn-collisionnelle avec la formation d'un forearc à la fin du Pliocène au début du Pléistocène ; et (c) Collisionnelle avec le plissement du bassin forearc. CARIB/NOAM définit le vecteur de mouvement de la plaque Caraïbe par rapport à la plaque nord-amérique obtenu par géodésie GPS et modélisation (Mann et al., 2002 ; Calais et al., 2016, 2016 ; Benford et al., 2012 ; Symithe et al., 2015). La ligne bleue continue (à l'ouest) représente la position de la côte nord de la République dominicaine au fil du temps. Des acronymes indiquent les affleurements du socle igné et métamorphique pré-Éocène au cœur des anticlinaux : ECBC, El Cacheal ; PPBC, Palma Picada ; PGBC, Pedro García ; PPIBC, Puerto Plata ; RSJBC, Río San Juan ; et SBC, Samaná. Ces six complexes forment le prisme subduction-accrétion des Caraïbes dans le nord d'Hispaniola. Eastern (E-SFZ), Central (C-SFZ) and Western (W-SFZ) northern segments of the Septentrional Fault Zone (SFZ); and the Eastern (EH-SFZ) and Central Haitian (CH-SFZ) southern segments of the Septentrional Fault Zone (SFZ). Other important onshore structures are the Camu (CFZ), Hispaniola Fault Zone (HFZ) ; Monte Cristi (MMFZ).

DEUXIÈME PARTIE

— *Données et méthodologie* —

CHAPITRE III : Données et méthodologie

III.1 Données

Cette thèse s'appuie sur des données recueillies lors de plusieurs campagnes océanographiques. Elles regroupent : (1) des données acoustiques (bathymétrie et imagerie multifaisceaux, de sismique très haute résolution en mode CHIRP, appelées également sondeurs de sédiments et sismiques multitraces, ainsi que (2) des données sédimentologiques (carottes sédimentaires d'une longueur variant entre 3 et 4.8m en moyenne).

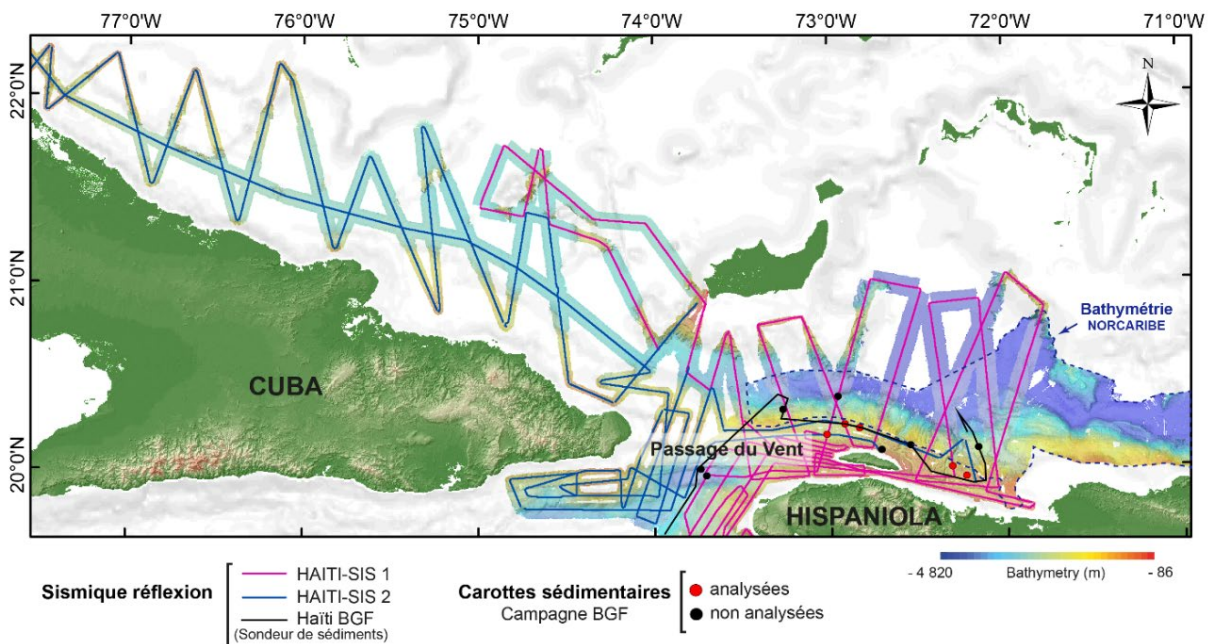


Figure III.1 : Plan de position des lignes de sismique réflexion et des données bathymétriques multifaisceaux utilisées dans le cadre de cette thèse. Les données bathymétriques proviennent principalement des missions HAITISIS (Leroy et al 2012 ; Leroy & Ellouz-Zimmermann 2013). Les données de la campagne NORCARIBE (Granja-Bruña 2013) sont représentées par une grille bathymétrique encadrée par une ligne en pointillés bleus.

La plupart des données de géophysique (bathymétrie et sismique réflexion, Figure III.1) ont été acquises pendant les campagnes HAITI SIS (2012) (Leroy, 2012) et HAITI SIS 2 (2013) (Leroy & Ellouz-Zimmermann, 2013) à bord du navire océanographique L'Atalante (Flotte Océanographique Française). La grille bathymétrique a été complétée par des données provenant de la campagne NORCARIBE (2013) réalisée à bord du navire océanographique espagnol Sarmiento de Gamboa (Figure III.1).

Les données de sondeurs de sédiments proviennent aussi majoritairement des expéditions HAITISIS. Lors de ces missions, elles ont été simultanément recueillies avec les données de bathymétrie multifaisceaux. Une partie des données de sondeur de sédiments a été obtenue lors de l'expédition Haïti BGF à bord du même navire océanographique L'Atalante (Ellouz-Zimmermann & Beaufort, 2015) (Figure III.1).

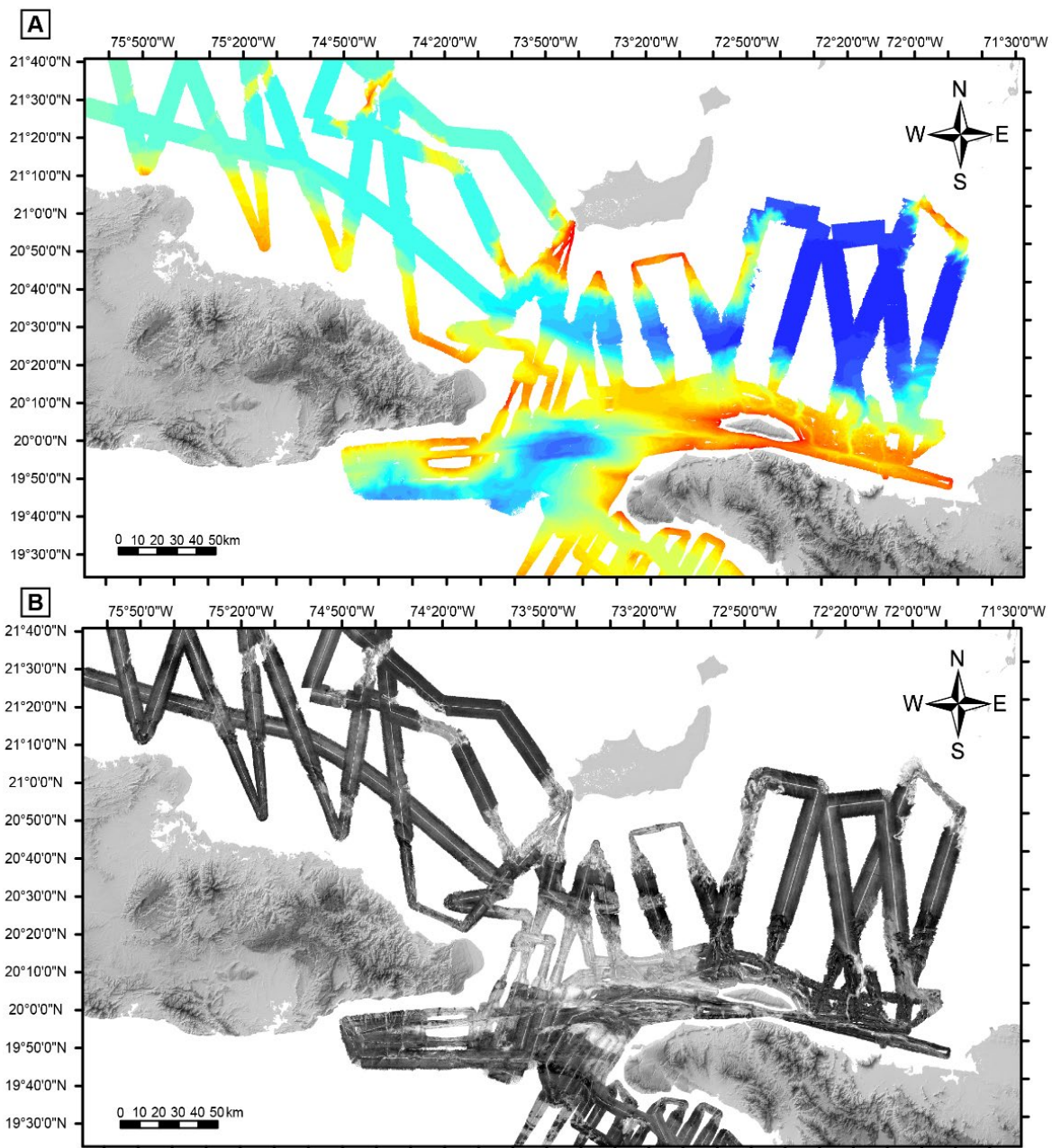
Les données de carottes sédimentaires proviennent de la campagne HAITI-SIS 1 (1 carotte) et de la campagne Haïti BGF (4 carottes) (Figure III.1).

III.1.1 Les données bathymétriques multifaisceaux

III.1.1.1 Acquisition

Les données de bathymétrie multifaisceaux couvrent une zone étendue sur environ 64436 km² depuis la région au nord de Cuba jusqu'à celle au Nord d'Haïti, et entre les deux, la région du détroit du Passage du vent (Figure III.1).

Les mesures bathymétriques, réalisées avec les sondeurs multifaisceaux EM122/710 (HAITISIS), ATLAS HYDROSWEEP DS (NORCARIBE), ont permis d'obtenir une carte bathymétrique d'une résolution de ~ 50m (Figure III.2). La carte bathymétrique a été complétée par des données provenant de l'atlas numérique GEBCO (https://www.gebco.net/data_and_products/gebco_digital_atlas/) avec une résolution de 800m.



III.1.1.2 Principe de la méthode

Le sondeur multifaisceaux est un instrument acoustique subaquatique conçu pour cartographier les fonds marins. Cet outil offre une capacité de génération rapide et précise de cartes topographiques du fond marin, permettant d'analyser la morphologie sous-marine et, par conséquent, les milieux de sédimentation. En plus de fournir des données bathymétriques, il capture des images acoustiques qui mettent en évidence les variations de réflectivité du plancher océanique.

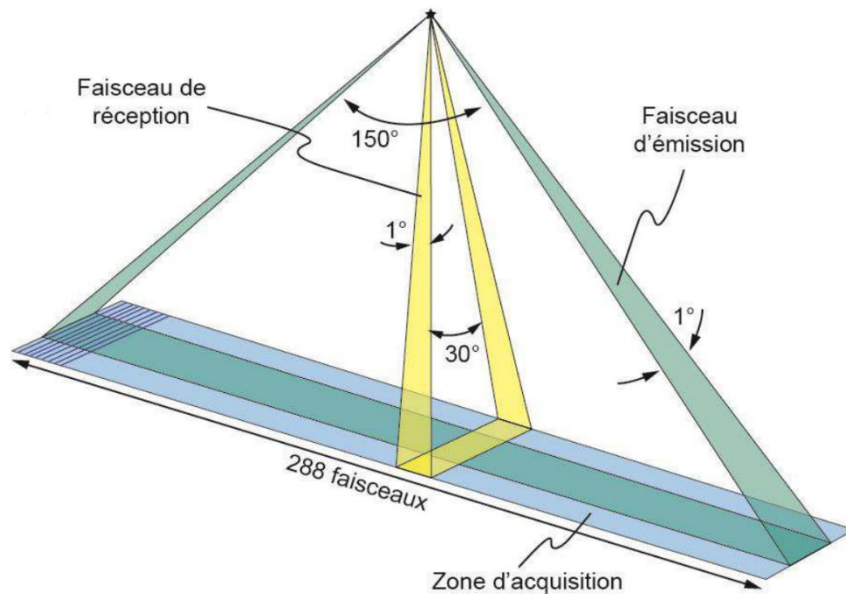


Figure III.3 : Schéma représentant la technique des faisceaux croisés de l'EMI22/710. D'après Augustin et al. (1996)

Le mécanisme d'acquisition repose sur la technique des "faisceaux croisés" (Figure III.3). Ce processus emploie un ensemble de faisceaux acoustiques élémentaires et directifs. Grâce à un unique signal émis, il est possible de recevoir de multiples réponses échogènes du fond, orthogonalement à la trajectoire du navire. L'angle d'ouverture latéral maximal s'élève à 150°, offrant une couverture vaste du fond marin, pouvant atteindre jusqu'à 6 à 7 fois la profondeur d'eau à cet endroit précis. Cet angle est ajusté en fonction de la profondeur et des propriétés du substrat (Unterseh, 1999). L'écho généré par l'intersection des faisceaux d'émission et de réception délivre deux catégories d'information : (i) Une donnée bathymétrique, dérivée du délai de l'onde sonore se propageant à travers l'eau (Figure III.2A-III.3); (ii) Une mesure de réflectivité, influencée par l'amplitude (en dB) de l'écho, qui découle des attributs physiques du sédiment (comme sa composition, sa texture et son état) et de la topographie locale du fond marin (Figure III.2B).

La réflectivité nous renseigne donc sur la nature du substratum, en permettant d'avoir une estimation sur les caractéristiques physiques de la roche, notamment sa "dureté", qui à son tour permet d'estimer la densité et le degré d'hydratation ou de compaction des sédiments. Des zones très réfléchives peuvent être observés le long de structures pentues. Les zones peu réfléchives (plus foncées sur la Figure III.2B) suggère la présence de sédiments peu consolidés et souvent saturés d'eau, tels que les argiles et les hémipélagites. Les zones à forte réflexion

(plus claires sur la Figure III.2B), sont le plus souvent associées à des sédiments plus denses, compactés ou à granulométrie plus grossière.

Les données issues de ces différentes missions ont permis de cartographier pour la première fois une grande partie des régions situées au large de Cuba et Haïti ainsi que la pente au sud des Bancs carbonatés des Bahamas à très haute résolution. Dans le cadre de cette étude, nous nous sommes attachés à détailler les différentes structures sédimentaires existantes sur cette marge.

III.1.2 Données sismiques

III.1.2.1 Acquisition

Lors des deux campagnes HAITI-SIS, les données sismiques ont été acquises avec le dispositif d'acquisition qui comprend deux canons à air de type Générateur-Injecteur ainsi qu'une flûte sismique de 24 traces. Au total, 244 profils de sismiques réflexion ont été acquis pendant ces 2 campagnes dont 48 ont été utilisés dans cette étude (Figure III.1).

Les données sismiques et bathymétriques des missions HAITI-SIS et NORCARIBE ont été traitées avant la présente étude par le logiciel SISPEED et Seismic Unix. Par contre, un traitement post mission sur le logiciel Reveal® a été effectué sur certaines lignes sismiques au nord de Cuba, afin d'obtenir une meilleure résolution des structures profondes sur ces lignes (principalement l'expression des bancs carbonatés enfouis). Ce traitement consistait à effectuer un filtrage pré-traitement différent en surface et en profondeur, afin de privilégier les hautes fréquences dans les sédiments et basses fréquences dans le socle acoustique.

III.1.2.2 Principe de la méthode

La sismique réflexion marine est une méthode géophysique d'exploration des interfaces, basée sur la génération et l'enregistrement d'ondes acoustiques. Ces ondes, émises depuis la surface de la mer, grâce à des canons, se réfléchissent au contact des interfaces géologiques situées sous le fond marin. Ces interfaces sont définies par des variations d'impédance acoustique, qui résultent du produit de la vitesse de propagation des ondes et de la densité du matériau traversé. Les facteurs dominants influençant l'impédance sont la lithologie, la porosité, la perméabilité, le type de fluides présents et l'anisotropie des formations rocheuses (Kearey et al. (1984).

Les ondes réfléchies sont captées à la surface à l'aide d'hydrophones, regroupés en configurations multitraces, sur une "flûte sismique". Les données recueillies sont ensuite transposées en sections sismiques, généralement exprimées en *Two Way Travel Time* (TWTT).

Le choix de la fréquence acoustique employée est primordial car il détermine la profondeur de pénétration et la résolution de l'imagerie géophysique. Les fréquences moyennes (50 à 500 Hz), typiques de la sismique Haute Résolution (HR), garantissent une exploration de 500 à 2000 m sous le fond avec une résolution verticale approximative de 10 à 15 m. Inversement, les fréquences élevées (300-2000 Hz) spécifiques à la sismique Très Haute Résolution (THR) offrent une excellente résolution verticale (1 à 2 m) mais limitent la profondeur d'investigation à 50-200 m.

III.1.3 Carottes Sédimentaires

III.1.3.1 Technique de Carottage par Carottier Kullenberg

La méthode de carottage avec le carottier Kullenberg repose sur la récupération de sédiments à partir d'un tube de prélèvement à pénétration gravitaire. Le carottier Kullenberg (Figure III.4) est composé d'un tube externe en acier à l'intérieur duquel est inséré un tube en PVC (appelé "chemise") ayant un diamètre de 10 cm. La partie supérieure de cet assemblage est équipée d'un lest ajustable, d'un bras d'armement, et d'un contrepoids, souvent désigné sous le nom de « messenger ». Ce dernier, lâché près du fond marin, optimise le déclenchement de la procédure de carottage (Figure III.4).

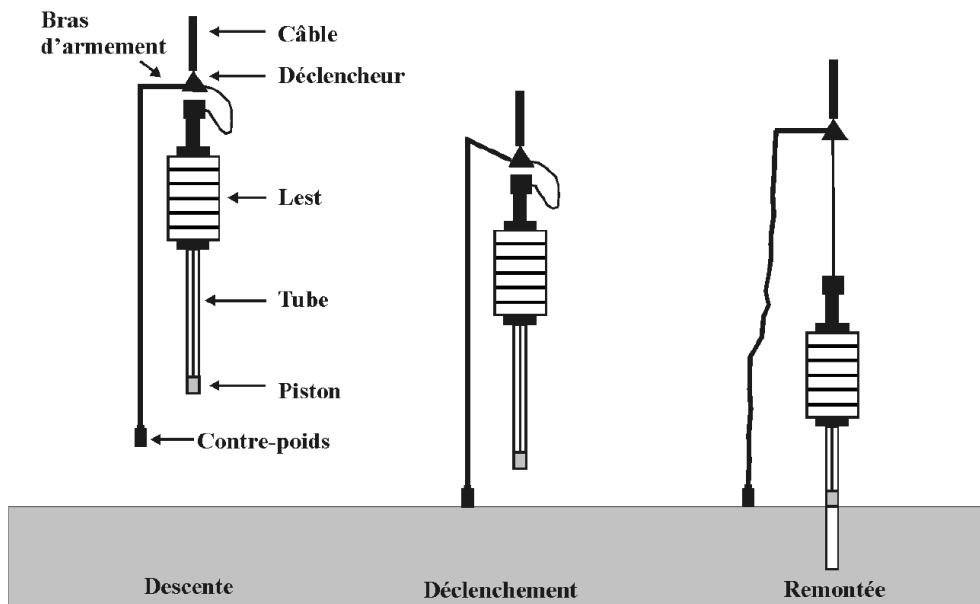


Figure III-4 : Principe du carottage à l'aide d'un carottier à piston de type Küllenberg (©Ifremer). D'après Principaud (2015)

Le bras d'armement, maintenu sous tension par un contrepoids, assure une mise en place efficace du dispositif. Selon les besoins spécifiques d'une mission, la longueur standard du tubage de 5 mètres peut être augmentée par l'ajout de sections supplémentaires, mesurant chacune 5 mètres.

La masse du lest, approximativement 250 kg, est modulable. Elle est constituée de plusieurs disques en fonte. Le réglage de ce poids est déterminé en fonction de la consistance du fond marin, de la profondeur de carottage souhaitée, et de la longueur totale du tubage utilisé (soit 5, 10 ou 15 m).

En action, le carottier est abaissé à l'aide d'un câble jusqu'à ce que le contrepoids atteigne le fond, déclenchant ainsi le carottage. La force gravitationnelle entraîne le carottier dans les sédiments (Figure III.4). Une fois la procédure achevée, le carottier est soigneusement retiré des sédiments et hissé à bord du navire. Le tube en PVC, qui contient le prélèvement sédimentaire, est extrait de la chemise métallique, scellé à ses deux extrémités, puis segmenté en tronçons. Chaque prélèvement est ensuite coupé en deux sections longitudinales, désignées comme demi-sections "travail" et "archive", conservés en tronçons d'un mètre et méticuleusement documentés pour de futures analyses en laboratoire.

III.2 METHODOLOGIE

III.2.1. Analyse des données acoustiques

Le traitement des données de bathymétrie multifaisceaux a été effectué à bord du navire par les électroniciens de Genavir, avec le logiciel de l'Ifremer Caraibes® (CARtographie Appliquée à l'Imagerie et la Bathymétrie des Sonars et sondeurs multifaisceaux). Les étapes de traitement ont eu pour objectif principal la génération de fichiers de sondes corrigées, validées et géolocalisées, facilitant la création de modèles numériques de terrain (MNT). Plusieurs MNTs à une résolution de 25 m ont été produits pour des zones définies, complétés par un MNT global à une résolution de 50 m.

L'analyse ultérieure de ces MNTs s'est effectuée par mes soins avec le logiciel ArcGIS, édité par ESRI. Dans ce contexte, l'utilisation du système d'information géographique (SIG) a assuré la géolocalisation, la consolidation, et la mise en forme des cartographies de distribution sédimentaire et des faciès acoustiques. De plus, une étude morphobathymétrique approfondie a été menée, comprenant la génération de cartes de gradients, de profils bathymétriques, et le calcul de superficies et volumes. Les données bathymétriques ont permis la localisation précise, l'identification, et la caractérisation morphologique des structures sédimentaires sur le fonds marin, telles que les canyons, les cicatrices d'érosion, les dépressions sous-marines, ou encore les monts carbonatés.

Concernant la réflectivité et sa relation à la lithologie, bien que le lien soit intrinsèquement complexe, une approche interprétative conventionnelle a été adoptée. Ainsi, les zones à faible réflectivité ont été associées à des sédiments fins, tandis que les zones à réflectivité élevée indiquent la présence de sédiments plus granuleux ou compactés. La cartographie de la réflectivité a joué un rôle clé pour délimiter les unités sédimentaires, postuler sur leur provenance et étudier les variations des faciès acoustiques en relation avec la lithologie, cette dernière étant corroborée par les échantillons de carottage.

III.2.2. Interprétation sismique

Cette analyse a été réalisée avec l'objectif d'identifier les principales caractéristiques architecturales de la région d'étude. L'interprétation sismique, selon les principes de la stratigraphie séquentielle (Catuneanu, 2006) a été effectuée en utilisant le programme Kingdom Suite®. Une analyse des faciès sismiques a été réalisée. Les principaux paramètres analysés sont l'amplitude (forte à faible), la fréquence (haute à basse) et la continuité des réflecteurs. Puis, la configuration interne des réflecteurs (organisation géométrique, contraste d'impédance) a été prise en compte afin de mettre en évidence des surfaces érosives et des ensembles génétiques de réflecteurs. Cela afin d'identifier des faciès et des géométries qui puissent indiquer la relation entre les systèmes sédimentaires observés sur la carte bathymétrique et l'architecture en profondeur des dépôts. Les structures tectoniques ont alors été identifiées sur les profils de sismique réflexion, telles que des failles normales, inverses, décrochantes, et des plis, en relation avec la déformation des séries sédimentaires caractérisées par la stratigraphie sismique.

Les profils sismiques multitraces (Figure III.1) ont été analysés afin d'en interpréter le style structural et de reconstituer l'architecture et l'évolution stratigraphique de la région d'étude.

III.2.3. Analyses sur carottes

L'étude sédimentologique de 5 carottes Küllenberg (Fig. III. 1), de 3 et 5 mètres de longueurs d'investigation, a été réalisée à l'Université de Bordeaux. Le protocole classique d'étude des sédiments en laboratoire s'est reposé sur plusieurs méthodes d'analyses dont les principes de fonctionnement ne seront pas détaillés dans ce chapitre. Elles comprennent cependant : (1) la photographie des tronçons de carottes, (2) la description de faciès sédimentaire, (3) l'imagerie par radioscopie rX, (4) l'analyse élémentaire par spectrométrie par fluorescence des rayons X (XRF), (5) l'analyse granulométrique, (6) l'analyse des teneurs en carbonates (CaCO_3), (7) la réalisation de lavages et de frottis et leurs observations à la loupe binoculaire et au microscope.

Dans le cadre de notre étude, ces carottes ont essentiellement servi à la caractérisation d'un point de vue faciès et processus sédimentaires ainsi que sur les conditions récentes de dépôts sur la marge au nord d'Haïti.

TROISIÈME PARTIE

— *Résultats* —

CHAPITRE IV : Evolution long-terme d'une limite de plaques - Cuba oriental

Ce chapitre correspond à un article soumis à Gcubed en septembre 2023 (special collection "A fresh look at the Caribbean plate geosystems").

La stratigraphie et la structure de la marge nord de l'Orient cubain (SE de Cuba) demeurent relativement peu explorées et les informations relatives aux dépôts marins sont quasi inexistantes. Ainsi, contrairement à sa partie occidentale, cette région a été largement négligée et non intégrée dans les études sur la compréhension de la tectonique globale.

L'étude menée dans la région au large de la côte nord-est de Cuba (Bloc de Cuba Oriental) s'est avérée cruciale pour une compréhension régionale de l'évolution de la frontière nord de la plaque Caraïbe. Celle-ci nous a éclairé sur la manière dont le registre sédimentaire de cette limite tectonique a varié d'est en ouest en réponse aux différentes phases de déformations associées à la collision diachrone avec le promontoire des Bahamas. Ce travail nous a également permis de formuler une chronologie des phases de déformation influençant les dépôts sédimentaires marins, en les intégrant aux événements géologiques majeurs survenus à Cuba depuis le Jurassique jusqu'à l'Éocène. Il montre l'importance de l'héritage tectonique des différents terrains mis en contact au cours du temps pour la dynamique long-terme de la frontière de plaque.

Dans cette étude, nous détaillons l'évolution de la limite Nord de la plaque Caraïbe, depuis l'abandon de son ancienne limite à travers le bloc de Cuba Oriental jusqu'à l'instauration du présent système de failles décrochantes Oriente-Septentrionale (SOFZ).

IV. The Protracted Evolution of a Plate Boundary: Eastern Cuba Block and Old Bahamas Channel

A. Oliviera de Sá¹, S. Leroy¹, E. d'Acremont¹, S. Lafuerza¹, J-L. Granja-Bruña², B. Moreno³, V. Cabiativa Pico¹, and J. Letouzey¹

¹ Sorbonne Université, CNRS, ISTeP, Institut des Sciences de la Terre de Paris, France

² Universidad Complutense, Madrid

³ Centro Nacional de Investigaciones Sismológicas, CENAI, Calle 17 No 61 e/4 y 6, Vista Alegre, Santiago de Cuba, Cuba

Key Points:

- The Old Bahamas Channel offers insights into the Caribbean's early tectonic history, dating back to the Pangea breakup.
- Bahamian carbonate banks formed as reefs on top of tilted blocks following the Pangea rift and were later affected by fault reactivation.
- The Eocene northern Caribbean plate boundary aligns with the Cuban Transform Fault, reactivated in Cuban orogenic and post-orogenic phases.

Abstract

The Eastern Cuban block has experienced a complex tectonic history characterized by plate interactions resulting in a diverse array of geological features observable in the offshore sedimentary record. We investigate the tectonic evolution of offshore Eastern Cuba, specifically in the Old Bahamas Channel and its surrounding areas, by integrating multi-channel seismic (MCS) reflection and published geological data. Our analysis employs stratigraphic frameworks and MCS data to assess deformation and key geological events in the region. We highlight the intricate tectonic history of the Eastern Cuban block, punctuated by significant geodynamic events, including rifting, the subduction of the oceanic Proto-Caribbean plate, and syntectonic orogenic and post-orogenic phases. The seismic units observed in the majority of the study area reveal the early evolution of the Northern Proto-Caribbean margin, subsequently impacted by the Cuban orogeny and the reactivation of the Cuban Transform Fault zone corresponding to a former plate boundary. We propose estimated ages for the seismic sequences, correlating them with available well data from neighboring regions. This study offers valuable insights into the tectonic history and geological evolution of offshore Eastern Cuba, contributing to a more comprehensive understanding of the region's geodynamic development.

IV.1. Introduction

The evolution of basins and structures at plate boundaries is strongly influenced by the vast history of plate movements they have undergone and the nature of these plates. In the Caribbean region, the North Cuba area was significantly impacted by regional plate motions that occurred during the fragmentation of Pangea, the emergence of the Proto-Caribbean arm of the Atlantic Ocean, and the north-eastern migration of the Caribbean plate between the Americas. Indeed, the origin of the Caribbean region can be traced back to the Triassic breakup of Pangea and the associated Proto-Caribbean continental passive margin linking the Gulf of Mexico to the Atlantic through the Cuba Fracture Zone (Klitgord et al., 1984). This evolution comprises the development of the Proto-Caribbean oceanic crust, its subduction below the Caribbean plate, and the Late Cretaceous collision and transfer of the NW Caribbean plate, including Cuba, to the North American plate (Pindell et al., 1988; Iturralde-Vinent & Lidiak, 2006).

The evolution of the Caribbean domain, from the early stages to its present configuration, is well-documented in the geology of Cuba. The thick Jurassic-Cretaceous strata and the interlayered basaltic rocks in Cuba provide significant evidence of the geological processes that occurred during the early evolution of the Proto-Caribbean continental passive margin. This margin was formed by the North American and South American plates facing the Proto-Caribbean Seaway (Figure IV. 1), which opened after the Pangea breakup. This vanished seaway connected the Atlantic and Pacific oceans from the Middle Jurassic to Early Cretaceous times. Remnants of the Proto-Caribbean oceanic lithosphere are present in ophiolitic units, outcropping along the northern Cuba (Ando et al., 1989; Iturralde-Vinent et al., 2016, Rui et al., 2022; Cobiella-Reguera, 2005) and also in the western part of the Demerara plateau (e.g., Gomez-Romeu et al., 2022).

During the Cretaceous-Paleocene period, arc activity due to Proto-Caribbean oceanic plate subduction caused the exhumation of metamorphic, volcanic, and sedimentary rocks, providing evidence of the various phases of the Cuban orogen's evolution (Iturralde-Vinent et al., 2016).

The Proto-Caribbean oceanic crust was entirely consumed due to subduction, leading to the collision of the northern border of the Caribbean plate with the Bahamas domain. This collision resulted in welding the Cuban Arc to the North American plate and played a significant role in establishing the current configuration of the Caribbean realm.

While the intricate, multi-phase history of this region, along with the tectonic plate interactions, were recorded onshore Cuba (Moretti et al., 2003; Rojas-Agramonte et al., 2008; Iturralde-Vinent et al., 2008, 2016), much of the history recorded offshore remains unexplored. This study presents a comprehensive offshore analysis of the Eastern Cuban Coast, using a multi-channel seismic reflection and swath-bathymetric dataset from the Haiti-SIS & 2 cruises (Leroy et al., 2015). We aim to establish a seismic stratigraphic framework for the offshore Western Cuban block by examining the reflection characteristics found within seismic sequences and correlating them with previously identified seismic sequences described in exploration wells and vintage seismic data within the surrounding regions.

Our analysis reveals that the seismic units observed in most of the area reflected the early evolution of the Northern Proto-Caribbean continental margin relative to the Bahamas Carbonate Province and were subsequently affected by the Cuban arc orogeny. We propose likely ages for the seismic sequences based on correlations with available well and dredge data from the neighboring regions. We show that the geological features in the offshore sedimentary records of Eastern Cuba are the result of various plate interactions, such as rifting, subduction, strike-slip, collision, and obduction, that have influenced its tectonic history.

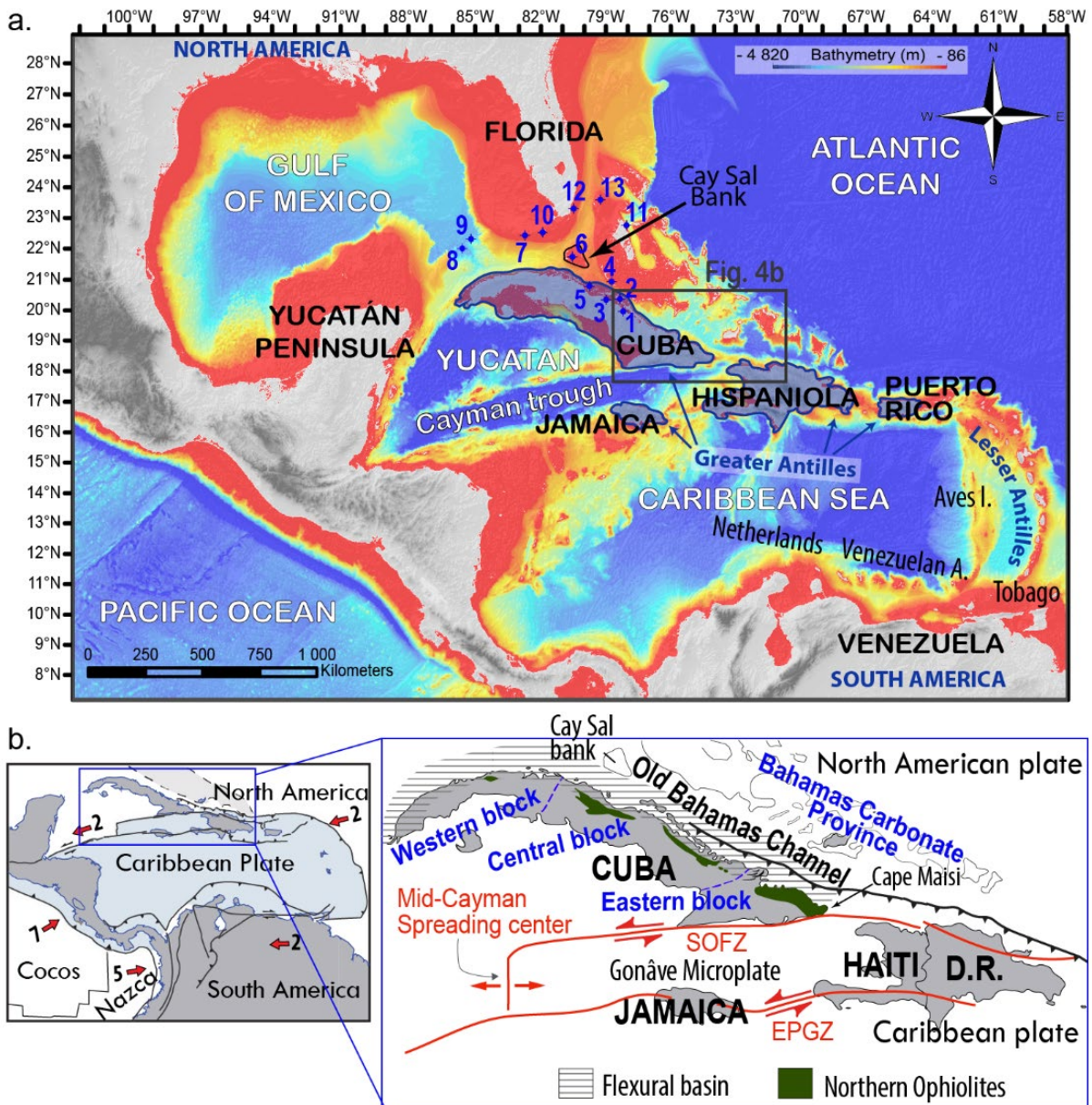


Figure IV. 1. Regional map of the Caribbean Sea area. (a) Topo-bathymetric map of the Caribbean Sea area. Onshore regions are in grey. The Greater Antilles archipelago consists of the four largest islands in the Caribbean: Cuba, Jamaica, Hispaniola, and Puerto Rico. Locations of academic and industrial key wells in South Florida, Bahamas, and Cuba are indicated by the blue dots with the following numbers: 1: Tina 1&2; 2: Cayo Coco 1&2; 3: Collazo 1; 4: Doubloon-Saxon. 5: Cayo Fragoso. 6: Cay Sal. 7: Marquesas 826; 8: ODP 535. 9: ODP 540; 10: Pine key; 11: Andros Island; 12: Williams; 13: Great Issac. (b) Main tectonic plates in the Caribbean region (numbers are in cm/y) and detailed view of the tectonic context of the Northern Boundary of the Caribbean Plate (on the right side). DR: Dominican Republic; SOFZ: Septentrional Oriente FZ; EPGFZ: Enriquillo Plantain Garden FZ.

IV.2. Geological setting: a synthesis

The Caribbean plate mainly consists of an oceanic igneous plateau with a 15 km-thick crust and, locally, some thick blocks of transitional and continental crust affinities and a few places of a 5 km-thick oceanic crust (Diebold et al., 1981; Burke et al., 1984; Mauffret & Leroy, 1997; Mauffret et al., 2001; Kerr & Tarney, 2005). Four plates surround the Caribbean plate: North American, South American, Cocos, and Nazca (Figure IV. 1b).

IV.2.1 Northern Proto-Caribbean Passive margin

North America, South America, and Africa formed the supercontinent Pangea during the Paleozoic and Early Triassic (Salvador, 1987). The rifting process between North America and Africa began in the Late Triassic, resulting in the stretching and thinning of continental crust during the Early and Middle Jurassic (Figures IV. 2a-b) (Marton & Buffler, 1993, 1994). During the continental breakup, the Bahamas-Cuba area was a transform zone linking the young Gulf of Mexico and the Atlantic Ocean (Figures IV. 2b-c) (Klitgord et al., 1984; Sheridan et al., 1988; Ross & Scotese, 1988; Marton & Buffler, 1994; Masferro & Eberli, 1999).

The Pangea rifting leads to the development of grabens and half-graben structures in the Proto-Caribbean margin (Salvador, 1987; Marton & Buffler, 1994; Pindell & Kennan, 2001; Padilla y Sánchez, 2016) (Figure IV. 2a). Syn-rift facies were intercepted by offshore wells (Figure IV. 1) (Jacobs, 1971; Iturralde-Vinent, 2003), which penetrated Jurassic redbeds (most like Callovian age) above crystalline basement rocks interpreted as belonging to the Proto-Caribbean continental crust (Meyerhoff & Hatten, 1968, 1974).

Graben and horst morphology prevailed during the Jurassic (Figure 2b) before the opening of the Gulf of Mexico and the upcoming Proto-Caribbean Ocean (Figure IV. 2c; Sheridan et al., 1981; Ladd & Sheridan, 1987; Schenk, 2008, Gaumet et al., 2002; Pindell & Kennan, 2001; Padilla y Sánchez, 2016). Most of the continental rifted zones emerged during the Middle Jurassic (Gaumet et al., 2004).

Early Jurassic rifting caused marine water influx, creating shallow water conditions (Ladd & Sheridan, 1987; Walles, 1993; Moretti et al., 2003; Epstein & Clark, 2009; Iturralde-Vinent et al., 2016). Middle Jurassic syn-rift redbeds were succeeded by evaporites in hypersaline lagoons (Figure IV. 2b; Gaumet et al., 2004; Padilla y Sánchez, 2016). Plate reconstructions by Klitgord et al. (1984) suggest that the Gulf of Mexico was isolated from Atlantic waters until the Callovian time due to the barrier formed by the elevated Florida-Bahamas region. However, plate reorganizations during the Early Callovian period (Figure IV. 2b-2c) may have opened up restricted waterways to the Proto-Caribbean margins (Klitgord et al., 1984).

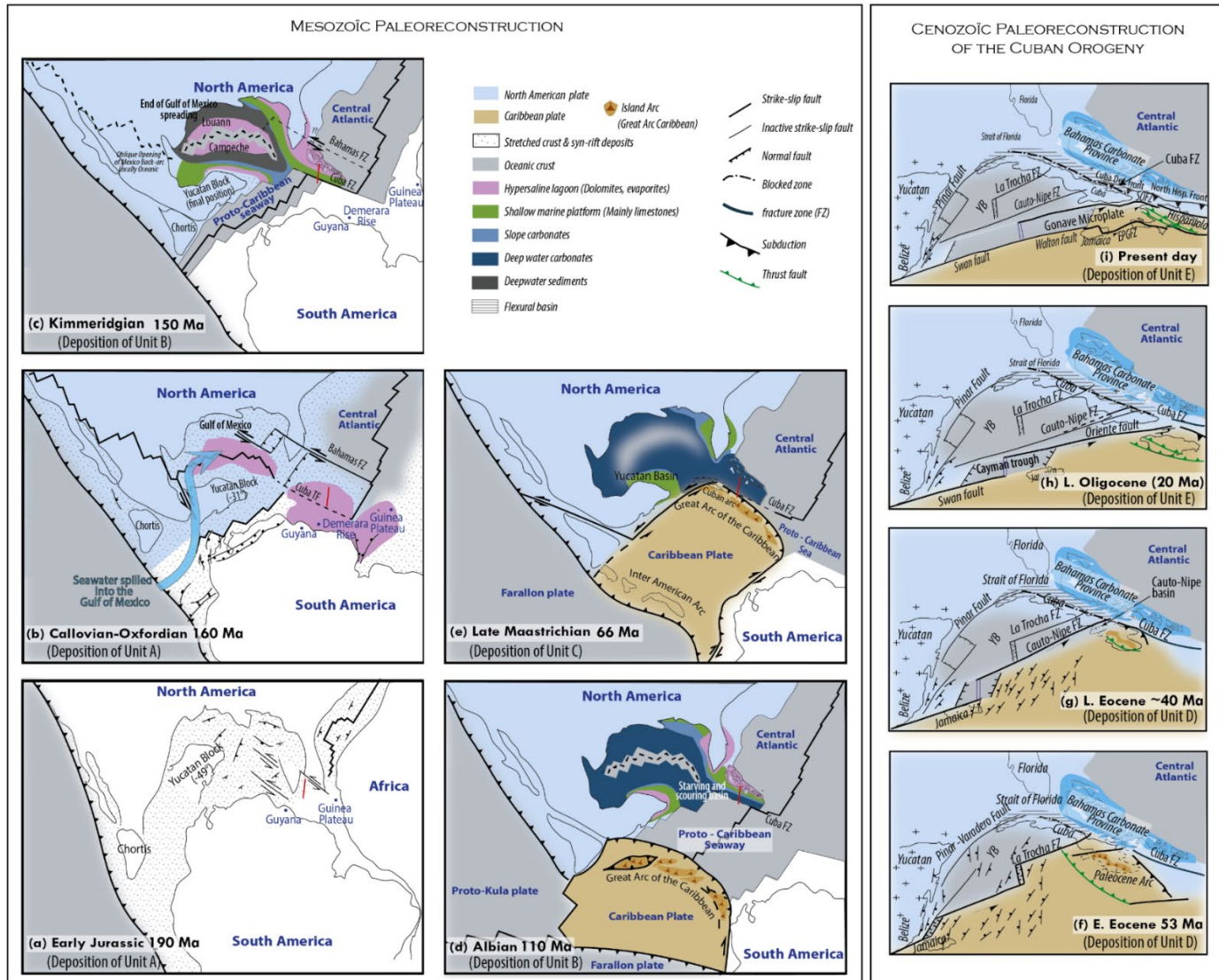


Figure IV. 2. Paleo-geodynamic reconstructions of the Caribbean region. Left panel: with the associated sediment deposits from Early Jurassic to Late Cretaceous. Right panel: Cenozoic paleo reconstruction of the Cuban orogeny from Early Eocene to Present-day. The sediments being very pellicular, they are not represented

The increased plate separation between North America and South America/Africa allowed a restricted influx of marine waters into the Gulf of Mexico from both the Pacific and potentially the Atlantic. Fossil-rich marine sediments in Mexico indicate a Pacific Ocean branch connected to the Gulf of Mexico in the Late Bathonian and Callovian periods (as shown by the blue arrow in Figure IV. 2b) (Salvador, 1987). Extensive salt deposits formed in the Gulf of Mexico, and a minor evaporite basin developed in the composite Bahamas domain, Demerara rise, and Guinea Plateau region (pink areas in Figure IV. 2b) (Lewis et al., 1991; Walles, 1993; Pindell & Kennan, 2001; Hudec et al., 2013).

The accumulation of 4,500—5,800 meters of shallow-water carbonates and evaporites found on Andros Island and Cay Sal Bank deep wells is attributed to subsidence during the Late Jurassic and Early Cretaceous periods, as documented by Furrázola-Bermúdez (1964), Khudoley, (1967), Uchupi et al., (1971) (Figure IV. 1a). A hundred meters of highly deformed halite and gypsum were found in the Punta Alegre Formation (Wells: Collazo-1 and Tina-1) (Figures IV. 1a and 3). The salt has been dated as Middle Jurassic, possibly Callovian (Figure IV. 3) (Cousminer, 1957).

Between the central Atlantic and Proto-Caribbean spreading systems, the Bahamas and Cuba fracture zones formed a wide transform area (Klitgord et al., 1984). These fracture zones (FZs) separate Mesozoic marginal sedimentary basins of the Proto-Caribbean continental passive margin as the Bahamas, South Florida, and the southeastern Gulf of Mexico basins (Figure IV. 2c) (Klitgord et al., 1984). During the Jurassic period, the Bahamas Fracture Zone formed first the southern boundary of the North American plate (Bahamas FZ in Figure IV. 2b). With the ongoing Proto-Caribbean spreading and the end of the Gulf of Mexico spreading, the Bahamas Fracture Zone is abandoned, and a narrow Jurassic transform zone, called the Cuba Fracture Zone, was formed (Cuban FZ in Figure IV. 2c) (Klitgord et al., 1984).

Between the Albian and Late Maastrichtian, the crust (Proto-Caribbean seaway) south of the Cuba FZ was consumed by the Cuban subduction zone (Figures IV. 2d-2e), and a thick carbonate pile was deposited in the southern and southeastern area of the Bahamas platform (Figure IV. 3).

IV.2.2 Bahamas domain

The Bahamas Carbonate Province was established during the Late Jurassic on the thinned crust formed by the breakup of Pangea (Masferro & Eberli, 1999). The Bahamian reef formation is also believed to have started in the Late Jurassic to the Mid-Cretaceous period due to shallow water conditions resulting from rifting, allowing a large carbonate deposition (green area in Figure IV. 2c). The steep-sided slopes of the Bahamas were built by reef accretion (Sheridan et al., 1969), and the distinctive "bank-trough" morphology observed in the Bahamas Carbonate Province is believed to have resulted from a combination of various tectonic events and the erosive action of deep-water currents (Mullins & Hine, 1989). During the Mesozoic, the Bahamas mega-platform evolved into a banking system (Denny et al., 1994). Two hypotheses have been proposed in the literature to explain the origin and morphology of Bahama's carbonate banks: (1) The first hypothesis, known as the "Graben hypothesis" (Mullins & Lynts, 1977), proposes that the modern physiography of the Bahamas arises from the configuration of rifted continental margins (horsts and grabens) formed when North America

rifted from Africa. According to this hypothesis, the deposition of shallow water carbonate banks was restricted to horsts/paleo-highs, while the grabens were filled with deep-water sediments. (2) The second hypothesis, known as the "Megabank hypothesis" (Meyerhoff & Hatten, 1968; Bryant et al., 1969; Schlager & Ginsburg, 1981), suggests that during the Late Jurassic to the Mid-Cretaceous, an extensive shallow-water carbonate platform developed from the West Florida shelf to the Bahamas. Carbonate banks persisted in various forms throughout the Bahamas region during the Late Cretaceous and the beginning of the Cenozoic (Sheridan et al., 1981; Eberli and Ginsburg, 1987, 1989; Ladd & Sheridan, 1987).

Shallow-water conditions persisted in some areas of the Bahamas archipelago during the Late Jurassic, and the Bahamas platform was characterized by a vast restricted marine lagoon under arid climate conditions during this time (Figure IV. 2c). Dolomitic facies from the Lower Cretaceous period discovered in deep exploratory wells in Florida attest to a shallow water environment at this period (Marquesas 826, Big Pine Key 373, and Williams 1, as reported by Applegate in 1984) (Figures IV. 1 and 2d). During the Albian, the Yucatan is shallow and suitable for the deposition of dolomites and evaporites (Figure IV. 2d). In addition to these findings, homogeneous hyper-saline lagoons were also observed to still develop in the Cayo Coco Formations (Figure IV. 2b) (Cayo Frago I and Cayo Coco 1-2 wells, Figure IV. 1; Gaumet et al., 2004).

The Bahamian area underwent a major transgressive event in the upper part of the Jurassic (Kimmeridgian) (Gaumet et al., 2004). The Upper Tithonian period then marked a deepening trend, enhancing connections between the Gulf of Mexico and the Proto-Caribbean domains. The transgression initially started in the Late Kimmeridgian had its peak during the Berriasian period, leading to the submersion of the region and the formation of deep carbonate deposits (Figures IV. 2c-d and 3) (Gaumet et al., 2004). In the southern part of the Florida-Bahamas Mega platform, dolomitic facies were followed by these slope and shallow carbonate deposits, while slope carbonate deposits expanded across the Eastern Cuban area (Figure IV. 2d). The deepening trend of the Late Jurassic-Early Cretaceous led to a reduction in reefal-lagoonal deposits in the southeastern Bahamas (Green and pink areas in Figure IV. 2d). However, localized shallow water build-ups persisted, contributing to the present "bank-through" morphology of the Bahamas (Figure IV. 1) (Gaumet et al., 2004).

While shallow conditions prevailed in the Bahamian area, the drowning event during the Berriasian period led to the sealing of the tilted blocks in Western and Central Cuba. This event caused a uniform deposition of deep-sea carbonates (blue in Figure IV. 2d) over the Jurassic syn-rift, which was characterized by a siliciclastic sequence interspersed with thin layers of black shales and sandstones (Moretti et al., 2003; Gaumet et al., 2004).

IV.2.3 The Proto-Caribbean Seaway

During the Lower Jurassic to the Early Kimmeridgian, the Yucatán block moved southward and rotated about 49° counterclockwise, causing the opening of the Gulf of Mexico and Proto-Caribbean seaways (Figures IV. 2a-2c) (Pindell & Dewey, 1982; Pindell, 1985; Schouten & Klitgord, 1994; Marton & Buffler, 1994; Pindell & Kennan, 2001). The oceanic crust underlying the central Gulf of Mexico drifted apart from the previous salt basin into two salt bodies, the southern (Campeche) and northern (Louann) (Marton & Buffler, 1994; Hudec et al.,

2013) (Figure IV. 2c). The Yucatan block reached its present position by the Early Kimmeridgian, and the Gulf of Mexico assumed its present configuration (Figure IV. 2c) (Padilla y Sánchez, 2016).

The cessation of Yucatán's rotation allowed for the formation of a single, slightly reorganized Proto-Caribbean oceanic ridge system, which linked the Pacific and Atlantic Oceans (Figure IV. 2c). Rui et al. (2022) suggest that the Proto-Caribbean plate was initiated before 137 Ma (Figure IV. 2c). The oceanic crust was generated at multiple spreading centers during the Jurassic and Early Cretaceous, forming an oceanic domain called the Proto-Caribbean Seaway (Figures IV. 2c and 2d) (Giunta & Orioli, 2011). This domain evolved into the Proto-Caribbean Seaway and will, thereafter, disappear in subduction under the Caribbean plate (Figure IV. 2d-e).

During the Early Cretaceous period, the east-dipping subduction of the paleo-Farallon plate bounds the North and South America plates and the Proto-Caribbean seaway (Figure IV. 2d). Much of the Proto-Caribbean crust has been overridden by the Pacific-derived Caribbean plate, leaving only fragments of Proto-Caribbean crust that have either been accreted to the Caribbean plate or thrust onto South America (Figure IV. 2d-2e) (Neil et al., 2014). During Late Cretaceous period, the east-dipping subduction beneath the inter-American Arc ceased and was superseded by SW-dipping subduction of the Proto-Caribbean oceanic crust, which resulted in the formation of the Great Arc of the Caribbean (Figure IV. 2d-2e) (Pindell & Dewey, 1982, Hastie and Kerr, 2010; Pindell et al., 2011; Hastie et al., 2013; Escuder-Viruete et al., 2014).

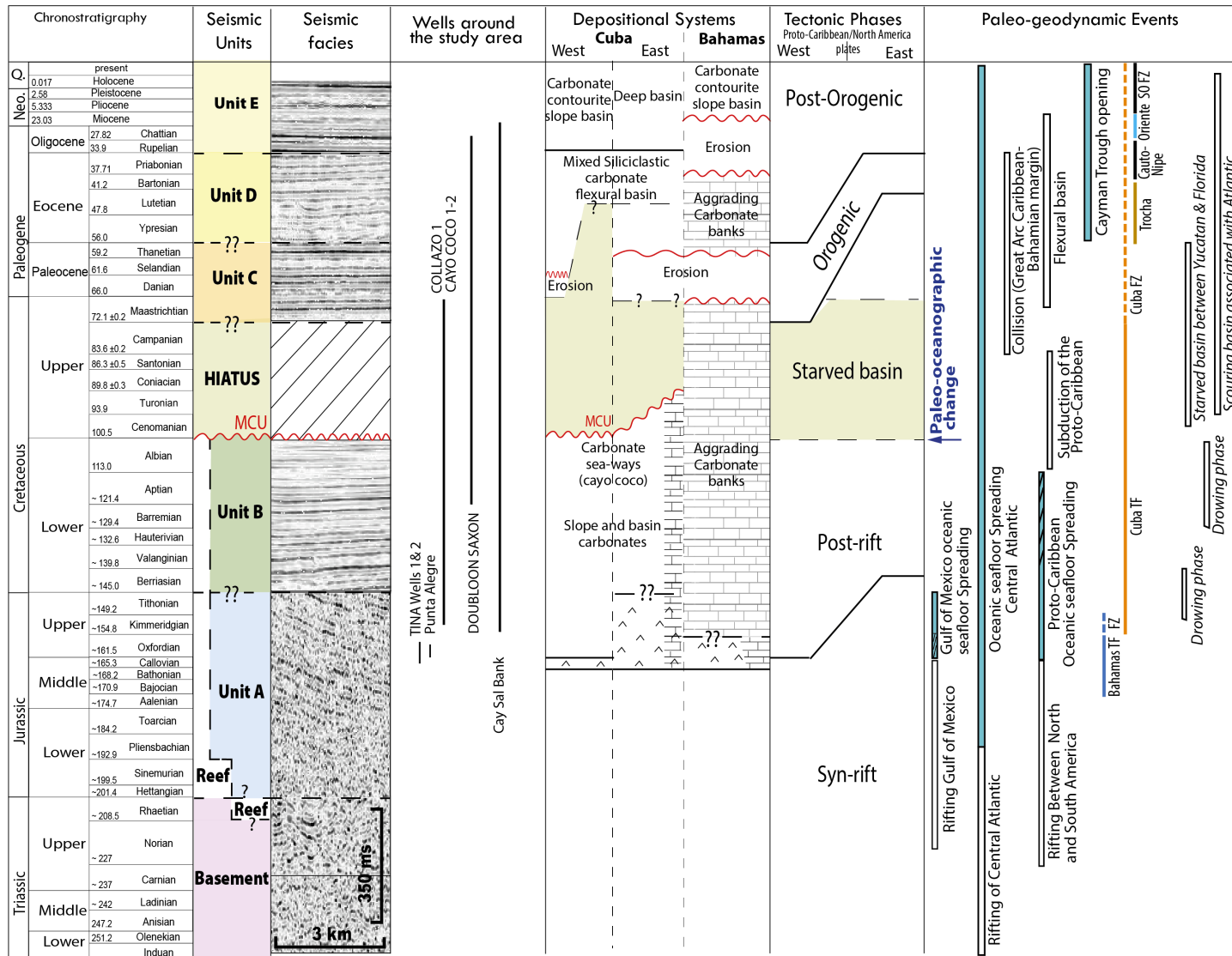


Figure IV. 3. Seismo-stratigraphic chart of the eastern Cuba-Bahamas area based on the seismic survey Haiti-Sis 2 and published wells. It enables the correlation of depositional systems, tectonic phases, and paleo-geodynamic events in the region.

IV.2.4 Cretaceous Caribbean plate

The subduction of the Proto-Caribbean seaway gave rise to the "Great Arc of the Caribbean" (as defined by Burke, 1988), which was a composite of several island arc systems with debated origin and complexity, including much of the present-day Great Antilles, Aves Ridge, and Netherlands-Venezuelan Antilles, as well as Tobago and allochthonous terranes in Venezuela (Figure IV. 1, Wright & Wyld, 2011; Neill et al., 2014).

The Great Arc of the Caribbean marked the leading edge of the Pacific-derived Caribbean plate from the Cretaceous to the Paleocene (Figures IV. 2d-2e). Remnants of the fossil convergent margin preserved in fore-arc units, along with the earliest magmatic arc sequences, provide evidence that this volcanic arc originated during the Early Cretaceous period and ended in the Paleogene period when the subduction ceased (Cobiella-Reguera, 2009). The subduction of the Proto-Caribbean plate first, then of the North American plate, ceased due to the collision between the Bahamian platform and the Caribbean plate and the termination of further northward motion of the Caribbean plate (Figure IV. 2f-2i).

By the Maastrichtian period (Figure IV. 2e), the position of the Caribbean plate was constrained to the North by evidence of accretion of the Eastern Cuba ophiolites (Figure IV. 4). These ophiolites are believed to be relics of the Proto-Caribbean oceanic lithosphere, emplaced during the Early Maastrichtian, before the Paleogene collision of the NW Caribbean and North American plates (Figures IV. 2d-2e, Andó et al., 1996; Cobiella-Reguera, 2005; Iturralde-Vinent et al., 2016; Rui et al., 2022). Cobiella-Reguera (2005) suggest that the eastern Cuba ophiolites were rapidly exhumed to the surface and displaced horizontally northward during an intense but brief tectonic event in the Early Maastrichtian.

IV.2.5 Cuban Arc

Cuba is the largest island in the Greater Antilles (Figure IV. 1). The Cuban Arc has witnessed and recorded numerous significant geological events within the Caribbean realm. Following the Cretaceous-Paleogene subduction beneath the Great Arc of the Caribbean, the collision between this volcanic arc and the southern margin of the North American plate resulted in a complex geological history linked to an orogenic phase (Figure IV. 2).

Cuban geology has been well-studied (Khudoley, 1967; Rosencrantz et al., 1988; Iturralde-Vinent, 1998; Moretti et al., 2003; Gaumet et al., 2004; Iturralde-Vinent et al., 2008, 2016; Pardo, 2009). Cuba is an archipelago of the Late Cretaceous-Eocene age that records geological units of three major tectonic phases: (i) A pre-orogenic phase, with the sedimentary evolution of the northern Proto-Caribbean Passive margin from the Jurassic up to Campanian (Figure IV. 3). (ii) An orogenic phase, when the northward displacement of the Great Arc of the Caribbean and the subduction of the Proto-Caribbean basin stopped, then the collision occurs in the southern margin of the North American plate between the Late Cretaceous (Figure IV. 2e) and Middle Eocene (Figure IV. 2g) (Malfait & Dinkelman, 1972; Echevarria-Rodriguez et al., 1991). During this process, Cuba was progressively welded to the North America plate (Leroy et al., 2000; Pindell et al., 2006; Oliveira de Sá et al., 2021) during a (iii) post-orogenic phase in which several left-lateral strike-slip faults shifted the Caribbean plate's relative motion from NNE (Maastrichtian) to E (Middle Eocene) (Pindell et al., 2005). As a consequence, these left-lateral strike-slip faults fragmented the Cuban orogen and formed several strike-slip corridors

(Figures IV. 2f to 2h). These corridors include the Eastern Yucatan Margin (Upper Cretaceous), the Pinar-Varadero (Paleocene), La Trocha (Early Eocene), Cauto-Nipe (Middle/Late Eocene), and Oriente Fault Zones (Early Oligocene) at the northern edge of the Cayman trough (Leroy et al., 2000; Oliveira de Sá et al., 2021) (Figures IV. 2f to 2h). According to this structural inheritance, the Cuban mainland is divided into three structural blocks, Western, Central, and Eastern Cuba (Lewis, 1990; Draper and Barros, 1994; Iturralde-Vinent, 1998) (Figure IV. 1b).

The sedimentary rocks outcropping in the west and center of Cuba have been assigned to the Eastern Yucatan margin (Haczewski 1976; Pindell 1985; Hutson et al. 1998; Ramos & Mann, 2023) and the southern margin of the Bahamas platform, respectively (Pardo 1975; Lewis & Draper 1990; Iturralde-Vinent 1994; Draper & Barros 1994; Pszczołkowski 1999). Mesozoic sedimentary rocks of the North American plate continental margin are widely distributed within the Western and Central Cuban blocks (Meyerhoff & Hatten, 1974). However, they do not crop out in the Eastern Cuba block (also called the Oriente block) (Figure IV. 1b).

The geological features of the Eastern Cuba block (Oriente block or Cuba Oriental) differ from those of the other regions in Cuba from the Upper Paleocene to the Early Middle Eocene. Up to the Early-Middle Eocene, the tectonic blocks of Eastern Cuba, Hispaniola, and Puerto Rico formed a single block (Figure IV. 2g). During this time, the Cauto-Nipe basin constituted an extension of the Yucatán basin (YB in Figures IV. 2f and 2i) *sensu lato*, representing the ancient boundary between the North American and Caribbean plates (Figure IV. 2g). This configuration explains the absence of arc-continental collision processes in Cuba Oriental during the Paleogene, as occurs in the rest of Cuba (Caballero & Cabrera, 2003a; Ramos & Mann, 2023).

During the Middle Eocene, the Eastern Cuban block collided with the Bahamas, and a left-lateral activity developed along the Cauto-Nipe basin (Figure IV. 2g) (Iturralde-Vinent & Macphee, 1999; Vázquez-Taset et al., 2020). Vázquez-Taset et al. (2020) describes a coexistence of extensive and compressive structures in the Cauto-Nipe Corridor. The authors associated these structures with local transtension and transpression regimes controlled by the left lateral activity of strike-slip faults in this corridor (Figure IV. 2g). The tectonic activity in the Cauto-Nipe fault zone began to wane in the upper Oligocene (Figure IV. 2h), which coincides with the transfer of slip to the Oriente Fault, the current boundary between the Caribbean and North American plates (Figure IV. 2h-i) (Iturralde-Vinent and Macphee, 1999; Rojas-Agramonte et al., 2008; Vázquez-Taset et al., 2020; Oliveira de Sá et al., 2021).

IV.3. Data and methods

Multi-channel seismic (MCS) reflection and multibeam bathymetric data were collected during HAITI-SIS 1-2 (2012-2013) cruises onboard the R/V L'Atalante from the *Flotte Océanographique Française* (Leroy, 2012; Leroy & Ellouz-Zimmermann, 2013; Leroy et al., 2015).

2D seismic reflection data are recorded using a source comprising two GI air guns (2.46 L, 300 in3) and a streamer with 24 channels (600 m-long) operated at c.a 9.7 knots (fast and light operating seismic system from GENAVIR/IFREMER). The multi-channel seismic reflection data were processed using a standard workflow, including CDP gathering (6-fold), binning at

25m, detailed dynamic velocity analysis, stack, and post-stack time migration. All the seismic reflection profiles presented are time-migrated using distinct filtering for the sediments and the seismic basement (bandpass filter for the sediments 20-28-100-128/12-18-32-70 Hz and for the basement 6-18-32-55-6-18-24-35 Hz).

Multibeam bathymetry data were acquired simultaneously along seismic profiles and gridded with a spacing of 50 m. The data from the NORCARIBE 2013 cruise (Rodríguez-Zurrunero et al., 2019, 2020) complement the bathymetric map. The gridded bathymetry data was completed with the GEBCO Digital Atlas (Weatherall et al., 2015) with an ~800 m resolution to provide almost full coverage (Figures IV. 1 and 4).

The processed seismic data are interpreted using Kingdom IHS Suite© software. Maps are plotted with ArcGIS© software. We use the seismic reflection dataset to identify seismic horizons and units, as well as their geometrical disposition, and then to interpret seismic units, deformation style, and spatiotemporal evolution of the tectonic structures. Morphological analysis of the seafloor based on swath-bathymetric data is carried out to determine the surface expression of tectonic features. We identify faults by either sediment horizon offsets or by the fault plane seismic reflection itself in the seismic profiles. It is important to note that the correlations done are only relative due to spatial gaps between areas with well-developed seismic stratigraphy, the gaps derived from wells and dredges, and the seismic data within the surrounding regions.

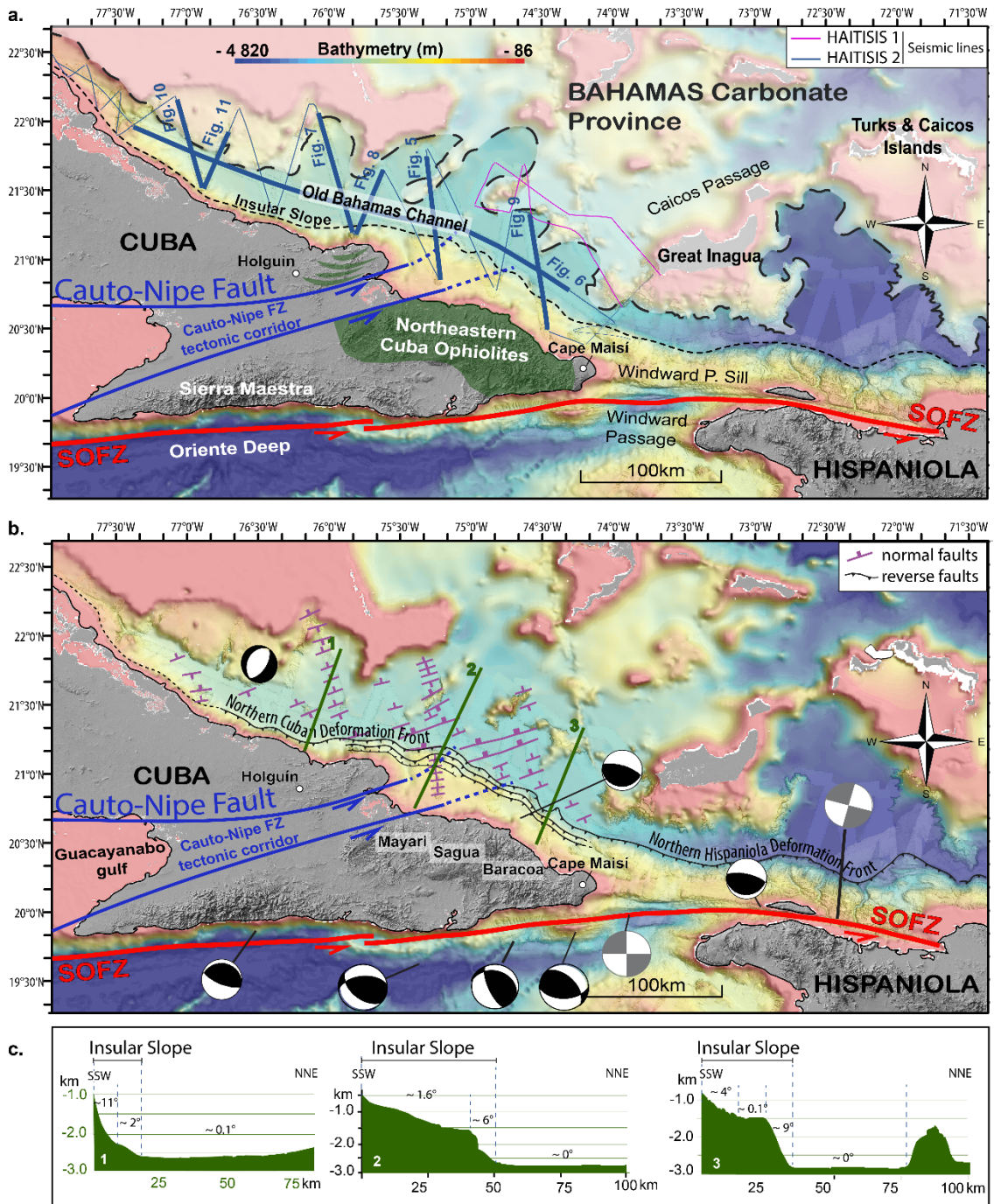


Figure IV. 4. (a) Bathymetric map showing the positions of seismic sections collected during cruises HAITI-SIS 1–2 (Leroy, 2012; Leroy & Ellouz-Zimmermann, 2013; Leroy et al., 2015). Bold lines show the location of the seismic profiles shown in this paper. The short-dashed black line represents the base of the insular slope. Large-dashed black line represents the limit of the banks and ridges (b) Structural map of the study area based on the interpretation of seismic profiles. The focal mechanisms are for $M > 5$ earthquakes from the CMT database, except for the $M_w 4.7$, Dec 17 2022 normal faulting on a NE-SW oriented fault plane in the south of the Bahamas Carbonate province (c) representative bathymetric profiles across the insular slope of Eastern Cuba, revealing depths up to 3 km and slope gradients ranging from 11° to zero. Locations of the bathymetric profiles are shown in Figure IV. 4b.

IV.4. Results

IV.4.1 Morphology of the study area

The Old Bahamas Channel is a strait that lies between the northern coast of Cuba and the southern edge of the Bahamas Carbonate Province (Figures IV. 1b and 4a). It spans from the Cay Sal Bank and runs in a southeasterly direction for about 160 km up to it reaches its endpoint between Cape Maisí in Cuba and Inagua Island in the Bahamas (Figures IV. 1b and 4).

The Old Bahamas Channel is approximately 22 km wide at its narrowest point, but it gradually widens south-eastward along the Holguín and Cape Maisí, reaching a width of about 70 km (Figure IV. 4a). On bathymetric maps, the channel is represented as a deep-water basin (around 2800 m-deep) punctuated northward by small banks and ridges (Figure IV. 4a). Its bathymetric expression is generally flat, (Figure IV. 4c), similar to those of abyssal plains. However, between the coast of Holguín and Cape Maisí, these flat gradients are contrasted by the steeper gradients of the Cuban insular slope, which can range from 1 to 9° (as seen in Figure IV. 4c). Compared to its western portion, the northern insular slope off Holguín and Cape Maisí is notably wider, with a range of 30 km wide to the North of Holguín up to 50 km wide in the area adjacent to the Cauto-Nipe tectonic corridor (Figure IV. 4).

IV.4.2 Seismic Stratigraphy

The 2D MCS data (represented by the solid lines shown in Figure IV. 4b) were used to determine the main seismic units and related structures in the study area. Interpretation of seismic profiles allowed us to recognize eight seismic units based on; i) their seismic facies (e.g., amplitude, lateral continuity, and frequency of internal reflectors), ii) bounding discontinuities, and iii) stratal architecture. The seismo-stratigraphic units were distinguished and labeled from older (Unit A) to younger (Unit E) in addition to the acoustic basement (Figure IV. 3). Other local but distinctive seismic units are the Bahamian reefs and ophiolites (Figures IV. 5 to 11).

IV.4.2.1 Basement

The study area's deepest reflectors consist of primarily disorganized and chaotic reflectors, referred to as the "acoustic basement." These chaotic reflectors of the acoustic basement are interrupted by normal faults that intersect the deepest traceable reflectors in the seismic sections, creating accommodation space for the deposition of Unit A above. Tilted blocks are inferred from the rugged and stepped morphology of the acoustic basement top (Figures IV. 5 to 11).

IV.4.2.2 Unit A

Unit A is the deepest seismic sedimentary unit, which exhibits distinct high-frequency parallel reflectors with moderate amplitude and local slight divergent geometry. This unit thickens towards the hanging wall of normal faults and gradually decreases in thickness towards tilted blocks with onlap terminations, forming syn-rift wedges (Figures IV. 3, 5, 7, 8, and 9). Toward the west, the roughness of the unconformity at the top of Unit A indicates that it has undergone significant erosional processes (Figures IV. 10 and 11). The eastern part of Unit A is disrupted by some growth faults (in blue Figures IV. 5b, 6, and 8)

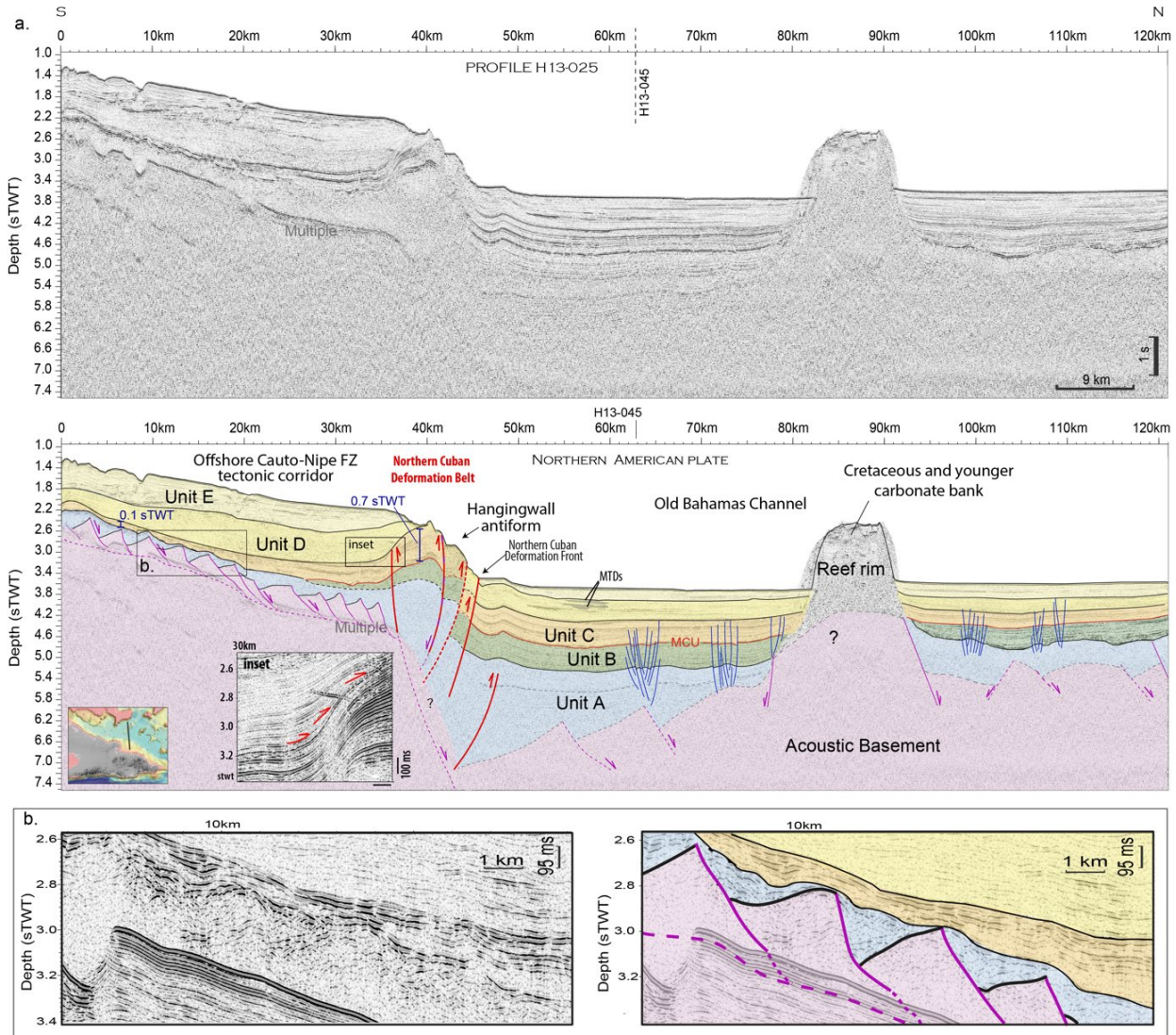


Figure IV. 5. Seismic line H13-025. a) Multichannel seismic profile across the Old Bahamas Channel, oriented south-north, showing the insular slope architecture created by the folding of seismic units towards the south. The associated pre- and syn-growth strata are discussed in section 5.1.2. The faults in red represent thrusts and reverse faults, forming the Northern Cuban deformation belt. Normal faults are delineated in violet. Dashed lines in violet denote inferred normal faults, deduced from the deformation architecture of Unit A. The blue faults illustrate steep minor faults which display a combination of normal and reverse offsets described in section 4.3.3. MCU: Mid-Cretaceous Unconformity. See the seismic line location in the inset and in Figure IV.4a. b) Enlarged sector showing a sequence of tilted blocks in a domino style affecting the basement of the insular slope (see location in Figure IV. 5b).

IV.4.2.3 Unit B

Unit B is characterized by high-frequency subparallel to parallel reflectors, displaying moderate to high amplitude, alternated by levels of low amplitude to transparent (Figures IV. 3, 7, and 8).

The deformation patterns within Unit B exhibit significant lateral variability. In the northern limit of the insular slope domain (faults in red in Figures IV. 5, 7, 8, and 9), Unit B is offset by numerous reverse faults and folds. In the western domain of the Old Bahamas Channel, Unit B is characterized by a rugged unconformity, indicated by the red horizons in the seismic profiles, Figures IV. 5 to 11). This unconformity is further accentuated by toplap terminations and truncated reflectors of the overlying Unit C (Figures IV. 6 and 10).

In contrast, moving eastward, the unconformity becomes less pronounced, and Unit B is observed as a draping layer, appearing relatively isopachous with minimal evidence of truncation (Figure IV. 6). However, unlike the western region, the eastern portion of Unit B is disrupted by a series of growth faults, which intersect with Unit A (in blue in Figures IV. 5b, 6, and 8).

IV.4.2.4 Unit C

Unit C is composed of moderate to high amplitude sub-parallel to parallel reflectors (Figure IV. 3). Seismic reflection profiles in the northern offshore area of the Cauto-Nipe tectonic corridor-(see Figure IV. 4a) reveal local thickness variations of Unit C, as the gradual increase seaward from around 0.1 sTWT to 0.7 sTWT along the hanging wall antiform (refer to Figure IV. 5a). This is not observed in other seismic profiles of the same orientation located to the west, outside the Cauto-Nipe tectonic corridor (Figures IV. 7 and 8).

The thickness of Unit C also exhibits variation towards the east (from 0.3 s TWT to 0.6 s TWT, Figure IV. 6). However, in the western portion of the Old Bahamas Channel, seismic reflections of Unit C display limited lateral continuity, adjacent to a large chaotic/transparent seismic body with only a few distinguishable reflectors (Figure IV. 6, km 20-100 and Figure IV. 10, km 20-40). These chaotic/transparent facies are interpreted as large mass transport deposits (MTDs) situated in the narrower part of the Old Bahamas Channel, toward the west.

IV.4.2.5 Unit D

Unit D is characterized mostly by parallel low to moderate-amplitude reflectors (Figure 3).

In the insular slope domain, Unit D fills the accommodation space created by the fold units beneath, outlining a syncline with an E–W axis (Figure IV. 5a, km 0-40) and NW-SE axis (Figure IV. 9, km 0-30). Its thickness reaches almost 1 sTWT (Figure IV. 5). The dip of Unit D reflectors progressively decreases upward near the fold from older to younger levels (Figure IV. 5 inset), creating a syn-tectonic wedge shape that onlaps the upper unconformity of Unit C (refer to Figure IV. 5, km 30-45). This geometry highlights Unit D as a growth strata.

Outside the insular slope domain, Unit D thickness is not greater than 0.4 sTWT (Figures IV. 8 and 9). In the eastern part of the Old Bahamas Channel, the topmost part of Unit D presents several isolated MTDs (Figure IV. 6, km 300-420).

IV.4.2.6 Unit E

Unit E is characterized by continuous plan-parallel reflectors with high amplitudes and high frequency (Figure IV. 3). It is deposited on Unit D mostly without deformation (Figure IV. 6). However, towards the west, where the Old Bahamas Channel is narrower, the upper portion of this unit has undergone extensive erosion (Figures IV. 10 and 11).

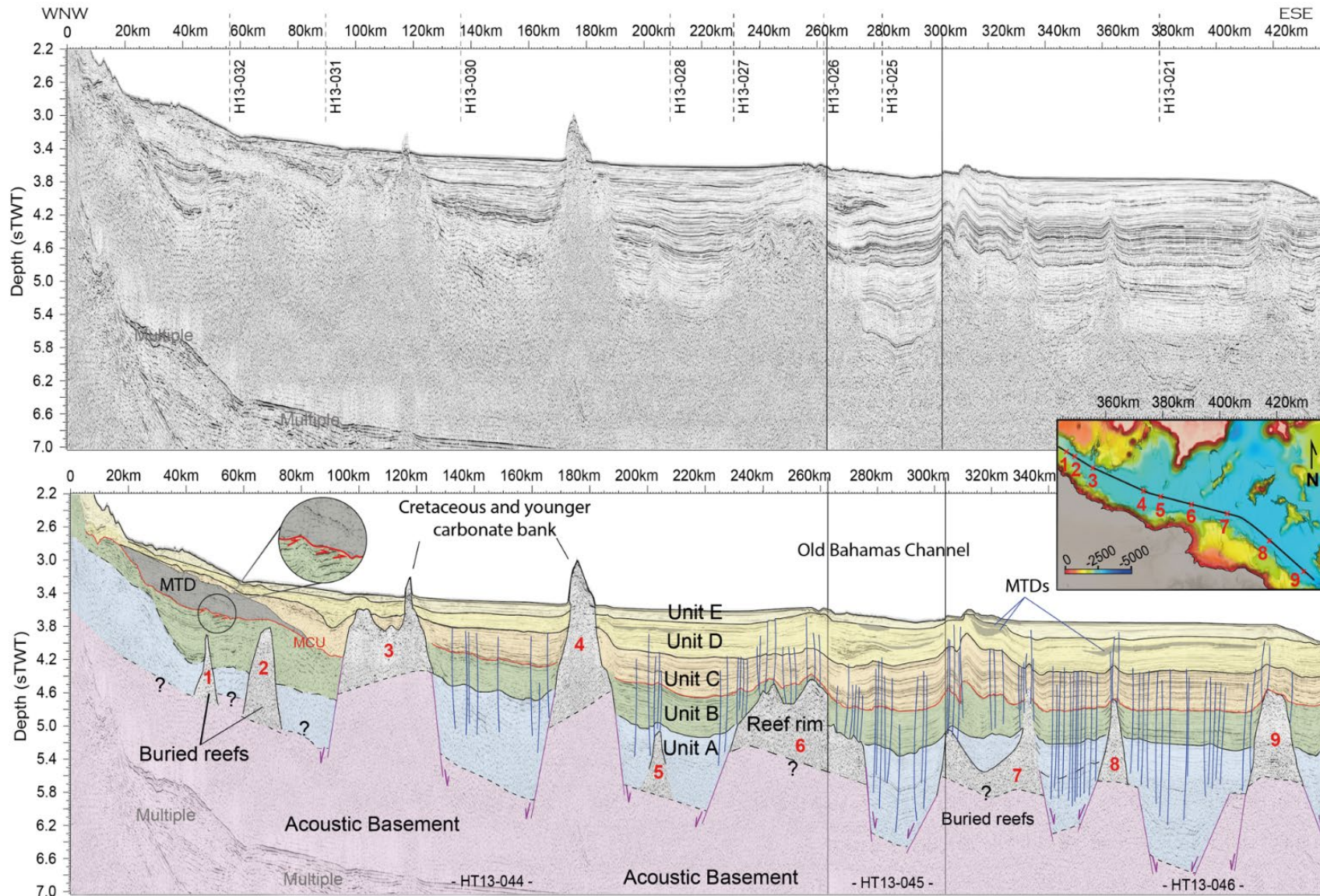


Figure IV. 6. Composite seismic profile (seismic lines HT13-004, HT13-045, and HT13-046) along the Old Bahamas Channel from WNW to ESE. The red numbers along the profile indicate the locations of identified carbonate mounds. While mounds 3 and 4 emerge on the seabed, the remaining carbonate mounds are buried. Notably, these buried carbonate mounds seem to be a continuation of the carbonate mounds that emerge further eastwards. This relationship is illustrated in the inset, which displays a bathymetric map indicating the position of the seismic profile and the distribution of carbonate mounds along its entire length. MTDs are represented in grey color. MCU: Mid-Cretaceous Unconformity. See Inset and Figure IV. 4a for the location of the profile.

IV.4.2.7 Other Seismic Features – Bahamian Highs and chaotic bodies

The seismic profiles intersect several Bahamian highs some of them also identifiable by the topographic features shown on the bathymetric map (Figure IV. 4). These highs have a distinctive mound shape on the seismic profile and are characterized by irregular, weak, discontinuous internal reflections (Figures IV. 4 and 5). Some highs reveal evidence of layering at their top (as in Figures IV. 5 and 7). However, reflections are highly attenuated with depth. Certain are well-developed and take the form of ridges on the ocean floor, oriented in a NE-SW direction (Figure IV. 4). However, others are completely buried by Units B, C, D, and E (e.g. Figure IV. 6). These buried highs appear to be the southwestern extension of the NE-SW oriented carbonate banks that emerge on the seafloor (inset in Figure IV. 6).

Unit B is seen overlapping the flanks of these dome-shaped formations up to it fully overlays them, whereas the more recent Units C, D, and E continue to deposit on top of them. Highs seem to be rooted in basement highs as horst or tilted blocks (Figures IV. 4c, 5, 6, and 7). Towards the east, sediment layers overlying the buried highs are tilted due to the upward growth of these highs (see Figure IV. 6, km 280-450). The onlap terminations against the highs are bent upwards along its flanks. Generally, the vertical upturn remains relatively consistent from Unit A to the top of Unit B, gradually decreasing upwards throughout Unit C (Figure IV. 6).

In the seismic profiles located off the northeastern Cuban Ophiolites, and Holguin ophiolites (Figures IV. 1 and 4a), seismic units from the basement up to Unit D terminate westward abruptly against a chaotic body situated on the north coast of Cuba (as shown in Figures IV. 7 and 8). However, due to intrinsic chaotic seismic signals and the presence of seabed multiples, the internal structures of this body are obscured, making the interpretation very difficult. The lateral contact between the chaotic body and the sedimentary seismic units up to Unit D is discordant, but Unit E is observed to overlie the chaotic body at its top.

IV.4.3 Structural analysis

IV.4.3.1 Tilted Basement blocks

Significant thickness variation in Unit A implies that it was formed in grabens and half-grabens that were actively subsiding (see Figures IV. 5, 6, and 7). This syn-sedimentary unit likely accumulated in half grabens and narrow basins during an extensional phase. The thickness of Unit A increases towards the south at the toe of the insular slope, where a major north-dipping normal fault could have played (Figures IV. 5 and 7). In several NNW-SSE trending seismic reflection profiles (Figures IV. 5, 7, 8, and 9), the basement is observed to be tilted towards the normal fault planes, exhibiting a tilted block geometry with a NE-SW orientation and forming asymmetrical half grabens (Figure IV. 4c). The size of the tilted blocks varies across the study area, with smaller blocks measuring approximately 3 to 5 km in the insular slope domain (Figure IV. 5b) and larger blocks ranging from 10 to 20 km in the deeper part of the Old Bahamas Channel domain (Figure IV. 6). In the insular slope domain, small tilted blocks are bounded by normal faults, likely situated above a concealed decollement (pink dashed line below the tilted blocks in Figure IV. 5a). This decollement is not visible in the seismic profiles due to the seabed's multiple (Figure IV. 5b).

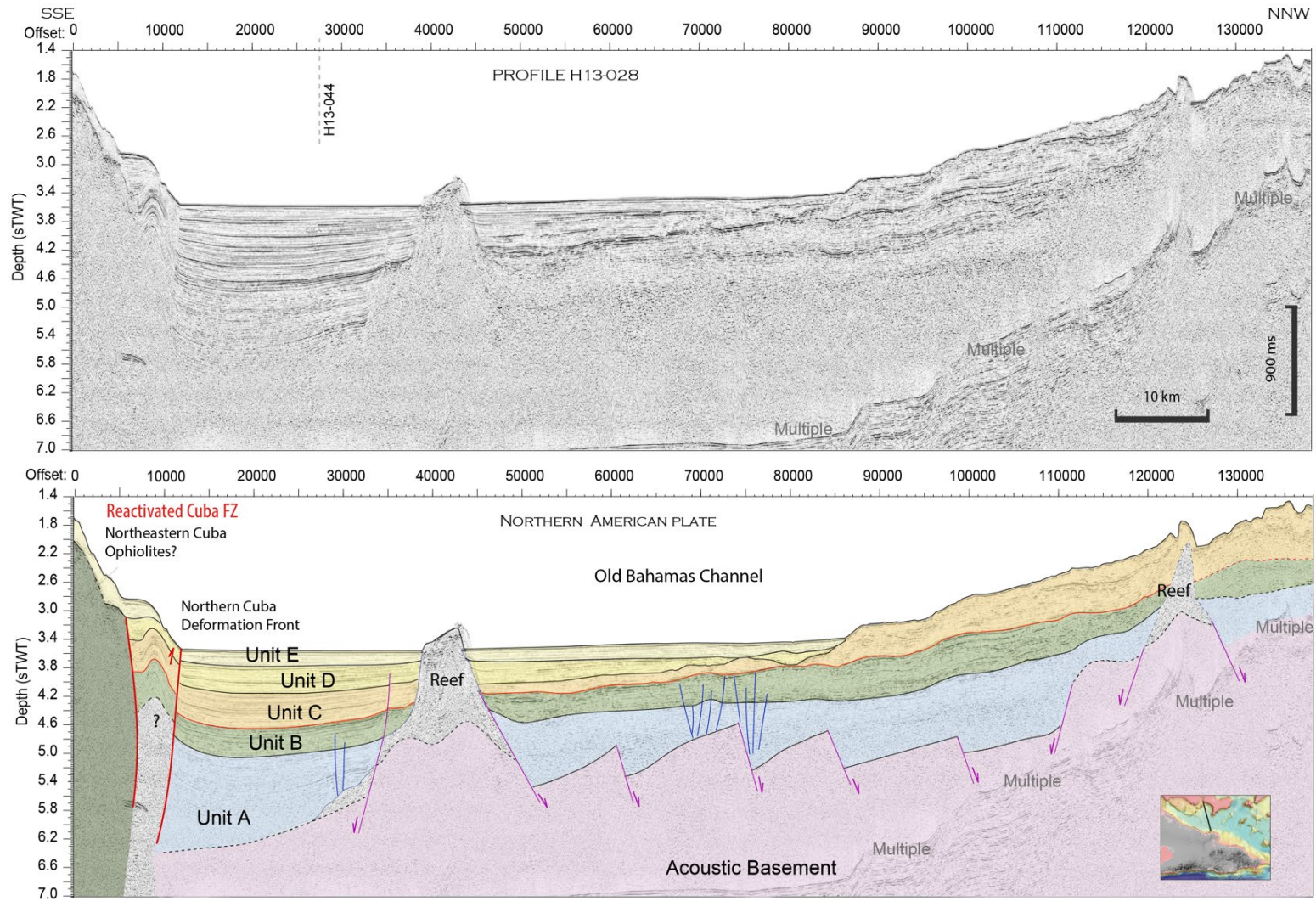


Figure IV.7. Seismic line H13-028. a) Multichannel seismic profile across the Old Bahamas Channel, oriented SSE-NNW, showing the abrupt contact between the seismic units A to D with a body towards the south we interpreted as the offshore part of the Northeastern Cuban ophiolites outcropping on land. MCU: Mid-Cretaceous Unconformity. See the seismic line location in the inset and in Figure IV. 4a.

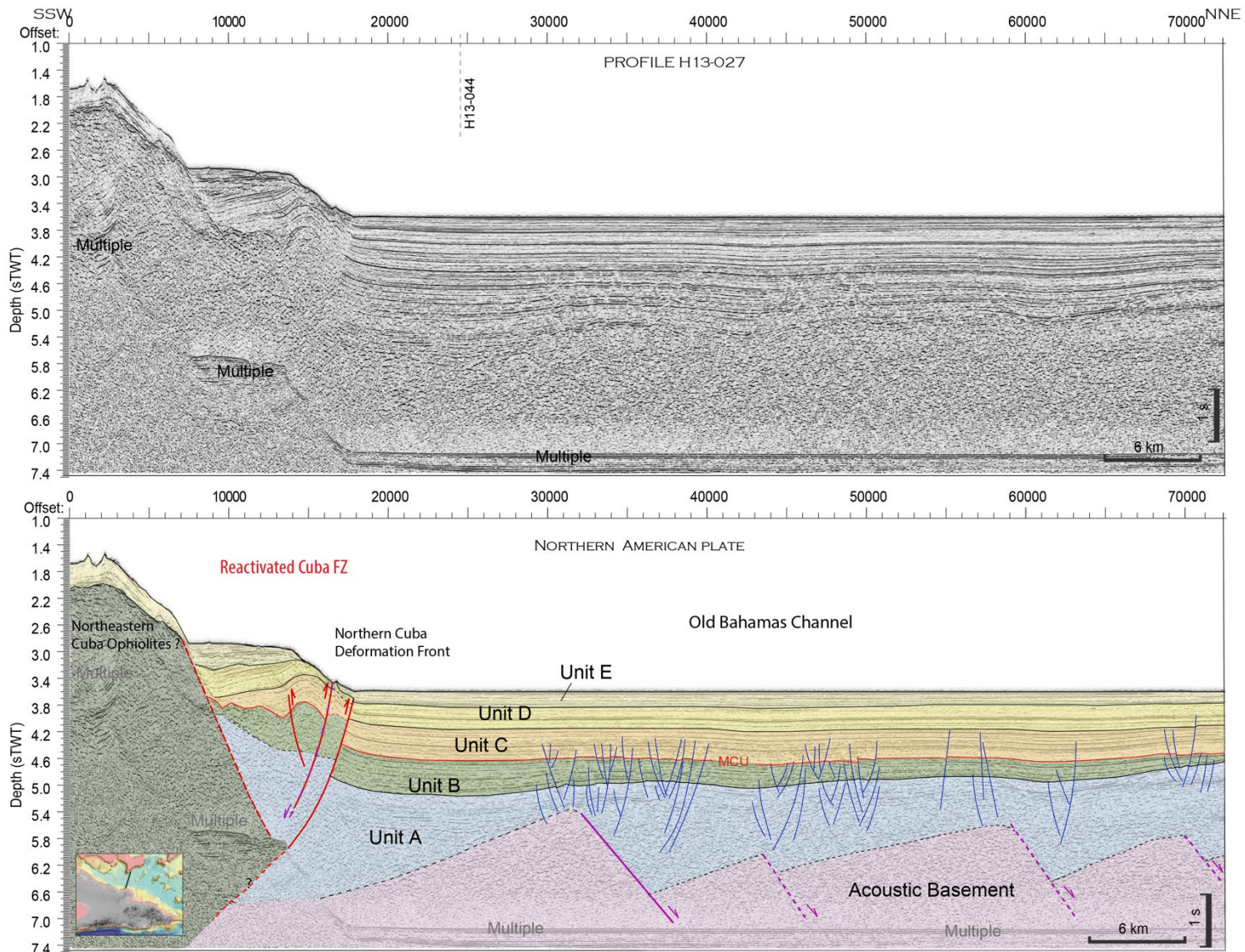


Figure IV.8. Seismic line H13-027. Seismic profile crossing the Old Bahamas Channel from SSW to NNE. MCU: Mid-Cretaceous Unconformity. See Figure IV. 4a and inset for the location of the profile.

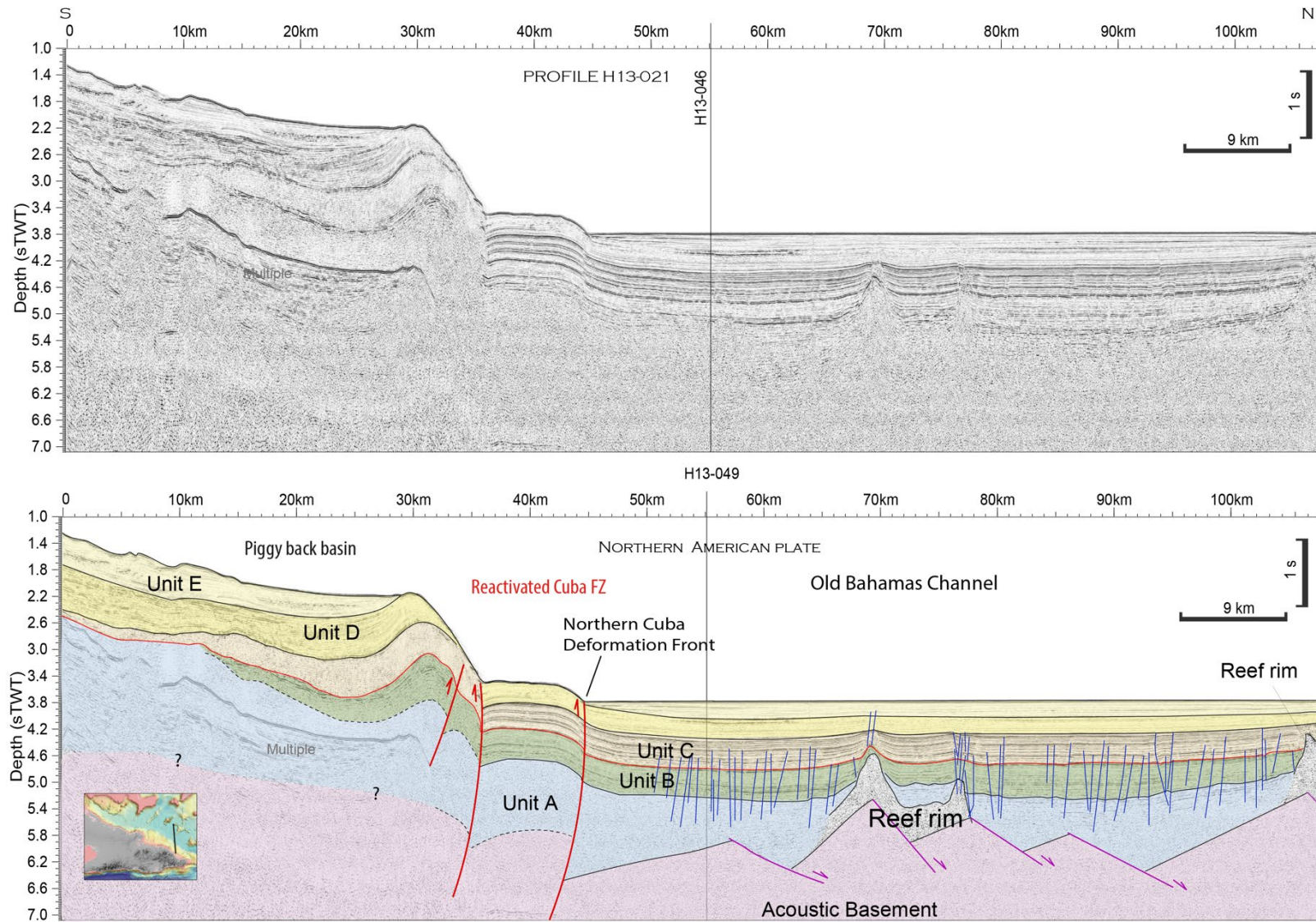


Figure IV.9. Seismic line H13-021. Seismic profile crossing the Old Bahamas Channel from south to north. MCU: Mid-Cretaceous Unconformity. See the inset and Figure IV.4a for the location of the profile.

IV.4.3.2 Thrust faults

Multibeam bathymetry over the insular slope shows one to three ridges displaying a WNW–ESE trend (Figure IV. 4c). This undulating surface morphology is mostly the expression of a narrow imbricate thrust belt where ridges are the surface expression of northward-verging fault-propagation folds along the offshore area adjacent to the Cauto-Nipe corridor (Figure IV. 5, km 35-50 and Figure IV. 9, km 35-45). Major frontal thrust faults at the insular slope base are inferred from the folded and faulted seismic units (Units A to D) in the Old Bahamas Channel.

In the offshore area at the toe of the insular slope, the thrust faults intersect the seafloor (Figures IV. 5, 7, 8 and 9). In contrast, towards the west, thrust fault tip points generally lie within Unit B (Figures IV. 10 and 11). In Figure IV.11, the folding of Unit B indicates contraction, implying the presence of buried thrusts within this unit. Deformation decreases upwards, with the upper Unit C barely folded. Note how the folding is less effective towards the West through Unit C in Figure IV.6. Anyhow, the folding is still ongoing in the eastern part of the study area, as shown in Figures IV. 7, 8, and 9.

Thrust faults along the Cauto-Nipe corridor deform the seismic units creating a typical contraction structure with asymmetrical hanging wall anticline and footwall, a large syncline ranging from 5 to 40km (Figure IV. 5). Note that Unit D thickens on the trough of the syncline while thinning on the crest of the anticline (inset in Figure IV. 5a), reflecting sedimentary response when the frontal thrust faults were active (Figure IV. 5, km 30-45). The complementary pairs of high-angle reverse faults bounding northward the Cauto- Nipe basin outlines a positive flower structure (Figure IV. 5, 35 km). The fault geometry and thickness variations that alternate in time and space may also suggest that this domain is a heavily sheared area that suffered from transtension and transpression before Unit D deposition along WNW–ESE-trending structures.

IV.4.3.3 Growth faults

The study area is affected by several steep growth faults that display both small normal and reverse offsets that locally converge at depth (blue lines in Figures IV. 5 and 8). Most of the faults die out downwards towards Unit A and seem directly correlated with the older normal faults disrupting the basement. The minor faults branches propagate upwards within Unit C, in the offshore area of the Eastern Cuban block and in the Bahamian domain (Figures IV. 5 to 10). Some of these faults extend over the tops of buried reefs and can impact the base of Unit D (Figures IV. 8 and 6).

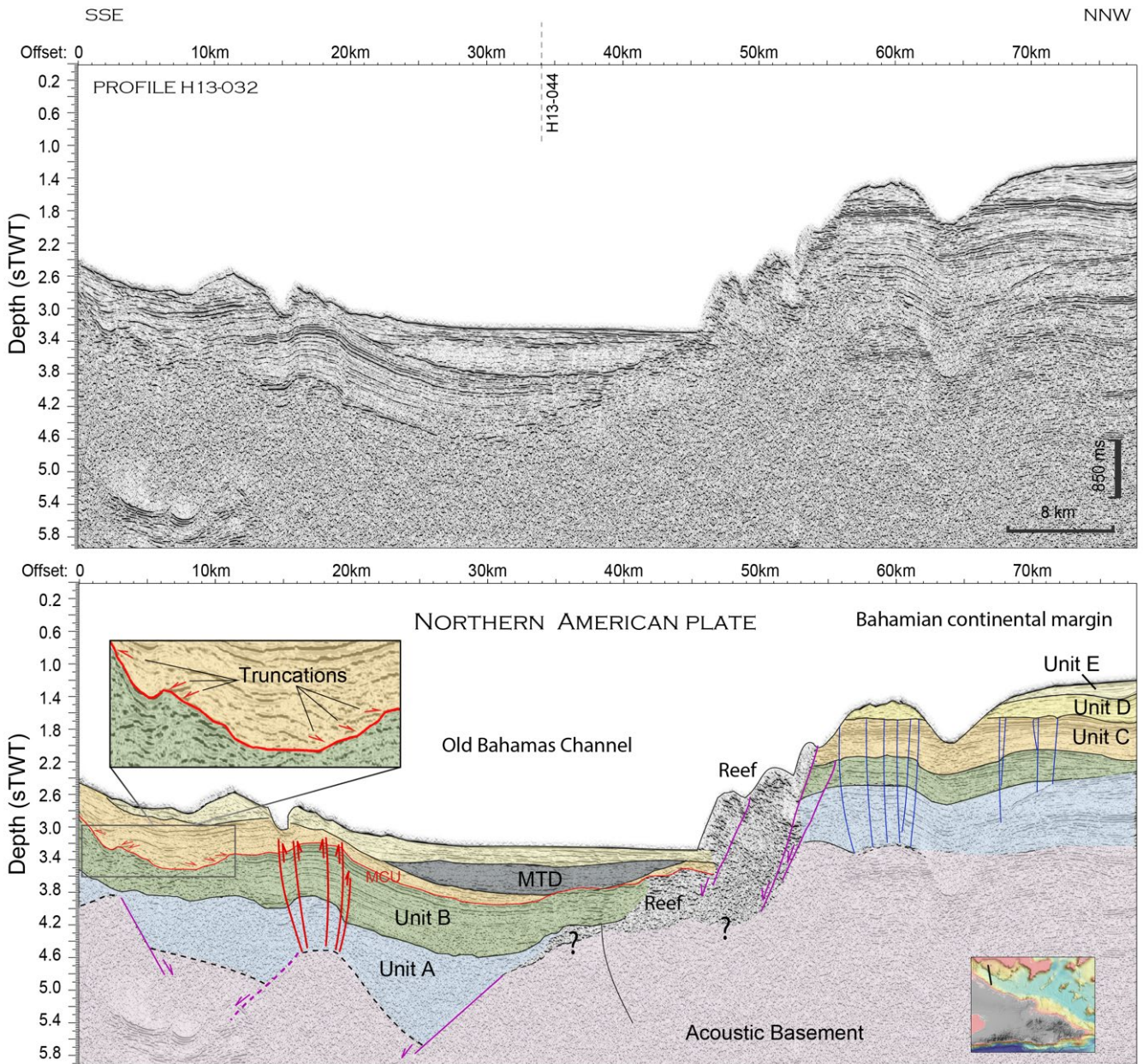


Figure IV. 10. Seismic line H13-032. Seismic profile crossing the Old Bahamas Channel from SSW to NNE. MCU: Mid-Cretaceous Unconformity. See the inset and Figure IV. 4a for the location of the profile.

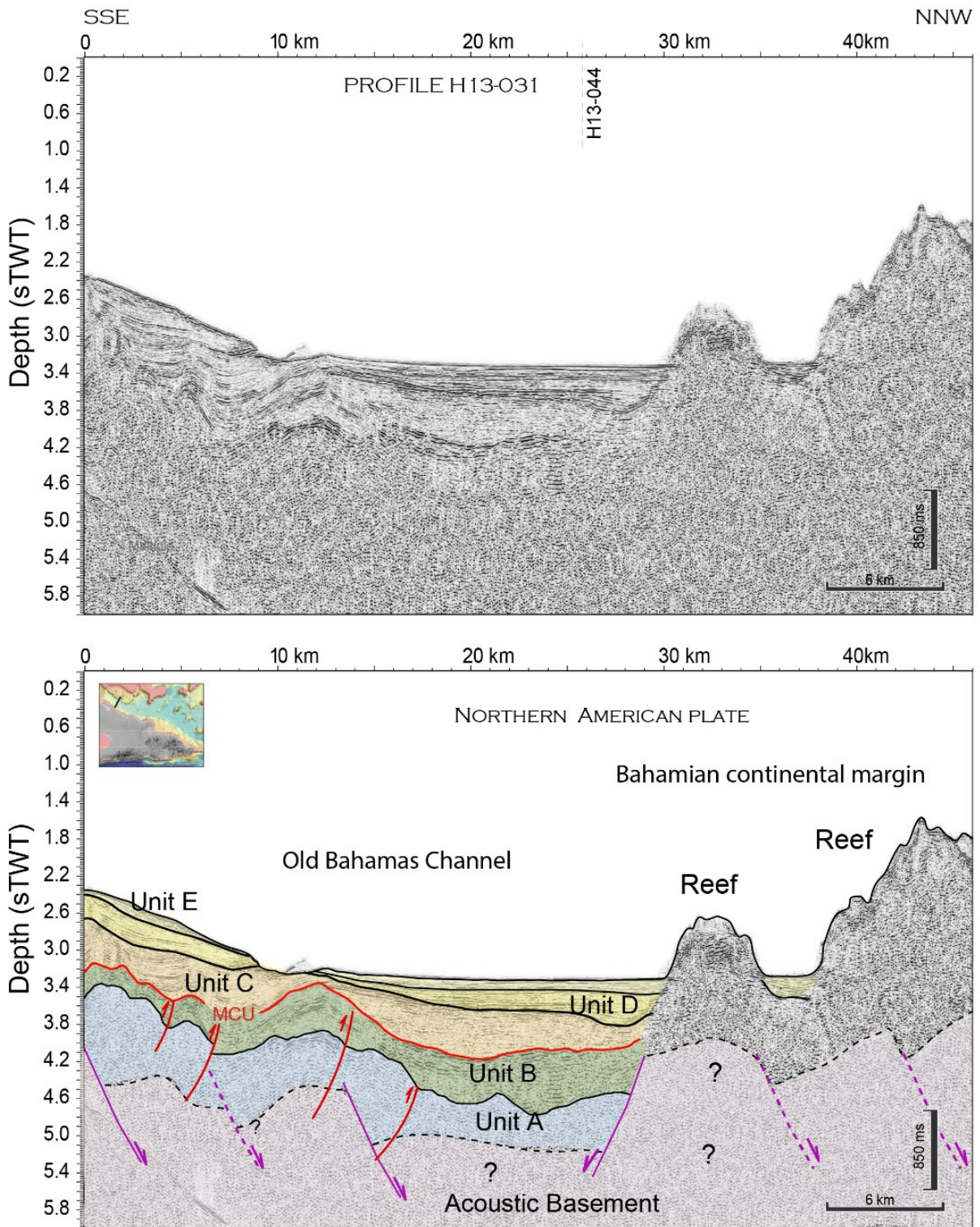


Figure IV. 11. Seismic line H13-031. Seismic profile crossing the Old Bahamas Channel from SSE to NNW. MCU: Mid-Cretaceous Unconformity. See the inset and Figure IV. 4a for the location of the profile.

IV.5. Discussion

IV.5.1 Age of Seismic Units

The stratigraphic framework for the offshore region of Western and Central Cuban blocks was proposed in several works based on outcrops in Cuba (Iturralde-Vinent, 1998; Caballero & Cabrera, 2003a, 2003b; Iturralde-Vinent et al., 2008; Cruz-Orosa et al., 2012; Vázquez-Taset et al., 2020) and in seismic data tied with industry offshore and onshore wells (Uchupi et al., 1971; Walles, 1993; Masafarro & Eberli, 1999; Moretti et al., 2003; Gaumet et al., 2004). However, the stratigraphic setting for the offshore Eastern Cuban block remains uncertain, and the limited availability of sediment cores poses a significant challenge to interpret the geological history of this region.

To determine the age of the sedimentary units in offshore Eastern Cuba, we reviewed the stratigraphic framework proposed in the literature and correlated it with our MCS data (Figure IV. 3). Time attributions were not directly assigned to the seismic units but were estimated based on the correlation of their facies and deformation patterns, possibly related to major paleo-geodynamic events in the Caribbean region (Iturralde-Vinent et al., 2016) (Figures IV. 2, 3, and 12).

IV.5.1.1 Unit A

Thickness variation in Unit A implies that it was formed in grabens and half-grabens that were actively subsiding and driven by phases of extension (see Figure IV. 5b). Half-grabens we also described in onshore outcrops in Western Cuba (e.g., San Cayetano Formation in Moretti et al., 2003). Masafarro and Eberli (1999) suggest that rifting in the southern Bahamas domain was controlled by several NW-striking strike-slip faults and NE extensional faults, which corroborates our structural interpretation showing similar NE-SW-striking normal faults separating tilted blocks (Figure IV. 4c).

Mullins & Lynts (1977) proposed that the deep-water channels surrounding and dissecting the Bahamas Carbonate Province are influenced by a northwest-southeast structural trend, which parallels the magnetic anomaly trends across the region. These channel patterns would correspond to the major fault pattern along the eastern continental margin of North America, resulting from the rifting of North America and Africa in the Early Jurassic (Sheridan, 1974a). In this case, the deep channels of the Bahamas are likely influenced and controlled by basement faults, as indicated by several studies (Talwani et al., 1960; Ball, 1967; Ball et al., 1968a, 1971; Lynts, 1970; Malloy and Hurley, 1970; Sheridan, 1971, 1974b; Glockhoff, 1973; Mullins & Lynts, 1976). The syn-sedimentary Unit A was probably deposited in half grabens and narrow basins formed during the former Pangea rifting phase (Figure IV. 2a). It is probable that the tilted blocks identified in seismic profiles offshore the Eastern Cuban block were formed during the Triassic-Jurassic interval (Figures IV. 2 and 12a).

Sedimentary rocks in eastern offshore Cuba should not be older than the Early Jurassic, or possibly Late Triassic, since the continents began to separate in the Middle Mesozoic. Thus, the syn-rift Unit A would have then a Jurassic age. This observation would be supported by offshore wells such as the Great Isaac well #1 (Jacobs, 1971; Iturralde-Vinent, 2003) (Figure IV. 1), which intercepted syn-rift facies, mostly Jurassic redbeds (most like Callovian age)

above crystalline basement rocks (Meyerhoff & Hatten, 1968, 1974). In Cuba, the oldest known sedimentary rocks of the Middle Jurassic age were observed on four salt diapiric structures (Cayo Coco area exposed at Punta Alegre (Collazo 1 well); La Isla de Turiganó, and near Loma de Cunagua (Tina 1 & 2 wells; Haczewski, 1976; Botton et al., 2016) (Figures IV. 3 and 12b).

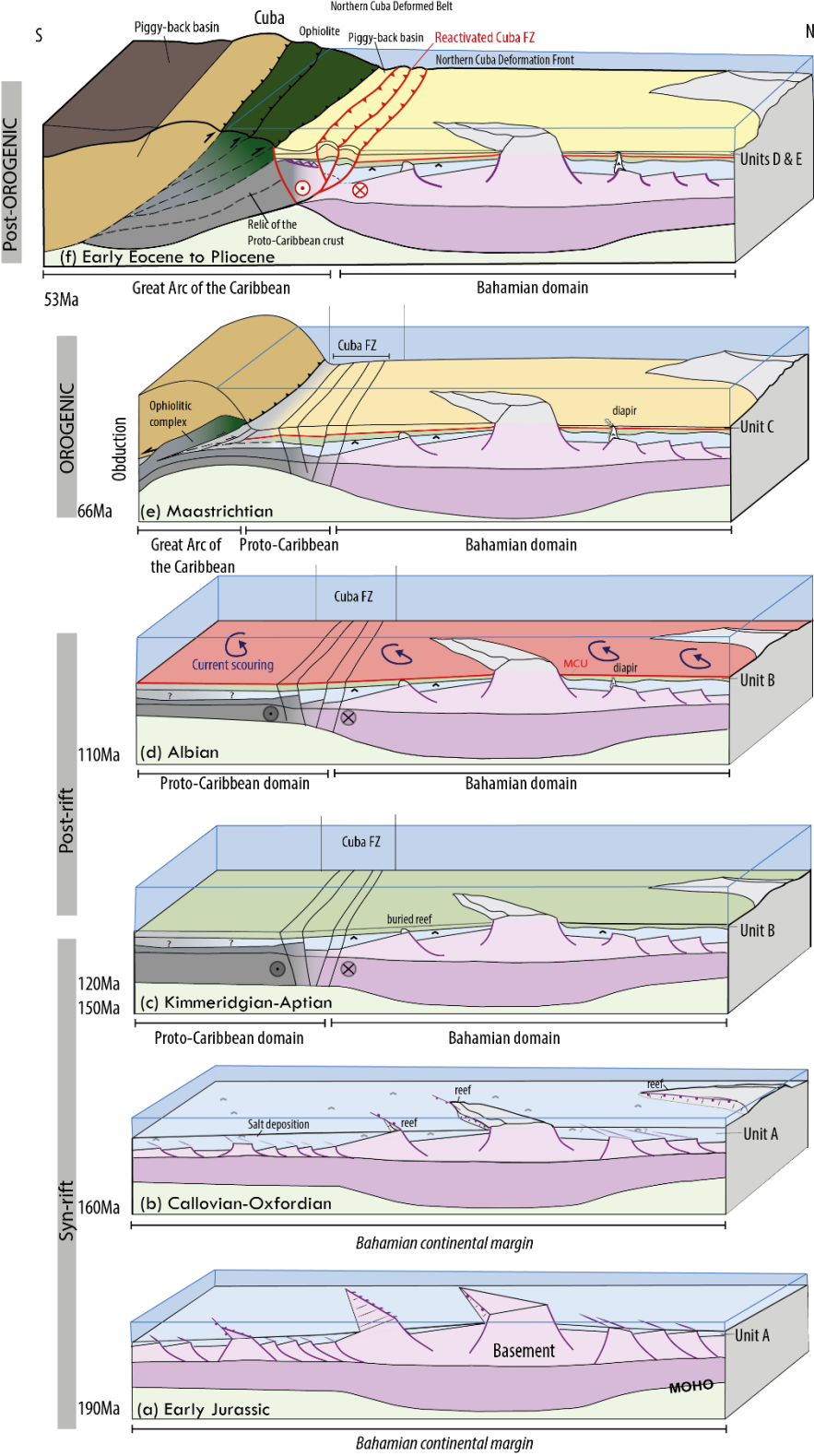


Figure IV. 12. Interpretative geodynamic model for the evolution of the Eastern Cuban Offshore area from Early Jurassic to Present-day. 3D geologic sketches are based on the H13-025 profile (Figure IV. 5) and paleo-reconstructions presented in Figure IV. 2. (a) During the Jurassic, Pangea rifting led to the development of NE-SW trending horsts and grabens in the proto-Caribbean and Bahamian continental margins. (b) The earliest carbonate banks of the Bahamas Carbonate Province were initiated as reefs accreted on the top of horsts and tilted blocks. (c) and (d) The emergence of the proto-Caribbean resulted in the creation of a Mid Jurassic-Lower Cretaceous Passive margin, which was later consumed by the subduction of the Proto-Caribbean crust. (e) In the late Cretaceous, the collision of the Caribbean plate with the North American plate formed the Cuban orogenic belt, a thrust system that transformed the Bahamas into a foreland basin. (f) During the Paleocene to Early Miocene, continuing northeastward migration led to regional uplift. The loading of the Cuban orogeny caused flexural drowning, which persisted until the Middle Eocene. By the Late Eocene, collision decreased, and the Cuban island arc became attached to the North American plate.

IV.5.1.2 Unit B

The peak of transgression during the Berriasian time resulted in a change from dolomitic facies to slope and basin carbonate deposits (Figures IV. 2d and 3) (Gaumet et al., 2004). During this time, restricted clastic inputs dominated western Cuba, with slope and basin carbonates being the primary facies association (Figure IV. 3) (ODP wells 535 & 540; Figure IV.1).

The seismic facies of Unit B could be correlated to the sequences of the Berriasian-Cenomanian interval in the study of Moretti et al. (2003). These series are similar in their seismic facies, characterized by high-frequency parallel reflectors that are coherent to transparent. It is likely that slope carbonate deposits also extended over the Eastern Cuban area during this time (Figure IV. 3), while shallow water build-ups persisted locally (as the reef rims showed in Figures IV. 5 and 6). The significant flooding event in the Berriasian time sealed all tilted blocks in Western and Central Cuba, resulting in the homogeneous deposition of deep carbonates over the Jurassic syn-rift (Gaumet et al., 2004). Hence, the Jurassic-Cretaceous boundary marks the end of the main syn-rift phase in the region, as the rifting in the southeastern Gulf of Mexico ceased (Figures IV. 2 and 3) (Gaumet et al., 2004).

The starvation of sediments resulted in erosion and non-deposition across Cuba, and Upper Cretaceous sediments were rarely deposited and preserved in the Gulf of Mexico and the Yucatan margin. A rough Post-Cenomanian unconformity called the "Mid-Cretaceous Unconformity – MCU" truncates the Early Cretaceous deposits in the Gulf of Mexico and Cuba (Gaumet et al. 2004; Moretti et al. 2003). In our MCS profiles, we image a rugged unconformity at the top of the Unit B, likely corresponding to the MCU (Figures IV. 5 to 11). The MCU represents a large hiatus of variable duration (Figure IV. 3). In some localities in the Gulf of Mexico, this hiatus spans almost the entire Late Cretaceous (Well 540, Schlager et al., 1984). In Cuba, MCU developed after the Late Cenomanian and continued until the Maastrichtian or later (Figure IV. 3) (Gaumet et al., 2004; Moretti et al., 2003). The MCU is a combined result of low sediment input, current scouring, and slumping on steep slopes along the Florida-Bahamas Platform (Schlager et al., 1984). However, the reasons for the prevailing non-deposition phenomenon from the Turonian up to the Campanian remain incompletely understood. The closure of the connection between the Pacific and the Proto-Caribbean by the Great Arc of the Caribbean likely caused palaeo-oceanographic changes, which may have led to the MCU regional hiatus (Figure IV. 2d) (Schlager et al., 1984; Malfait & Dickelman, 1972; Sykes et al., 1982; Gaumet et al., 2004).

IV.5.1.3 Units C, D, and E

Unit C recovered the MCU and was deposited in the Old Bahamas Channel as deep-sea sediments (high frequency, coherent, and parallel reflectors). It would consist of clastics and flysch deposited in the deeper part of the Cuban flexural (foreland) basin (Figure IV. 1b) (Gordon et al., 1997; Moretti et al., 2003; Cobiella-Reguera, 2009). The origin of the large MTD in Figures IV. 6 and 10 is likely associated with the sliding of a portion of Unit C. The MTD deposit displays a few discernible reflectors, suggesting that it comprises blocks likely derived from Unit C. The blocks may slide gradually during a folding phase caused by a collisional event.

Determining pre- and syn-orogenic strata related to the onset of collision indicates that sedimentary units preceding the deposition of Unit D are pre-orogenic strata. In contrast, Unit D is syn-orogenic (Figures IV. 3 and 5), while the continuous plan-parallel reflectors of Unit E indicate post-orogenic strata. This classification implies that the pre-orogenic units are at least as old as the Early Eocene (Figure IV. 3).

IV.5.2 Main structural and geological features

IV.5.2.1 Rifting of the Eastern Cuban Block

The Pangea rifting led to the development of NE-SW horst and grabens in the Proto-Caribbean and Bahamian continental margins during the Jurassic (Figures IV. 2 and 12; Salvador, 1987; Marton & Buffler, 1994; Pindell & Kennan, 2001; Padilla y Sánchez, 2016).

As extension proceeds and uplift occurs on the proximal margin, the differential vertical movement between the proximal and distal parts of the margin increases the slope of the margin. The tilted small blocks in domino observed on the top of the basement in the Cuban margin probably occurred at the end of the rifting along a decollement layer in the pre-rift series (Figure IV. 5b). Such destabilization of tilted block tops has already been observed and proposed on several continental margins in the Gulf of Aden and southern Somalia, for example (e.g., Autin et al., 2010; Sapin et al., 2023).

IV.5.2.2 Reef related to basement features and sea-level rises

The Bahamian highs corresponding to reefs in the studied region display a distinct NE-SW orientation, indicating that the tilted blocks supporting these reefs and the faults bounding them also have a NE-SW orientation (Figures IV. 4a and 4c). It would support the idea that carbonate bank deposition likely began concurrently with or shortly after the extensional phase ended. Likely, the growth of carbonate reefs occurred concurrently with the deposition of Unit A, as shown in Figures IV. 3, 5, and 6. Given the stratigraphic position of the reef rims in seismic profiles shown in Figures IV. 5, 9, and 11, the reef accretion likely developed on top of tilted blocks and ended in the Late Jurassic to the Mid-Cretaceous (Figure IV. 12c). This would agree with the 'Graben hypothesis' (Mullins & Lynts, 1977), in which the earliest carbonate banks may have initiated as reefs on the top of tilted blocks raised into the photic zone (Pindell, 1985).

The bathymetric data show that the carbonate banks of the Bahamas become deeper towards the south until they disappear in the Old Bahamas Channel (Figure IV. 4). Only a few carbonate banks outcrop in the Old Bahamas Channel, where most of these reefs are buried by Unit B, as in the seismic profiles shown in Figures IV. 6 and 9.

The rate of reef accretion depends on a range of environmental factors, including sea level changes, water temperature, nutrient availability, and ocean circulation patterns (Kuffner, 2018). During periods of sea level rise or tectonic subsidence, coral reefs may be able to keep pace by growing vertically to maintain their position relative to the water surface. However, if the rate of sea level rise or subsidence exceeds the rate at which the coral reef can grow vertically, the reef may become submerged and eventually die off (Kuffner, 2018). The reef burial asymmetry between the northeast and the southwest cannot be explained by a sea level variation that would have had a regional consequence. However, a subsidence rate more important in the south than the North could explain the burying of these features.

In the Aptian period, the Bahamas Platform underwent back-stepping due to eustasy and subsidence, as documented by Sanchez et al. (1999). Back-stepping of the southern region of the Bahamas platform is probably associated with the ongoing subduction of the Proto-Caribbean seaway under the Caribbean plate from the Middle to Late Cretaceous (Figures IV. 2 and 12). The subduction of the Proto-Caribbean crust beneath the Great Arc of the Caribbean during the Cretaceous period likely caused a flexure in the upper plate (Bahamian domain), which further accentuated subsidence in its southern domain. This process is evidenced by the deepening of the basement towards the south, resulting in increased subsidence in the southern area of the Old Bahamas Channel. The progressive burial of the Bahamian reefs in the southern part and the deepening of the top basement is likely the result of this flexural subsidence (as illustrated in Figures IV. 5 to 9).

The establishment of a deep basin environment during the Middle-Upper Cretaceous in the southern domain of the Bahamas platform is likely attributed to the flexural subsidence. This phenomenon probably caused the drowning of carbonate banks in the area and their subsequent burial during the Unit B deposition (Figures IV. 2d and 3).

IV.5.2.3 Evidence of salt

Some dome-shaped forms interpreted as buried reefs (features 1, 2, and 5 in Figure IV. 6) are geometrically similar to salt diapirs, with overlain sediment layers upturned (Figure IV. 6, in grey lines km 340 and km 360) and a localized deformation at the top layers by minor radial faults. In this case, the hypothesis of salt deposition during the extensional phase in the Eastern Cuba region (Figure IV. 2ab) would be evoked, supporting the idea of an evaporative basin where salt deposition occurred in the Old Bahamas Channel.

The salt occurrence in the Punta Alegre Formation in western Cuba (possibly Callovian age, e.g., Cousminer, 1957) implies that it is possible to find some salt deposition offshore Cuba. Salt diapirs outcropping on land in the Cayo Coco area (Figure IV. 1) are related to Jurassic evaporite deposits (Meyerhoff & Hatten, 1968; Bouton et al., 2016). This supports Pindell & Kenan (2001)'s interpretation that a second evaporite basin with lesser salt was deposited in the Bahamas domain during the Middle-Upper Jurassic under shallow water conditions (Figure IV. 2b).

Salt diapirs were previously reported offshore in the Bahamas mega-platform (Lidz, 1973; Ball et al., 1985). The hundreds of meters of evaporites found on Andros Island, Cay Sal Bank, and Doubloon Saxon deep wells (Figure IV. 1) would support the hypothesis that a Middle-Upper Jurassic evaporitic basin may extend until the Eastern Cuba area. In this case, the upper portion of Unit A would contain evaporitic layers that were subsequently mobilized as upward-moving salt as salt domes or along the flanks of buried carbonate reefs. Deformation patterns and upward domes, potentially salt diapirs, coming from Unit A suggest the earliest salt deposition in the Eastern Cuba area during this syn-rift phase. The upward bending of the onlap terminations against the flanks of the buried reefs implies that these reefs have either undergone upward displacement or that a highly viscous fluid rheology material has moved upwards along their flanks (Figures IV. 6 and 9).

However, the seismic resolution of our seismic lines cannot image these structures in detail. Moreover, considering the geometry of domes 1, 2, and 5, visible in Figure IV. 6, and their similarity and proximity to the buried carbonate banks, we prioritize the hypothesis of buried reefs to explain the origin of these structures.

IV.5.2.4 Structure and Deformation in Insular Slope: strike-slip, compression, reactivation

The appearance of a bi-vergent fold-and-thrust system similar to a positive flower structure downslope in the insular slope domain could be interpreted as a result of a compressional phase or due to the reverse reactivation of strike-slip faults formed at the onset of a contractional phase. However, the thickening of Units B and C in the insular slope domain, shown in Figures IV. 6 and 10, may have resulted from strike-slip deformation with an extensional component, possibly related to an ancient shear zone. This suggests the possibility of strike-slip activity during the deposition of Units B and C. During this period (Cretaceous), the study area was located on the Cuba FZ, which was considered the plate boundary between the Proto-Caribbean plate and the Bahamian domain (Central Atlantic domain, Figures IV. 2d-e and 12) (Klitgord et al., 1984).

In the offshore prolongation of the Cauto-Nipe tectonic corridor, Units B and C are marked by a variation in thickness which may be related to a transtensive play during their deposition (Figure IV. 4). This area may correspond to the ancient location of the NW-SE-oriented Cuba FZ, which was lately affected by the activity of the nearly E-W-oriented Cauto-Nipe Fault Zone (Figure IV. 2f). The reactivation of these ancient shear faults during a contractional phase would result in the formation of a flower structure at the deformation front (Figures IV. 5, 8 and 12).

The reactivation of faults is likely associated with a reorganization of the regional stress regime (Bellahsen et al. 2006). This change in the stress regime is also manifested by the presence of minor faults that affect Unit C in the Old Bahamas Channel (shown as blue faults in Figures IV. 5 and 6). These minor faults exhibit both normal and reverse offsets that converge at depth. Most of these faults terminate downward towards Unit A and appear to be directly correlated with older normal faults, suggesting that they are also linked to the stress reorganization that occurred at the beginning of the Unit C deposition. However, their activity diminishes as Unit C is deposited, and they appear to be no longer active during the deposition of Unit D. This plate reorganization could be associated with the end of the subduction of the

Proto-Caribbean oceanic plate and the consequent extinction of the Cuba fracture zone (Figure IV. 2e, Paleo-geodynamic events inset in Figure IV. 3).

Sedimentary units up to Unit E exhibit folding and the northern boundary of the insular slope is delineated by several imbricated thrusts. These features suggest that a period of contractional activity affected the sedimentary record in the Old Bahamas Channel and, in particular, at the northern boundary of the insular slope indicating a deformation front to the north.

Analysis of pre- and syn-orogenic strata shows that Units A, B, and C are pre-folding strata, while Unit D represents syn-folding strata (Figure IV. 5). The folding mechanism that affected Units A, B, and C created an anticline ridge along the hanging wall frontal thrust and a syncline on top of the moving thrust sheet, forming a piggyback basin that runs alongside the continental slope. This basin extends from the offshore region of the Cauto-Nipe tectonic corridor and eastward until the Windward Passage area (Figures IV. 4, 5, and 9). This piggyback basin trapped the syn-orogenic deposition of Unit D. These compressive features could follow the end of the subduction of the Proto-Caribbean oceanic plate when the Cuba Fracture Zone was located against the deformation front (Figure IV. 2e) and associated with the start of the Great Arc of the Caribbean- Bahamian collision phase (Figures IV. 2f and 12).

IV.5.3 Geological evolution of the Old Bahamas Channel, Eastern Cuba Block

The geological history of the Eastern Cuba Block has been shaped by various geodynamic events, including the syn-rift and post-rift phases, the syn-tectonic orogenic phase, the post-orogenic phase and the cumulative effect of shear episodes (Bahamas, Cuba, Cauto-Nipe Transfer/Transform/Fracture Zones) (Figures IV. 2, 3, and 12). The stratigraphic findings discovered in Eastern offshore Cuba could be interpreted within the context of these events, as discussed in the following sections.

IV.5.3.1 Post-rift phase

Unit B is relatively isopachous and deposited as a draping sequence without tectonic activity, indicating the end of an extensional phase. This unit, along with the younger units above it, is characterized by high-frequency, coherent, and parallel reflectors that are typical of deep basin environments. The hypothesis may be that the extensional phase is followed by a water depth increase due to subsidence and/or a sea level rising creating space for the deposition of Unit B. This vertical movement impacted the vertical growth of some reefs that were unable to keep up their vertical accretion, leading to their abandonment and eventual burial during Unit B deposition (Figures IV. 6 and 9).

The Bahamas Carbonate Province was likely well-developed during the Upper Kimmeridgian period, with carbonate platforms extending southwards, partially documented in the Cayo Coco Fm. in Central Cuba (Gaumet et al., 2004) (Figure IV. 2c). However, the subsequent drowning phase during the Tithonian time resulted in a regional transgression giving place to deep carbonatic deposits (Gaumet et al., 2004).-The deepening trend during the Upper Tithonian made more connections between the Gulf and Proto-Caribbean domains (Figure IV. 2). According to Uchupi (1971), the reefal-lagoonal deposits in the southeastern Bahamas diminished as the region began to subside during Early Cretaceous times. Therefore, channels

became deep, and some ancient reefs were buried (Figures IV. 6, 9, and 12d). However, some reefs eventually were perpetuated by reef growth, as in Figures IV. 5, 6, and 11, giving rise to the current "bank-through" morphology of the Bahamas (Figures IV. 1 and 2c).

The progressive drowning of the Bahamas platform led to the formation of a deep marine seaway (Gaumet et al., 2004). Since then, several deep marine seaways have continued to dismember the Bahamas Carbonate Province contributing together with tectonics the actual bank configuration. The slope of the banks is characterized by strong bottom currents, including turbidites and contourites, and features channelized systems. At the toe of the bank slope, intense current scouring eroded the sedimentary record (see "starved basin and MCU" in Figure IV. 3). Our seismic profiles suggest that the MCU may correspond to the top erosional unconformity of Unit B, unconformity due to the activity of these bottom currents, particularly in the western area of the Old Bahamas Channel (Figures IV. 6, 10, and 11). However, towards the east, this unconformity shows less evidence of erosion and is likely more related to a non-deposition hiatus (Figure IV. 6). It is possible that the eastward basin was deeper than its westward continuity during the Cretaceous period, as the Cuban basins started to deepen after the Aptian (Moretti et al., 2003).

IV.5.3.2 Orogenic phase

In the Upper Cretaceous, the Proto-Caribbean Seaway was closed, leading to the reactivation of the Cuba Fracture Zone, the obduction of the ophiolitic complex, and the collision between the Great Arc of the Caribbean and the Bahamian domain (Figures IV. 2, 3, and 12ef). Pre-existing Bahamas and Cuba Jurassic faults certainly played an important role in the style of deformation generated by the Cuban convergent orogeny.

Eastern Cuba experienced an obduction process during the Maastrichtian (Ophiolitic domain of Holguín and Mayari-Sagua-Baracoa Mountains, shown in Figure IV. 4a,b). On the seismic lines crossing the insular slope off Holguín province (Figures IV. 7 and 8), seismic units are shown overlying a thick chaotic body, which could be interpreted as the offshore continuation of the Ophiolitic complex in the Northeastern Cuban block (Figure IV. 12e).

During the Late Cretaceous (Maastrichtian)/Early Paleocene, the Bahamas Carbonate Province became involved in the Caribbean-American collision (Figure IV. 2e) (Ross & Scotese, 1988; Masferro & Eberli, 1999; Mullins & Sheridan, 1983; Mullins, 1984; Pindell & Barrett, 1990; Mann and Burke, 1990; Mann et al., 1995; Leroy et al 2000; Boschmann et al., 2014).

According to Massafero and Eberli (1999), this reorganization of the stress regime caused the reactivation of Jurassic faults and, in particular, the major Cuban Transform Fault, which is interpreted in this study as being located at the plate boundary between the Proto-Caribbean plate and the Bahamian domain (Central Atlantic domain, Figures IV. 2e and 12d-e). Individual faults branched out from the deep basement resulting in localized deformation at the toe of the insular slope (Figure IV. 5, km 30-45). Ancient faults were also reactivated in the Cretaceous carbonate platform, and the southern Bahamas underwent fragmentation (see Figure IV. 10, km 45-55 and, Figure IV. 11, km 28-45) (Klitgord et al., 1984; Ladd & Sheridan, 1987; Sheridan et al., 1988).

The collision of the Great Arc of the Caribbean with the Bahamas Carbonate Province resulted in a drastic reorganization of the northern boundary of the Caribbean plate. The collision resulted in the formation of the Cuban orogenic belt, characterized by a thrust system, and turned the Bahamas region into a foreland basin. Consequently, the Bahamas' southern margin was diachronically imbricated in thrusts (Moretti et al., 2003; Saura et al., 2008; Stanek et al., 2009). As a result, a fold-and-thrust belt developed in northern Cuba (Iturralde-Vinent et al., 2008). The accreted belts extend parallel to the axis of the Island (Kerr et al., 1999). The steep margin that rimmed the northern coast of Cuba follows the same thrust front separating the thrust belt from the deep flexural basin northward (the Old Bahamas Channel). Cuban fold-and-thrust belt moves from West to East, with the earliest deformation (Maastriachian-Palaeocene) occurring in western Cuba and the youngest (Middle Eocene) deformation occurring to the east in eastern Cuba (Figure IV. 2f to 2i) (Iturralde-Vinent, 1998; Vázquez-Taset et al., 2020).

The MTDs recorded in the Old Bahamas Channel support this diachronism, as they are younger towards the east (Figure IV. 6). Our observations suggest that MTDs strongly correlate to ongoing collision in the eastern Cuban block. As the collision starts earlier towards the west, the MTDs are recorded at the Paleocene-Early Eocene (Figure IV. 6, km 20-100 and, Figure IV. 10, km 20-45). However, as the collision progresses eastward and culminates in the collision of the paleo-arc terranes in Eastern Cuba against the paleo-margin of the Bahamas in the Middle Eocene (Quintas et al., 1994; Cazañas et al., 1998), the MTDs are recorded later in the eastern part of the Old Bahamas Channel (likely in the Middle Eocene, Figure IV. 6, km 300-420). MTDs in the study area may illustrate periods of intense tectonic activity accompanied by seismicity and high sedimentation rates offshore due to onshore erosion.

The pre-orogenic strata of Units A, B, and C have folded along the hanging wall frontal thrust, forming an anticline ridge illustrated in Figure IV. 5. This folding mechanism has resulted in the development of a syncline on top of the moving thrust sheet, which is a common mechanism for forearc basins (Noda, 2016). This process has given rise to a stretched basin that runs parallel to the continental slope, contributing to the present morphology of the insular slope in the Eastern block (Figure IV. 4b). We interpret this depression as a minor piggyback basin that has trapped the syn-orogenic deposition of Unit D (Figure IV. 12f). The syn-tectonic wedge shape of Unit D suggests that its deposition occurred concurrently with the development of the syncline.

The widening of the insular slope and its current morphology would be related to establishing this piggyback basin on the northeastern Cuban coast (Figure IV. 4b). The basin extends westward from the offshore region of the Cauto-Nipe tectonic corridor until the Windward Passage area (Figure IV. 4a). According to Oliveira de Sá et al. (2021), the Windward Passage structure is associated with the emplacement of a piggyback basin during the Late Eocene. The diachronous collision with the Bahamas Carbonate Province probably created this piggyback basin that extends eastward.

The asymmetry observed in the deformation pattern between the west and east domains of the Old Bahamas Channel could be explained by the presence of blocks with different rheologies as the rigid Bahamas platform, which may lock the subduction, the shear propagation and lead to collision in a scissors-like manner from west to east (Figures IV. 2d, e).

IV.5.3.3 Post-Orogenic phase and shear zone jumps

According to Mann et al. (1995), Leroy et al. (2000), and recently synthesized by Wessels (2019), there was a shift in relative motion between the Caribbean and the North American plates from NNE during the Maastrichtian period to E during the Middle Eocene period. This change in relative motion led to the formation of NE-SW-oriented left-lateral strike-slip faults and caused the thrust belt to fragment. This was caused by the eastward escape of the Caribbean plate and the presence of the Bahamas rigid block (Figure IV. IV.12f to i). Several studies have documented this process, including Rosencrantz (1990), Mann et al (1995); Gordon et al. (1997), Leroy et al. (2000), Pubellier et al. (2000), and Rojas-Agramonte et al. (2006), Oliveira de Sa et al. (2021).

The onset of the Cauto-Nipe fault zone is Middle-Late Eocene (Leroy et al., 2000; Rojas-Agramonte et al., 2008; Vázquez-Taset et al., 2020) forming a sedimentary basin that separates the two ophiolite massifs exposed in eastern Cuba (Holguín and Northeastern Cuban (Mayari-Sagua-Baracoa) ophiolites; Figures IV. 2, 4 and 5). The deformation front corresponds in this place to this zone (Figures IV. 4 and 5). The strata in the Old Bahamas Channel were probably folded during the Early Eocene during the collision of Cuba with the Bahamas Carbonate Province. The youngest strata of the topmost Unit E (post-orogenic strata) are not folded, testifying to a calmer tectonic phase or a localized one. This phase might be related to the Eastern Cuban microplate displacement that could not continue northeastward, ending the tectonic activity in the Cauto-Nipe fault zone during the upper Oligocene (Oliveira de Sa et al., 2021).

In the uppermost Lower Eocene, the oceanic seafloor spreading of the Cayman through halted volcanic activity in Sierra Maestra (Figure IV. IV.2f, Unit D). During the Middle Eocene period, Eastern Cuba underwent a significant geological change (Figure IV. IV. 2g, Unit D). During this time, this block was characterized by shallow basins where volcanogenic molasses accumulated, while to the North, a deep basin developed with deposits of fine-grained tuffs. However, deep seas were prevalent in Eastern Cuba during the Middle Eocene.

During the Middle/Late Eocene period, the collision stopped as the Oriente Fault emerged (Figure IV. IV.12h), causing the separation of Eastern Cuba's terrain from the surrounding region and joining it with the North American plate (Oliveira de Sa et al., 2021). This occurrence is supported by seismic sections, which depict the cessation of tectonic activity through horizontal seismic reflections in the topmost layer, known as Unit E (refer to Figure IV. IV. 12). Nevertheless, some faults affect relatively recent seismic reflections, suggesting the possibility of ongoing tectonic activity localized on the deformation front as shown by seismic activity and the still active uplift of the Cuba coast (Authemayou et al., 2023; Calais et al., 2023) (refer to Figures IV. 4b, 5, 8, and 9).

IV.6. Summary and conclusions

Our results reveal that the Old Bahamas Channel, Cuba's insular slope, and south Bahamas Carbonate Province experienced multiple phases of deformation since the Jurassic, linked to the complex plate boundary evolution. The presence of normal faults bounding tilted blocks indicates an earlier extensional phase, while the occurrence of thrust faults and folds overprinting these structures along the Cuban margin suggests a subsequent contractional phase

with local inversion. Additionally, the presence of wrench faults nucleated in pre-existing structures implies a shear component.

Syn-sedimentary faulting during the rifting phase resulted in tilted blocks and deposition of syn-rift Unit A in the Jurassic period. Carbonate reef accretion in the Southeastern Bahamas began concurrently with or shortly after the syn-rifting phase ended. Earliest carbonate banks initiated as reefs on top of tilted blocks raised into the photic zone during the subsequent drowning phases.

Some buried carbonate reefs could show deformation patterns at their top, which may resemble diapirs and could suggest early salt deposition in Eastern Cuba. Perhaps, during the Callovian period, a scenario emerged wherein a constrained influx of waters was initiated due to plate reorganization, and as the North America and South America/Africa plates underwent increased separation, it gave rise to potential water pathways leading into the Proto-Caribbean margin, both from the Pacific and conceivably from the Atlantic. Is there a potential connection between the salt deposits in the offshore Eastern block of Cuba and the hypersaline basin formation in northern Cuba during the Callovian era, and could this be related to salt deposition in the Gulf of Mexico?

During the Late Jurassic-Early Cretaceous period (post-rift phase), the Proto-Caribbean margin was characterized by shear zones and basement hinge zones. The Cuba FZ separated the Proto-Caribbean Ocean from the Bahamian margin, which was the composite of the North of Cuba and the Bahamas at this time. The Cuba FZ likely formed due to the activation of shear zones along the reactivation of faults that tilted the underlying Triassic-Early Jurassic basement.

The Bahamian margin was a relatively stable tectonic domain characterized by a deep basinal environment from the Middle-Upper Cretaceous until the Proto-Caribbean oceanic crust was entirely consumed beneath the Caribbean plate, leading to the collision of the northern border of the Caribbean plate with the Bahamas domain. This collision led to folding, shortening, and localized salt upwelling along the flanks and atop the Bahamian buried reefs offshore the Eastern Cuban block. This collision resulted in the welding of Cuba to the North American plate and played a significant role in establishing the current configuration of the Caribbean. These changes also resulted in the establishment of the northeastern Cuban Ophiolites.

The reactivation of ancient Jurassic faults played an important role in the offshore positioning of the northern limit of the Caribbean plate during the Middle Eocene. The present-day frontal deformation at the insular slope corresponds to the cumulative tectonic processes of the Cuba Fracture zone, then the Cauto-Nipe tectonic corridor. Indeed, the offshore placement of the Cauto-Nipe strike-slip system probably corresponds to the ancient Cuban TF, which represents a crustal barrier during the collision of the Eastern Cuban Block with the North American plate. The collision ceased during the Middle to Late Eocene with the development of the Oriente fault, linking Eastern Cuba's terrain to the North American plate. However, reverse faults at the deformation front affect the seafloor, suggesting a potential ongoing localized tectonic activity offshore the Eastern Cuban block.

Our findings contribute to understanding the geological history of the Eastern Cuban block, providing valuable insights into the region's tectonic evolution despite limited sediment

core availability and stratigraphic framework uncertainties. The tectonic history of Eastern Cuba has been shaped by a variety of processes related to tectonic plate interactions, including rifting, subduction, strike-slip and transfer fault zones, collision, and obduction. These processes linking the Central Atlantic, Gulf of Mexico, Proto-Caribbean, and Caribbean plates have resulted in distinct geological features that can be observed in the present-day offshore basement and sedimentary records.

Further research, including acquiring additional seismic data and sediment cores, is essential to refine our understanding of the tectonic evolution and its influence on the sedimentary record in this region. The ages provided by our study should be utilized in future research to establish better correlations between Eastern Offshore Cuba and other Cuban blocks.

Acknowledgments:

We thank Captain Moimeaux, the crews and technicians of the RV L'Atalante (IFREMER/GENAVIR), and the scientific team. We are indebted to the French Embassies in Haiti, Bruno Asseray, Cuba, Aurelie Nogues, and Oliver Tenes. We also thank the local authorities, as well as Daysarih Tapanes Robau from CITMA, Claude Prepetit from BME, and R. Momplaisir, D. Boisson, and J. Jadotte from UEH. We thank Dr. Bernard Mercier de Lépinay for his precious time and helpful comments. A. Oliveira de Sá is supported by funding from Sorbonne University.

IV.7 References

- Andó, J., Kosék, M., & Rios-Martinez, Y. (1996). Caracterización general de la asociación ofiolítica Holguín-Moa y el papel de las ofiolitas en el desarrollo estructural de Cuba. *Minería y Geología*, 7(1), Article 1.
- Applegate, A. V. (1984). Brown Dolomite Zone of Lehigh Acres Formation (Aptian) in South Florida--a Potentially Prolific Offshore Producing Zone. *AAPG Bulletin*, 68(9), 1209-1209.
- Authemayou, C., Nuñez, A., Pedoja, K., Peñalver, L., Chauveau, D., Dunán-Avila, P., Martín-Izquierdo, D., de Gelder, G., Husson, L., Castellanos Abella, E., Benítez Frómata, P. de J., & Pastier, A.-M. (2023). Oblique Collision of the Bahamas Platform at the Northern Boundary of the Caribbean Plate Recorded by the Late Cenozoic Coastal Terraces of SE Cuba. *Tectonics*, 42(8). <https://doi.org/10.1029/2023TC007806>
- Ball, M. M., Martin, R. G., Bock, W. D., Sylwester, R. E., Bowles, R. M., Taylor, D., Coward, E. L., Dodd, J. E., & Gilbert, L. (1985). Seismic Structure and Stratigraphy of Northern Edge of Bahaman-Cuban Collision Zone. *AAPG Bulletin*, 69(8), 1275-1294. <https://doi.org/10.1306/AD462BD2-16F7-11D7-8645000102C1865D>
- Bellahsen, N., Fournier, M., d'Acremont, E., Leroy, S., & Daniel, J. M. (2006). Fault reactivation and rift localization : Northeastern Gulf of Aden margin. *Tectonics*, 25(1). <https://doi.org/10.1029/2004TC001626>
- Boschman, L. M., van Hinsbergen, D. J. J., Torsvik, T. H., Spakman, W., & Pindell, J. L. (2014). Kinematic reconstruction of the Caribbean region since the Early Jurassic. *Earth-Science Reviews*, 138, 102-136. <https://doi.org/10.1016/j.earscirev.2014.08.007>
- Bryant, W. R., Meyerhoff, A. A., Brown, N. K., Jr., Furrer, M. A., Pyle, T. E., & Antoine, J. W. (1969). Escarpments, Reef Trends, and Diapiric Structures, Eastern Gulf of

- Mexico1. *AAPG Bulletin*, 53(12), 2506-2542. <https://doi.org/10.1306/5D25C971-16C1-11D7-8645000102C1865D>
- Burke, K., Cooper, C., Dewey, J. F., Mann, P., & Pindell, J. L. (1984). Caribbean tectonics and relative plate motions. *162*, 31-64. <https://doi.org/10.1130/MEM162-p31>
- Caballero, F. Q., & Cabrera, E. C. (2003a). Estratigrafía y paleogeografía del límite Eoceno Inferior-Eoceno Medio en el terreno Cuba oriental y en la Cuenca Cauto-Nipe. *Revista Geológica de América Central*, 29, Article 29. <https://doi.org/10.15517/rgac.v0i29.7772>
- Caballero, F. Q., & Cabrera, E. C. (2003b). Geological evolution of the Caribbean region; A plate-tectonic perspective. *Geological evolution of the Caribbean region; A plate-tectonic perspective*, 21-34.
- Calais, E., Gonzales, O., Arango-Arias, E. D., Moreno, B., Clares, R. P., Cutie, M., Diez, E., Montenegro, C., Roche, E. R., Garcia, J., Castellanos, E., & Symithe, S. (2023). Current Deformation Along the Northern Caribbean Plate Boundary from Gns Measurements in Cuba. <https://doi.org/10.2139/ssrn.4537779>
- Cobiella-Reguera, J. L. (2009). Emplacement of the northern ophiolites of Cuba and the Campanian-Eocene geological history of the northwestern Caribbean-SE Gulf of Mexico region. *Geological Society, London, Special Publications*, 328(1), 315-338. <https://doi.org/10.1144/SP328.13>
- Cobiella-Reguera, J. (2005). Emplacement of Cuban Ophiolites. *Geologica acta: an international earth science journal*, ISSN 1695-6133, Vol. 3, No. 3, 2005, pags. 273-294, 3.
- Cousminer, H. L. (1957). Palynological determination in Tina 1 Well. Hatten, Ch. W.: O. E. Schooler; N. R. Giedt; y A. A. Meyerhoff. *Geology of Central Cuba, Eastern Las Villas and Western Camagüey, Provinces, Cuba*.
- Cruz-Orosa, I., Sàbat, F., Ramos, E., Rivero, L., & Vázquez-Taset, Y. M. (2012). Structural evolution of the La Trocha fault zone : Oblique collision and strike-slip basins in the Cuban Orogen. *Tectonics*, 31(5). <https://doi.org/10.1029/2011TC003045>
- Diebold, J., Stoffa, P., Buhl, P., & Truchan, M. (1981). Venezuela Basin crustal structure. *Journal of Geophysical Research*, 86, 7901-7923. <https://doi.org/10.1029/JB086iB09p07901>
- Echevarria-Rodriguez, G., Hernandez-Perez, G., Lopez-Quintero, J. O., Lopez-Rivera, J. G., Rodriguez-Hernandez, R., Sanchez-Arango, J. R., Socorro-Trujillo, R., Tenreyro-Perez, R., & Yparraguirre-Pena, J. L. (1991). Oil and Gas Exploration in Cuba. *Journal of Petroleum Geology*, 14(2), 259-274. <https://doi.org/10.1111/j.1747-5457.1991.tb00311.x>
- Epstein, S. A., & Clark, D. (2009). Hydrocarbon potential of the mesozoic carbonates of the Bahamas. *Carbonates and Evaporites*, 24(2), 97-138. <https://doi.org/10.1007/BF03182088>
- Gaumet, F., Letouzey, J., & Sanchez, J. R. (2004). Paleogeographic Evolution of the Southeastern Region of the Gulf of Mexico (NW Cuba – Deep Waters). *AAPG International Conference, Cancun, Mexico*.
- Giunta, G., & Orioli, S. (2011). The Caribbean Plate Evolution : Trying to Resolve a Very Complicated Tectonic Puzzle. <https://doi.org/10.5772/18723>
- Gordon, M. B., Mann, P., Cáceres, D., & Flores, R. (1997). Cenozoic tectonic history of the North America-Caribbean plate boundary zone in western Cuba. *Journal of Geophysical Research: Solid Earth*, 102(B5), 10055-10082. <https://doi.org/10.1029/96JB03177>
- Haczewski, G. (1976). Sedimentological reconnaissance of the San Cayetano Formation : An accumulative continental margin in the Jurassic of western Cuba. *Acta geologica Polonica*, 26, 331-357.

- Hu, H. Y., Stern, R. J., Rojas-Agramonte, Y., & Garcia-Casco, A. (2022). Review of Geochronologic and Geochemical Data of the Greater Antilles Volcanic Arc and Implications for the Evolution of Oceanic Arcs. *Geochemistry, Geophysics, Geosystems*, 23(4). <https://doi.org/10.1029/2021GC010148>
- Hudec, M. R., Norton, I. O., Jackson, M. P. A., & Peel, F. J. (2013). Jurassic evolution of the Gulf of Mexico salt basin. *AAPG Bulletin*, 97(10), 1683-1710. <https://doi.org/10.1306/04011312073>
- Iturralde-Vinent, M. A. (2003). Ensayo sobre la paleogeografía del Cuaternario de Cuba. 74.
- Iturralde-Vinent, M. (1998). Sinopsis de la Constitución Geológica de Cuba. *Acta geológica hispánica*; Vol.: 33 Núm.: 1 -4, 33(1-4).
- Iturralde-Vinent, M. A., García-Casco, A., Rojas-Agramonte, Y., Proenza, J. A., Murphy, J. B., & Stern, R. J. (2016). The geology of Cuba : A brief overview and synthesis. *GSA Today*, 4-10. <https://doi.org/10.1130/GSATG296A.1>
- Iturralde-Vinent, M., & Macphee, R. (1999). Paleogeography of the Caribbean Region : Implications for Cenozoic biogeography. *Bulletin of the American Museum of Natural History*, 238, 1-95.
- Iturralde-Vinent, M., Otero, C., Garcia-Casco, A., & van Hinsbergen, D. (2008). Paleogene Foredeep Basin Deposits of North-Central Cuba : A Record of Arc-Continent Collision between the Caribbean and North American Plates. *International Geology Review*, 50. <https://doi.org/10.2747/0020-6814.50.10.863>
- Jacobs, C. (1971). Jurassic Lithology in Great Isaac 1 Well, Bahamas : Discussion'. *The American Association of Petroleum Geologists Bulletin*, 61(3), 443.
- Kerr, A. C., Iturralde-Vinent, M. A., Saunders, A. D., Babbs, T. L., & Tarney, J. (1999). A new plate tectonic model of the Caribbean : Implications from a geochemical reconnaissance of Cuban Mesozoic volcanic rocks. *Geological Society of America Bulletin*, 111, 1581. [https://doi.org/10.1130/0016-7606\(1999\)111<1581:ANPTMO>2.3.CO;2](https://doi.org/10.1130/0016-7606(1999)111<1581:ANPTMO>2.3.CO;2)
- Kerr, A. C., & Tarney, J. (2005). Tectonic evolution of the Caribbean and northwestern South America : The case for accretion of two Late Cretaceous oceanic plateaus. *Geology*, 33(4), 269-272. <https://doi.org/10.1130/G21109.1>
- Khudoley, K. M. (1967). Principal Features of Cuban Geology. *AAPG Bulletin*, 51. <https://doi.org/10.1306/5D25C0BF-16C1-11D7-8645000102C1865D>
- Klitgord, K. D., Popenoe, P., & Schouten, H. (1984). Florida : A Jurassic transform plate boundary. *Journal of Geophysical Research: Solid Earth*, 89(B9), 7753-7772. <https://doi.org/10.1029/JB089iB09p07753>
- Kuffner, I. B. (2018). Sea-level rise could overwhelm coral reefs. *Nature*, 558(7710), 378-379. <https://doi.org/10.1038/d41586-018-04879-7>
- Ladd, J. W., & Sheridan, R. E. (1987). Seismic Stratigraphy of the Bahamas1. *AAPG Bulletin*, 71(6), 719-736. <https://doi.org/10.1306/94887898-1704-11D7-8645000102C1865D>
- Leroy, S. (2012). HAITI-SIS cruise, L'Atalante R/V. <https://doi.org/10.17600/12010070>
- Leroy, S., & Ellouz-Zimmermann, N. (2013). HAITI-SIS2 cruise, L'Atalante R/V. <https://doi.org/10.17600/13010080>
- Leroy, S., Ellouz-Zimmermann, N., Corbeau, J., Rolandone, F., Mercier De Lépinay, B., Meyer, B., Momplaisir, R., Bruña, J.-L. G., Battani, A., Baurion, C., Burov, E., Clouard, V., Deschamps, R., Gorini, C., Hamon, Y., Lafosse, M., Leonel, J., Pourhiet, L. L., Estrada, P. L., ... Muñoz, S. (2015). Segmentation and kinematics of the North America-Caribbean plate boundary offshore Hispaniola. *Terra Nova*, 27(6), 467-478. <https://doi.org/10.1111/ter.12181>
- Leroy, S., Mauffret, A., Patriat, P., & Mercier de Lépinay, B. (2000). An alternative interpretation of the Cayman trough evolution from a reidentification of magnetic

- anomalies. *Geophysical Journal International*, 141(3), 539-557. <https://doi.org/10.1046/j.1365-246x.2000.00059.x>
- Lewis, J., Amarante, A., Bloise, G., G., J. G., & Dominguez, H. (1991). Lithology and stratigraphy of Upper Cretaceous volcanic and volcanoclastic rocks of the Tiroo Group, Dominican Republic, and correlations with the Massif du Nord in Haiti. *Geologic and tectonic development of the North American-Caribbean plate boundary in Hispaniola*, 262, 143-163. <https://doi.org/10.1130/SPE262-p143>
- Lidz, B. (1973). Biostratigraphy of Neogene Cores from Exuma Sound Diapirs, Bahama Islands. *AAPG Bulletin*, 57(5), 841-857. <https://doi.org/10.1306/83D90D5E-16C7-11D7-8645000102C1865D>
- Malfait, B. T., & Dinkelman, M. G. (1972). Circum-Caribbean Tectonic and Igneous Activity and the Evolution of the Caribbean Plate. *GSA Bulletin*, 83(2), 251-272. [https://doi.org/10.1130/0016-7606\(1972\)83\[251:CTAIAA\]2.0.CO;2](https://doi.org/10.1130/0016-7606(1972)83[251:CTAIAA]2.0.CO;2)
- Marton, G., & Buffler, R. T. (1993). Application of simple-shear model to the evolution of passive continental margins of the Gulf of Mexico basin. *Geology*, 21(6), 495. [https://doi.org/10.1130/0091-7613\(1993\)021<0495:AOSMT>2.3.CO;2](https://doi.org/10.1130/0091-7613(1993)021<0495:AOSMT>2.3.CO;2)
- Marton, G., & Buffler, R. T. (1994). Jurassic Reconstruction of the Gulf of Mexico Basin. *International Geology Review*, 36(6), 545-586. <https://doi.org/10.1080/00206819409465475>
- Masaferro, J. L., & Eberli, G. P. (1999). Chapter 7 Jurassic-cenozoic structural evolution of the southern great Bahama bank. In P. Mann (Éd.), *Sedimentary Basins of the World* (Vol. 4, p. 167-193). Elsevier. [https://doi.org/10.1016/S1874-5997\(99\)80041-0](https://doi.org/10.1016/S1874-5997(99)80041-0)
- Mauffret, A., & Leroy, S. (1997). Seismic stratigraphy and structure of the Caribbean igneous province. *Tectonophysics*, 283(1), 61-104. [https://doi.org/10.1016/S0040-1951\(97\)00103-0](https://doi.org/10.1016/S0040-1951(97)00103-0)
- Mauffret, A., Leroy, S., Vila, J.-M., Hallot, E., de Lépinay, B., & Duncan, R. (2001). Prolonged Magmatic and Tectonic Development of the Caribbean Igneous Province Revealed by a Diving Submersible Survey. *Marine Geophysical Researches*, 22, 17-45. <https://doi.org/10.1023/A:1004873905885>
- Meyerhoff, A. A., & Hatten, C. W. (1968). Diapiric Structures in Central Cuba. In J. Braunstein & G. D. O'Brien (Éds.), *Diapirism and Diapirs : A symposium* (Vol. 8, p. 0). American Association of Petroleum Geologists. <https://doi.org/10.1306/M8361C21>
- Meyerhoff, A. A., & Hatten, C. W. (1974). Bahamas Salient of North America. In C. A. Burk & C. L. Drake (Éds.), *The Geology of Continental Margins* (p. 429-446). Springer. https://doi.org/10.1007/978-3-662-01141-6_31
- Moretti, I., Tenreiro, R., Linares, E., Lopez, J. G., Letouzey, J., Magnier, C., Gaumet, F., Lecomte, J. C., Lopez, J. O., & Zimine, S. (2003). Petroleum system of the Cuban Northwest offshore zone. 125-128.
- Mullins, H. T., & Hine, A. C. (1989). Scalloped bank margins : Beginning of the end for carbonate platforms? *Geology*, 17(1), 30-33. [https://doi.org/10.1130/0091-7613\(1989\)017<0030:SBMBOT>2.3.CO;2](https://doi.org/10.1130/0091-7613(1989)017<0030:SBMBOT>2.3.CO;2)
- Mullins, H. T., & Lynts, G. W. (1977). Origin of the northwestern Bahama Platform : Review and reinterpretation. *GSA Bulletin*, 88(10), 1447-1461. [https://doi.org/10.1130/0016-7606\(1977\)88<1447:OOTNBP>2.0.CO;2](https://doi.org/10.1130/0016-7606(1977)88<1447:OOTNBP>2.0.CO;2)
- Neill, I., Kerr, A. C., Chamberlain, K. R., Schmitt, A. K., Urbani, F., Hastie, A. R., Pindell, J. L., Barry, T. L., & Millar, I. L. (2014). Vestiges of the proto-Caribbean seaway : Origin of the San Souci Volcanic Group, Trinidad. *Tectonophysics*, 626, 170-185. <https://doi.org/10.1016/j.tecto.2014.04.019>
- Noda, A. (2016). Forearc basins : Types, geometries, and relationships to subduction zone dynamics. <https://doi.org/10.1130/B31345.1>

- Oliveira de Sá, A., d'Acremont, E., Leroy, S., & Lafuerza, S. (2021). Polyphase Deformation and Strain Migration on the Septentrional-Oriente Fault Zone in the Windward Passage, Northern Caribbean Plate Boundary. *Tectonics*, 40(8), e2021TC006802. <https://doi.org/10.1029/2021TC006802>
- Padilla y Sánchez, R. J. (2016). Late Triassic-Late Cretaceous Paleogeography of Mexico and the Gulf of Mexico. In C. M. Lowery, J. W. Snedden, & N. C. Rosen (Éds.), *Mesozoic of the Gulf Rim and Beyond : New Progress in Science and Exploration of the Gulf of Mexico Basin* (Vol. 35, p. 0). SEPM Society for Sedimentary Geology. <https://doi.org/10.5724/gcs.15.35.0273>
- Pardo, G. (2009). Overview. In G. Pardo (Éd.), *The Geology of Cuba* (p. 1-47). The American Association of Petroleum Geologists. <https://doi.org/10.1306/13141059St583328>
- Pindell, J. (1985). Alleghenian reconstruction and subsequent evolution of the Gulf of Mexico, Bahamas, and Proto-Caribbean. <https://doi.org/10.1029/TC004I001P00001>
- Pindell, J., & Dewey, J. F. (1982). Permo-Triassic reconstruction of western Pangea and the evolution of the Gulf of Mexico/Caribbean region. *Tectonics*, 1(2), 179-211. <https://doi.org/10.1029/TC001i002p00179>
- Pindell, J., & Kennan, L. (2001). Kinematic Evolution of the Gulf of Mexico and Caribbean. In R. H. Fillon, N. C. Rosen, P. Weimer, A. Lowrie, H. Pettingill, R. L. Phair, H. H. Roberts, & H. H. van Hoom (Éds.), *Petroleum Systems of Deep-Water Basins—Global and Gulf of Mexico Experience* (Vol. 21, p. 0). SEPM Society for Sedimentary Geology. <https://doi.org/10.5724/gcs.01.21.0193>
- Pindell, J., Kennan, L., Maresch, W. V., Stanek, K.-P., Draper, G., & Higgs, R. (2005). Plate-kinematics and crustal dynamics of circum-Caribbean arc-continent interactions : Tectonic controls on basin development in Proto-Caribbean margins. In H. G. A. Lallemand & V. B. Sisson, *Caribbean-South American plate interactions, Venezuela*. Geological Society of America. <https://doi.org/10.1130/0-8137-2394-9.7>
- Pindell, J., Kennan, L., Stanek, K., Maresch, W., & Draper, G. (2006). Foundations of Gulf of Mexico and Caribbean evolution : Eight controversies resolved. *Geologica acta: an international earth science journal*, 4(1-2), 303-341.
- Ramos, J. P., & Mann, P. (2023). Late Cretaceous-Recent Tectonostratigraphic Evolution of the Yucatan Back-Arc Basin, Northern Caribbean Sea. *Geochemistry, Geophysics, Geosystems*, 24(8), e2023GC010933. <https://doi.org/10.1029/2023GC010933>
- Rodríguez-Zurrunero, A., Granja-Bruña, J. L., Carbó-Gorosabel, A., Muñoz-Martín, A., Gorosabel-Araus, J. M., Gómez de la Peña, L., Gómez Ballesteros, M., Pazos, A., Catalán, M., Espinosa, S., Druet, M., Llanes, P., & ten Brink, U. (2019). Submarine morpho-structure and active processes along the North American-Caribbean plate boundary (Dominican Republic sector). *Marine Geology*, 407, 121-147. <https://doi.org/10.1016/j.margeo.2018.10.010>
- Rodríguez-Zurrunero, A., Granja-Bruña, J. L., Muñoz-Martín, A., Leroy, S., ten Brink, U., Gorosabel-Araus, J. M., Gómez de la Peña, L., Druet, M., & Carbó-Gorosabel, A. (2020). Along-strike segmentation in the northern Caribbean plate boundary zone (Hispaniola sector) : Tectonic implications. *Tectonophysics*, 776, 228322. <https://doi.org/10.1016/j.tecto.2020.228322>
- Rojas-Agramonte, Y., Neubauer, F., Garcia-Delgado, D. E., Handler, R., Friedl, G., & Delgado-Damas, R. (2008). Tectonic evolution of the Sierra Maestra Mountains, SE Cuba, during Tertiary times : From arc-continent collision to transform motion. *Journal of South American Earth Sciences*, 26(2), 125-151. <https://doi.org/10.1016/j.jsames.2008.05.005>
- Rosencrantz, E., Ross, M. I., & Sclater, J. G. (1988). Age and spreading history of the Cayman Trough as determined from depth, heat flow, and magnetic anomalies. *Journal of*

- Geophysical Research: Solid Earth, 93(B3), 2141-2157.
<https://doi.org/10.1029/JB093iB03p02141>
- Ross, M., & Scotese, C. (1988). A hierarchical tectonic model of the Gulf of Mexico and Caribbean Region. *Tectonophysics*, 155, 139-168. [https://doi.org/10.1016/0040-1951\(88\)90263-6](https://doi.org/10.1016/0040-1951(88)90263-6)
- Rui, H.-C., Yang, J.-S., Zheng, J.-P., Llanes Castro, A. I., Liu, F., Wu, Y., Wu, W.-W., Valdes Mariño, Y., & Masoud, A. E. (2022). Early Cretaceous subduction initiation of the proto-Caribbean plate : Geochronological and geochemical evidence from gabbros of the Moa-Baracoa ophiolitic massif, Eastern Cuba. *Lithos*, 418, 106674. <https://doi.org/10.1016/j.lithos.2022.106674>
- Salvador, A. (1987). Late Triassic-Jurassic Paleogeography and Origin of Gulf of Mexico Basin. *AAPG Bulletin*, 71(4), 419-451.
- Sanchez, J. R., S. Blanco, Tenreyro, R., Rodriguez, M., & Valladares, S. (1999). Aptian Transgressive Event in the continental margin of Cuba and regional comparisons -A review. Dimas Dias-Brito, Joel Cameiro de Castro, Rosemarie Rohn. 1er Simposio Sobre O Cretáceo do America del Sur, Editors: Boletim do 5 Simposio Sobre O Cretáceo do Brasil, 11-18.
- Saura, E., Vergés, J., Brown, D., Lukito, P., Soriano, Sofía, Torrecusa, S., García, R., Sánchez, J. R., Sosa, C., & Tenreyro, R. (2008). Structural and tectonic evolution of western Cuba fold and thrust belt. *Tectonics*, 27. <https://doi.org/10.1029/2007TC002237>
- Schenk, C. J. (2008). Jurassic-Cretaceous Composite Total Petroleum System and geologic models for oil and gas assessment of the North Cuba Basin, Cuba. (p. 94).
- Schlager, W., Jr, J., Corso, W., McNulty, C., Fluegel, E., Renz, O., & Steinmetz, J. (1984). Early Cretaceous platform reentrant and escarpment erosion in the Bahama. *Geology*, 12. [https://doi.org/10.1130/0091-7613\(1984\)12<147:ECPRAE>2.0.CO;2](https://doi.org/10.1130/0091-7613(1984)12<147:ECPRAE>2.0.CO;2)
- Schouten, H., & Klitgord, K. (1994). Mechanistic solutions to the opening of the Gulf of Mexico. *Geology*, 22. [https://doi.org/10.1130/0091-7613\(1994\)022<0507:MSTTOO>2.3.CO;2](https://doi.org/10.1130/0091-7613(1994)022<0507:MSTTOO>2.3.CO;2)
- Sheridan, R. E., Crosby, J. T., Bryan, G. M., & Stoffa, P. L. (1981). Stratigraphy and Structure of Southern Blake Plateau, Northern Florida Straits, and Northern Bahama Platform from Multichannel Seismic Reflection Data1. *AAPG Bulletin*, 65(12), 2571-2593. <https://doi.org/10.1306/03B59A08-16D1-11D7-8645000102C1865D>
- Sheridan, R. E., Mullins, H. T., Austin, J. A., Jr., Ball, M. M., & Ladd, J. W. (1988). Geology and geophysics of the Bahamas. In R. E. Sheridan & J. A. Grow (Éds.), *The Atlantic Continental Margin: Vol. I-2*. Geological Society of America. <https://doi.org/10.1130/DNAG-GNA-I2.329>
- Sheridan, R. E., Smith, J. D., & Gardner, J. (1969). Rock Dredges from Blake Escarpment Near Great Abaco Canyon1. *AAPG Bulletin*, 53(12), 2551-2558. <https://doi.org/10.1306/5D25C975-16C1-11D7-8645000102C1865D>
- Stanek, K. P., Maresch, W. V., & Pindell, J. L. (2009). The geotectonic story of the northwestern branch of the Caribbean Arc: Implications from structural and geochronological data of Cuba. Geological Society, London, Special Publications, 328(1), 361-398. <https://doi.org/10.1144/SP328.15>
- Uchupi, E., Milliman, J. D., Luyendyk, B. P., Bowin, C. O., & Emery, K. O. (1971). Structure and Origin of Southeastern Bahamas1. *AAPG Bulletin*, 55(5), 687-704. <https://doi.org/10.1306/819A3C56-16C5-11D7-8645000102C1865D>
- Vázquez-Taset, Y. M., Sàbat, F., Cabello, P., Cruz-Orosa, I., & Ramos, E. (2020). Cenozoic tectonostratigraphic evolution of the strike-slip Cauto-Guacanayabo Basin, Eastern

- Cuba. *Journal of South American Earth Sciences*, 100, 102592. <https://doi.org/10.1016/j.jsames.2020.102592>
- Walles, F. E. (1993). Tectonic and diagenetically induced seal failure within the south-western Great Bahamas Bank. *Marine and Petroleum Geology*, 10(1), 14-28. [https://doi.org/10.1016/0264-8172\(93\)90096-B](https://doi.org/10.1016/0264-8172(93)90096-B)
- Weatherall, P., Marks, K. M., Jakobsson, M., Schmitt, T., Tani, S., Arndt, J. E., Rovere, M., Chayes, D., Ferrini, V., & Wigley, R. (2015). A new digital bathymetric model of the world's oceans. *Earth and Space Science*, 2(8), 331-345. <https://doi.org/10.1002/2015EA000107>
- Wessels, R. J. F. (2019). Chapter 15—Strike-Slip Fault Systems Along the Northern Caribbean Plate Boundary. In J. C. Duarte (Éd.), *Transform Plate Boundaries and Fracture Zones* (p. 375-395). Elsevier. <https://doi.org/10.1016/B978-0-12-812064-4.00015-3>
- Wright, J., & Wyld, S. (2011). Late Cretaceous subduction initiation on the eastern margin of the Caribbean-Colombian Oceanic Plateau: One Great Arc of the Caribbean (?). *Geosphere*, 7, 468-493. <https://doi.org/10.1130/GES00577.1>





CHAPITRE V : Déformation polyphasée et migration de la déformation le long du Système de failles décrochantes sénestres Septentrionale-Oriente

Tectonics

RESEARCH ARTICLE
10.1029/2021TC006802

Accepted 19 JUL 2021

Polyphase Deformation and Strain Migration on the Septentrional-Oriente Fault Zone in the Windward Passage, Northern Caribbean Plate Boundary

A. Oliveira de Sá¹ , E. d'Acremont¹ , S. Leroy¹ , and S. Lafuerza¹ 

¹Sorbonne Université, CNRS-INSU, Institut des Sciences de la Terre Paris, Paris, France

Après notre étude de la région au large du bloc de Cuba Oriental, abordée dans le chapitre précédent, une question centrale émerge : comment la limite de la plaque Caraïbe a-t-elle migré dans le temps et l'espace depuis son ancienne frontière au nord du bloc Cuba Oriental ? Quelles contraintes tectoniques sont nécessaires pour une telle évolution ? Cette étude, centrée sur la région du Passage du Vent, vise principalement à (i) détailler la morphologie du fond marin situé dans cette région, entre le sud-est de Cuba et le nord-ouest d'Haïti, en identifiant les mécanismes géologiques dominants qui en sont à l'origine et (ii) de reconstituer les dynamiques de déformation à travers la corrélation des séquences sismiques observées avec les phases majeures de déformations terrestres survenues depuis l'Éocène.

Le détroit du Passage du Vent, stratégiquement positionné entre le sud-est de Cuba et le nord-ouest d'Haïti, s'avère être une localité essentielle pour l'analyse et la compréhension des segments actifs de la SOFZ (Zone de Faille Oriente Septentrionale). Grâce à la proximité des terrains émergés, il a été possible d'établir une corrélation robuste entre les événements tectoniques observés en mer et ceux décrits à terre. Cette approche intégrée offre une vision qui se veut claire de l'évolution de la limite nord de la plaque Caraïbe, depuis le nord de Cuba Oriental à la fin de l'Éocène, jusqu'à sa position actuelle, à la faveur de plusieurs migrations de zones de faille décrochantes.

V. Polyphase deformation and strain migration on the Septentrional-Oriente Fault Zone in the Windward Passage, Northern Caribbean Plate boundary

A. Oliveira de Sá¹, E. d'Acremont¹, S. Leroy¹, and S. Lafuerza¹

¹ Sorbonne Université, CNRS-INSU, Institut des Sciences de la Terre Paris, ISTeP, 75005 Paris, France

Key Points:

- The present-day structure in the Windward Passage implies a polyphase evolution with at least 4 stages of deformation.

- Motion on the Septentrional-Oriente Fault in the Windward Passage began in early Pliocene time and has generated an estimated ~80 km offset
- Onset of motion in the Windward Passage is key to revealing Neogene structural evolution of the northern Caribbean plate.

Abstract

Oblique collision between the Caribbean plate and the Bahama Banks has led to an eastward migration of the northern Caribbean plate boundary by successive southward jumps of major strike-slip faults. The Septentrional-Oriente Fault zone (SOFZ) defines the present-day northern Caribbean plate boundary accommodating most of the eastward escape of the Caribbean plate. Here, we reevaluate the complex history of the SOFZ along the Windward Passage area between the easternmost region of Cuba and the northwest of Haiti. Based on seismic reflection and swath-bathymetric dataset we interpret the structure and tectonic pattern of the Windward Passage. The tectono-sedimentary framework of this large strait shows contrasting patterns of deformation linked to a complex polyphase tectonic history of dominantly strike-slip faulting. SOFZ segments offset the seismic units and yield key markers of displacement along the fault system. Our study provides structural and stratigraphic insights into the relative timing of deformation along the Windward Passage and presents new elements that constrain the southeastward jump of the north Caribbean plate boundary to its present-day position. We propose dates for the identified seismic units based on the correlation of offshore deformation phases recorded in the Windward Passage sedimentary cover with major paleogeographic reorganization episodes described onland (Late Eocene, Late Oligocene, Middle Miocene and Late Pliocene). By restoring the offset of the seismic units, we demonstrate that at least ~80 km of left-lateral motion has occurred on the SOFZ, and that the SOFZ has been active since the Pliocene.

V.1 Introduction

Relative plate motion at most convergent plate boundaries is oblique to the boundary itself (Philippon & Corti, 2016). Oblique convergence settings display strain partitioning into boundary-normal and boundary-parallel components of the plate motion vector (Jarrard, 1986; Demets, 1992; ten Brink & Lin, 2004; Chemenda et al., 2000). In oblique convergence settings, the oblique component of motion is often accommodated by strike-slip faults that dominate plate interactions (Teyssier et al., 1995; Chemenda et al., 2000). In such cases, strike-slip faults may also form along the edge of the overriding plate to accommodate boundary-parallel components (Fitch, 1972; Jarrard, 1986). This process is called slip partitioning and it has been observed in oblique convergence contexts such as offshore Sumatra (Jarrard, 1986), the Philippine fault (Fitch, 1972), in Taiwan (Lallemand et al., 1999) and in the Lesser Antilles (Symithe et al., 2015; Laurencin et al., 2019). Along the Caribbean–North American plate boundary, the degree of obliquity varies from ~50° North of Cuba, ~20° in the northern Hispaniola Island arc, to up to 72° in the northern Lesser Antilles (Calais et al. 2016; Laurencin et al., 2019; Rodríguez-Zurrunero et al., 2020). To the north of Hispaniola, the eastward motion of the Caribbean Plate is slowed by its collision with the Bahama Banks. Caribbean plate motion is highly oblique to this portion of the plate boundary (Figure V.1)(Demets, 1992; Mullins et al., 1992; Calais et al., 2016). This ongoing oblique collision results in a strong stress coupling between the plates and slip partitioning along the northern edge of Hispaniola (Rodríguez-Zurrunero et al., 2020). North-verging fold propagation faults sub-parallel to the Caribbean plate displacement accommodates part of the convergence in Hispaniola's northern coast

(Calais et al., 2010). Oblique motion is also accommodated by a large-scale, seismically active strike-slip fault system, known as the Septentrional-Oriente Fault Zone (SOFZ), which forms the current northern Caribbean Plate boundary (Leroy et al., 2015; Calais et al., 2016)(Figure V.1).

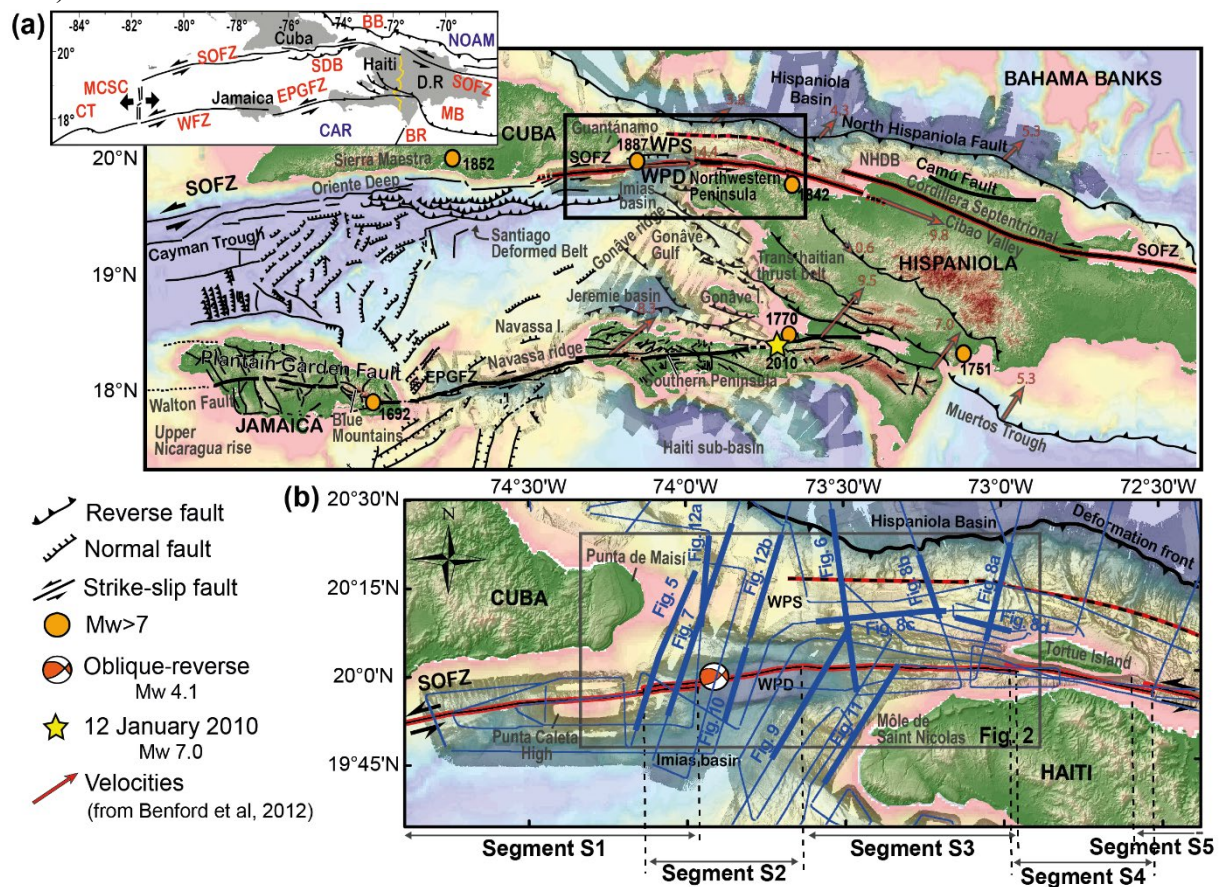


Figure V.1. Tectonic map of the northern Caribbean plate boundary. (a) Orange dots indicate the presumed epicenters of $M_w > 7$ historical earthquakes (from Syed Tabrez et al., 2008). Velocities in mm. $a-1$ are reported from a block model incorporating the available GPS data, velocity vectors are relative to the North American plate (Benford et al., 2012). The parts of the fault system studied in this paper are outlined in red. Red line with black dots represent the fault strand identified by Rodriguez-Zurrunero et al. (2020) in the Windward Passage Sill (WPS). Faults in black are from previous studies (Calais & Mercier de Lépinay, 1989, 1991; Corbeau et al., 2016; Leroy et al., 2015; Granja Bruña et al., 2014; Leroy et al., 1996; Mann et al., 1995, 1998; Mauffret & Leroy, 1997). Inset: Geodynamic map. NOAM: North American plate; CAR: Caribbean plate; MB: Muertos Belt; MCSC: Mid-Cayman spreading center; CT: Cayman trough; D.R.: Dominican Republic; OFZ: Oriente Fault zone; EPGFZ: Enriquillo–Plantain Garden Fault zone; WFZ: Walton Fault zone; SDB: Santiago Deformed Belt; BB: Bahamas platform; BR: Beata Ridge (modified from Leroy et al., 2015). (b) Bathymetric map of the Windward Passage area showing the active segments of the Oriente-Septentrional Fault Zone (SOFZ) inferred from distinct geometric fault complexities. Active SOFZ Segments are outlined in red. Blue lines represent the seismic sections collected during cruises HAITI-SIS 1-2 (Leroy, 2012; Leroy & Ellouz-Zimmermann, 2013; Leroy et al., 2015). Bold pink and blue lines indicate positions of seismic sections in this paper (Figures V.5 and 13). Boxe of detailed bathymetry (Figure V.2). EPGFZ: Enriquillo-Plantain-Garden Fault Zone; NHDB: Northern Hispaniola Deformation Belt; SOFZ: Septentrional–Oriente fault zone, WPS: Windward Passage Sill, WPD: Windward Passage Deep.

The SOFZ trends almost E-W as it runs along the southern coast of Cuban, and straight across the Windward Passage until it steps onland in northern Hispaniola (Figure V.1a). The geological setting of the region has been strongly controlled by this large-scale strike-slip fault

system (de Zoeten & Mann, 1991; Mann et al., 1995; Rojas-Agramonte et al., 2008). Previous seismic reflection data has led to an initial description of the SOFZ and its related structural framework (Calais & Mercier de Lépinay, 1991; Dillon et al., 1992; Calais & Mercier de Lépinay, 1995; Leroy et al., 2015). However, the initiation of SOFZ remains poorly constrained, as well as the understanding of how the various segments of the system may have functioned as the convergent plate boundary evolved.

This paper documents the sedimentary and structural framework associated with the active segments of the SOFZ in the Windward Passage. The study area is located at the contact zone between the North American Plate and the northern boundary of the Caribbean Plate. The Windward Passage may have recorded a wealth of information concerning tectonic events at the Caribbean–North American plate boundary. It is thus a critical witness to the kinematic evolution of the Caribbean Plate.

The main goal of this study is to understand how the tectonic context of oblique collision with strain partitioning within the Windward Passage since the Eocene has led to the current sedimentary and structural framework. We present high-resolution multibeam bathymetry and ~3000 km of multi-channel seismic reflection profiles that image the Windward Passage domains, mapping the SOFZ fault trace and related morphological features (Figure V.2). Deformation events recorded in the sedimentary cover were time-correlated with major onland deformation events in southern Cuba and Northern Hispaniola. Our intent is to (i) constrain the deformation styles in time through interpretation of the sedimentary record, (ii) infer the structural framework that existed prior to inception of the SOFZ, and (iii) better understand the current structures associated to this major fault system. We discuss the critical time markers for inferring the stratigraphic interval that defines a timeframe for the initiation of left-lateral strike-slip motion on the SOFZ within the Windward Passage and its subsequent migration. We accurately define the active tectonics of the Northern Caribbean plate boundary, providing a better understanding of the regional tectonics.

V.2 Tectonic Settings

Since Paleocene times, the Caribbean–North American plate boundary has undergone progressive reorganization in response to the diachronous collision between the Cuban-Hispaniola Arc and the Bahama Banks (Gordon et al., 1997; Iturralde-Vinent & Macphee, 1999; Mann et al., 2002). This collision has caused a change in the Caribbean-North American relative plate motion from NNE to E (Pindell et al., 2005; Boschman et al., 2014). Along the Cuban Arc, strain partitioning and large-scale strike-slip faulting took place. The northern Caribbean plate boundary underwent a series of jumps. During the initial stages of collision, the boundary coincided with the eastern Yucatan transform margin. Accommodation of relative plate motion migrated progressively southward as each new fault systems developed and was subsequently replaced by a younger fault system starting with the development of the Pinar fault (Paleocene), followed by the La Trocha fault (Early Eocene), and then the Cauto fault (middle Eocene) in Cuba (Figures V.3a and 3b). As the plate boundary shifted southward to the Oriente Fault zone (OFZ) (early Oligocene), the Cuban block became attached to the North American Plate resulting in the separation of Cuba and Hispaniola, which until then had formed a single block (Figure V.3c)(Calais & Mercier de Lépinay, 1992; Leroy et al., 2000; Rojas-Agramonte et al., 2008; Wessels, 2019). The OFZ transcurrent plate boundary must have been located north of Hispaniola during the Miocene until Pliocene times (Figures V.3d, 3e and 3f)(Erikson et al., 1998). However, as the system evolved the northern end of the OFZ gradually became inactive and the strike-slip motion between Cuba and Hispaniola shifted southward (Calais & Mercier de Lépinay, 1995), extending into the northwestern peninsula of Hispaniola to form the

Septentrional fault (Late Pliocene) and establish the current Septentrional-Oriente Fault Zone (SOFZ) (Figures V.1b, 3f and 3g) (Calais et al., 2016; Escuder-Viruete and Pérez, 2020).

On the Island of Hispaniola, the SOFZ and the North Hispaniola fault (Deformation front) partition the oblique convergence into boundary-parallel and boundary-normal components (Rodríguez-Zurrunero et al., 2019, 2020). The SOFZ accommodates most of the left-lateral strain of the current Caribbean-North American relative plate motion as a major transpressional fault system. Using GPS measurements and block modelling, Calais et al. (2010) estimate that the SOFZ currently accumulates elastic strain at a rate of $12 \pm 3 \text{ mm yr}^{-1}$. While the North Hispaniola fault accommodates 2 to 6 mm/yr of \sim N-S shortening, and the Trans-Haitian belt accommodates about 4 mm yr^{-1} of \sim N-S shortening (Figure V.1a).

The Windward Passage area is a large strait separating the eastern extremity of Cuba from the northwestern peninsula of Hispaniola (Figure V.1b) (Calais, 1990). The area consists of a submarine plateau, the Windward Passage Sill (WPS) (Goreau, 1989) and an adjacent sedimentary basin, the Windward Passage Deep (WPD) (Calais & Mercier de Lépinay, 1995). A forward-propagating imbricated zone of contractional structures characterizes the WPS on its northern edge and delimits the deformation front (Figure V.2)(Goreau, 1989; Dillon et al., 1992, 1996; Rodríguez-Zurrunero et al., 2019). There, sediments of the adjacent Hispaniola basin are tilted to the north and incorporated into the WPS structure. To the south, the WPS is bounded by the WPD, an east-west trending elongated basin. The WPD is about 120 km long and 15 km wide with depths ranging from 1100 to 3780 m (Figure V.2a). The evolution of the WPD is interwoven with SOFZ formation, which crosses its entire length running from the southern Cuban margin eastward to the northern Hispaniola margin (Figure V.2b). Calais & Mercier de Lépinay (1995) correlate offshore seismic sequences recognized in the WPD to successive tectonic and sedimentary events recorded onshore in Cuba and Hispaniola. These authors associate these correlated onshore-offshore events with the successive collisions of the northern Caribbean mobile terranes against the Bahama Bank.

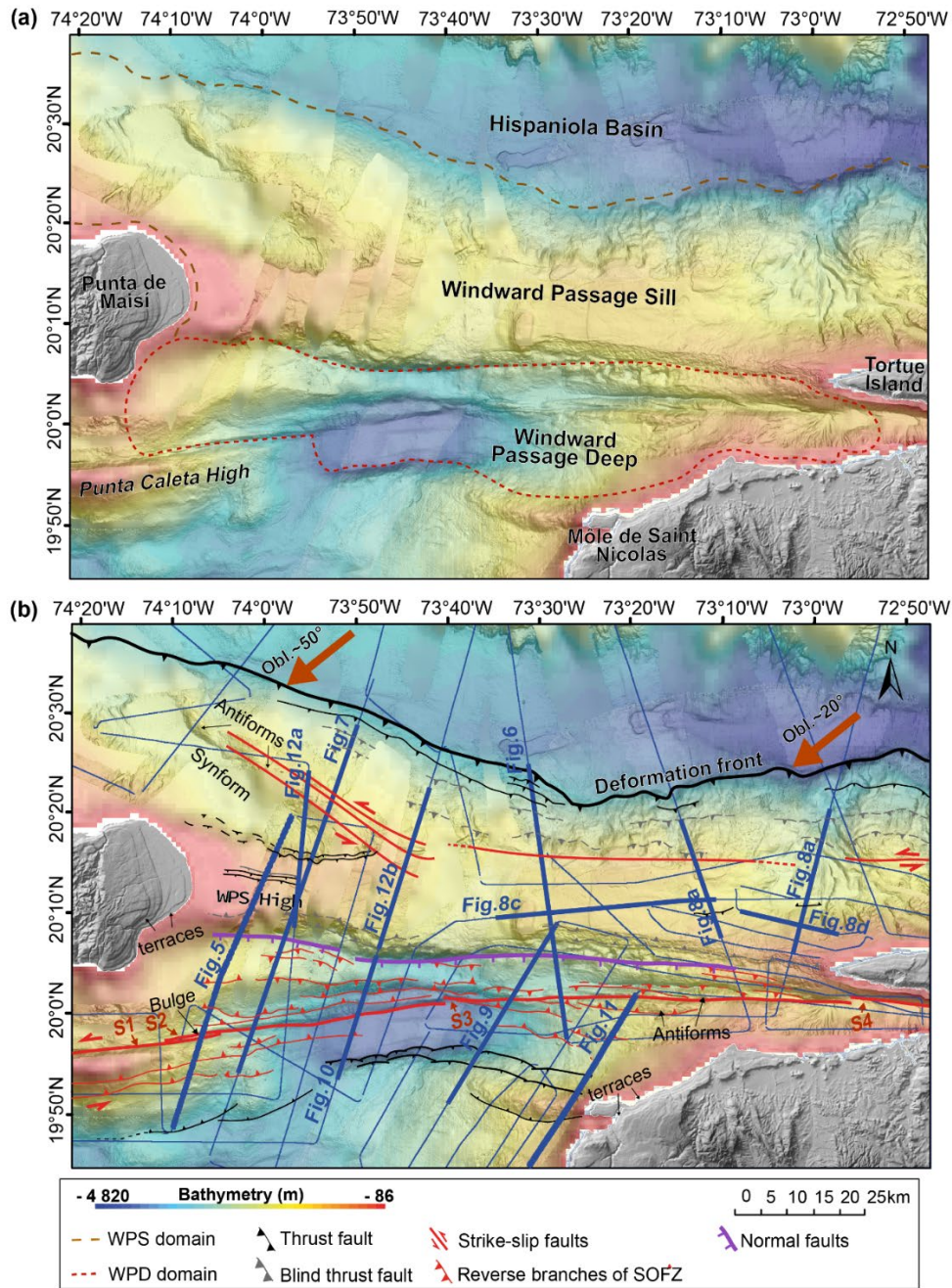


Figure V.2. (a) Detailed bathymetric map of the Windward Passage Sill and Deep areas. (b) Bathymetric map with structural interpretations. See Figure V.1 for location of the map. In the Windward Passage Sill area, the activity of wrench faults forms a relief about 350 m high structured by an antiform and a synform trending E-W and NW-SE. The Septentrional Oriente Fault Zone (SOFZ) represented in bold red lines by the S1 to S4 fault segments, cross-cuts the Windward Passage Deep area. Red arrows show the average plate convergence direction of the North American plate with respect to the Caribbean (Calais et al., 2016). Multibeam bathymetry data from the HAITI-SIS cruises and NORCARIBE (Leroy, 2012; Leroy and Ellouz-Zimmermann, 2013; Leroy et al., 2015; Granja-Bruna et al 2014) completed with the GEBCO Digital Atlas (https://www.gebco.net/data_and_products/gebco_digital_atlas/).

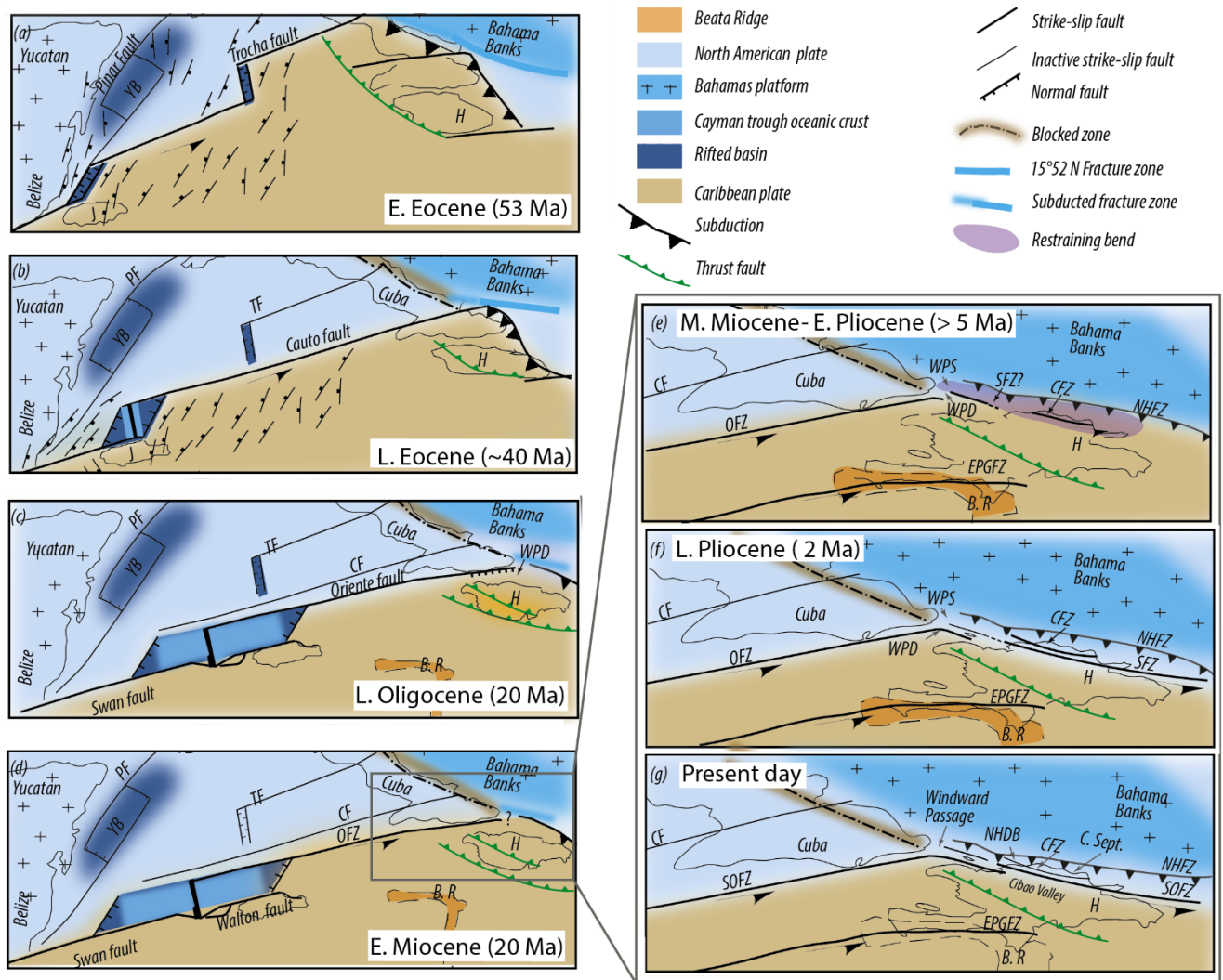


Figure V.3. Tectonic setting of the northern boundary of the Caribbean plate from Early Eocene to Present-day times, modified from Leroy et al. (2000). See text for discussion. B.R.: Beata Ridge ; C. Sept. CF: Cauto Fault; CFZ: Camú Fault Zone; EPGFZ: Enriquillo-Plantain-Garden Fault Zone; H: Hispaniola block; J: Jamaica; NHDB: Northern Hispaniola Deformed Belt; NHFZ: Northern Hispaniola Fault Zone. OFZ: Oriente Fault Zone; SFZ: Septentrional Fault Zone; SOFZ: Septentrional Oriente Fault Zone; WPD: Windward Passage Deep; WPS: Windward Passage Sill; YB: Yucatan Basin; TF: Trocha fault.

V.3 Data and Methods

Multichannel seismic reflection and multibeam bathymetric data were collected during cruises HAITI-SIS 1-2 (2012-2013) onboard the R/V L'Atalante from the Flotte Océanographique Française (Leroy, 2012; Leroy and Ellouz-Zimmermann, 2013; Leroy et al., 2015). Multibeam bathymetric data collected during NORCARIBE geophysical cruise in November–December 2013 aboard the Spanish R/V Sarmiento de Gamboa is used to fill the gaps in our data coverage (Leroy et al 2015; Rodríguez-Zurrunero et al., 2020). In this paper, we focus on the Windward Passage area where ~3000 km of seismic profiles have been acquired (Figure V.1b). Seismic reflection data are recorded using a source comprising two GI air guns (2.46 L, 300 in3) and a streamer with 24 traces (600 m long) operated at c.a 9.7 knots (fast and light seismic system). The multichannel seismic reflection data were processed using

classical steps including CDP gathering (fold 6), binning at 25m, detailed velocity analysis, stack and post-stack time migration. All the seismic reflection profiles presented are time migrated. Multibeam bathymetry data were acquired simultaneously along seismic profiles and gridded with a spacing of 50 m. The gridded bathymetry data was augmented with the GEBCO Digital Atlas (https://www.gebco.net/data_and_products/gebco_digital_atlas/) with an 800m resolution to provide an almost full coverage (Figure V.1a). The processed seismic data are interpreted using Kingdom IHS Suite© software. Maps are plotted with ArcGIS© software. We use the seismic reflection dataset to identify sedimentary units, deformation style and spatio-temporal evolution of the tectonic structures. Morphological analysis of the seafloor based on swath-bathymetric data is carried out to identify the surface signature of tectonic features (Figure V.2). We identify faults by either sediment horizon offsets or by the fault plane seismic reflection itself in the available seismic profiles.

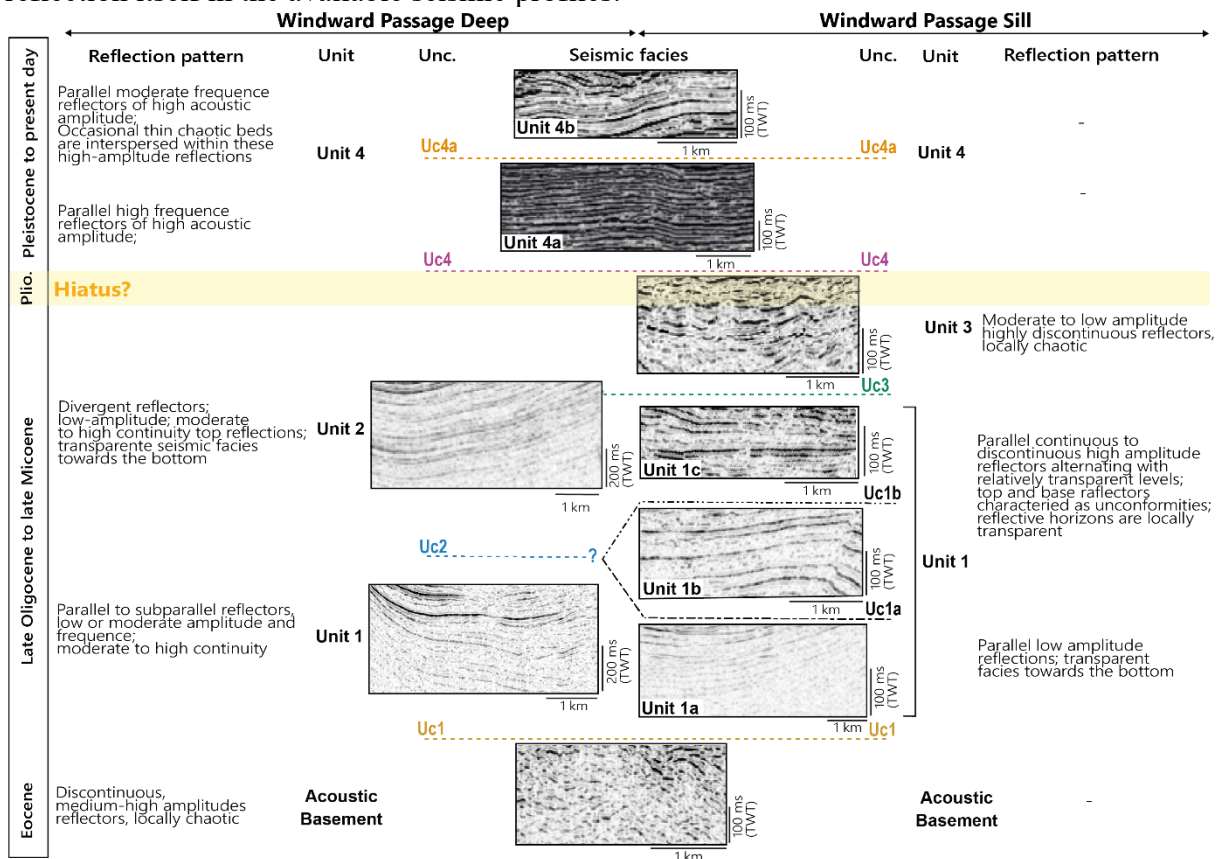


Figure V.4. Overview of interpreted seismic units through the WPD and the WPS areas from Eocene to Present-day. A time calibration is proposed. Units 1, 3 and 4 were first named in the work of Calais & Mercier de Lépinois (1995) as B, A' and A, respectively. Unc.: unconformity.

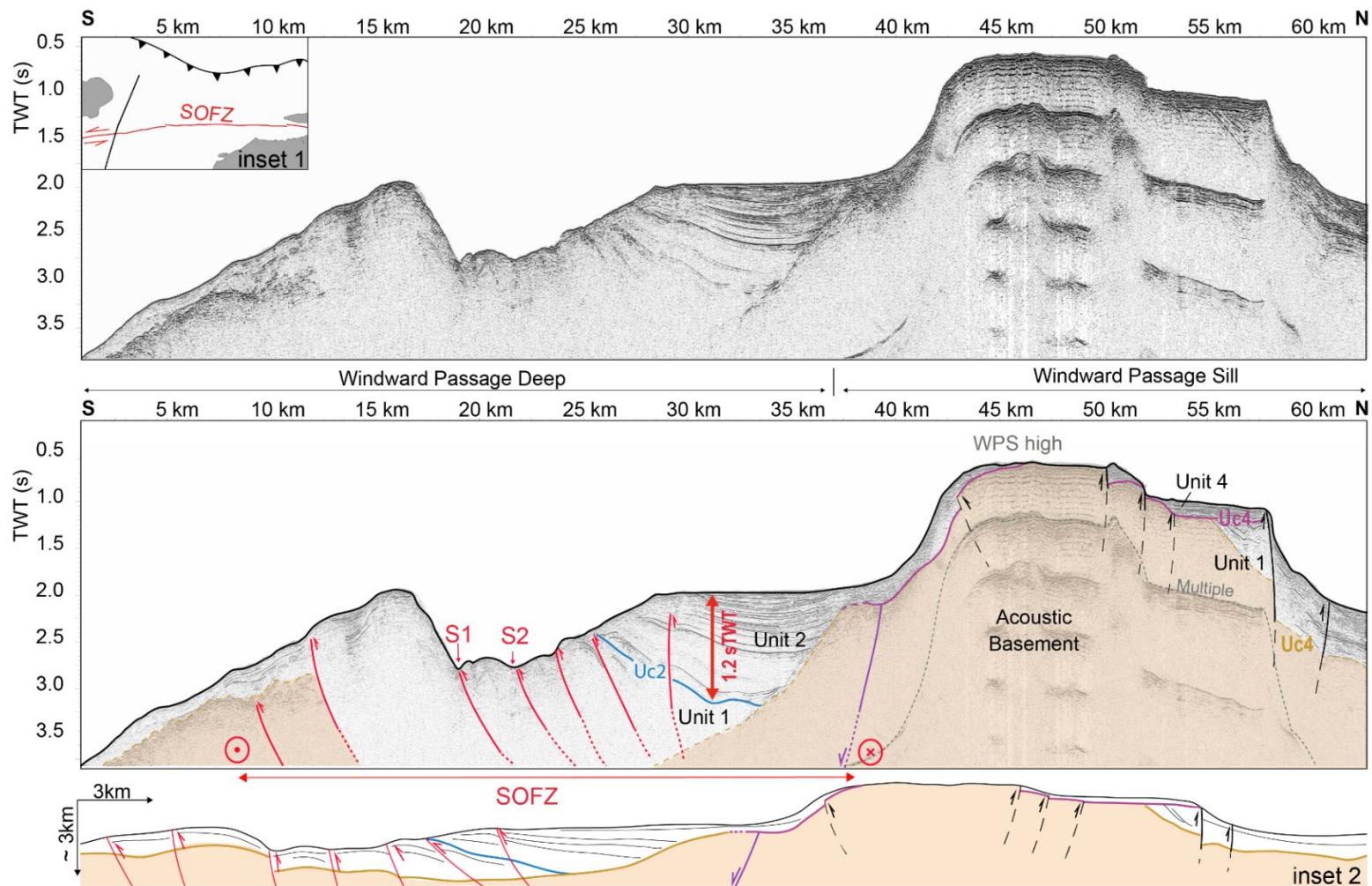


Figure V.5. Seismic profile covering the Windward Passage Deep (south) and part of the Windward Passage Sill (north). Unit 2 is perched and laterally discontinuous southward. The WPS high active reverse faults propagate upwards reaching the seafloor. Faults in red are upward spreading strands of wrench faults. Normal and thrust faults are, respectively, outline in violet and black colors. Inset 1: Location of the seismic line. Inset 2: Seismic line displayed with no vertical exaggeration according to the seafloor.

V.4 Results

V.4.1 Seismic stratigraphy

Seismic units are hereafter described by geographic sectors and ordered from the acoustic basement to the most recent one (Unit 4). We summarize the corresponding facies in a table (Figure V.4). For both areas, WPS and WPD, the top of the acoustic basement corresponds to a rough surface on some profiles (Figures V.5, 6 and 7), and it may outcrop in the structural highs of the study area (Figure V.5, km 40-55). Acoustic energy is insufficient to image beneath the top of the observed acoustic basement (labelled unconformity Uc1). The presence of seabed multiples usually hampers the description of internal geometry of the acoustic basement. When seismic reflections are observed within the acoustic basement, the reflectors are discontinuous to chaotic, medium-high amplitudes that may terminate upward against the irregular and rugged unconformity Uc1 (Figures V.4, 5 and 6).

V.4.1.1 Windward Passage Sill

Within the Windward Passage Sill (WPS), we define three main seismic units above the acoustic basement that correspond to seismic units previously defined by Calais and Mercier de Lépinay (1995). The lower unit (Unit 1) is characterized by a thick series (>1s TWT) with at least two internal angular unconformities (Uc1a and Uc1b, Figures V.6 and 7) that separate distinct sub-units of distinct facies and geometries (Units 1a, 1b and 1c; see Figure V.4 for detailed reflections attributes).

At the base of Unit 1, the seismic facies is transparent (Unit 1a in Figures V.4 and 7, km 65-85), then well-defined by parallel high frequency reflections in its upper part (Unit 1c, Figure V.4). Most of Unit 1, especially its base, appears to have been folded and then eroded as indicated by unconformities Uc1a and Uc1b (Figure V.7, km 65-85). In the northern flank of the WPS high, Units 1a and 1b onlap the angular unconformity Uc1 (Figure V.6, km 33-43) and Unit 2 is not present. The second seismic unit in the WPS (Unit 3) is separated from the Unit 1 by an angular unconformity labelled Uc3 (Figures V.4 and 6). Unit 3 layers are tilted and folded and were deposited in the syncline depressions formed by the previous folding of Unit 1, with a succession of onlap terminations in a well-layered sequence (Figure V.6, km 25-40).

The angular unconformity Uc4 is observed at the top of Unit 3 and separates Unit 3 from the more horizontally layered high-frequency reflectors of uppermost Unit 4 (Figures V.4 and 6). Our seismic profiles through the WPS illustrate the lateral thickness variation of Unit 4. The thickness of this unit increases from north to south (Figure V.6, km 40-20) and more clearly from west to east: increasing from 160 m in the western part (conversion of 0.2 s TWT by using a P-wave velocity of 1600 m/s for less consolidated sediments; Figure V.7) to up to 480 m in its eastern part near the Tortue Island (Figures V.6 and 8d).

Toward the east, close to Tortue Island, the seismic profiles display an unconformity that truncates the horizontally stratified, undisturbed reflectors of Unit 4 (unconformity Uc4a in Figures V.8b and 8c). Unit 4 is therefore subdivided into two sub-units: Unit 4a that shows parallel high frequency reflectors and Unit 4b with parallel moderate frequency, low-amplitude reflectors interspersed with thin chaotic beds (see Figure V.4). The thickness of Unit 4b varies from north to south (Figures V.8a and 8b) and from west to east (Figures V.8c and 8d). On the northern slope off Tortue Island its thickness reaches 0.6 s TWT (~480m thick)(Figure V.8d, km 25-30).

Westward, this sub-unit is almost completely eroded (Figures V.6 and 8c). Recent mass wasting processes probably affected the shape of the slope in the WPS area, eroding the upmost part of Unit 4b.

V.4.1.2 Windward Passage Deep

Sedimentary units in the WPD area do not show clear correlations with those found in the WPS. Units 1 and 4 are common to both areas (Figures V.4 and 6). However, in the WPD these units show some slightly differences in their facies (Figure V.4):

As observed in the WPS area, Unit 1 consists of parallel to sub-parallel high-amplitude and low-frequency reflections onlapping the basement in the WPD area (Figure V.6). Punctually, its seismic facies become transparent to chaotic and the unit displays lateral variations of thickness (Figure V.4). Its bottom geometry is barely visible on seismic data. In the WPD area the Unit 1 does not clearly display distinct sub-units as described in the WPS area.

Unit 2 is a distinct sedimentary unit present only in the WPD area (Figures V.6, 7 and 9). It overlies Unit 1 on the angular unconformity Uc2 (Figure V.10). Its thickness and internal reflection pattern vary throughout the basin. In the north wall of the WPD (southern flank of the WPS), Unit 2 is perched (Figure V.5). Unit 2 is thus defined by parallel to sub-parallel continuous reflectors, which are onlapping the steeply dipping Uc1 unconformity at its northern boundary (Figure V.5, km 25-40). Its thickness is about 1.2s TWT (~960m thick; conversion of 1.2 s TWT by using a P-wave velocity of 1600 m/s for less consolidated sediments), and it thickens slightly northward (Figures V.5 and 6). In the basin, the southern part of Unit 2 displays lateral variations of thickness from east to west (Figures V.7 and 9). Unit 2 reaches a thickness of almost 1.3s TWT (~1040m thick) in its eastern part (Figure V.11). The internal reflection pattern changes gradually from plane-parallel reflectors, low-amplitudes and low-frequency at its base to flat-lying, high amplitudes and high-frequency at its top (Figure V.4). Its seismic facies, thickness and deformation pattern changes laterally within individual seismic lines. For example, the thickness can be about 0.6s TWT (~480m thick) southward and 1.2s TWT northward (see Figure V.10). The most recent upper parts of Unit 4 are characterized by flat-lying strata that overlie Unit 2 strata in the deep basin (Figure V.9).

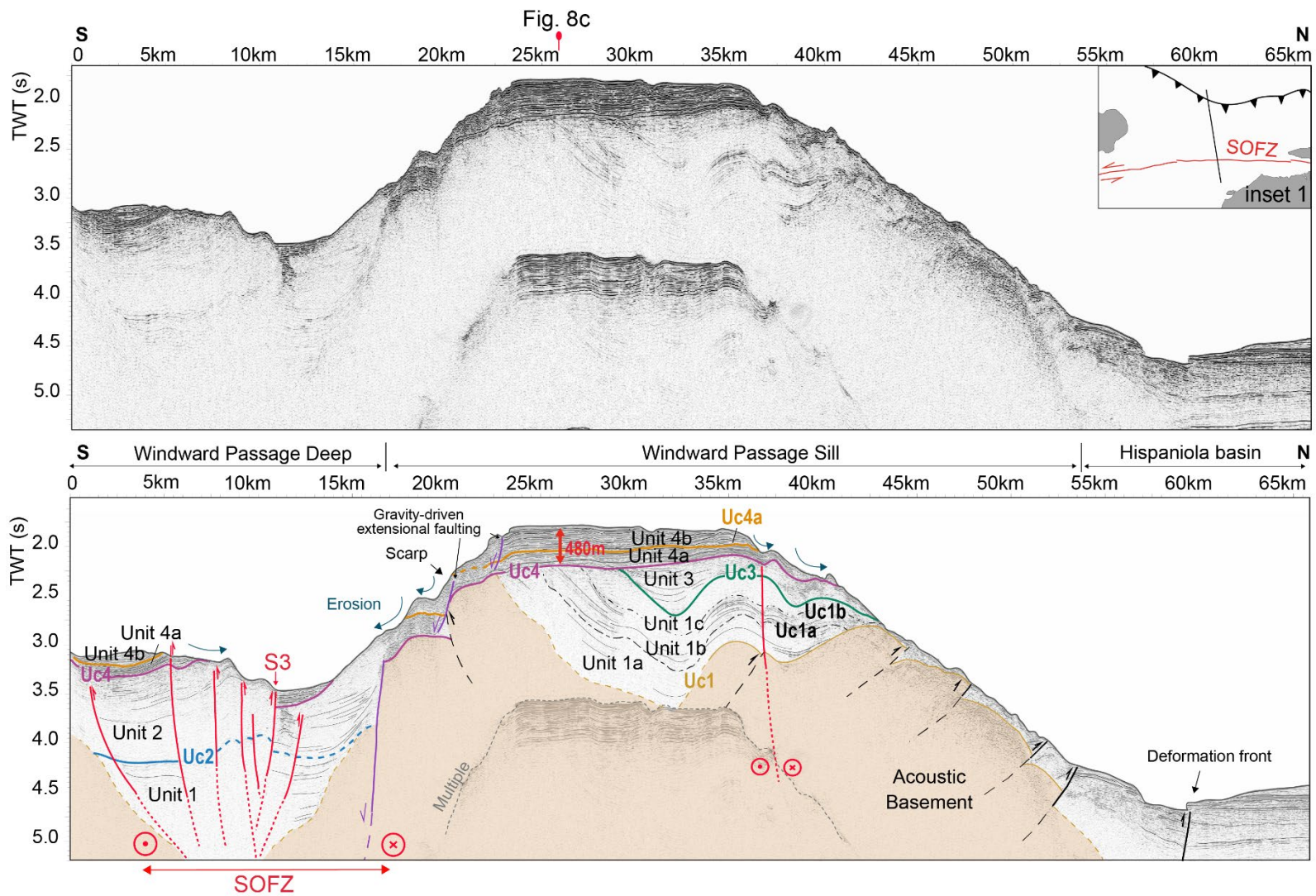


Figure V.6. Seismic profile crossing the Windward Passage Deep (south) and Windward Passage Sill (north). In the Windward Passage Sill, sediments of unit 1 are deformed by older thrust faults. Black dashed lines are inferred faults based on the folded unconformities Uc1 and Uc3. Inset 1: Location of the seismic line.

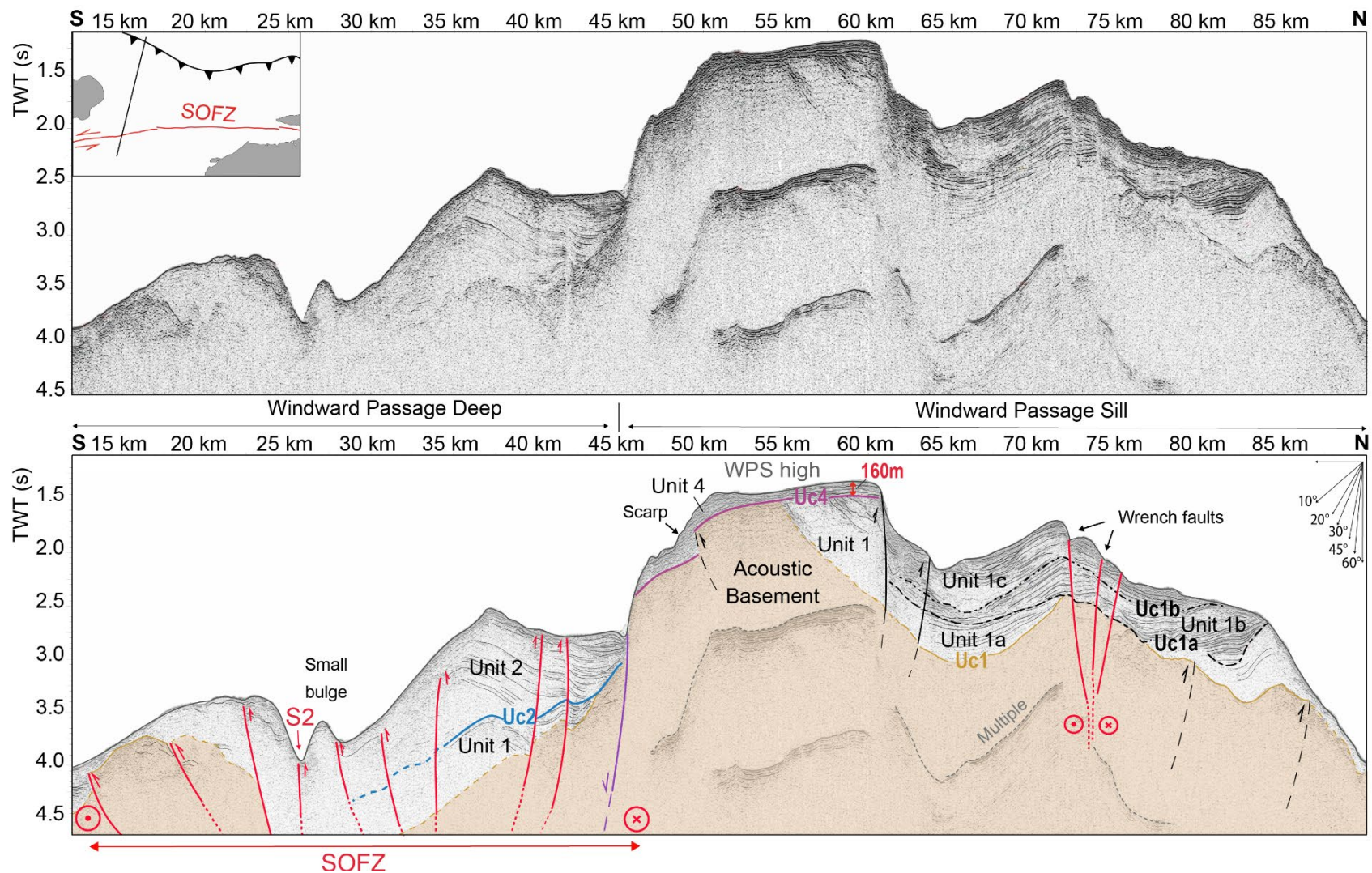


Figure V.7: Seismic profile crossing the Windward Passage Deep (south) and Windward Passage Sill (north). Wrench faults offset the Windward Passage Sill and developed a positive flower structure. The WPS high buildup-structure bordered by reverse faults indicates uplift along the Windward Passage Sill. See inset and Figure V.2 for location of profile.

V.4.2. Structural Analysis

V.4.2.1. Windward Passage Sill structural features

WPS area is characterized in seismic reflection profiles by a topographic high deformed by faults and series of folds (Figure V.7). Numerous imbricated thrusts, mainly synthetic to the deformation front to the north (Figure V.6, km 40 - 60), affect the acoustic basement and progressively steepen its northern slope. On the southern slope of the WPS, north dipping blind thrust faults are inferred from the geometry of the folded and shifted acoustic basement. Presently, gravity-driven normal faults shift the seafloor on the southern edge of the WPS as proposed by Rodríguez-Zurrutero et al. (2020).

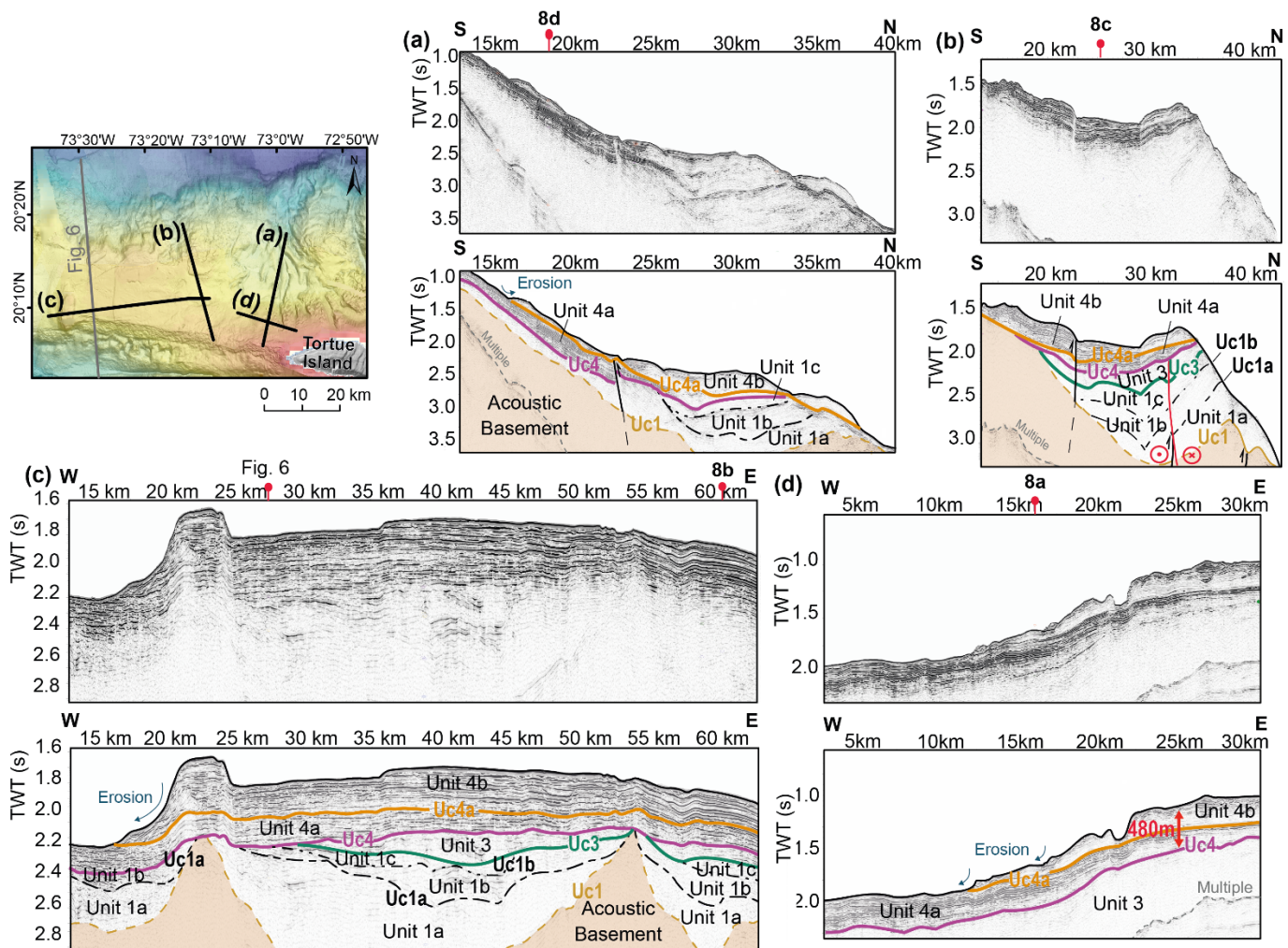


Figure V.8. Seismic profiles in the Windward Passage Sill with interpreted seismic units and its relative unconformities. Inset map shows seismic lines location.

A near-straight fault trace runs towards west along the north flank of the WPS (Figures V.6, km 35-40, and Figure V.7, km 70- 80). The recent study carried out by Rodríguez-Zurrutero et al. (2020) revealed that this fault strand seems to be aligned with the neotectonic SOFZ segment in the south flank of Septentrional Cordillera (Figure V.1a). Its westward termination coincides

with a narrow deformation zone with sub-vertical faults that displace the acoustic basement and the sediment layers in the central part of the WPS (wrench faults in Figure V.12a, km 60-65). The deformation can be followed eastward on parallel seismic lines (Figures V.7, km 70-77, and Figure 12b, km 48-53) and interpreted as a positive flower structure oriented NW-SE. The overlying, parallel-bedded sediments appear to be tilted and displaced by the uplift of this positive flower structure (Figures V.7 and 12a). This uplift of the seabed by the wrench fault strands of the flower structure created a wide synform located south of the wrench faults (Figures V.2 and 12a). This synform is clearly observable in the seabed as an elongated east-west trending depression (Figure V.2). In the westernmost part of the WPS, this positive flower structure takes the form of an NNW-SSE trending antiform with relief of about 350m (Figure V.2). The disturbance of the seafloor and shallow sediments indicate tectonic activity is currently occurring along this structure (Figure V.12).

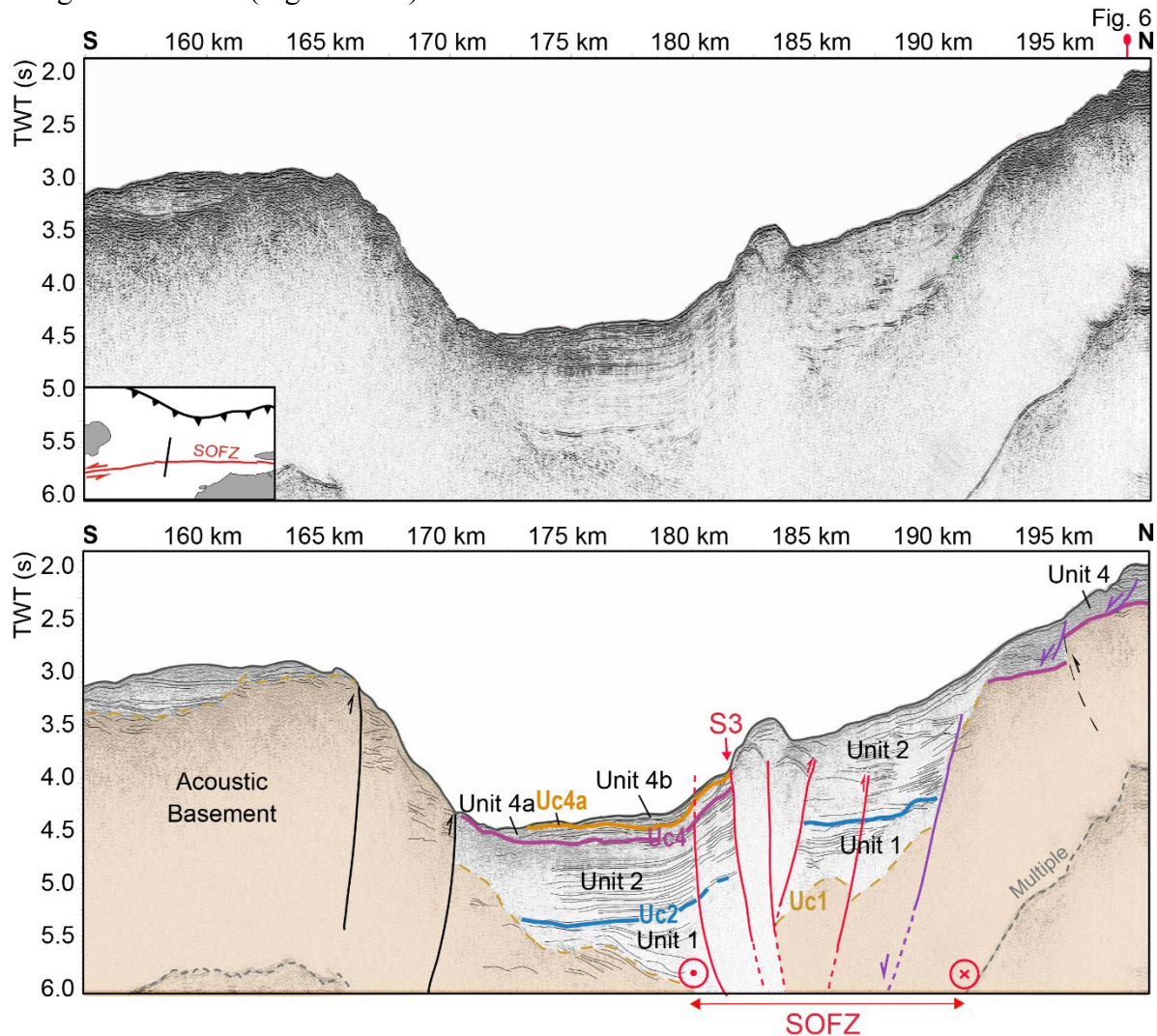


Figure V.9. Seismic profile across the Windward Passage Deep. Sets of reverse faults are identified on either edge of the basin. See inset and Figure V.2 for profile location.

Confined between the WPS synform and the WPD, an isolated structural high characterizes the southwestern part of the WPS, named the WPS high (Figures V.2, 5 and 7). This structural high is bound by opposing north- and south-dipping reverse faults (Figure V.12a, km 35-50). These bounding reverse faults trending E-W with opposing $\sim 45^\circ$ dips delimit the WPS E-W high. The highly benched slope of the WPS, may be the direct consequence of activity on these reverse faults. However, the stepped morphology of the slope suggests that gravity-driven mechanisms may play an important role in its shape by promoting slope erosion (Figure V.6, km 20-25).

V.4.2.2 The Windward Passage Deep structural features

SOFZ activity has clearly left a morphologic imprint on the seafloor study area (Figure V.2) and affected the entire sedimentary record of the WPD area (Figures V.5 to 11).

A network of reverse faults forms a small bulge and trough (1.5 km wide) (Figure V.5, km 18-23). These faults are sub-vertical and seem to merge at depth along a main fault strand that may be associated with the SOFZ (Figure V.9). The internal structure, which displays faults with an opposing dips on either side of this bulge, is typical of a positive flower structure (Figure V.10, km 25-30). The main fault segments and several subordinate strands of this flower structure are imaged on the seafloor mainly as the edges of antiforms (Figure V.2).

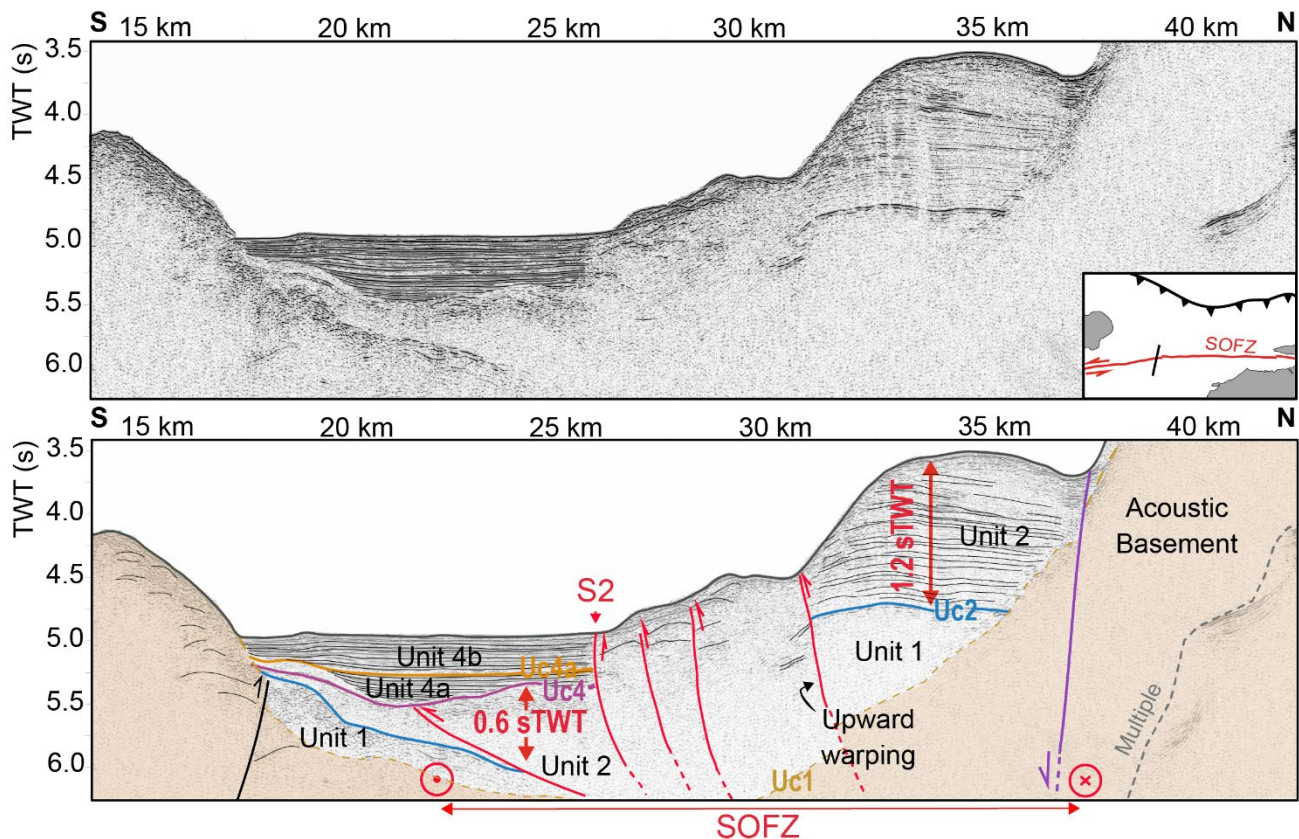


Figure V.10. Seismic profile across the Windward Passage Deep. The unit 2 are uplifted in its northern border. Faults in red highlight the typical expression of the Septentrional–Oriente Fault zone (SOFZ) in the Windward Passage Deep. Pre-existing northern border fault firstly with a normal component and secondly with a reverse component is represented in violet. See inset and Figure V.2 for location of profile.

Expression of the SOFZ on seafloor of the WPD allows us to identify five distinct segments according to azimuth changes. The western 83-km-long segment, Segment 1 (S1 in Figure V.1), runs offshore Cuba through the Punta Caleta high, from 74°50'W to 74°05'W and trends N82°E. A second 50-km-long segment (S2) runs from 74°10'W to 73°35'W and trends N83°E. Segments S1 and S2 have been considered as individual segments based on two distinct traces on the seismic sections and bathymetric data (Figures V.1 and 2), despite short interruptions of rupture traces on the seabed (Figure V.2). The boundary between S1 and S2 corresponds to a contractional jog which forms a relatively small bulge (about ~300m high, Figures V.2 and 7), associated with a distinct change in azimuth of almost 1°. The boundary between Segments 2 and 3 is marked by a change of slope oriented N015° and a sharp azimuth change of 7-8° (Figure V.2). Segment 3 is 74-km-long and trends N90°E. At its western end it runs along the rupture at 73°40'W. Eastward, over a distance of a few kilometers, the fault trace is characterized by a large azimuth change of 10°, that marks the boundary between S3 and S4. From 72°57'W, a Segment 4 trends N100°E to the south of the Tortue Island (Figure V.1).

These active segments of the present-day SOFZ identified on the bathymetric map also appear at depth, in the seismic reflection data (identified on the figures by segments S1 to S4). The width of deformation associated with the SOFZ is narrower in the central part of the WPD (Figure V.2, 73°40'W and 20°02'N) and wider at its extremities (6 km wide). Deformation linked to the flower structure spreads out eastward and the sedimentary cover is highly affected by its fault branches (Figures V.6, 9, and 11). In this area, the most recent sedimentary units (Units 2 and 4) and the unconformities Uc4 and Uc4a appear to have been folded and faulted (Figures V.6 and 11). The present-day offset and roughness of the seafloor indicate ongoing faulting in this area.

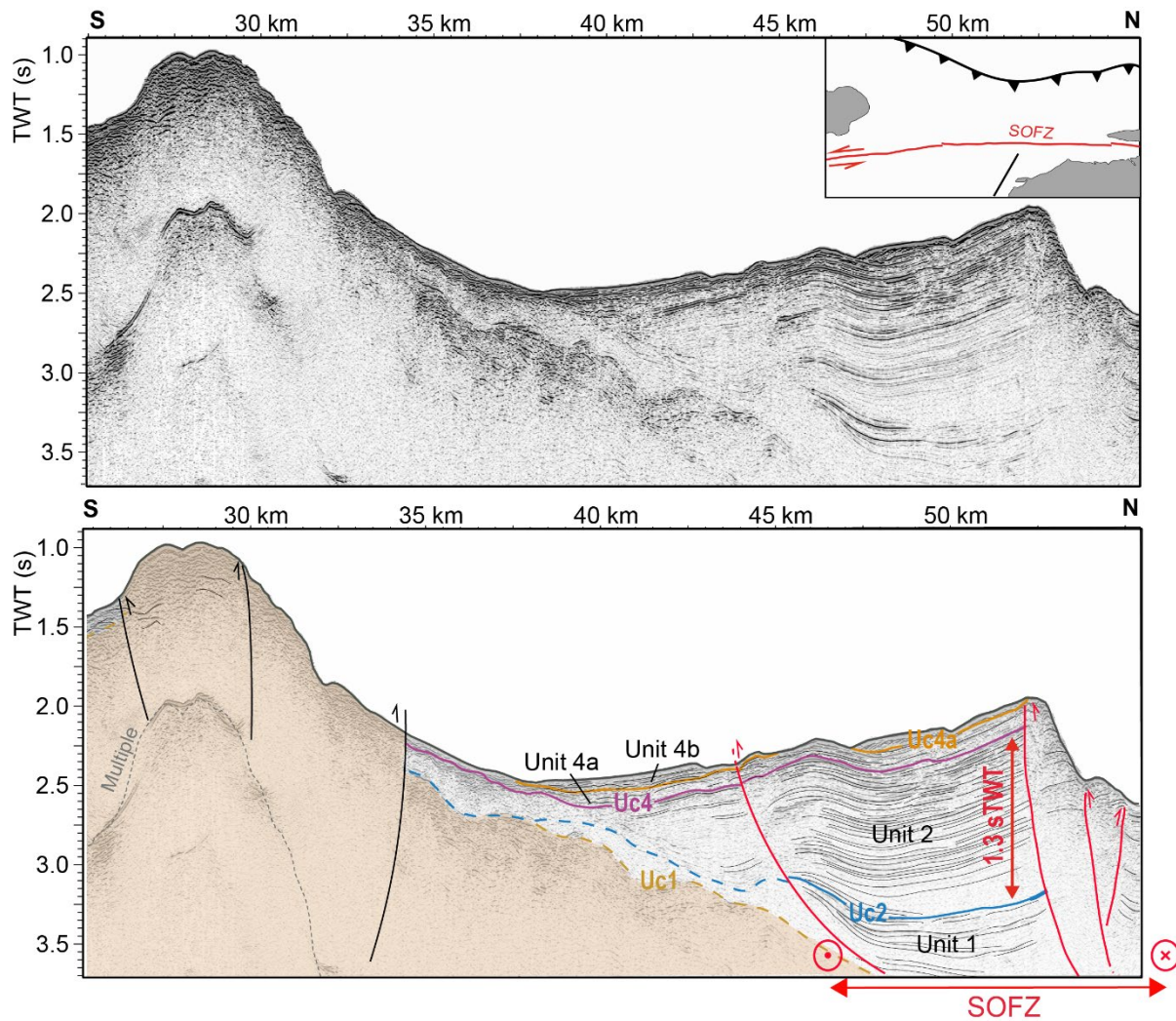


Figure V.11. Seismic profile across the Windward Passage Deep. Sets of reverse faults structural high on the southern edge of the basin. The unit 2 thickens toward the fault highlighting a syntectonic wedge related to a normal faulting. See inset and Figure V.2 for profile location.

These E-W oriented SOFZ segments divides the WPD into a northern block, which we assume to be fixed, and an eastward-moving southern block. Deformation seems to be concentrated in the northern block forming a perched sedimentary block (~10 to 20 km wide, Figures V.7, km 30-45, and 5; km 20-40) characterized by a thick sedimentary deposit (about 1.2 s TWT, Figure V.5). Upwarping of Units 1 and 2 and the folding along this perched sedimentary block, indicate that the WPD northern block is under a compressional stress field. The perched block is bound to the north by a southward-dipping normal fault that offsets the Units 1 and 2 and the acoustic basement (Figures V.5, 6, 7 and 9). Unit 2 thickens northwards toward the fault, highlighting a syntectonic wedge related to an earlier stage of normal faulting (Figures V.5 and 7).

At the southern boundary of the WPD, a set of reverse and thrust faults forms a ridge-like structural high (Figures V.2 and 11, km 25-35). This feature is characterized in the bathymetric data by a steep, uniform, east-west trending scarp ridge. This ridge becomes higher eastward and

seems to extend onshore. The scarp may correspond physiographically to the Môle de Saint-Nicolas area in the Northwestern Peninsula (Haiti) (Figures V.1 and 2).

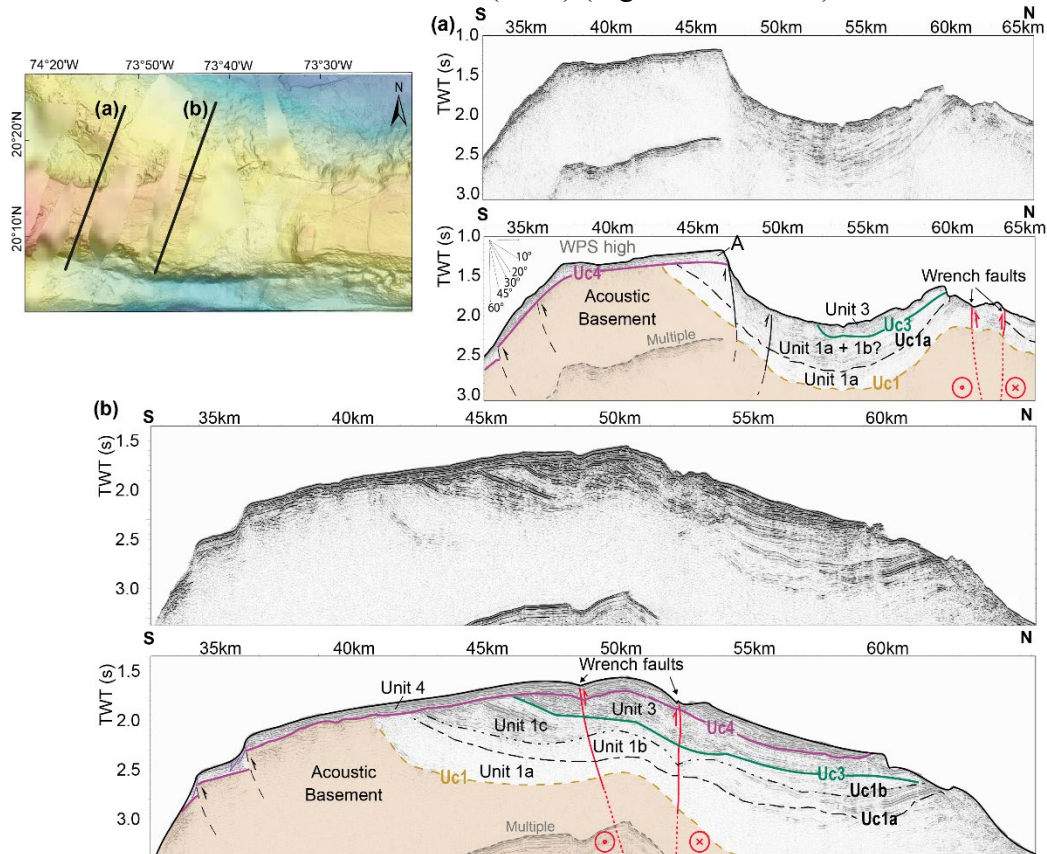


Figure V.12. Two seismic profiles located in the Windward Passage Sill (see inset for location) with interpreted seismic units and its relative unconformities. (a) A narrow wrench fault deformation zone shifts acoustic basement and the sediment layers in the WPS central part. (b) The deformed area can be followed westward on parallel seismic lines. See inset and Figure V.2 for profile location.

In summary, the seismic reflection profiles allowed us to establish a precise structural map of the Windward Passage Deep (Figures V.2 and 13). The sedimentary and structural framework are much more complex than found in previous studies. Seismic data demonstrate that the WPD sedimentary cover is deformed by the multiple, near-vertical fault strands of the SOFZ, forming a large deformation corridor crossing the whole length of the basin (Figure V.13).

V.5. Discussion

Our results reveal distinct deformation styles across the Windward Passage with several phases (at least 3 stages of deformation discussed in section 5.1). Thrust faults and folds in the deeper units of the WPS (Figure V.6, km 25-45) are compatible with a predominantly contractional deformation phase, while the WPD thick sedimentary cover suggests an extensional deformation phase overprinted by a current transpressive deformation (e.g. Figure V.6).

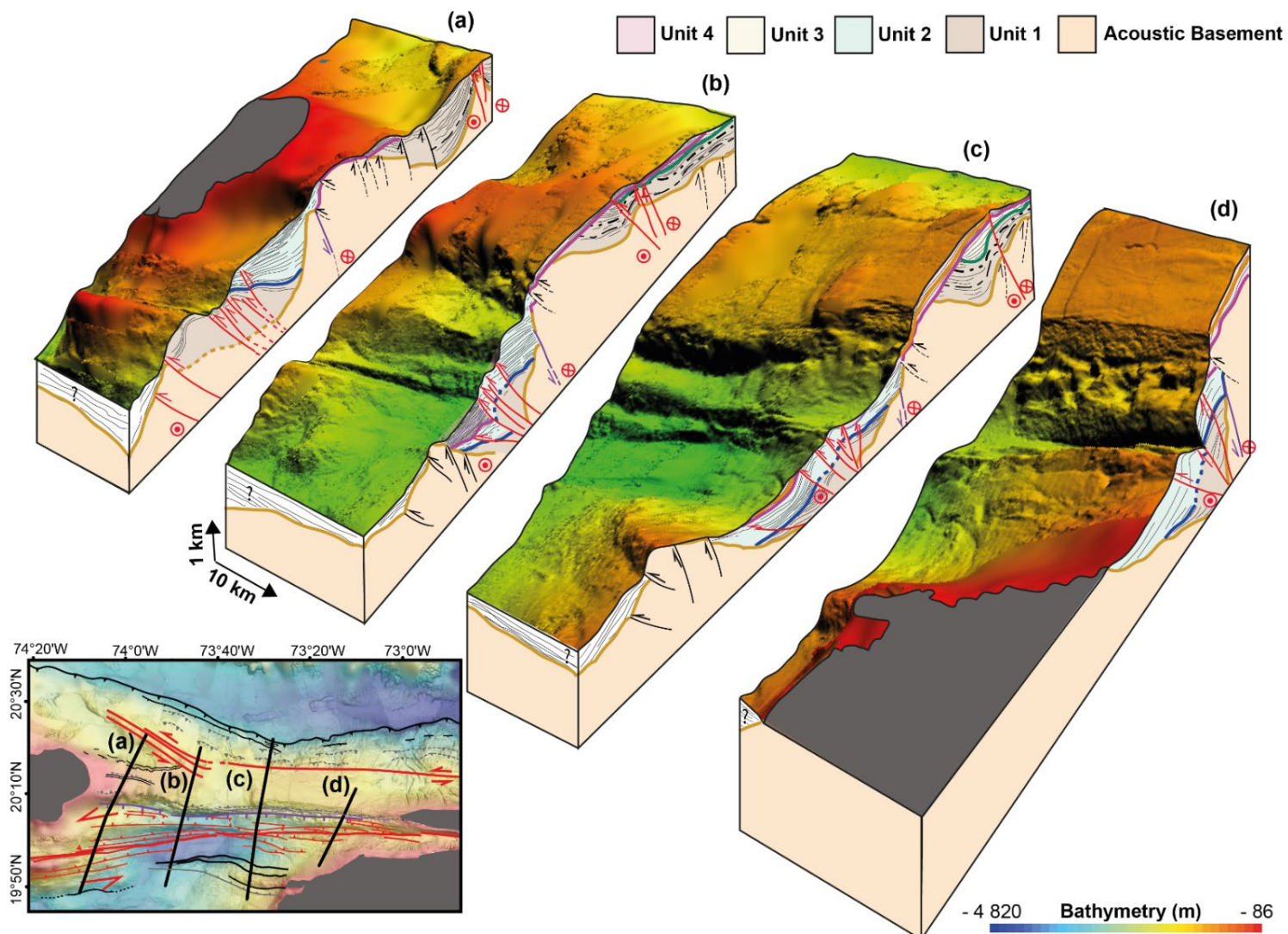


Figure V.13. Four cross-sections across the Windward Passage area showing our summary schematic interpretation from the tectonic framework, as discerned from seismic images presented in this paper. Summary schematic interpretation of the tectonic framework across the Windward Passage, as discerned from seismic images presented in this paper. Inset map shows seismic lines location.

Strike-slip systems usually create conditions that allow for the juxtaposition of normal and reverse faults over a comparatively short distances and periods of time. The most likely hypothesis is a polyphase evolution with a compressive phase followed by a short extensional phase and then a recent transpressive phase. In this scenario, the normal faults offset the WPS southern border are the primary mechanism for WPD opening. Flower structures affecting the most recent WPD sedimentary record represent the current transpressive deformational style in the area.

V.5.1 Deformation events in the Windward Passage

Since the deformation patterns in the WPS and the WPD are quite different, we discuss them separately in this section, before proposing correlations and time constrains for both areas in section 5.2.

V.5.1.1 Windward Passage Sill

The folded Unit 1 records the first deformation event in the Windward Passage Sill domain (Figure V.6). As proposed by Calais & Mercier de Lépinay (1995), folding of Units 1a, 1b and 1c (Figure V.6) suggests that a contractional deformation pulse affected the WPS. The presence of minor unconformities within Unit 1 (unconformities Uc1a and Uc1b in Figures V.6, 7 and 12) indicates intermittent episodes of erosion during its deposition. Units 1a, 2b and 3b are broadly similar in style and orientation, which implies that their top unconformities correspond to rapid episodes of erosion.

The first episode of contractional deformation may have been active until the deposition of Unit 3, which displays less folding than the underlying unconformable Unit 1. The gentler folding of Unit 3 may be due to weaker contractional deformation, suggesting a second compressive pulse in the WPS.

Angular unconformity Uc4 separates the horizontally ponded strata of Unit 4 from the older folded layers of Units 1 and 3, highlighting a sedimentation hiatus (Figures V.4 and 6). Overlying horizontal layers of Unit 4 suggest that the contractional deformation is less pronounced than the earliest contractional stages (Calais & Mercier de Lépinay, 1995). However, relatively flat reflectors do not mean a quiet period as proven by the presence of active reverse faults affecting Unit 4 in the WPS (Figure V.5, km 40 - 60). The southward thickening of Unit 4 and tilting of unconformity Uc4 suggest ongoing contractional deformation (Figure V.6). It implies a southward tilt of the WPS, possibly related to a recent activity of the imbricated thrust zone shearing off the WPS sedimentary strata on its northern slope (Figure V.6, km 40-55). Such observations suggest an ongoing compressional stress field in WPS, in particular on its northern limit (Rodríguez-Zurrunero et al., 2020).

The positive flower structure in the middle part of the WPS provides evidence of a current strike-slip component in WPS area (Figures V.12a, km 60-65, and Figure V.12b, km 48- 53)(Rodríguez-Zurrunero et al., 2020). Such a fault pattern, suggests that lateral slip, together with thrusting, are the two major styles of deformation operating in the WPS. Both styles of deformation reflect a transpressional tectonic regime that is likely a combined response of the large-scale present-day oblique collision between the Caribbean Plate and the Bahama Banks.

V.5.1.2 Windward Passage Deep

In contrast to the folding observed in the WPS, the Units 1 and 2 in the WPD seem relatively less disturbed by the early stages of compressional stress (Figure V.6). At the northern edge of the WPD, the acoustic basement is tilted southward and the presence of northward dipping syntectonic wedges through the Unit 2 (Figures V.6 and 7) suggests an early N-S

extensional tectonics in the WPD area. This extensional stage probably follows Unit 1 deposition, which implies that the onset of Unit 1 deposition precedes the opening of the WPD area. A similar extensional stage affecting older folded sedimentary series is described by Calais & Mercier de Lépinay (1991) in the Imias Basin, just to the south of the study (Figure V.1).

This early extensional tectonic event was related to the opening of the WPD domain and appears to have ceased after Unit 2 deposition. The normal fault identified at the northern boundary of the WPD seems presently inactive since the most recent overlying sediments in the WPD show no evidence of lateral thickening (Figures V.5 and 6). The current morphology of WPD area seems to be controlled by transpressional regime with block “ramps” upward along both sides of the basin (Figure V.9).

The neotectonic strike-slip regional component in the Windward Passage is apparent in the major SOFZ that crosses the entire length of the WPD (Figure V.2). Sets of inward dipping faults that form part of this fault system converge at depth with the main SOFZ segments forming a large positive flower-structure (Figures V.5 and 7). The positive flower structure formed by transpressional shear reflects the current transpressional tectonic setting in the area. Because positive flower structures allow only a small amount of shortening, the dominant type of motion on a thoroughgoing fault characterized by this feature must be strike-slip with a transpressive component (Biddle & Christie-Blick, 1985). Our structural observations lead us to infer that the present-day WPD deformation pattern is currently ruled by significant transpression.

V.5.2 Tectonic interpretation of deformation events and onshore correlations

Due to the lack of direct sampling, sedimentary units in the Windward Passage can only be time-correlated based on onshore observations. Calais & Mercier de Lépinay (1995) were the first to time-correlate deformation events in the Windward Passage with four major paleogeographic periods in both southern Cuba and northern Hispaniola domains. The late Eocene, Oligocene, Middle Miocene and Late Pliocene paleogeographic stages are largely described onshore (Calais, 1990; Pindell & Draper, 1991; de Zoeten & Mann, 1991; Calais et al., 2016; Mann et al., 2002). Each one of these periods corresponds to a drastic reorganization of the Caribbean northern plate boundary geometry (Calais & Mercier de Lépinay, 1995). Based on recent kinematic and advances in onshore field work in southern Cuba (Rojas-Agramonte et al., 2008) and northern Hispaniola (Leroy et al., 2015; Escuder-Viruete et al., 2015; Escuder-Viruete & Pérez, 2020), we propose an alternative correlation of deformation stages in the Windward Passage with the four aforementioned paleogeographic framework in the northern Caribbean Plate (Figure V.14).

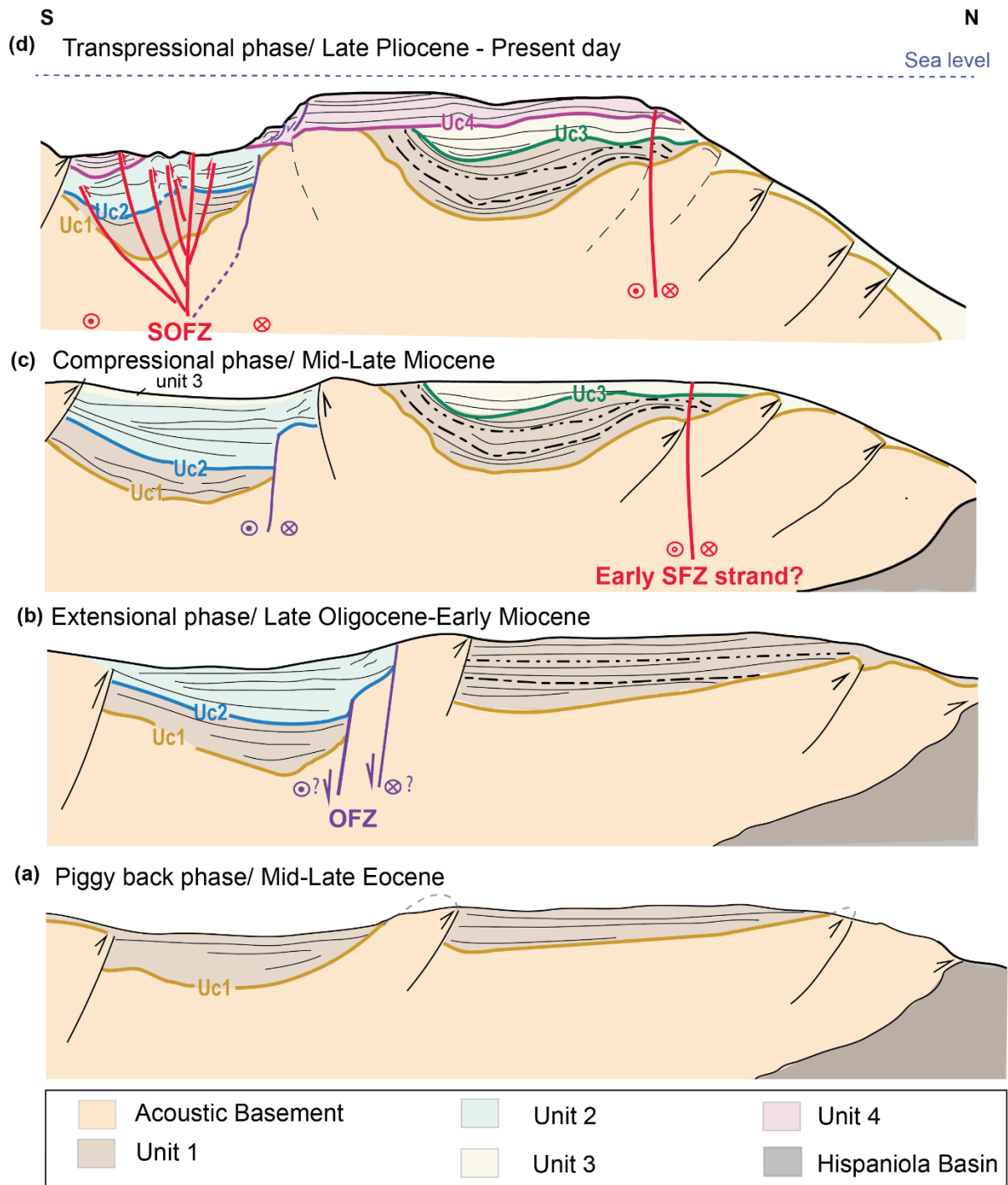


Figure V.14. Sketches of the Windward Passage tectonic evolution in four main tectonic phases from Mid-late Eocene to Late-Pliocene to Present-day. Not to scale.

V.5.2.1 Eocene Deformation: Piggyback basins phase

The acoustic basement high observed at the southern boundary of the WPD (Figure V.11, km 25-35) may outcrop in the northwestern peninsula of Hispaniola. If this is the case, the acoustic basement sedimentary series would be the equivalent to the detrital sedimentary rocks of Abullot Formation of Early/Middle Eocene (possibly Paleocene) age (Butterlin, 1960).

The Eocene is a period of intense contractional deformation with a broad overthrusting and progressive superposition of geologic formations in Cuba and Hispaniola (Mann et al., 1991; Iturralde-Vinent, 1994; Iturralde-Vinent & Gahagan, 2002; Rojas-Agramonte et al., 2008). The Cuban-Hispaniolan arc-continent collision with the Bahama Banks takes place in the Paleocene/middle Eocene (de Zoeten & Mann, 1991; Draper et al., 1994). During this time, the exhumation of ophiolitic and metamorphic rocks occurred, as well as the cessation of arc volcanism in Hispaniola (Escuder-Viruete et al., 2015). Structures in upper Paleocene to middle Eocene sedimentary rocks are consistent with an evolution from a forearc basin into piggy-back basins at the top of an advancing accretionary wedge (Escuder-Viruete et al., 2015). The folding and thrust faulting of Eocene rocks that induced regional uplift and associated piggy-back basins resulted from the convergence between the north-facing Hispaniola Island arc and the Bahama Banks (de Zoeten & Mann, 1991; Escuder-Viruete et al., 2015). The deformation style of the acoustic basement which is characterized by steep horizons, may reflect a complicated set of older stacked geological units inherited from this middle Eocene paleogeographic framework (Figure V.3a). Enhanced uplift during the arc-continent collision may have resulted in subaerial exposure and formation of the basal angular unconformity Uc1 that cuts through previously tilted strata (Figure V.6).

In the late Eocene, the WPS was probably the northernmost continuation of the early piggyback basin formed at the top of the accretionary wedge (Figure V.14a, Pindell & Draper, 1991; Escuder-Viruete et al., 2015). Its current structure would thus be inherited from this compressive scenario. However, according to Escuder-Viruete et al. (2015), the progressive movement of the orogenic wedge toward the NE onto the continental margin may have produced a short subsidence period. This brief subsidence episode that took place in the Late Eocene must have created the space that accommodated deposition of Unit 1 above Uc1 (Figure V.2a). Unconformities Uc1a and Uc1b were probably formed by local episodes of erosion, as the sub-units of Unit 1 are similar in both style and orientation (Figure V.6). Outcrops of formations onshore suggest that this subsidence period was followed by deposition of deep-marine sequences (Upper Eocene to lower Miocene) in a relatively stable forearc basin.

V.5.2.2 Late-Oligocene: Extensional Phase

We interpret the extensional phase, that peaked during the earliest stages of development of the WPD, to be late Oligocene in age (Figures V.3c and 14b). Disruption of Hispaniola and Eastern Cuban blocks started in Early Oligocene (Leroy et al., 2000). The eastern Cuban block becomes attached to the North American plate as the plate boundary jumps to the Oriente fault (Figure V.3c, Leroy et al., 2000; Rojas-Agramonte et al., 2008; Wessels, 2019). Oligocene time is described as a tectonically stable period onshore without any significant compressional event on Hispaniola (Pindell & Draper, 1991; de Zoeten & Mann, 1991). However, several authors propose an extensional event related to the northern Caribbean boundary stress reorganization that occurred when the Oriente fault development during Oligocene (Calais & Mercier de Lépinay 1992; Iturralde-Vinent, 1998; Rojas-Agramonte et al., 2008). Onshore observations of Rojas-Agramonte et al. (2008) in the Sierra Maestra region suggest that contractional structures were overprinted by widespread extensional structures, mainly southward dipping normal faults, in the late Oligocene to Miocene (Figure V.3c). Calais & Mercier de Lépinay (1991) also relate a transtensional regime in the offshore southern Cuban coast, which is accompanied significant subsidence of the Oriente deep. Normal faulting on the northern edge of the WPD is probably related to this transtensive episode (Figure V.14b). Unit 1 and the acoustic basement are tilted toward the normal fault planes creating accommodation space for the syntectonic deposition of Unit 2 above the unconformity Uc2, which is likely late Eocene-Early Oligocene in age (Figures V.3c et 14b). Syntectonic deposition of Unit 2 in the WPD may be coeval to the continuous Unit 1 deposition in the WPS area.

V.5.2.3 Middle Miocene Deformation: Compressional phase

We interpret the compressive episode in which Units 1 and 2 undergo contraction to be middle Miocene in age (Figures V.3e and 14c). This event is mainly recorded in the WPS. According to Calais & Mercier de Lépinay (1991), a similar event is observed in the Oriente deep area (Figure V.1a), where the basin sedimentary infill begins to undergo compression at this time. Extensional tectonic may have ceased in the early/middle Miocene times, when the onshore Oligocene basins sedimentary infill begins to fold (de Zoeten and Mann, 1999). From late Oligocene to early/middle Miocene time, the OFZ is the locus of large strike-slip faults, with only minor vertical movement (Figure V.3d; de Zoeten and Mann, 1991). de Zoeten and Mann (1991) interpret the lack of angular unconformities during this interval as the lack of a significant contractional component. This interpretation is consistent with the oceanic spreading history in the Cayman Through, along the western extension of the Oriente Fault Zone (de Zoeten & Mann, 1991; Leroy et al., 2000). Oceanic magnetic anomalies in the Cayman Through suggest more than 200km of left-lateral strike-slip displacement since late Oligocene-early Miocene time (Rosencrantz et al., 1988; Leroy et al., 2000).

Late Eocene-Early Miocene formations on Hispaniola (Altamira, Las Lavas, and La Toca Formations, e.g de Zoeten and Mann, 1991) are folded and faulted by a minor compressional episode during the middle Miocene (Pindell & Draper, 1991; de Zoeten & Mann, 1991; Calais & Mercier de Lépinay, 1995; Erikson et al., 1998; Escuder-Viruete & Pérez, 2020). This minor compressional event is associated with the initial development of a restraining bend in northern Hispaniola (Figure V.3e) (Erikson et al., 1998; de Zoeten & Mann, 1991, 1999). As restraining bends do not efficiently accommodate the regional transcurrent shear of the fault system (Cooke et al., 2013), the middle Miocene was probably a period of active fault evolution including the abandonment and the development of new fault strands. Initiation of new fault strands in the WPS (Figure V.3e) and its subsequent migration into the WPD (Figure V.3f) may have allowed the fault system to more efficiently accommodate strike-slip stress. At this time, the whole of the Caribbean Plate to the south also experiences an episode of compression (Mauffret & Leroy, 1997; Mauffret & Leroy, 1999).

We propose that during this middle Miocene compressive episode, thrust faults formed in the WPS northern slope. Ongoing compression in the WPS, folded Unit 1 and created space to accommodate Unit 3 deposition (Figure V.14c). Simultaneously, the SFZ strand evolved to accommodate part of the ongoing strike-slip stress (Figure V.14c). Calais & Mercier de Lépinay (1995) propose an erosional episode during which Unit 1 may have been partially eroded and that the eroded material may have filled up the syncline depressions formed by the previous folding of Unit 1, thus depositing Unit 3. Another possible interpretation is that Unit 3 is the equivalent of the Upper Miocene to Lower Pliocene carbonate platform (Villa Trina Fm, e.g. Escuder-Viruete and Pérez, 2020) deposited during a transgressive cycle in the Lower Miocene to late-middle Pliocene in northern Hispaniola (Escuder-Viruete & Pérez, 2020). In the Cordillera Septentrional (Figure V.1), the carbonate platform rocks are tilted, faulted and folded in synclines of the upper Eocene-middle Miocene age (Escuder-Viruete & Pérez, 2020). In this case, the local angular unconformity separating upper Eocene-middle Miocene rocks from less folded carbonate rocks onshore in the Cordillera Septentrional (de Zoeten and Mann, 1999) could be the equivalent of unconformity Uc3 observed in the WPS.

V.5.2.4 Pliocene to Present Deformation: Transpressional phase

We interpret the current transpressive component in the Windward Passage to have been initiated during Pliocene time (Figures V.3f, 3g and 14d). The Pliocene is described as a period of dramatic reorganization of the northern Caribbean Plate boundary (Calais & Mercier de Lépinay, 1995; Calais et al., 2016). It is marked by the oblique collision of the northern

Hispaniola block within the Bahama Banks (Figure V.3f; Calais et al., 2016; Escuder-Viruete and Pérez, 2020). Obliquity of the maximum horizontal stress has promoted the development of a transpressional zone, with oblique motion between Hispaniola and Bahama Banks (Pindell & Draper, 1991). This, in turn, caused activation of WNW- to W-trending left-lateral strike-slip faults that accommodated and continue to accommodate part of the oblique convergence between the Caribbean and North American Plates. This may also be the case for the Septentrional Fault Zone (SFZ) which formed during the Pliocene as well (Figure V.3g; Leroy et al., 2015; Calais et al., 2016; Escuder-Viruete and Pérez, 2020). Formation of the Septentrional-Orient Fault Zone (SOFZ) in the Windward Passage occurred when the Oriente Fault Zone (OFZ) joined the Septentrional Fault Zone (SFZ) (Figure V.3f). The SOFZ segments in the WPD likely formed in the early Pliocene (Figure V.14d). Transpressive deformation due to oblique collision prompted the development of positive flower structures in the Windward Passage (Figures V.5, 6 and 7). In the WPD area, the positive flower structure forms an antiformal corridor over the SOFZ trace. Units 2 and 3 were folded and uplifted (Figure V.14d) and this uplift created a strong erosional surface over the whole area, unconformity Uc4 (Figures V.7 and 14d).

The Pliocene is also marked by the uplift of the Cordillera Septentrional (C. Sept. in Figure V.3g, Calais et al., 2016; Escuder-Viruete and Pérez, 2020). The great regional uplift triggered the destruction of the upper Miocene-lower Pliocene forearc carbonate platform (Escuder-Viruete & Pérez, 2020). The onset of collision with the Bahama Banks during the mid-Pliocene in this area was followed by a regional sedimentary hiatus that persists until late Pleistocene in the northern Cordillera Septentrional (Escuder-Viruete and Pérez, 2020). We correlate the sedimentary hiatus highlighted by the overlying horizontal layers of Unit 4 above the folded Units 1 and 3 (unconformity Uc4 in Figures V.4 and 6) to be the offshore equivalent of this regional sedimentary hiatus. If this is the case, Unit 4 would be middle- to late-Pleistocene in age. If so, the onshore equivalent would be the Quaternary coral reef terraces of northern Hispaniola (Isabela Fm, e.g. Escuder-Viruete and Pérez, 2020). This Quaternary formation that includes two main facies onshore, may correspond to Units 2a and 2b in the Windward Passage (Figures V.4 and 8).

The system of Quaternary coral reef terraces on along the northwest coast of Hispaniola and the southeast coast of Cuban (Môle de St. Nicolas in Figure V.1b; Sorel et al., 1991; Calais & Mercier de Lépinay, 1992) implies a period of active compressional tectonic uplift (Escuder-Viruete et al., 2020). The onshore extensions of the Western WPS high and of the Eastern WPD correspond to the uplifted areas of Guantánamo and Môle de St. Nicolas respectively (Figure V.1b). The WPS displays enhanced uplift at its both extremities. Sorel (1991) dates the most recent marine terrace at Môle de St. Nicolas as 80 Ka. In Cuba, Rojas-Agramonte et al. (2008) relate a general uplift of the reefs and detrital limestones from late Miocene to Quaternary as part of a system of marine terraces. The first Pleistocene terrace can be seen at several localities along the Cuban coast, with up to 20 m in Guantanamo area (southeastern Cuba coast, Figures V.1 and 3). Marine terraces in Guantanamo are more elevated (up to 400 m, Muhs et al., 2017) than others described along Cuban coast supporting the notion of strong and rapid uplift (Iturralde-Vinent, 2003). Rojas-Agramonte et al. (2008) interpret this terrace to be related to active tectonic movements along the SOFZ.

Active reverse faults cutting the topmost layers of Unit 4 in the WPS high may be associated with the current compressional pulse recorded in the Northern Hispaniola. The collision with the Bahama Banks is also recorded by the formation of fold-thrust structures in the northwestern submarine accretionary wedge, known as the Northern Hispaniola Deformation Belt (NHDB in Figure V.1a)(Dillon et al., 1992; Dillon et al., 1996; Rodríguez-Zurrunero et al., 2019). Southward tilting of Unit 4 could also be explained by this recent

tectonic pulse in the Caribbean-North American Plate boundary that activated thrust faults along the northern limit of the WPS (Figure 5, km 40-60). Moreover, the narrow positive flower structure affecting the most recent sedimentary layers in its middle part of the WPS indicates that the area is undergoing current transpressional deformation (Figure V.2).

The presence of current transpressive structures across the Windward Passage area confirms the influence of the active transpressional strike-slip component in the area. An oblique-reverse focal mechanism located in the WPD is evidence of transpression in this area (Corbeau et al., 2019). However, the regional approach of Corbeau et al. (2019) shows the scarcity of this type of event in the northern Caribbean Plate in which most focal mechanisms are thrust-fault related. The lack of focal mechanisms with left lateral strike-slip component may suggest that the accommodation of the horizontal component of displacement may be mostly aseismic (Rodríguez-Zurrunero et al., 2020) or that there are not enough seismometers to properly record it. Current compressional deformation is mainly N-S to NNE-SSW as the result of the collision between the Bahama Banks and Hispaniola (Corbeau et al., 2019).

V.5.2.2 Timing constraints for the SOFZ propagation

The closely spaced seismic lines crossing the SOFZ main segments allowed us to infer critical time indicators that bracket the interval in the stratigraphic section during which horizontal strike-slip motion began in the WPD. As the Early Miocene locus of Caribbean North-American Plate displacement was north of the Cordillera Septentrional (Figure V.3d) (Calais & Mercier de Lépinay, 1995; Erikson et al. 1998), the strike-slip displacement may not have affected the early WPD sedimentary record at this time.

Geometry trends of Units 1 and 2 suggest that these two units predate initiation of horizontal movement on the SOFZ in the WPD (Figures V.5 and 10). Strike-slip motion of S1, S2, S3 and S4 segments appears to have taken place after Units 1 and 2 were deposited (Figure V.1b). The approximately E-W trending of these segments divides the WPD into a southern block and a northern block moving past each other as left-lateral strike-slip movement occurs on the fault system. Thickness changes in Unit 2 between the WPD northern and southern blocks may be due to the left-lateral southern block displacement (Figures V.5, 10, and 11). Bohannon (1975) describes a similar observation elaborated by the correlation of Oligocene and Miocene rocks in southern California. In this region, these formations were originally deposited in continuous nonmarine basin formed by extensional tectonics, but subsequent right-slip faults evolved and have displaced these formations to their present positions. More examples are described in the Wecoma fault in the Cascadia basin, in the offshore Oregon convergent margin (Goldfinger et al., 1993), and at strike-slip fault zones in the offshore regions of Fukushima and Miyagi, Japan (Arato, 2017).

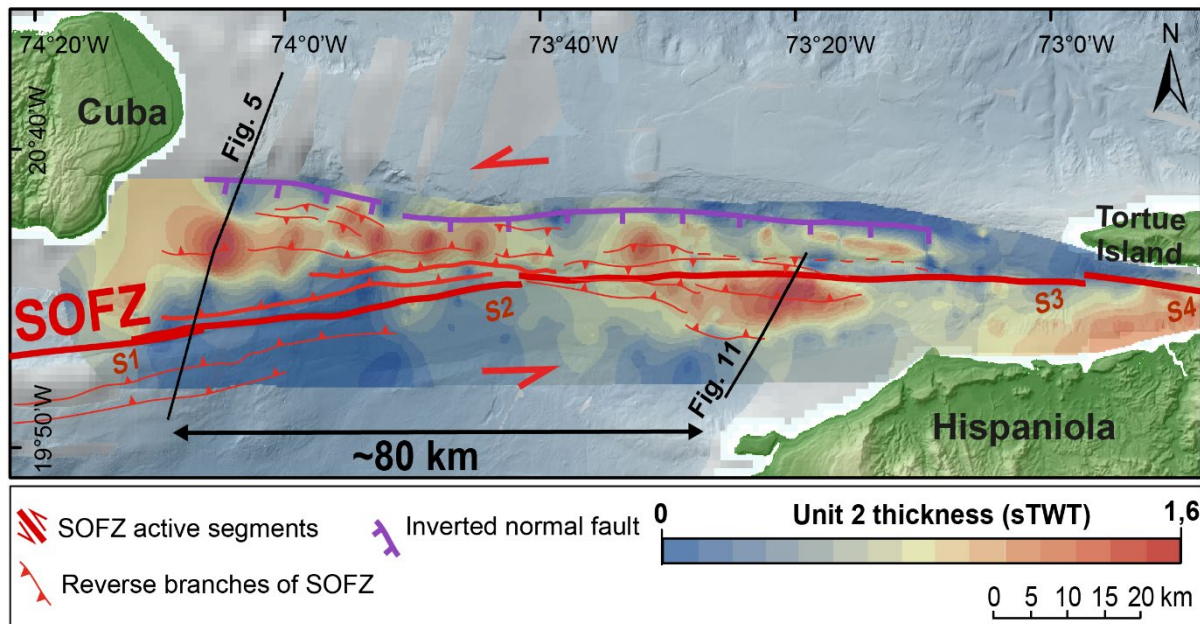


Figure V.15. Isopach map of the unit 2 showing the 80km displacement of the Windward Passage Deep depocenter through east. Note that the bold reverse branches of SOFZ (north to the S2 segment) delimit well the unit 2 depocenter. These two fault strands probably accommodate part of the lateral relative motion during the left-lateral displacement of this unit.

Unit 2 thickness and seismic facies are used to estimate the left-lateral strike-slip displacement since the inception of the SOFZ segments. Basin configuration before strike-slip fault propagation should be identifiable after restoration of left slip displacement (Goldfinger et al., 1993). The horizontal plane sections are restored to estimate the onset of strike-slip motion. The southern block is translated right-laterally until Unit 2 thickness and seismic facies match on the opposite side of the fault. Corresponding Unit 2 thickness and seismic facies are found on seismic lines separated by 80 km in Figures V.11 and 5, thus the horizontal distance needed to restore the section is at least ~80 km (Figure V.15). However, as each fault strand accommodates part of the lateral relative motion, the left-lateral displacement of this unit must have taken place over a much larger deformation zone rather than along a single fault segment (Figure V.15). We infer an age of 5.4 ± 0.2 Ma for the onset of SOFZ segments in the WPD. Our estimate is based on the current $\sim 14\text{--}15$ mm yr⁻¹ of left-lateral motion predicted by Benford et al. (2012) for the Oriente Fault and our estimation of 80 km-net slip in the WPD. Time of fault propagation in the WPD is then coincident with the Pliocene paleogeographic reorganization. This estimated fault age may include a large error as we consider a slip-rate constant since the late Miocene time. Even though it is known that strike-slip fault systems change the apportionment of fault slip rates as they evolve and some slip rate discrepancy may occur over time (Cooke et al., 2020).

Timing relationship between Oriente and Septentrional fault segments (OFZ and SFZ respectively, e.g. Figure V.3) is not clear. According to Calais & Mercier de Lépinay (1995) the plate boundary has been migrating since Late Oligocene-Early Miocene time when the locus of Caribbean-North American Plate motion shifted to the Oriente fault and splayed eastward (Figure V.3f). The transcurrent plate boundary must have been located north of Hispaniola during the Miocene until the Pliocene (Calais & Mercier de Lépinay, 1995). However, Pliocene oblique collision of the Bahama Banks with northern Hispaniola (Escudier-viruet and Perez, 2020) slowed down the Hispaniola's eastward motion with respect to the North American Plate (Calais et al., 1992). Obliquity of the collision transmitted far-field stress to the overriding plate and prompted activation of strike-slip and contractional components within Hispaniola.

Partitioning of the external stress field caused activation of the SFZ and uplift of the Cordillera Septentrional (Figures V.3g and 3f, Mann et al., 2002; Calais et al., 2016). Because of SFZ formation, the previously location of the major strike-slip fault in the Hispaniola basin was abandoned (Calais & Mercier de Lépinay, 1995). The major strike-slip motion shifted south to the present-day trace of the plate boundary, transferring part of northern Hispaniola (the present-day Cordillera Septentrional of the Dominican Republic) to the North-American plate (Calais & Mercier de Lépinay, 1995; Erikson et al., 1998; Leroy et al., 2015; Calais et al., 2016; Escudier-Viruete & Perez, 2020).

Our estimate of the age of the SOFZ segments in the WPD correlates well with ages inferred for onshore strike-slip faults on Hispaniola (Draper et al., 1994; Erikson et al., 1998, Escudier-Viruete and Perez, 2020). Erikson et al. (1998) estimate a similar offset of 85 km for the Septentrional fault segment in Cibao basin in the Cibao Valley (northern Hispaniola, Figure V.1). Escudier-Viruete and Perez (2020) suggests a similar horizontal displacement of ~88 km, which implies an average ~25 mm. yr⁻¹ slip rate for the last 3.5 Ma. Draper et al. (1994) related that the CFZ (subparallel to the onshore SFZ; Figure V.3g) has accommodated at least 60 km of left-lateral strike-slip since the Eocene. During the Pliocene collision, the major strike-slip motion probably shifted south to the SFZ present location (Calais et al., 2016) as the Oriente fault system splayed eastward running across the WPD and into northern Hispaniola to form the SOFZ (Figure V.3f; Calais & Mercier de Lépinay, 1995; Leroy et al., 2015). Moreover, the estimate 16.5 km offset along the Septentrional fault zone segment offshore does presume an onset of motion at 1.8 Ma (Leroy et al., 2015).

These discrepancies of displacements imply that until the uppermost Pliocene, the regional stress field is accommodated mainly by the SFZ but that some local-field stress transferred to subparallel splays, such as the Camú fault zone (Figure V.1a)(Rodríguez-Zurrunero et al., 2020). However, in the uppermost Pliocene the trace of the OFZ extends offshore parallel to the northern coast of Haiti until it connects with the SFZ in northwestern Dominican Republic (Figure V.3f, Leroy et al., 2015). The result of this last regional paleogeographic reorganization formed the current plate boundary which is represented by the SOFZ present-day trace (Figure V.3g; Calais et al., 1992; Leroy et al., 2015; Calais et al., 2016). The uppermost Pliocene is also the age inferred by Escudier-Viruete and Perez (2020) for the oblique collision of the Bahama Banks with the northern Hispaniola.

V.5 Conclusions

Tectono-sedimentary evolution in the Windward Passage provides critical constraints for the diachronous evolution of the northern Caribbean Plate boundary over Neogene times. Four main seismic units were identified above the acoustic basement in the Windward Passage. Sedimentation in the Windward Passage Sill (WPS) and in the Windward Passage Deep (WPD) probably occurred in a common paleogeographic framework until the inception of the early Oriente Fault zone (OFZ). Therefore, syntectonic deposition of Unit 2, distinct to the WPD, marks the beginning of strike-slip stress field in the area. Discrepancies in seismic facies and the deformation patterns present in the seismic units in both geographic areas probably reflects the structural evolution of the earlier transcurrent plate boundary represented by the OFZ until the initiation of the current SOFZ.

The Windward Passage has recorded at least 4 tectonic events related to the ongoing oblique collision between the Caribbean Plate and the Bahama Banks. In this context, the first tectonic event in the area may correspond to the period of Cuban-Hispaniola Arc collision, in which the sedimentary cover of the ancient forearc basin was gradually uplifted recording the formation of piggyback basins along a syn-collisional margin. The second tectonic event records a period of transition between mainly contractional and transcurrent motions. This

period is marked by an important paleogeographic reorganization that corresponds to a brief transtensional event that resulted in the opening of the Windward Passage Deep during the OFZ initiation and the consequent disruption of the Cuban and Hispaniola blocks. The last two events are characterized by contractional and then the current transpressional deformation mainly reflects (i) the progressive collision between the Bahama Banks and Hispaniola blocks and (ii) the Caribbean Plate's eastward escape relative to the North American plate. These last stages of deformation are particularly well recorded in the Windward Passage sedimentary cover, which was folded and displaced left-laterally shifted by the SOFZ. Through the Windward Passage Deep, the estimated ~80 km offset of the sedimentary cover on either side of the major fault suggests an early Pliocene inception for the SOFZ segments in this area. This result provides important time constraints on the SOFZ southeastward migration as well as additional information on the time-related evolution of the northern Caribbean Plate boundary.

Acknowledgments

We thank Captain Moimeaux, the crews and technicians of the RV L'Atalante (IFREMER/GENAVIR) and the scientific team. We are indebted to the French Embassies in Haiti, Bruno Asseray and Cuba, Aurelie Nogues and Oliver Tenes. We also thank the local authorities, as well as Daysarih Tapanes Robau from CITMA, Claude Prepetit from BME, and R. Momplaisir, D. Boisson and J. Jadotte from UEH. We thank Dr Bernard Mercier de Lépinay for his precious time and helpful comments. We also want to thank the Associate Editor Dr Laura Giambiagi, and the reviewers Dr Jose-Luis Granja Bruña and Dr Serge Lallemand for their helpful comments on the first version of this paper. We deeply thank Dr Heather Sloan for post-editing the English style and grammar. A. Oliveira de Sá is supported by funding from Sorbonne University. The processed data will be available on demand on the website Seanoe.org.

V.6 References

- Arato, H. (2017). Cenozoic Fault Zone Activity and Geologic Evolution of the Offshore Regions of Fukushima and Miyagi Prefectures, Northeastern Japan, Based on Petroleum Exploration Data. In Y. Itoh (Ed.), *Evolutionary Models of Convergent Margins - Origin of Their Diversity* (pp. 29-48). Croatia: IntechOpen. <http://dx.doi.org/10.5772/67391>
- Benford, B., DeMets, C., & Calais, É. (2012). GPS estimates of microplate motions, northern Caribbean: evidence for a Hispaniola microplate and implications for earthquake hazard. *Geophysical Journal International*, 191(2), 481–490. <https://doi.org/10.1111/j.1365-246X.2012.05662.x>
- Biddle, K. T., & Christie-Blick, N. (Eds.) (1985). *Strike-Slip Deformation, Basin Formation, and Sedimentation*. Tulsa, OK: SEPM Society for Sedimentary Geology. <https://doi.org/10.2110/pec.85.37>
- Bohannon, R.G. (1975). Mid-Tertiary conglomerates and their bearing on Transverse Range tectonics, southern California, in J.C. Crowell (Ed.), *San Andreas fault in southern California - a guide to San Andreas fault from Mexico to Carrizo Plain* (Special Report 118, p. 75-82): Sacramento, CA: Division of Mines and Geology.
- Boschman, L. M., van Hinsbergen, D. J. J., Torsvik, T. H., Spakman, W., & Pindell, J. L. (2014). Kinematic reconstruction of the Caribbean region since the Early Jurassic. *Earth-Science Reviews*, 138, 102–136. <https://doi.org/10.1016/j.earscirev.2014.08.007>
- Butterlin, J. (1960). Géologie régionale de la République D'Haïti. In J. Butterlin (Ed.), *Géologie générale et régionale de la république d'Haïti* (pp. 29-118). Paris: Éditions de l'IHEAL.

- Calais, É. (1990). Relations cinématique/déformation le long des limites de plaques en coulissage : l'exemple de la limite de plaques Nord Caraïbe de Cuba à Porto Rico, (Doctoral dissertation). Nice: University of Nice.
- Calais, É., & Mercier de Lépinay, B. (1989). Des données nouvelles sur la Cordillère Septentrionale de République Dominicaine: ses relations avec la limite de plaques décrochante. *Comptes rendus de l'Académie des sciences*, 309, 409–415.
- Calais, É., & Mercier de Lépinay, B. (1991). From transtension to transpression along the northern Caribbean plate boundary off Cuba: implications for the Recent motion of the Caribbean plate. *Tectonophysics*, 186(3), 329–350. [https://doi.org/10.1016/0040-1951\(91\)90367-2](https://doi.org/10.1016/0040-1951(91)90367-2)
- Calais, É., & Mercier de Lépinay, B. (1992). La limite de plaques décrochante Nord Caraïbe en Hispaniola: évolution paléogéographique et structurale cénozoïque. *Bull. Soc. Géol.*, 3(163), 309–324.
- Calais, É., & Mercier de Lépinay, B. (1995). Strike-slip tectonic processes in the northern Caribbean between Cuba and Hispaniola (Windward Passage). *Marine Geophysical Researches*, 17(1), 63–95. <https://doi.org/10.1007/BF01268051>
- Calais, É., Freed, A., Mattioli, G., Amelung, F., Jónsson, S., Jansma, P., et al. (2010). Transpressional rupture of an unmapped fault during the 2010 Haiti earthquake. *Nature Geoscience*, 3(11), 794–799. <https://doi.org/10.1038/ngeo992>
- Calais, É., Symithe, S., Mercier de Lépinay, B., & Prépetit, C. (2016). Plate boundary segmentation in the northeastern Caribbean from geodetic measurements and Neogene geological observations. *Comptes Rendus Geoscience*, 348(1), 42–51. <https://doi.org/10.1016/j.crte.2015.10.007>
- Chemenda, A. I., Burg, J.-P., & Mattauer, M. (2000). Evolutionary model of the Himalaya–Tibet system: geopoem: based on new modelling, geological and geophysical data. *Earth and Planetary Science Letters*, 174(3), 397–409. [https://doi.org/10.1016/S0012-821X\(99\)00277-0](https://doi.org/10.1016/S0012-821X(99)00277-0)
- Cooke, M. L., Schottenfeld, M. T., & Buchanan, S. W. (2013). Evolution of fault efficiency at restraining bends within wet kaolin analog experiments. *Journal of Structural Geology*, 51, 180–192. <https://doi.org/10.1016/j.jsg.2013.01.010>
- Cooke, M. L., Toeneboehn, K., & Hatch, J. L. (2020). Onset of slip partitioning under oblique convergence within scaled physical experiments. *Geosphere*, 16(3), 875–889. <https://doi.org/10.1130/GES02179.1>
- Corbeau, J., Rolandone, F., Leroy, S., Meyer, B., Mercier de Lépinay, B., Ellouz-Zimmermann, N., et al. (2016). How transpressive is the northern Caribbean plate boundary?. *Tectonics*, 35(4), 1032–1046. <https://doi.org/10.1002/2015TC003996>
- Corbeau, J., Gonzalez, O., Clouard, V., Rolandone, F., Leroy, S., Keir, D., et al. (2019). Is the local seismicity in western Hispaniola (Haiti) capable of imaging northern Caribbean subduction? *Geosphere*, 15 (6), 1738–1750. <https://doi.org/10.1130/GES02083.1>
- DeMets, C. (1992). Oblique convergence and deformation along the Kuril and Japan Trenches, *J. Geophys. Res.*, 97(B12), 17615– 17625. <https://doi.org/10.1029/92JB01306>
- de Zoeten, R., & Mann, P. (1991). Structural geology and Cenozoic tectonic history of the central Cordillera Septentrional, Dominican Republic. In Geological Society of America Special Papers (Vol. 262, pp. 265–280). *Geological Society of America*. <https://doi.org/10.1130/SPE262-p265>
- de Zoeten, R., & Mann, P. (1999). Chapter 11 Cenozoic el mamey group of northern hispaniola: a sedimentary record of subduction, collisional and strike-slip events within the north America-Caribbean plate boundary zone. In P. Mann (Ed.), *Sedimentary Basins of the World* (Vol. 4, pp. 247–286). Elsevier. [https://doi.org/10.1016/S1874-5997\(99\)80045-8](https://doi.org/10.1016/S1874-5997(99)80045-8)

- Dillon, W. P., Austin, J. A., Scanlon, K. M., Terence Edgar, N., & Parson, L. M. (1992). Accretionary margin of north-western Hispaniola: morphology, structure and development of part of the northern Caribbean plate boundary. *Marine and Petroleum Geology*, 9(1), 70–88. [https://doi.org/10.1016/0264-8172\(92\)90005-Y](https://doi.org/10.1016/0264-8172(92)90005-Y)
- Dillon, W., Edgar, N., Scanlon, K., & Coleman, D. (1996). A Review of the Tectonic Problems of the Strike-Slip Northern Boundary of the Caribbean Plate and Examination by GLORIA. In J. Gardner, M. Field, & D. Twichell (Eds.), *Geology of the United States' Seafloor: The View from GLORIA* (pp. 135-164). Cambridge: Cambridge University Press. <https://doi.org/10.1017/CBO9780511529481.013>
- Draper, G., Mann, P., & Lewis, J. F. (1994). Hispaniola. In S. K. Donovan & T. A. Jackson (Ed.), *Caribbean Geology: An Introduction* (pp. 129–150). Jamaica, CA: University of the West Indies Publishers Association.
- Erikson, J., Pindell, J., Karner, G., Sonder, L., Fuller, E., & Dent, L. (1998). Neogene Sedimentation and Tectonics in the Cibao Basin and Northern Hispaniola: An Example of Basin Evolution Near A Strike-Slip-Dominated Plate Boundary. *The Journal of Geology*, 106(4), 473-494. <https://doi.org/10.1086/516036>
- Escuder-Virueite, J., Suárez-Rodríguez, A., Gabites, J., & Pérez-Estaún, A. (2015). The Imbert Formation of northern Hispaniola: a tectono-sedimentary record of arc-continent collision and ophiolite emplacement in the northern Caribbean subduction-accretionary prism. *Solid Earth Discussions*, 7(2), 1827–1876. <https://doi.org/10.5194/sed-7-1827-2015>
- Escuder-Virueite, J., & Pérez, Y. (2020). Neotectonic structures and stress fields associated with oblique collision and forearc sliver formation in northern Hispaniola: Implications for the seismic hazard assessment. *Tectonophysics*, 784, 228-452. <https://doi.org/10.1016/j.tecto.2020.228452>
- Fitch, T. J. (1972). Plate convergence, transcurrent faults, and internal deformation adjacent to Southeast Asia and the western Pacific. *Journal of Geophysical Research*, 77(23), 4432–4460. <https://doi.org/10.1029/JB077i023p04432>
- Goldfinger, C., Kulm, L. D., Yeats, R. S., Appelgate, B., MacKay, M., & Cochrane, G. R. (1996). Active strike-slip faulting and folding of the Cascadia plate boundary and forearc in central and northern Oregon. In A.M. Rogers, T. J. Walsh, W. J. Kockelman, and G. Priest (Eds.), *Assessing and Reducing Earthquake Hazards in the Pacific Northwest, U.S. Geol. Surv. Prof. Pap. (Vol. 2, pp. 223-256)*. Denver, CO: U.S. Geological Survey. <https://doi.org/10.3133/pp1560>
- Gordon, M. B., Mann, P., Cáceres, D., & Flores, R. (1997). Cenozoic tectonic history of the North America-Caribbean plate boundary zone in western Cuba. *Journal of Geophysical Research: Solid Earth*, 102(B5), 10055–10082. <https://doi.org/10.1029/96JB03177>
- Goreau, P. D. (1989). The tectonic evolution of the North Central Caribbean plate margin.
- Granja Bruña, J. L., Carbó-Gorosabel, A., Llanes Estrada, P., Muñoz-Martín, A., ten Brink, U. S., Gómez Ballesteros, M., et al. (2014). Morphostructure at the junction between the Beata ridge and the Greater Antilles island arc (offshore Hispaniola southern slope). *Tectonophysics*, 618, 138–163. <https://doi.org/10.1016/j.tecto.2014.02.001>
- Iturralde-Vinent, M. A. (1994). Cuban Geology: A New Plate-Tectonic Synthesis. *Journal of Petroleum Geology*, 17(1), 39–69. <https://doi.org/10.1111/j.1747-5457.1994.tb00113.x>
- Iturralde-Vinent, M.A. (1998). Sinopsis de la constitución geológica de Cuba. *Acta Geologica Hispanica*, 33, 9–56.
- Iturralde-Vinent, M., & Macphee, R. (1999). Paleogeography of the Caribbean Region: Implications for Cenozoic biogeography. *Bulletin of the American Museum of Natural History*, 238, 1–95.

- Iturralde-Vinent, M. A. (2003). *Ensayo sobre la paleogeografía del Cuaternario de Cuba*. Paper presented at the V Congreso Cubano de Geología y Minería, Memorias Geomin, La Habana.
- Iturralde-Vinent, M., & Gahagan, L. (2002). Latest Eocene to Middle Miocene tectonic evolution of the Caribbean: Some principles and their implications for plate tectonic modeling. In T. A. Jackson (Ed.), *Caribbean geology into the third millennium: Transactions of the Fifteenth Caribbean Geological Conference* (pp. 47–62), Kingston: University of the West Indies Press.
- Jarrard, R. D. (1986). Terrane motion by strike-slip faulting of forearc slivers. *Geology*, 14(9), 780-783. [https://doi.org/10.1130/0091-7613\(1986\)14<780:TMBSFO>2.0.CO;2](https://doi.org/10.1130/0091-7613(1986)14<780:TMBSFO>2.0.CO;2)
- Lallemant, S., Liu, C.-S., Dominguez, S., Schnürle, P., Malavieille, J., and the ACT scientific crew. (1999). Trench-parallel stretching and folding of forearc basins and lateral migration of the accretionary wedge in the southern Ryukyus: A case of strain partition caused by oblique convergence; *Tectonics*, 18 (2), 231-247. doi:10.1029/1998TC900011
- Laurencin, M., Marcaillou, B., Graindorge, D., Lebrun, J. -F., Klingelhofer, F., Boucard, M., et al. (2019). The Bunce Fault and Strain Partitioning in the Northern Lesser Antilles. *Geophysical Research Letters*, 46(16), 9573–9582. <https://doi.org/10.1029/2019GL083490>
- Leroy, S., Mercier de Lépinay, B., Mauffret, A., & Pubellier, M. (1996). Structural and Tectonic Evolution of the Eastern Cayman Trough (Caribbean Sea) From Seismic Reflection Data. *AAPG Bulletin*, 80(2). 222-247. <https://doi.org/10.1306/64ED8796-1724-11D7-8645000102C1865D>
- Leroy, S., Mauffret, A., Patriat, P., & Mercier de Lépinay, B. (2000). An alternative interpretation of the Cayman trough evolution from a reidentification of magnetic anomalies. *Geophysical Journal International*, 141(3), 539–557. <https://doi.org/10.1046/j.1365-246x.2000.00059.x>
- Leroy, S. (2012). HAITI-SIS cruise, L'Atalante R/V. <https://doi.org/10.17600/12010070>
- Leroy, S., & Ellouz-Zimmermann, N. (2013). HAITI-SIS2 cruise, L'Atalante R/V. <https://doi.org/10.17600/13010080>
- Leroy, S., Ellouz-Zimmermann, N., Corbeau, J., Rolandone, F., Mercier de Lépinay, B., Meyer, B., et al. (2015). Segmentation and kinematics of the North America-Caribbean plate boundary offshore Hispaniola. *Terra Nova*, 27(6), 467–478. <https://doi.org/10.1111/ter.12181>
- Mann, P., Taylor, F. W., Edwards, R. L., & Ku, T.-L. (1995). Actively evolving microplate formation by oblique collision and sideways motion along strike-slip faults: An example from the northeastern Caribbean plate margin. *Tectonophysics*, 246(1), 1–69. [https://doi.org/10.1016/0040-1951\(94\)00268-E](https://doi.org/10.1016/0040-1951(94)00268-E)
- Mann, P., Prentice, C., Burr, G., Peña, L., & Taylor, F. (1998). Tectonic geomorphology and paleoseismology of the Septentrional fault system, Dominican Republic. In J.F Dolan & P. Mann (Eds.), *Active Strike-Slip and Collisional Tectonics of the Northern Caribbean Plate Boundary Zone, Geological Society of America Special Papers* (Vol. 326, pp. 63-124). Boulder, Colo: GSA Books. <https://doi.org/10.1130/0-8137-2326-4.63>
- Mann, P., Draper, G., & Lewis, J. F. (1991). An overview of the geologic and tectonic development of Hispaniola, *Geological Society of America Special Papers*, 262, 1–28. <https://doi.org/10.1130/SPE262-p1>
- Mann, P., Calais, É., Ruegg, J.-C., DeMets, C., Jansma, P. E., & Mattioli, G. S. (2002). Oblique collision in the northeastern Caribbean from GPS measurements and geological observations. *Tectonics*, 21(6), 1057–1083. <https://doi.org/10.1029/2001TC001304>

- Mauffret, A., & Leroy, S. (1997). Seismic stratigraphy and structure of the Caribbean igneous province. *Tectonophysics*, 283(1), 61–104. [https://doi.org/10.1016/S0040-1951\(97\)00103-0](https://doi.org/10.1016/S0040-1951(97)00103-0)
- Mauffret, A., & Leroy, S. (1999). Neogene intraplate deformation of the Caribbean plate at the Beata ridge. In P. Mann (Ed.), *Sedimentary Basins of the World* (Vol. 4, pp. 627–669), Elsevier. [https://doi.org/10.1016/S1874-5997\(99\)80055-0](https://doi.org/10.1016/S1874-5997(99)80055-0)
- Muhs, D. R., Schweig, E. S., Simmons, K. R., & Halley, R. B. (2017). Late Quaternary uplift along the North America-Caribbean plate boundary: Evidence from the sea level record of Guantanamo Bay, Cuba. *Quaternary Science Reviews*, 178, 54–76. <https://doi.org/10.1016/j.quascirev.2017.10.024>
- Mullins, H. T., Breen, N., Dolan, J., Wellner, R. W., Petruccione, J. L., Gaylord, M., et al. (1992). Carbonate platforms along the southeast Bahamas-Hispaniola collision zone. *Marine Geology*, 105(1), 169–209. [https://doi.org/10.1016/0025-3227\(92\)90188-N](https://doi.org/10.1016/0025-3227(92)90188-N)
- Philippon, M., & Corti, G. (2016). Obliquity along plate boundaries. *Tectonophysics*, 693, 171–182. <https://doi.org/10.1016/j.tecto.2016.05.033>
- Pindell, J., Kennan, L., Maresch, W. V., Stanek, K.-P., Draper, G., & Higgs, R. (2005). Plate-kinematics and crustal dynamics of circum-Caribbean arc-continent interactions: Tectonic controls on basin development in Proto-Caribbean margins. In H. G. A. Lallemand & V. B. Sisson (Eds.), *Caribbean-South American plate interactions, Venezuela*. CA: Geological Society of America. <https://doi.org/10.1130/0-8137-2394-9.7>
- Pindell, J. L., & Draper, G. (1991). Stratigraphy and geological history of the Puerto Plata area, northern Dominican Republic. In P. Mann, G. Draper, J. F. Lewis (Eds.), *Geologic and Tectonic Development of the North America-Caribbean Plate Boundary in Hispaniola*, Geological Society of America Special Papers (Vol. 262, pp. 97–114). <https://doi.org/10.1130/SPE262-p97>
- Rodríguez-Zurrunero, A., Granja-Bruña, J. L., Carbó-Gorosabel, A., Muñoz-Martín, A., Gorosabel-Araus, J. M., Gómez de la Peña, L., et al. (2019). Submarine morpho-structure and active processes along the North American-Caribbean plate boundary (Dominican Republic sector). *Marine Geology*, 407, 121–147. <https://doi.org/10.1016/j.margeo.2018.10.010>
- Rodríguez-Zurrunero, A., Granja-Bruña, J. L., Muñoz-Martín, A., Leroy, S., ten Brink, U., Gorosabel-Araus, J. M., et al. (2020). Along-strike segmentation in the northern Caribbean plate boundary zone (Hispaniola sector): Tectonic implications. *Tectonophysics*, 776, 228–322. <https://doi.org/10.1016/j.tecto.2020.228322>
- Rojas-Agramonte, Y., Neubauer, F., Garcia-Delgado, D. E., Handler, R., Friedl, G., & Delgado-Damas, R. (2008). Tectonic evolution of the Sierra Maestra Mountains, SE Cuba, during Tertiary times: From arc-continent collision to transform motion. *Journal of South American Earth Sciences*, 26(2), 125–151. <https://doi.org/10.1016/j.jsames.2008.05.005>
- Rosencrantz, E., Ross, M. I., & Sclater, J. G. (1988). Age and spreading history of the Cayman Trough as determined from depth, heat flow, and magnetic anomalies. *Journal of Geophysical Research: Solid Earth*, 93(B3), 2141–2157. <https://doi.org/10.1029/JB093iB03p02141>
- Sorel, D., Purser, B. H., & Senatos, H. (1991). Strike-slip tectonic processes in the northern Caribbean between Cuba and Hispaniola (Windward Passage). Essai de Datation Des Récifs Soulevés d’Haiti Par La Méthode Du Forçage Climatique Orbital. *Comptes rendus de l’Académie des sciences*, 313, 1277–1281.
- Syed Tabrez, A., Freed, A. M., Calais, É., Manaker, D. M., & McCann, W. R. (2008). Coulomb stress evolution in Northeastern Caribbean over the past 250 years due to coseismic,

- postseismic and interseismic deformation. *Geophysical Journal International*, 174(3), 904–918. <https://doi.org/10.1111/j.1365-246X.2008.03634.x>
- Symithe, S., Calais, É., Chabalier, J. B., Robertson, R., & Higgins, M. (2015). Current block motions and strain accumulation on active faults in the Caribbean. *Journal of Geophysical Research: Solid Earth*, 120(5), 3748–3774. <https://doi.org/10.1002/2014JB011779>
- ten Brink, U., & Lin, J. (2004). Stress interaction between subduction earthquakes and forearc strike-slip faults: Modeling and application to the northern Caribbean plate boundary. *Journal of Geophysical Research: Solid Earth*, 109, B12310. <https://doi.org/10.1029/2004JB003031>
- Teyssier, C., Tikoff, B., & Markley, M. (1995). Oblique plate motion and continental tectonics. *Geology*, 23(5), 447–450. [https://doi.org/10.1130/0091-7613\(1995\)023<0447:OPMACT>2.3.CO;2](https://doi.org/10.1130/0091-7613(1995)023<0447:OPMACT>2.3.CO;2)
- Wessels, R. J. F. (2019). Chapter 15 - Strike-Slip Fault Systems Along the Northern Caribbean Plate Boundary. In J. C. Duarte (Ed.), *Transform Plate Boundaries and Fracture Zones* (pp. 375–395). Elsevier. <https://doi.org/10.1016/B978-0-12-812064-4.00015-3>

CHAPITRE VI : Évolution de la limite de plaque Nord Caraïbe au Nord d'Haïti

Ce chapitre correspond à un article en préparation pour soumission à *Tectonophysics*.

L'analyse tectono-sédimentaire de la région Nord de Cuba oriental et de la région du Passage du Vent, ont fait émerger de nouvelles questions : Quelle est la chronologie de la progression vers l'Est du système de faille à la frontière nord Caraïbe ? depuis l'activation des segments de la Faille Oriente jusqu'à la mise en place du système de failles Septentrional-Oriente ? Comment les éléments morphologiques du fond sont affectés par la mise en place de ces segments ? Quelles sont les conséquences du partitionnement de la déformation dû à la collision oblique sur les systèmes tectoniques et sédimentaires ?

Cette étude, réalisée sur la marge au large de la côte nord Haïtienne, révèle que le remplissage sédimentaire ainsi que la signature fond de mer diffèrent d'Est en Ouest. Nous discutons des différences structurales et sédimentaires observées d'est en ouest sur cette marge. Nous proposons différents processus qui semblent être à l'origine de cette variabilité géomorphologique du fond de mer. Ceci indique qu'il existe une relation étroite entre les éléments morphologiques de surface observés et la tectonique décrochante régionale.

VI. Dynamic Evolution of the Northern Caribbean Plate Boundary: Impact on Seabed and Tectonics from Miocene to Present

Oliveira de Sá A.¹, Leroy S.¹, d'Acremont E.¹, Lafuerza S.¹, Granja-Buña J.L.², Momplaisir R.³, Boisson D.³, Watremez L.⁴, Moreno B.⁵

1 Sorbonne Université, CNRS, IStEP, Institut des Sciences de la Terre de Paris, France

2 Universidad Complutense, Madrid, Spain

3 Université d'Etat d'Haïti, Port-au-Prince, Haïti

4 Université de Lille

5 CENAI, Santiago de Cuba, Cuba

Abstract

The northern margin of Haiti is characterised by a complex morpho-structure shaped by geodynamic, tectonic, and sedimentary interplays. We use HAITISIS cruises data to investigate the northern Caribbean plate boundary, marked by oblique convergence. Here, we elucidate the relationship between fault-driven tectonic activity, seabed morphology, and the effects of strike-slip and compressive deformations.

Distinct Eastern and Western morpho-structural domains are identified along the Haitian northern coast. These domains, with their unique sedimentary patterns and seabed structures, were differentiated during the paleogeographic reorganisation of the Upper Miocene-Pliocene along the Caribbean plate's northern boundary. Regional changes are

associated with Hispaniola and Bahamas oblique collision onset. This tectonic event led to the formation of an accretionary prism and activated segments of the Northern-Oriente Fault Zone (SOFZ), resulting in lateral sediment source displacements, and influencing sedimentary infill and deformation patterns in the study area. The Eastern domain exhibits a mass transport deposit (MTD) believed to have formed during this period of tectonic instability. The MTD influences the seabed through differential compaction and the remobilisation of recent seismic units. In the Western domain, the MTD is absent. Additionally, canyons are present in the eastern domain and absent in the western domain. Our findings shed light on the initiation of SOFZ segments along the offshore Haitian coast from the early Miocene to the present. The evolution of the SOFZ differs from previous assumptions of continuous eastward propagation. Changes in seafloor morphology, as lateral shifts in canyon paths, provide a chronology for establishing strike-slip and thrust faults along the margin up to the development of active SOFZ segments. Our findings enhance comprehension of tectonic-sedimentary-geomorphological interactions along Haiti's northern margin, presenting new perspectives on the Northern Caribbean Plate boundary's formation.

VI.1 Introduction

Active tectonic margins, including shear and subduction margins, represent an important proportion of continental margins. The seabed morphology of active tectonic margins is governed by climatic, sedimentary, and oceanographic processes similar to passive margins. However, active tectonic controls the morphology at both local and regional scales (Emery, 1980). Through folding, faulting, uplift, or subsidence, seafloor deformation has been shown to directly affect the location, alignment, and geometry of many geomorphological seabed features (Harris & Whiteway, 2011; McAdoo et al., 2000; Micallef et al., 2014). Therefore, it is essential to characterise tectonics' influence on the emplacement and evolution of sedimentary systems, as this aspect remains poorly explored.

The Northern Haitian margin offers an invaluable opportunity for investigating the interaction between fault-related tectonic activity and seabed morphology in an oblique collision setting (Figures VI.1 and 2). The Septentrional-Oriente Fault Zone (SOFZ) delineates the Northern boundary of the Caribbean plate, tracing a WNW-ESE trajectory along this margin (Figures VI.1 and 2) (Leroy et al., 2015; Oliveira de Sá et al., 2021). Given the oblique movement of the Caribbean plate relative to the North American plate in this area, this plate boundary is characterised by a strain partitioning with the coexistence of the Northern Hispaniola Deformed Belt (NHDB) and the SOFZ accommodating the shortening and longitudinal strain components respectively (Calais et al., 2002; Mann et al., 2004; Rodríguez-Zurrunero et al., 2020). Then, strike-slip and compressive deformations are witnessed, leading to a diverse range of tectonic structures (Figure VI.2b) (Calais et al., 2016; Rodríguez-Zurrunero et al., 2020). These tectonic structures significantly shape sedimentary filling and the seabed morphology. Understanding this partitioned deformation system necessitates thoroughly examining the current northern boundary of the Caribbean plate and its geodynamic evolution. This requires the characterisation of the morpho-structures and the evolution of

seabed morphologies. These factors collectively yield insights into the mechanics and dynamics of this active system and the tectonic impact on the regional geological features.

Our study aims to characterise the structural framework of the Northern Haitian margin with seismic reflection data and conduct a detailed geomorphological analysis using high-resolution bathymetry data acquired during the HAITISIS 1 and 2 oceanographic expeditions (Leroy, 2012; Leroy & Ellouz-Zimmermann, 2013). Our objective is to determine the influence of tectonically induced subsurface deformation on the seabed morphology and sedimentary systems in a plate boundaries context. We investigate the geomorphological seabed features and large-scale submarine canyon network intersected by strike-slip faults along the northern Haitian margin. The canyons' deflections highlight the regional strike-slip tectonic's signature and the recent initiation of the SOFZ segment along the offshore Haitian coast. Furthermore, we discuss the variability of morphological seabed features, predominantly tied to the structural settings. This comprehensive examination enhances our understanding of the complex tectonic processes, their influence on the geological and morphological features over time, and the current geometry of the Northern boundary of the Caribbean plate.

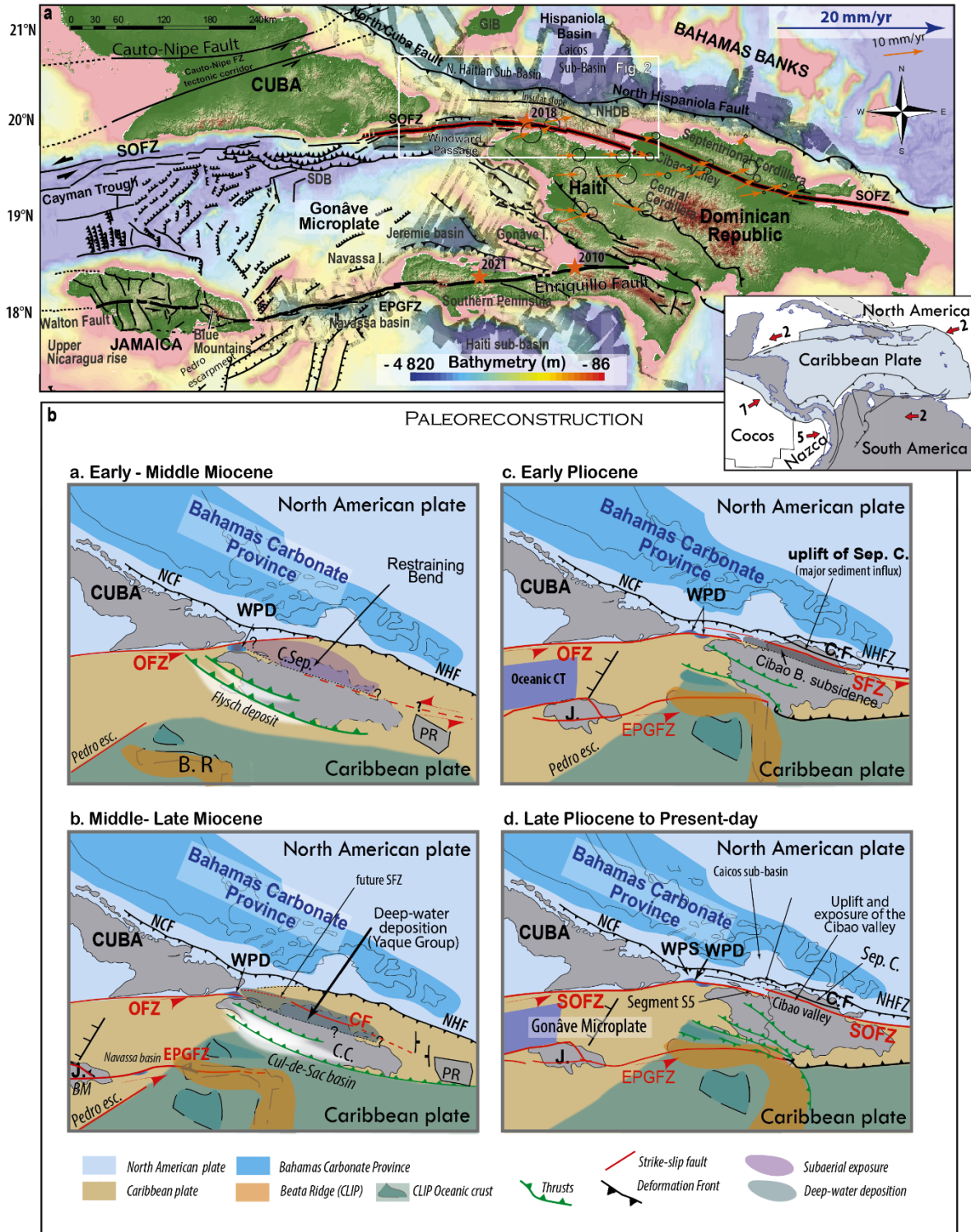


Figure VI.1. a) Tectonic map of the northern Caribbean plate boundary. NHDB: Northern Hispaniola Deformed Belt; SDB: Santiago Deformed Belt; SOFZ: Septentrional-Oriente Fault Zone, EPGFZ: Enriquillo Plantain Garden Fault Zone. The orange arrows indicate a GPS-derived velocity map expressed in the North American plate referenced frame (NAM08) with an ellipse error of 95% confidence (modified from Rodriguez-Zurrunero et al. 2020). Inset: Large-scale tectonic setting with arrows showing GPS-derived plate velocities in cm/y. The stars correspond to the main earthquakes since 2010. b) Paleo-reconstruction/Tectonic setting of the northern boundary of the Caribbean plate from Early-Middle Miocene to Late Pliocene – Present day, modified from Leroy et al. (2000), Calais et al. (2016) and, Oliveira de Sá et al. (2021). See text for discussion. B.R.: Beata Ridge; Pedro Esc.:

Pedro Escarpment; NHF: North Hispaniola fault; NCF: North Cuba Fault; BM: Blue Mountains; J. Jamaica; C. Sept.: Septentrional Cordillera; PR: Porto Rico EPGFZ: Enriquillo-Plantain-Garden Fault Zone; OFZ: Oriente Fault Zone; CF: Camu Fault; SFZ: Septentrional Fault Zone; SOFZ: Septentrional Oriente Fault Zone; WPD: Windward Passage Deep; WPS: Windward Passage Sill.
 Geological setting.

V.I.2.1 Regional Tectonic Setting

The oblique collision between the Caribbean plate and the Bahamas Banks has led to an eastward migration of the northern Caribbean plate boundary by successive southward jumps of major strike-slip (Figure VI.1b; Mann et al., 1996; Leroy et al., 2000; Rojas-Agramonte et al., 2008; Iturralde-Vinent et al., 2016; Oliveira de Sá et al., 2021). In the Miocene, Cuba was already welded to the North American plate, and the major strike-slip fault, the Oriente Fault Zone (OFZ), ran along its southern coast (Figure VI.1b step a-b). During this time, the Northern Hispaniola margin has ongoing a paleogeographic reorganisation related to the active oblique convergence (Calais et al., 2016; de Zoeten & Mann, 1999).



Figure VI.2: a) Bathymetric map showing the main morpho-structural domains of the Northern Haitian margin. Grey lines show the high-resolution 2D seismic reflection data used in the study. Violet lines indicates the location of the seismic lines used in this paper. White rectangles: detailed bathymetry maps shown in Figure VI.3. b) Structural map of the area. Red dots: aftershocks of the Mw 5.9 earthquake of October 6 (2018). Source: USGS Catalog.

In the middle Miocene period, the continuous oblique stress resulted in the initiation of a strand of the future Septentrional Fault Zone (SFZ) and the development of a restraining bend along the margin of Northern Hispaniola (Figure VI.1b step a-b). Geological formations in the Septentrional Cordillera (Figure VI.1a) experienced tilting, faulting, and folding (de Zoeten & Mann, 1991, 1999; Erikson et al., 1998; Escuder-Viruete & Pérez, 2020).

The eastward motion of the Caribbean Plate was slowed by its oblique collision with the Bahamas Carbonate Province (Figure VI.1b) (Calais et al., 2016; Oliveira de Sa et al., 2021). The major strike-slip motion shifted successively south (Calais et al., 2016). The Oriente fault system splayed eastward, running across the Windward Passage Deep into northern Hispaniola to form the present-day Septentrional-Oriente Fault Zone (SOFZ) (the current northern Caribbean Plate boundary, Figure VI.1b step d) (Oliveira de Sa et al., 2021; Calais & Mercier de Lépinay, 1995; Leroy et al., 2015). The Windward Passage Deep sedimentary cover shows a left-lateral offset of approximately 80 km on either side of the SOFZ segments (Figure VI.1b step c-d; since 5.4 ± 0.2 Ma, e.g., Oliveira de Sa et al., 2021).

Northern Hispaniola is also marked by a significant paleogeographic reorganisation related to its late Pliocene oblique collision with the Bahamas Carbonate Province (Calais et al., 2016; Calais & Mercier De Lépinay, 1991; de Zoeten & Mann, 1999). From the Pliocene, a great regional uplift resulted in the emergence of the Septentrional Cordillera (Calais et al., 2016; Erikson et al., 1998). With the initiation of the SFZ, the present-day Septentrional Cordillera (the northern Dominican Republic, Figure VI.1a) was transferred to the North-American plate (Calais et al., 2016; Calais & Mercier De Lépinay, 1995; Erikson et al., 1998; Leroy et al., 2015; Rodríguez-Zurrunero et al., 2019, 2020).

The Pliocene paleogeographic reorganisation resulted in the widespread strain distribution across the northern margin of Hispaniola. Oblique motion is mainly accommodated by the SOFZ, which runs sub-parallel to the collision margin and accommodates the movement perpendicular to the margin at a rate of 10–12 mm/yr. While the Northern Hispaniola Prism (with its Deformation Front, Figure VI.2b) accommodates the motion normal to the margin with an elastic strain at a rate of 1–3 mm/yr (Benford et al., 2012; Calais et al., 2010; Dolan et al., 1998; Mann et al., 1995, 2002; Symithe et al., 2015).

VI.2.2 Morpho-structural settings

The northern Haitian margin (Figures VI.2 and 3) extends 250 km from Windward Passage and the northern coast of Haiti to the toe of the shallow platform eastward of the Dominican Republic (Figures VI.1a and 2a; Monte Cristi). The seabed is at water depths from 200 m to 4000 m.

The region of the North Haitian Margin is occupied by the Northern Hispaniola Prism (Figure VI.2b), which we consider an accretionary prism defined by three domains (upper, middle, and lower prisms, Figure VI.4). The accretionary prism is also called the Northern Hispaniola Deformed Belt (NHDB, Figure VI.1a) (Dillon et al., 1992, 1996; Rodríguez-

Zurrunero et al., 2020). It alternates roughly E-W trending broad anticline ridges and narrow troughs, sub-parallel to the compressive deformation front (Figure VI.2b). This prism can be followed toward the east along the northern Dominican Republic (Rodríguez-Zurrunero et al. 2020) and to the west into the Old Bahamas Channel along the northern Cuban coast (Oliveira de Sá et al., *subm.*) (Figure VI.1a).

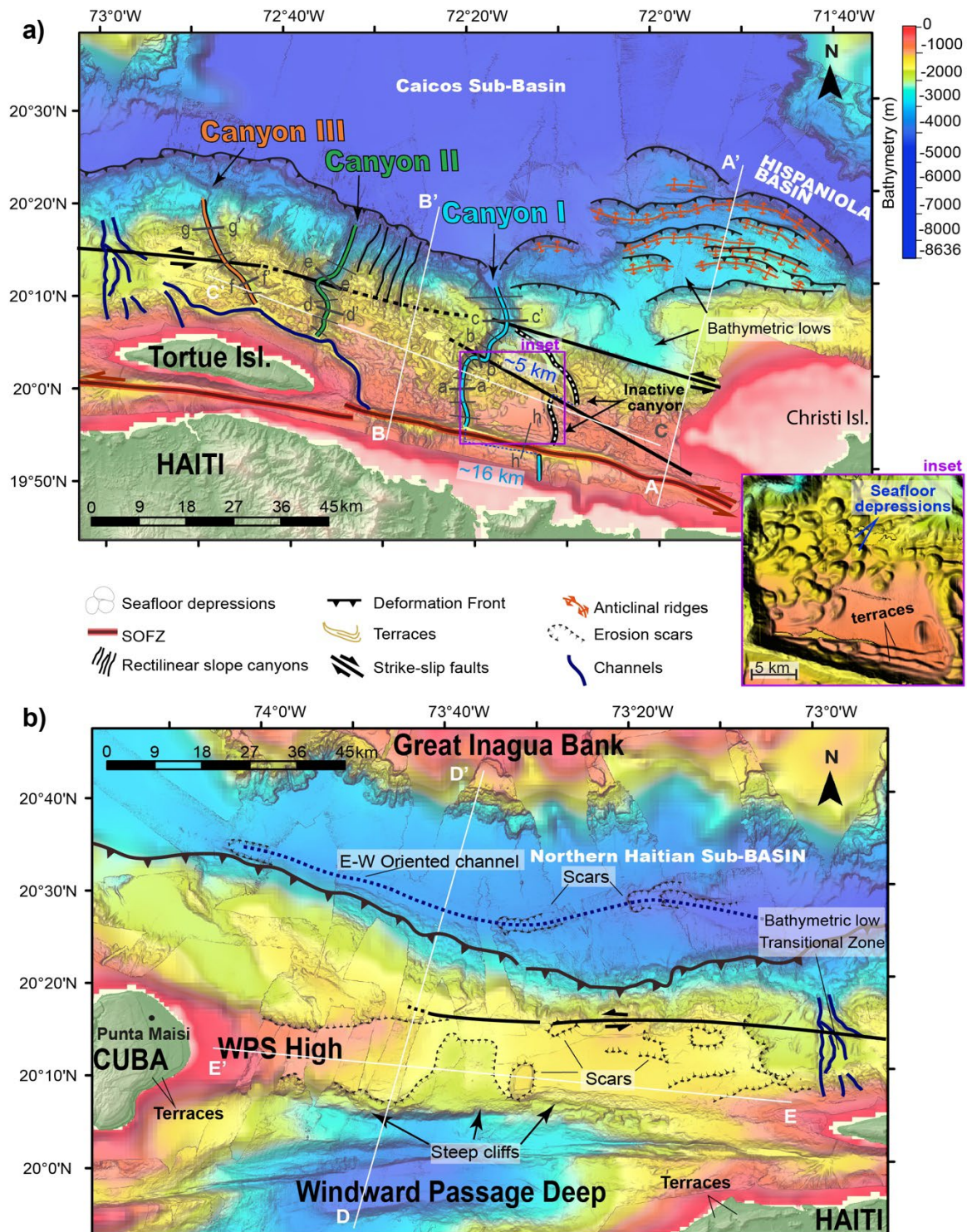


Figure VI.3. Bathymetric map with the interpretation of the principal seafloor geomorphological elements in the Eastern (a) and Western domains (b). WPS High: Windward Passage Sill High. The

Hispaniola basin is divided into two sub-basins, here in the study area, which are the Caicos sub-basin in the east and the Northern Haitian sub-basin, as proposed by Rodriguez-Zurrunero et al. 2020. The blue canyon shows a 16 km shift, corresponding to 2 Ma of SOFZ activity (Leroy et al. 2015). See Authemayou et al. (2023) for terraces in Southern Cuba.

From 72°10' to 72°50'W, a system of deeply incised canyons stretches along the margin, following a north-south direction (Figure VI.3a). The head of these canyons are shifted from about 16 km by segment 5 of the SOFZ ~2 Ma ago (Figures VI.2b and 3a; Leroy et al. 2015). The seabed in this region is also affected by several seafloor depressions (inset in Figure VI.3a).

Beyond 72°50', the edge of the Great Inagua Bank comes within 30 km of the Windward Passage Sill, creating a narrow basin (Northern Haitian sub-basin; Figure VI.2b). Within this basin, the seabed's elevation differs by roughly 500 meters in comparison to the seafloor of the Caicos sub-basin. In the Northern Haitian sub-basin, the slope of the E-W-oriented channel floor gently inclines towards the east, aligning with the basin's direction (Figure VI.3b). Large U-shaped scars (between 72°50' and 74°' in Figure VI.3b) at the seafloor of this channel are probably the result of slumping (Goreau, 1981), perhaps from sediments that are flowing towards the Caicos sub-basin from the west (Figures VI.1, 2, and 3).

VI.2 Data and Methodology

Multichannel seismic reflection and multibeam bathymetric data were collected during HAITISIS 1-2 (2012-2013) cruises onboard the R/V L'Atalante (Flotte Océanographique Française (Leroy, 2012; Leroy & Ellouz-Zimmermann, 2013)). Multibeam bathymetric data collected during the NORCARIBE geophysical cruise in 2013 aboard the Spanish R/V Sarmiento de Gamboa allows us to fill the gaps in our data coverage (Leroy et al. 2015; Rodríguez-Zurrunero et al., 2020). Our study focuses on the Northern Haiti area and the Windward Passage sill, where ~800 km of seismic profiles were acquired (Figure VI.2a). Seismic reflection data are recorded using a source comprising two GI air guns (2.46 L, 300 in³) and a streamer with 24 traces (600 m long) operated at c.a 9.7 knots (fast and light seismic system). The multichannel seismic reflection data were processed using classical steps, including CDP gathering (fold 6), binning at 25 m, detailed velocity analysis, stack, and post-stack time migration. All the seismic reflection profiles presented are time-migrated with Seismic Unix®. Multibeam bathymetry data were acquired simultaneously along with seismic profiles and gridded with a spacing of 50 m. The gridded bathymetry data was augmented with the GEBCO Digital Atlas (https://www.gebco.net/data_and_products/gebco_digital_atlas/) with an 800 m resolution to provide almost complete area coverage (Figure VI.2a).

The processed seismic data were interpreted using Kingdom IHS Suite© software. Maps are plotted with ArcGIS® and Global Mapper® software. We use the seismic reflection dataset to identify sedimentary units and deformation styles and infer the spatiotemporal evolution of the tectonic structures. Morphological analysis of the seafloor based on swath-bathymetric data is carried out to identify the surface signature of tectonic features (Figure VI.2). We identify faults by either sediment horizon offsets or by the fault plane seismic reflection itself in the available seismic profiles.

VI.3. Results

The Northern Haitian margin exhibits two distinct domains: the eastern domain extending from Christi Islands to Tortue Island (Figure VI.2a), and the western domain located to the south of the Great Inagua Bank, including west of Tortue Island and Punta Maisi in Cuba (Figure VI.2b).

VI.3.1 Submarine canyons and channels

Submarine canyons are present only on the seabed of the Eastern domain (Figure VI.3a). The 3 largest canyons in the area (labelled I to III in Figures VI.3a and 4) stretch from the margin with a north-south trend, reaching depths of approximately ~4000 m (Figure VI.4B).

The head of Canyon I (east of Tortue Island) is rooted at the SOFZ channel (up to 1500 m depth, Figure VI.3a). The total length of this U-shaped canyon is about 35 km (Talweg topography shown in Figure VI.4, inset a). After 17 km N-S, the canyon axis bends towards the east, taking an NNE-SSW direction, which it maintains for 8 km until it changes its direction again to an NNW-SSE direction (Figure VI.3a). The axial depth varies between 600 to 800 m, and its width spans from 3000 to 7000 meters from rim to rim (sections a-a', b-b', and c-c' in Figure VI.4). To the east of Canyon I, a narrow, steep-sided valley begins its incision with a nearly N-S trend over 9 km until it is beheaded and deflected, changing its direction to an NNW-SSE trend (white dots in Figure VI.3a). This valley joins the canyon I mouth at $72^{\circ}15'W$ (Figure VI.3a), reaching its maximum width at this point (~6 km wide from rim to rim, section c-c' in Figure VI.4). These canyons do not seem to be the present-day extension of any coastal river, as proposed by Leroy et al. (2015). Five large terraces with depths ~1100m, ~ 1030 m, ~ 930 m, ~ 900 m, and 875m uplift the northern edge of the fault trace (section h-h', Figure VI.4 inset b).

A nearly NW-SE trend channel runs the northern border of Tortue Island and connects to two branches, canyon II and III (Figure VI.3a), that cut the insular slope with a nearly N-S trend (Figure VI.3a). These canyons also show a deflection of their trajectory after 10 km (Figure VI.3a). The canyon II shows a sinuosity in its path but returns to its direction NNE-SSW. Canyon III presents a slight deflection in its pattern, continuing with a more NNW-SSE trend (Figure VI.3a). All canyons present U-shaped profiles and similar geomorphological evolution (sections a-a' to f-f,' in Figure VI.4, inset a).

Several N-S rectilinear channel morphologies incise the insular slope's northern part (rectilinear channels in Figure VI.3a). The head of these rectilinear channels coincides with the local deflection of canyons II and III (Figure VI.3a).

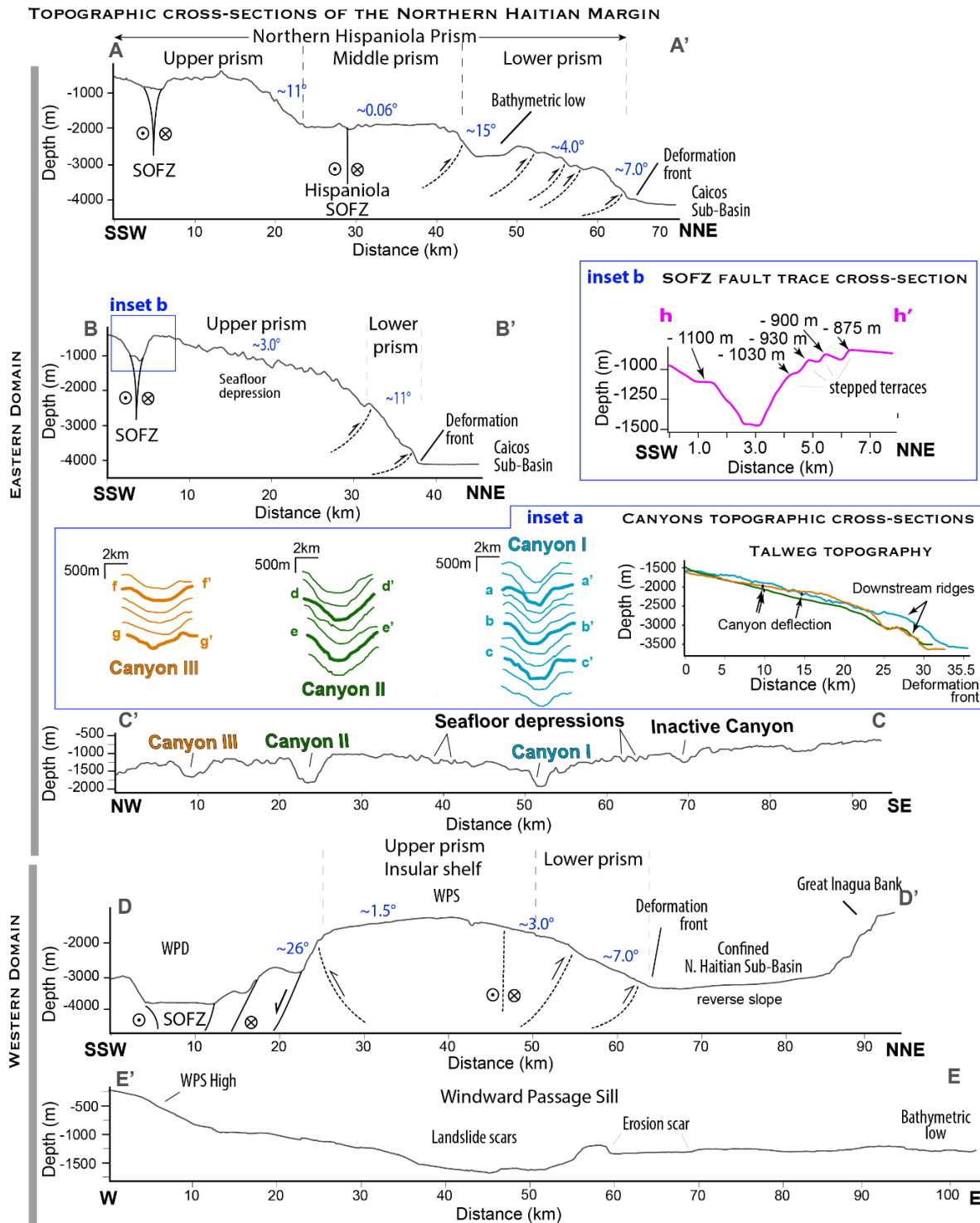


Figure VI.4: Bathymetric analysis of the eastern and western domains of the Northern Haitian margin. Topographic cross-sections with morphological analysis of surface features (canyons, depressions, scars, terraces) and schematic positioning of structural features at depth (strike-slip, thrusts). See Figure VI.3 for profiles locations. A-A'; B-B' and D-D' cross-sections exhibit the Northern Hispaniola Prism with its lower, middle and upper prism parts. The middle prism is cut by the offshore continuity of the SOFZ in Hispaniola. Inset a: Topographic cross-sections across the canyons I, II and III. See Figure VI.3a for location. Profiles a-a' to g-g' show the talweg topography along the three canyons. Blue is Canyon I; green is Canyon II, orange is Canyon III. Inset b: Cross-sections of the fault SOFZ (Septentrional Oriente Fault Zone) showing the stepped terraces. WPS: Windward Passage Sill. WPD: Windward Passage Deep.

V1.3.2 Seafloor Depressions

The Eastern domain is affected by a closely packed set of alternating seabed depressional ponds and raised ridges (section C-C' in Figure VI.4). They are kilometre-scale features that appear in water depths that range from 600 to 2000 m (inset in Figure VI.3a). The narrow-raised ridges that define individual walls of these structures have a complex morphological pattern, which gives rise to shapes ranging from circular to irregular (inset in Figure VI.3a).

The Western domain has broad bathymetric lows and scars (Figures VI.3b and 4, section E-E'). There are no indications of seafloor depressions at the Windward Passage Sill (WPS) (Figure VI.2b). The depressions are only located in the Eastern domain of the study area that occur in the northern and eastern part of Tortue Island, covering an area of ca 2224 km² (Figures VI.3a).

VI.3.3 Seismic stratigraphy

Seismic units are hereafter named and ordered from the acoustic basement to the most recent one, Unit 4, as proposed by Oliveira de Sá et al. (2021) in the Windward Passage region.

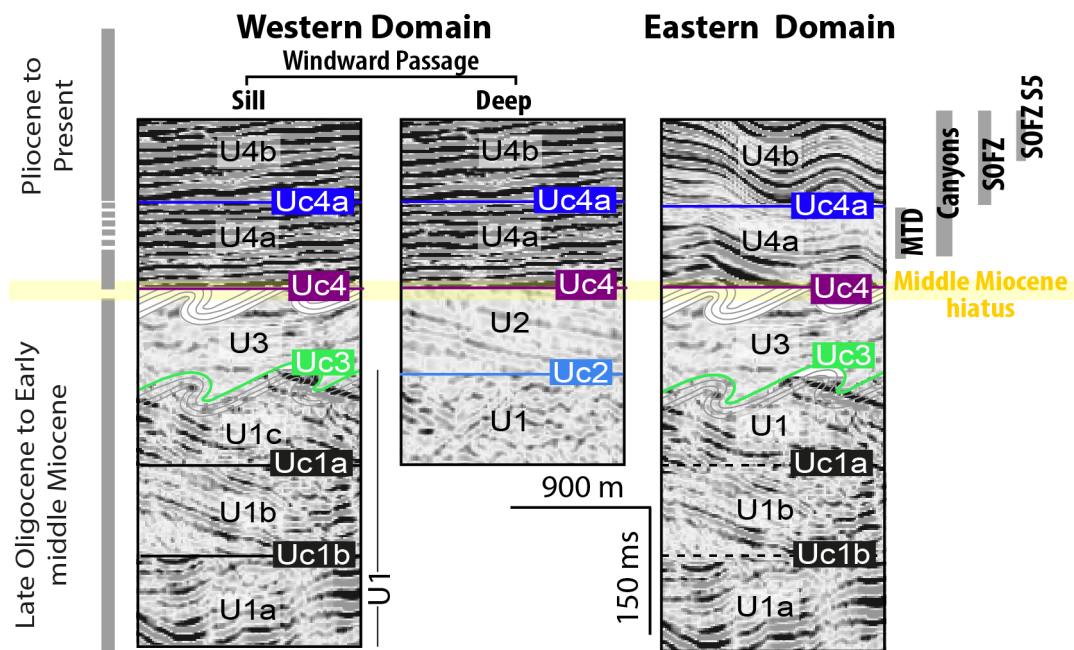


Figure VI.5 : Diagrams illustrating a synthetic log of the seismic units and their seismic patterns. An age estimation of these units is provided, as well as the timing of the MTD installation, the initiation of canyon incisions, the establishment of the Northern-Oriente Fault Zone (SOFZ), and its most recent S5 segment.

The units are described on the northern Haitian margin through correlation and cross-referencing with Oliveira de Sa et al. (2021) profiles located in the Windward Passage area (Figure VI.5). The seismic signal is mainly insufficient to accurately image the reflectors of Units 1 and 3 in the Eastern domain, revealing only the reflectors in the uppermost of its units.

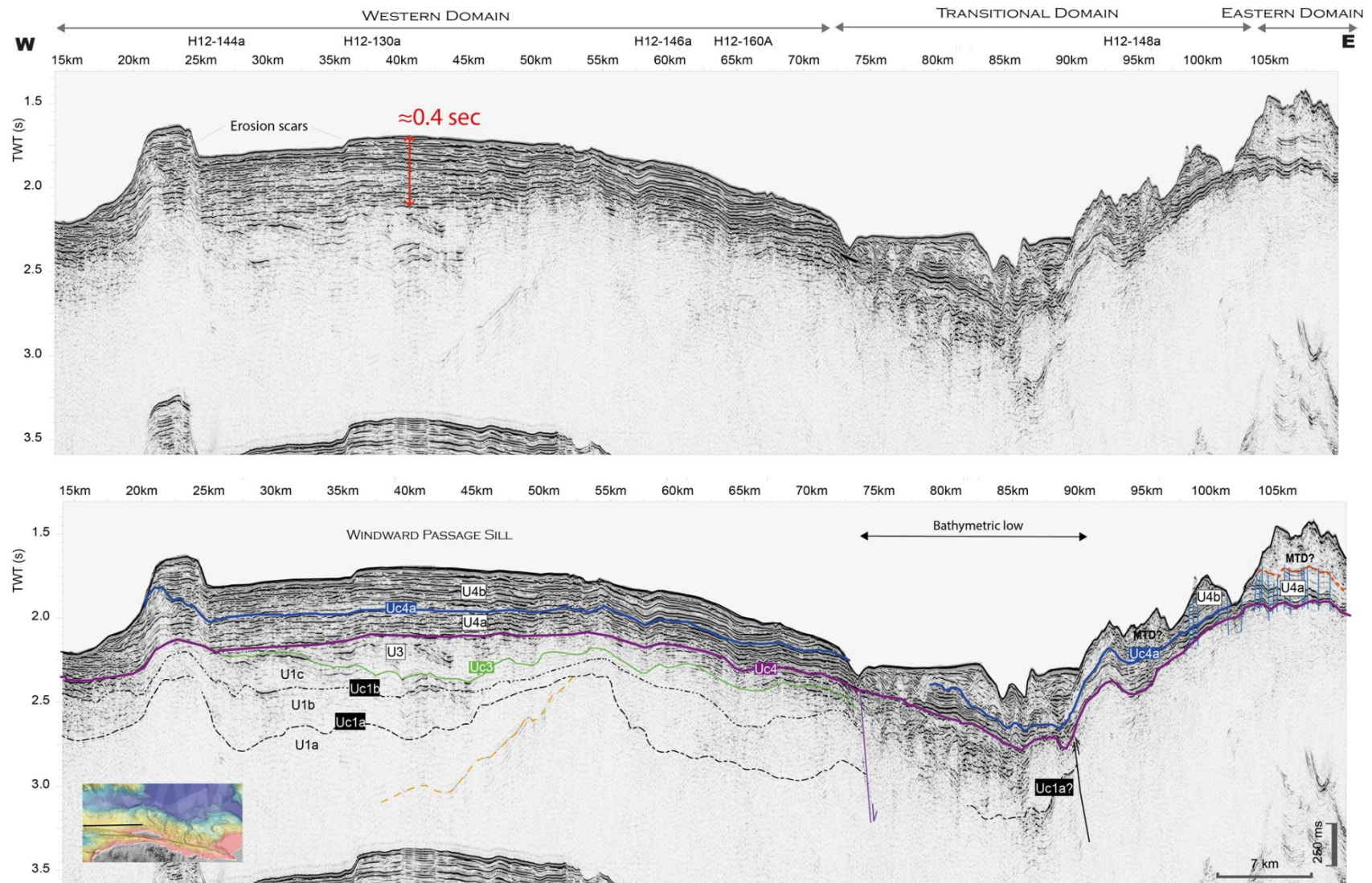


Figure VI.6: Seismic line H12-122. At the top, the uninterpreted seismic line with a W-E orientation illustrates the West and East domains of the study region, as well as the transition zone between these two domains, which corresponds to the location of a bathymetric low. See location in Figure VI.2a.

In the Western domain, Unit 1 consists of a relatively thick series (0.4 - 0.8 s TWT) with two internal angular unconformities (Uc1a and Uc1b) that separate distinct sub-units of distinct facies and geometries (Units 1a, 1b and 1c). The sub-units within Unit 1 and its associated unconformities are discernible in Figures VI.6 and 7, km 23-35, through the correlation plot of the seismic profiles extending towards the western region (e.g., Figure VI.7 of Oliveira de Sa et al., 2021). However, they remain quite faint on the seismic profiles due to the attenuation of the seismic signal.

The Unit 2 was is not identified in the study area. This unit was described by Oliveira de Sá et al. (2021) only in the Windward Passage Deep (Figure VI.2). This syn-tectonic unit is associated with the opening of the Passage between Cuba and Hispaniola (Oliveira de Sá et al., 2021).

Unit 3 is characterised by tilted and folded reflectors, filling the synclines depressions formed by the previous folding of Unit 1 (Figures VI.6, 7, and 8b) (Oliveira de Sá et al., 2021). Unit 3 is delimited at its top by the Uc4 unconformity (purple).

Unit 4 shows well-stratified and high-amplitude reflections in the western part of Tortue Island (Figures VI.6, 7, and 9). Towards the east, the horizontally layered high-frequency reflectors of Unit 4 turn into complex internal reflections with greater thickness (Figure VI.9, km 80-140). Unit 4 is characterised by nearly parallel, wave-like seismic reflections in this area.

Unit 4 is divided into two subunits: U4a, and U4b. Subunit U4a is bounded by the unconformities Uc4 (purple) and Uc4a (blue) (Figure VI.6). The strata thickness varies across the study area, thickening towards the east (≈ 0.4 sec westward, ≈ 0.75 sec eastward; Figures VI.6 and 9).

Within the Western domain, the U4a unit is characterised by continuous and parallel high-amplitude reflections from Uc4 to Uc4a unconformities (Figure VI.9 km 0-30). Within the Eastern domain, the lower portion of the U4a subunit is marked by a high-amplitude layer, showing continuous high-amplitude reflections (Figure VI.9). This high-amplitude layer exhibits a double-wedge shape, thickening as it approaches the central axis of the major canyons (III and II) that incise the U4 unit in the Eastern domain (Figure VI.9, km 80-110 and km 112-130). Away from the channel-fill, this layer is relatively thin, and the signature at some locations is characterised by the two continuous high amplitude reflections from its top and base (Figure VI.9 between km 120-125). The internal seismic pattern of the U4a unit, from unconformities Uc4 to Uc4a, is characterised locally by relatively continuous and parallel, high to moderate amplitude reflections (Figures VI.9, km135 and 10 between the km 3-5, 11 between the km 0-1.5). Vertically and laterally, the facies change from well-bedded, visible reflections to more transparent ones. This particular unit is interpreted as a Mass Transport Deposit (MTD). The lower part of this MTD is marked by horizon A (Dotted orange line), and its upper part by horizon B (Dotted green line) (Figures VI.10, 11, and 12).

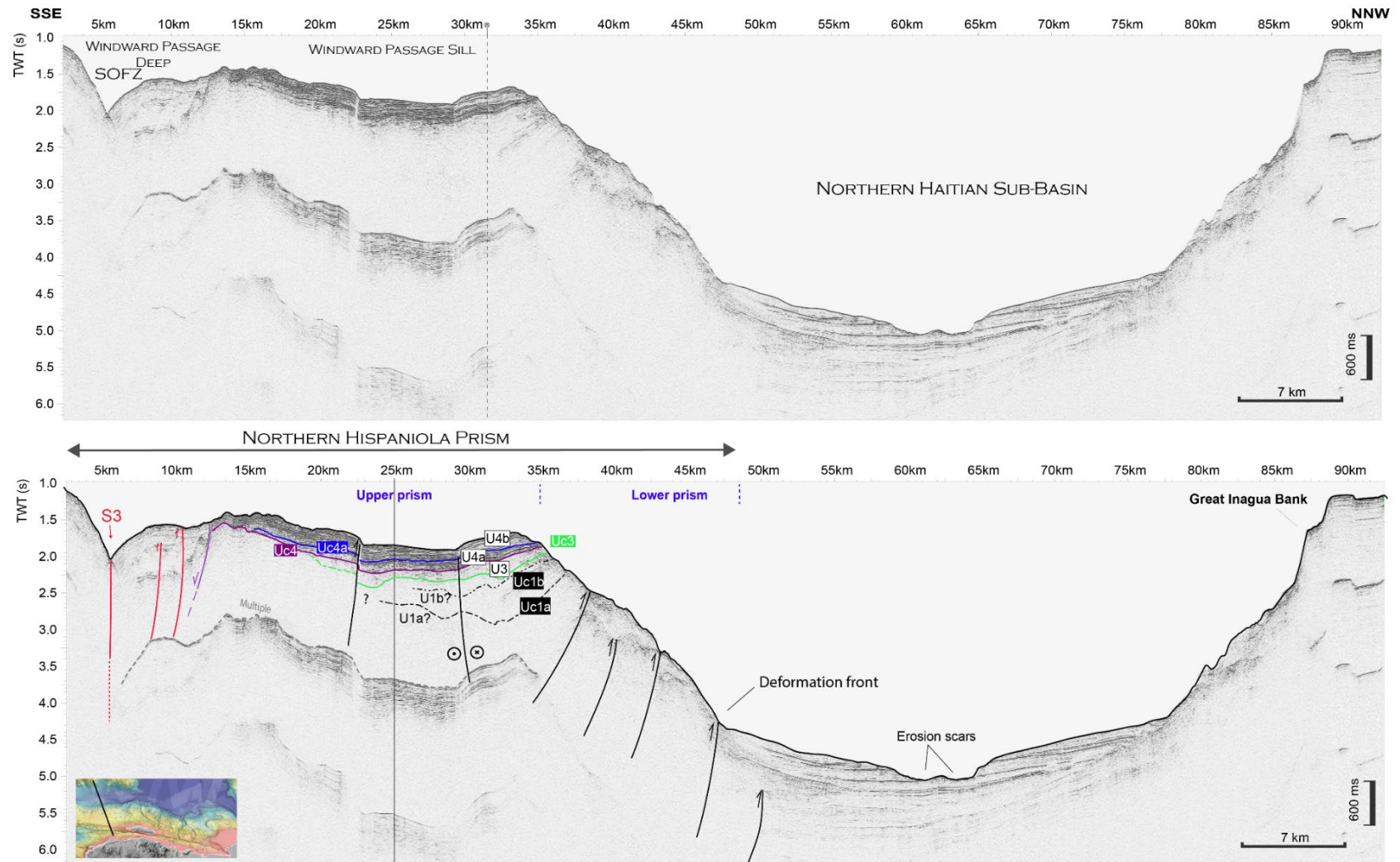


Figure VI.7. Seismic line H12-146. At the top, the uninterpreted seismic line crossing the western domain of the study region displays the Windward Passage Sill and the Haiti sub-basin. At the bottom, the interpreted seismic line shows the reverse faults on the lower prism, as well as the westward continuation of the strike-slip fault that offsets the path of the canyons from the eastern domain, and reverse faults (km 20.5) affecting the most recent sedimentary cover. See location in Figure VI.2a.

On the Eastern domain, this MTD truncates the top of Subunit U4a (Figures VI.10, 11, and 12). It is characterised by internal transparent to chaotic seismic facies, although some continuous reflections can be seen within this deposit (Figures VI.10, 11, and 12). This MTD truncates the Subunit U4a across almost the entire extent of the Eastern domain.

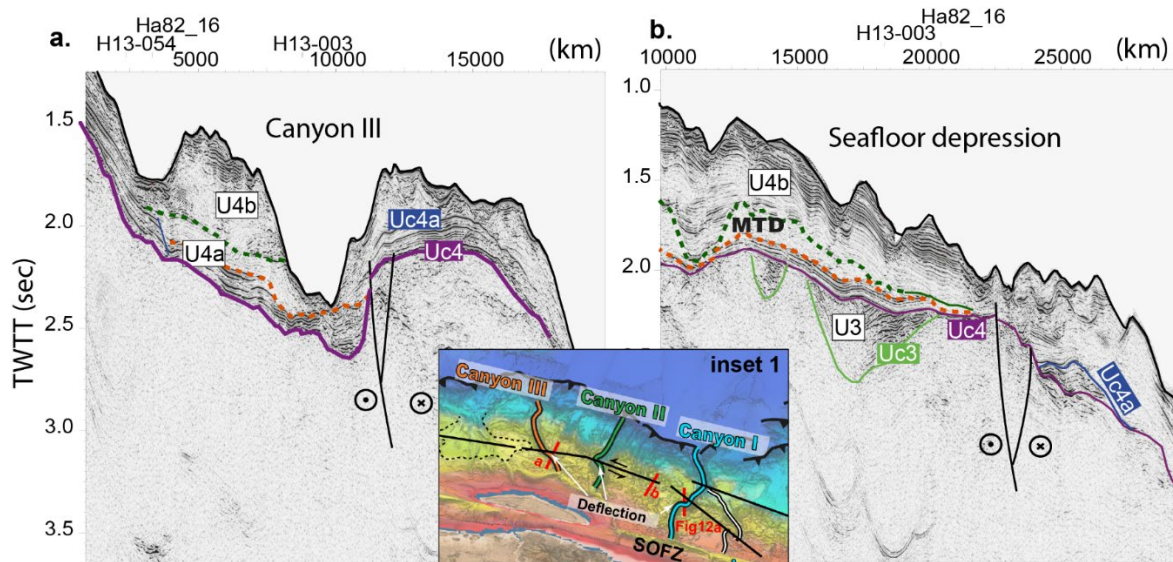


Figure VI.8. a) Seismic line HI2-149, and b) Seismic line HI2-124. The figure shows segments of these seismic lines showing the presence of deep strike-slip faults that seem to be related to the offset of canyon paths visible on bathymetric maps, like the one visible in Inset 1. In Inset 1, the canyon offset corresponds to the position of these strike-slip faults.

Some amplitude anomalies are found above U4a, as the V-shaped anomaly consists of two bedding-concordant limbs dipping towards a shared basal apex in Figures VI.9 “wing” (km 120) and 12b (inset 1). The limbs of these “wing-like” reflections are discordant to the surrounding stratal reflections (inset 1 in Figure VI.12b).

Subunit U4b constitutes the uppermost strata of the sedimentary fill in the Northern Haitian margin (Figure VI.9). In the western domain, the subunit U4b is bounded by the basal unconformity Uc4a (blue) (Figures VI.5 and 9). In this domain, the Subunit U4b displays well-stratified high-amplitude reflections (Figures VI.7, 8, and 9). The thickness of Subunit U4b varies throughout the study area. In the Eastern domain, the subunit U4b is thicker and bounded at its base by the unconformity Uc4a or by the horizon B at the top of the MTD when present. Then, the horizon B at the top of the MTD, when present, represents the base of this subunit (Figures VI.9 and 10). In this domain, the upper part of the Subunit U4b is cut by numerous seabed depressions, affecting the entire eastern sector (inset in Figure VI.3 and Figures VI.9, 10, 11, 12, and 13). The reflectors have a complex wave-like geometry (inset in Figure VI.9). The amplitude of the reflectors is higher at the top of the unit, transitioning to lower amplitude reflectors at greater depths (Figures VI.9 and 10). The horizon B overlapped the basal reflectors of the subunit U4b, forming a very undulated contact (Figure VI.10, inset 3).

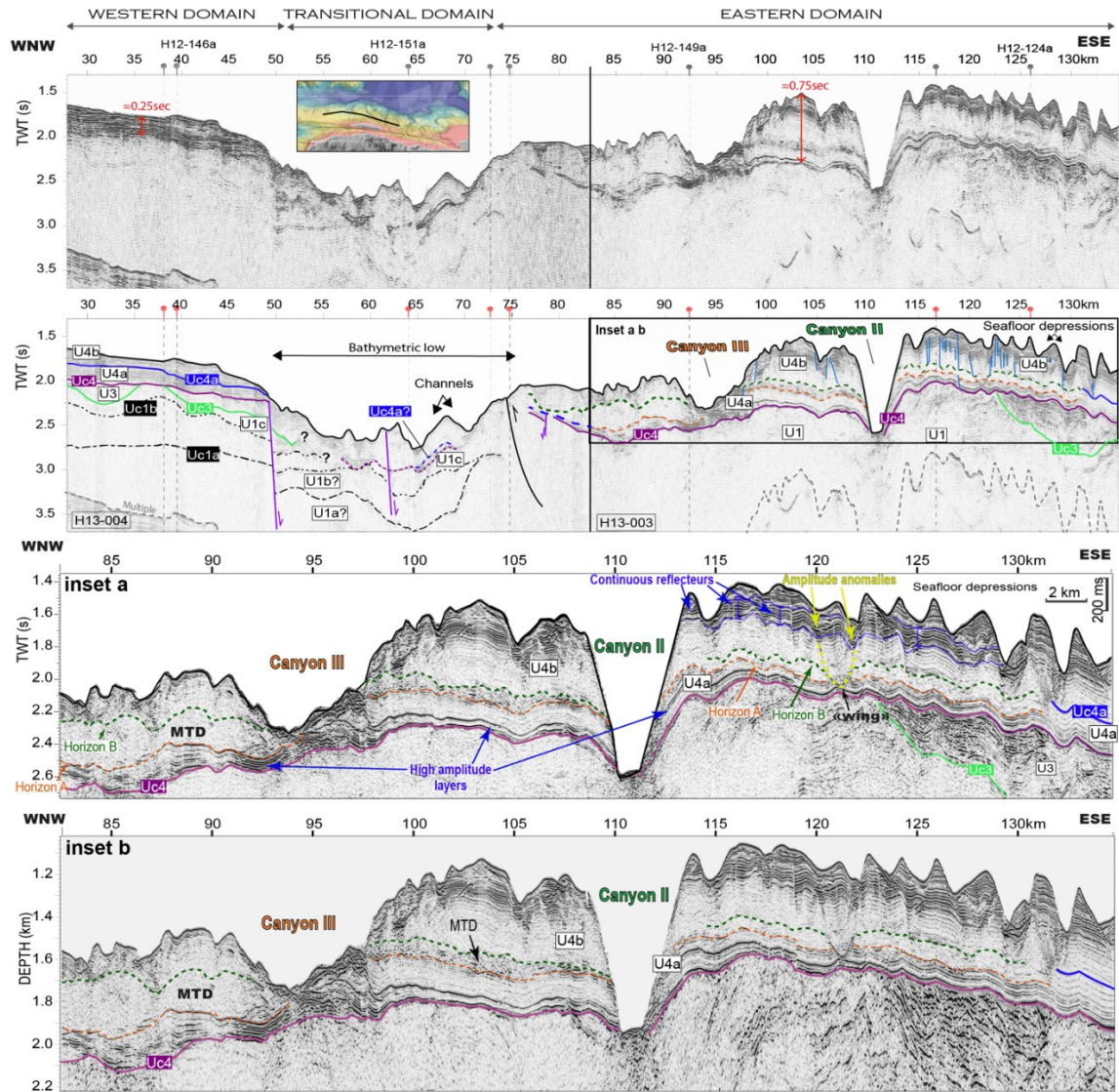


Figure VI.9: Combined seismic line from seismic profiles H13-003 and H13-004. a) W-E trending seismic profile covering the Northern Haitian margin. See location in Figure VI.2a. b) Detailed inset of Unit 4 showing the fault network and the attenuation of the amplitude of Unit 4 reflections with depth.. The seismic profile has been converted in depth by using the following velocity law. From 1500 to 2000m/s at the U_{c4} unconformity and from 2500 to 4000m/s at the base of the selected profile.

VI.3.4 Deformation front

In the Northern Hispaniola Prism, the sedimentary filling is progressively deformed by imbricate thrust faults, forming narrow and smooth E-W trending anticline ridges on the seafloor, suggesting active deformation in this area (Figure VI.2b). These thrust faults imbricate the thicker Caicos sub-basin infill (Figures VI.10 and 13). This prism can be followed toward the east along the Northern Dominican Republic (called NHDB, Rodriguez-Zurrunero et al. 2020) and to the west into the Old Bahamas Channel along the northern Cuban coast (Oliveira de Sá et al. subm.). However, the geometry of the deformation front and the extent of the prism varies from East to West.

The deformation front shows two pronounced undulations between 73°W and 71°30'W (Figure VI.2b). Offshore Dominican Republic (71°40' to 72°20'W), the margin stretches out for

almost 70 km, and ridges at the sea floor remain prominent (Figures VI.3a and 4, section A-A'). In this area, the prism is characterised by three distinct tiers (upper, middle, and lower prisms) (section A-A' Figure VI.4). The upper prism corresponds to the insular shelf, while the lower prism extends on the insular slope from the deformation front to a plateau corresponding to the middle Prism (Figures VI.1, 4, and 13). In contrast to the lower prism, the middle prism appears slightly deformed, with no significant thrusts. The upper prism is crossed by the SOFZ (Figure VI.4). The irregular inter-ridge pattern creates topographic lows (Figures VI.3a and 4, section A-A'). North of the Tortue Island, the Northern Haitian margin becomes narrower than its easternmost portion, ~30 km, with only the lower and upper prisms present (section B-B', in Figures VI.4; 10). The fold vergence is slightly northeast (Figures VI.4 and 13). Far from the ridges, the deep Caicos sub-basin floor is smooth and flat further north.

In the western region (from 73°W of longitude) encompassing the Windward Passage Sill (WPS), the deformation front exhibits a more linear east-west orientation (Figure VI.2b). This is characterised in the seismic profile by tightly folded thrust sheets interpreted as belonging to the lower prism domain (Figure VI.7). These buried thrusts are overlaid by sediments from the slope, concealing this inactive north-verging imbricate system (refer to Figure VI.7). The WPS corresponds to the upper prism in the continuity of the insular shelf.

VI.3.5. Morpho-structural domains

The Northern Haitian margin can then be divided into two morphostructural domains: the Western and Eastern domains (Figure VI.2a). A significant variation in seafloor morphology between these two domains exists (Figure VI.3).

In the Eastern domain (Figure VI.3a), the seafloor is very complex, with deeply incised canyons (Figure VI.4, section C-C' and inset a) beheaded and disconnected from the onshore supplies by the lateral motion of the SOFZ (Figure VI.3a). The SOFZ underlies the seabed as a linear east-west trend valley on the Northern Haiti coast (Figures VI.3a and 4B, inset b). The Eastern domain is also punctuated by various geomorphological features such as seafloor depressions (Figure VI.3a), terraces, gullies, the presence of a buried MTD, and the anticlinal ridges of the lower Prism (Figures VI.2, 4, and 13). The middle prism is only expressed in the most eastern part of the eastern domain. In the western part, upper and lower prisms are observed (Figures VI.4; BB' and 10).

At a longitude of 73°00'W to the west of Tortue Island (see Figure VI.3), the extensive network of deeply incised canyons is absent, and the deformation front becomes more linear (Figure VI.3b). Instead, smaller canyons can be observed, cutting into a relatively shallow bathymetric low (~250 m deeper than the surrounding areas to the east and west, Figure VI.3). Beyond this bathymetric low begins the western domain of the study region (Figure VI.3b).

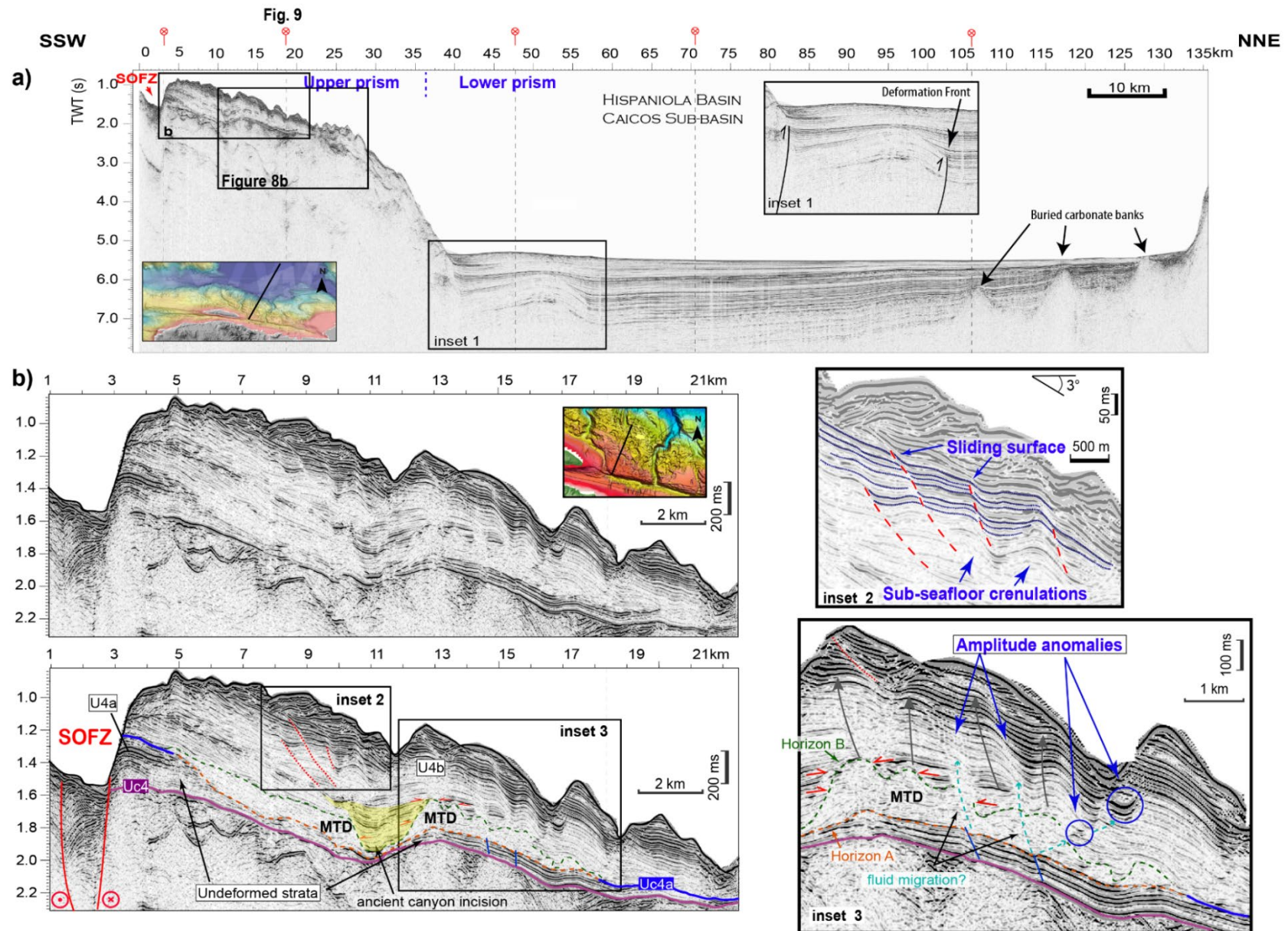


Figure VI.10. Seismic line H12-124. a) Uninterpreted seismic profile showcasing the northern prism of Hispaniola and the Caïcos sub-basin. Buried carbonate mounts are indicated at the northern tip of this basin. See location in Figure VI.2a. b) Close-up of the recent sedimentary cover of the upper prism. The MTD deposit is highlighted, along with the valley shaped by the trace of the SOFZ. Inset 1: Close-up on the frontal fault (deformation front) showing that this fault does not propagate into the most recent deposits of the Caïcos sub-basin. Inset 2: Displays listric faults affecting the reflectors of the U4b subunit, creating subsurface crenulations. Inset 3: Close-up on the distal part of the MTD, which appears more chaotic. The reflectors of the U4b unit onlap the MTD and seem to be "whitened" by potential fluids migrating upwards from the MTD. These fluid exits are inferred by the local amplitude loss of the U4b unit reflectors in contact with this MTD. Grey-coloured arrows indicate that the reflectors of unit U4b mimic the reliefs of Horizon B.

The Western domain pertains to the region encompassing the Windward Passage, situated west of Tortue Island (Figures VI.2 and 3b). In the area referred to as the WPS by Oliveira et al. (2021), the water depth gradually diminishes as it extends westward towards the Punta Maisi region and the WPS high (Figures VI.2, 3b, and 4, section E-E'). In the Western domain, the seafloor on the shelf between Cuba and Tortue Island shows no signs of canyon incisions or channels, no buried MTD, and none of the surface depressions visible in the seafloor of the Eastern domain. The seabed is essentially flat but with some irregularities, such as large erosion scars, some of which create elevations exceeding 300 meters on the seafloor (WPS High west of section E-E' in Figure VI.4). Unlike longitudinal sections, cross-sections show a relatively flat seafloor, dipping $\sim 3.0^\circ$ towards the north and about 1.5° towards the south, in the direction of the Windward Passage Deep (Figure VI.4, section D-D'). This domain is bounded by striking cliffs along the northern and southern edges, particularly adjacent to the Windward Passage Deep (Figure VI.3b; 26° dip Figure VI.4D). The Northern Haitian sub-basin is very narrow toward the north, confined between the WPS and the Great Inagua Bank (Figure VI.4 section D-D').

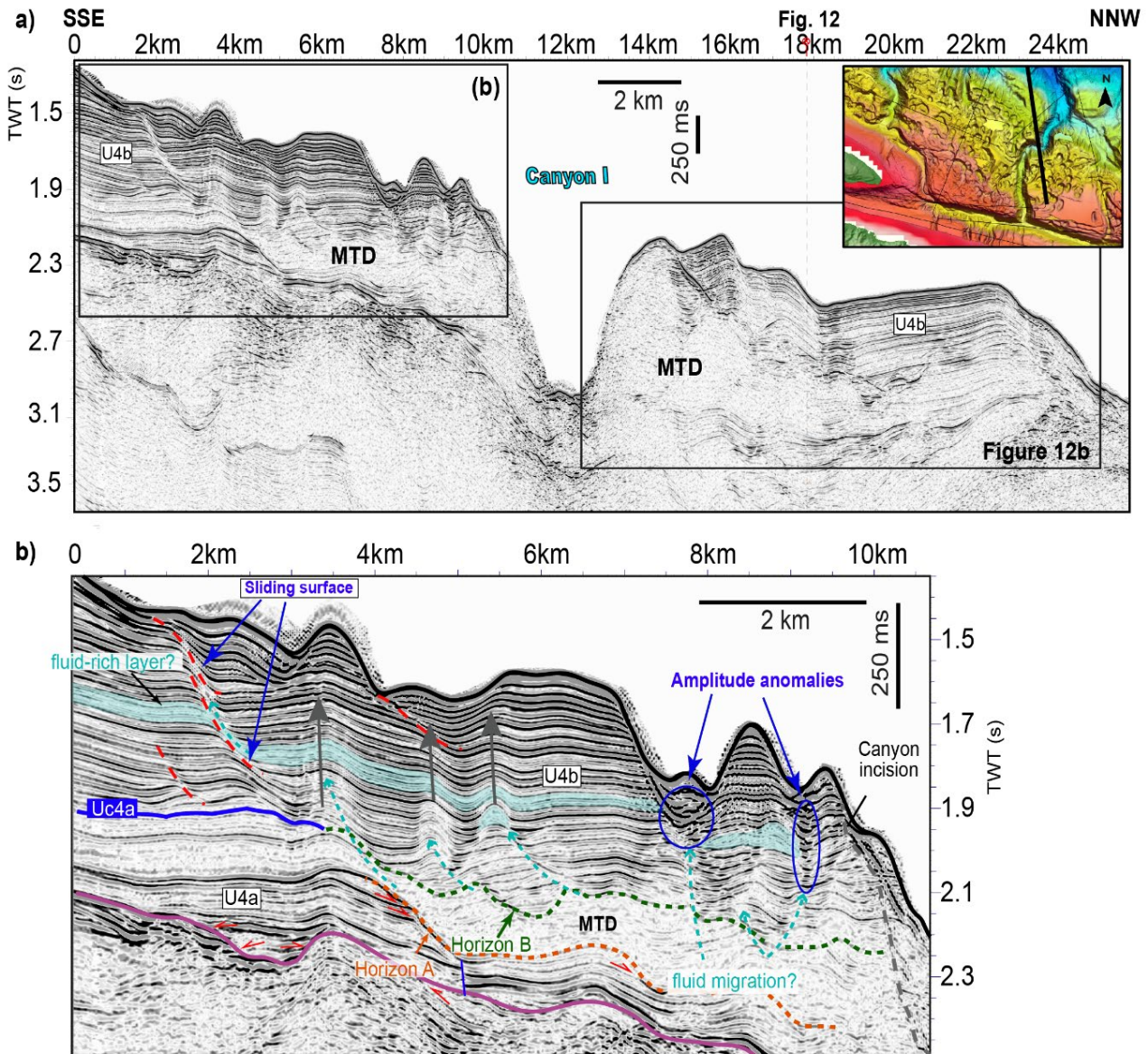


Figure VI.11. Seismic line H12-128. a) Uninterpreted seismic line displaying Unit 4 impacted by depressions on the seafloor of the eastern domain of the study region. See location in Figure VI.2a. b) Close-up on Unit U4 showing the MTD continuous with sub-unit U4a. Amplitude anomalies are visible at the top of the MTD, from which fluids appear to be migrating upwards. Grey-coloured arrows indicate that the reflectors of unit U4b mimic the reliefs of Horizon B.

VI.4. Discussion

The morpho-structural analysis and seismic stratigraphic interpretation allow us to study the relationships between the eastward migration of the SOFZ, the Bahamas Carbonate Province, the deformation front, the morphological seabed features and the architecture of the sedimentary cover. The strike-slip activity spanned from the Oligocene to the Late Pliocene when its latest segment started offshore Haiti (referred to as segment S5 in Figures VI.1b and 2b; Leroy et al. 2015; Oliveira de Sá et al. 2021). The propagation of the SOFZ segments in the Northern Haitian margin did not happen continuously eastward (Oliveira de Sá et al., 2021). Instead, it involved the establishment of strike-slip fault segments along the Northern Haitian margin. This process initiated a series of strike-slip segments north and south of Tortue

Island (Oliveira de Sá et al., 2021). These tectonic activities significantly impacted the region', as observed in the stratigraphic record and the seabed morphology along two distinct morpho-structural domains. Their origin is discussed herein.

VI.4 Stratigraphic record and seafloor morphology variability

Seismic units underlying unconformity Uc4 show comparable deformation characteristics in both domains of the study region. Precisely, the sedimentary succession within unit U1 is folded, and the accommodation space created by these folds is filled by the deposition of Unit 3 (Figures VI.6, 7, and 9). A significant erosion phase cannibalises these units, establishing unconformity UC4. In both domains, the erosive unconformity UC4 is indicated by the toplap terminations of folded horizons (km 10-40 and inset of km 113-140 in Figure VI.9).

The significant difference between the Eastern and Western domains is attributed to the distinct thickness and internal architecture of Unit U4. The high-amplitude and well-stratified reflection pattern within Unit 4 in the Western domain (0.4 s TWT thick, Fig. 6) contrasts well with the complex wave-like pattern of seismic reflectors within the thicker Unit 4 in the Eastern domain (0.75 s TWT thick, Figure VI.9). In particular, the occurrence of (i) a high-amplitude layer at the base of Subunit U4a and (ii) the MTD at the base of Subunit U4b, is exclusively documented within the Eastern domain. Moreover, on the eastern domain, subunit U4b exhibits wave-like internal reflections and a greater thickness compared to the western domain (Figures VI.10, 11, 12).

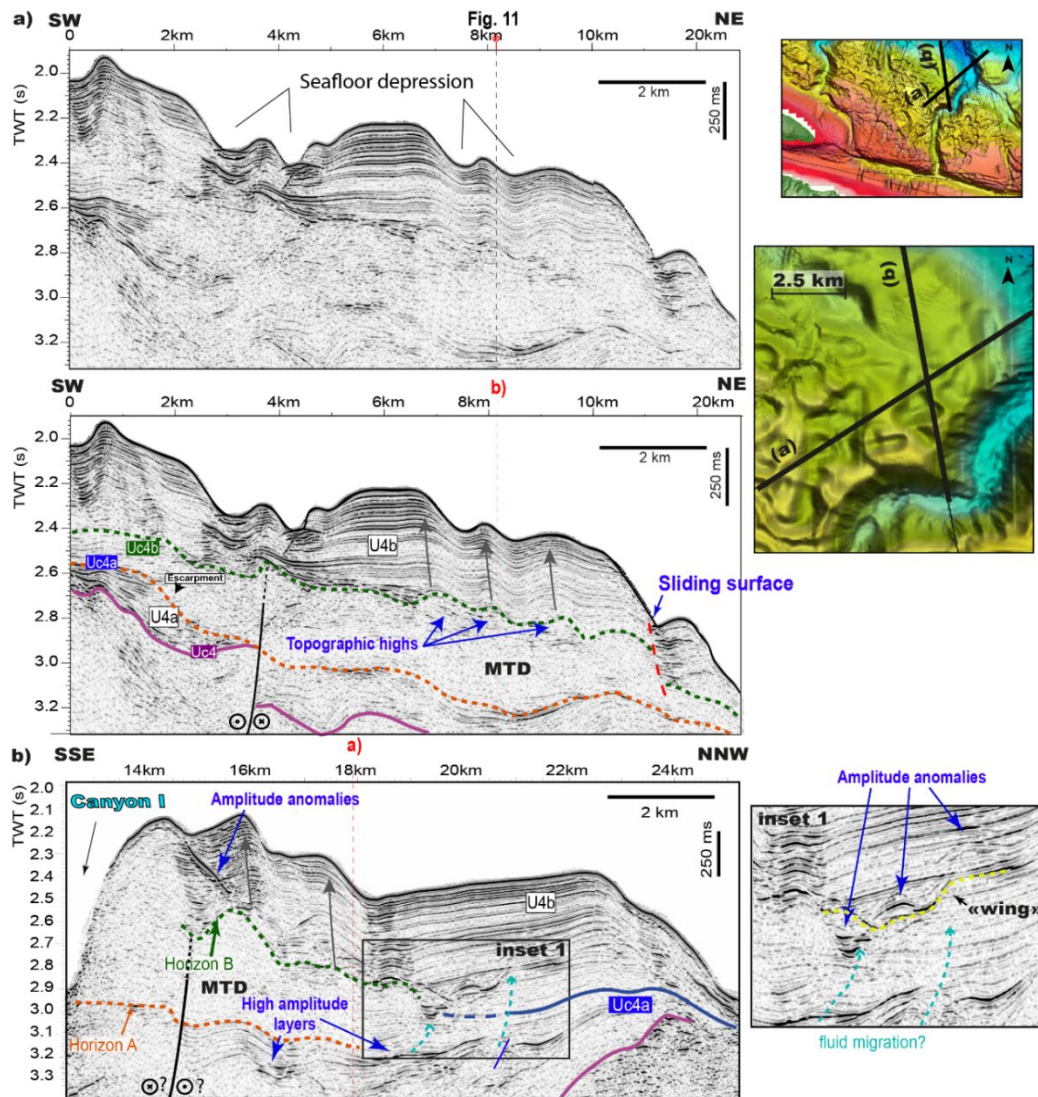


Figure VI.12 : a) Seismic line H13-002. Uninterpreted seismic line on top showing Unit 4 impacted by depressions on the seafloor of the eastern domain of the study region. See location in Figure VI.2a. At the bottom, the interpreted seismic line particularly displays the wavy geometry of horizon B, which defines the top of the MTD. b) Profile shown on a larger scale in Figure VI.11a. Inset 1 displays amplitude anomalies typical of sandy intrusions, known as "wings". Grey-coloured arrows indicate that the reflectors of unit U4b mimic the reliefs of Horizon B.

VI.4.1 Evidence of post-depositional remobilisation within Unit U4

The high amplitudes of the reflectors identified at the base of unit U4a could indicate the early deposition of sand-rich strata (Ma et al., 2020). The presence of significant sandstone-bearing units in the study area cannot be proved as no long sediment cores have been logged. However, Middle/Late Miocene up to middle Pliocene deposits in the Cibao basin (Figure VI.1b - step c, Yaque Group, e.g. Erikson, 1998) show successions of thick intervals of sandstone and conglomerate deposits (middle neritic to upper bathyal) (Erikson, 1998). The Cibao basin can be considered, in a paleogeographic reconstruction, as the proximal part of the study area during the Pliocene (Figure VI.1b). In this case, the presence of sand-rich deposits could be explained by the deposition of turbidity currents transported from submarine canyons to the deep environment of the study region. Analogous sand-rich deposits are also found on the adjacent coast of Tortue Island, where sand-rich deposits prevail (Figure VI.1a) (Cotilla-

Rodríguez, 2021). Furthermore, the double-wedge shape thinning away from the channel fill in Figure VI.9 can be interpreted as external channel levee deposits, which develop adjacent to channel belts (Kane & Hodgson, 2011; Saller & Dharmasamadhi, 2012; Shepard, 1965). In this context, we interpret that the subunit U4a sand-rich deposits acted as a source of fluids, formed during the Middle/Late Miocene up to the Middle Pliocene when the study region was characterised by a deep depositional environment (Figure VI.1b) (Erikson et al., 1998). These deposits are likely associated with a large channel-levee system that transported sandstone from sediments derived from the Central Cordillera and the uplifting and eroding Septentrional Cordillera (Figure VI.1b and c).

Excess pore fluid pressure within buried sand strata can arise due to differential compaction, fluid buoyancy, lateral pressure transmission, and silica diagenesis (Davies et al., 2006; Huuse et al., 2007; Osborne & Swarbrick, 1998). This renders these formations vulnerable to displacement and injection in case of seal layer failure (Gay et al., 2004; Hurst et al., 2003; Monnier et al., 2014). Suggested mechanisms that can potentially initiate seal failure include earthquakes, the development of polygonal faults, and the propagation of fractures due to differential compaction (Huuse et al., 2007; Jackson, 2007; Lonergan et al., 2000; Monnier et al., 2014). A common characteristic of remobilised and injected sands is the presence of wing-like sandstone intrusions (e.g. East Greenland, Surlyk et al., 2007; Northern England Kane, 2010, Barents Sea, Safronova et al., 2012). These features can assume diverse configurations, ranging from dike-like structures to dikes culminating in sills (Monnier et al., 2014). These sandy injections propagate outward from their origin through conduits and occasionally traverse the sedimentary layers, intersecting different stratification planes within the rock (Jackson, 2007; Kane, 2010; Lonergan et al., 2013).

"Wings" are observed in seismic data as prominent high-amplitude reflections originating from sandy bodies. The observation of wing-like anomalies atop the high amplitude basal layers of subunit U4a, coupled with the existence of minor faults that subtly disrupt the reflectors within unit U4—likely attributed to the effects of differential compaction—strengthens the proposition of an excess of fluid pressure in a sandstone lower level (Figures VI.10, 11 and 12).

VI.4.2 Significance of the MTD in the Eastern Domain

The position of the MTD above and in the lateral continuity of the undeformed strata of subunit U4a suggests that the MTD deposit affects U4a only (Figures VI.11b and 12b). This is supported by the MTD being the same thickness as the laterally adjacent, undeformed interval of subunit U4a. The presence of discernible reflectors inside this MTD (Figure VI.11b) supports the interpretation that the displacement was limited and experienced minimal deformation near the leading edge. However, chaotic reflectors in the downslope direction show that it has undergone the most significant deformation towards the north (inset 3 in Figure VI.10). We interpret that the MTD deposit was translated northwards along the slope (Figures VI.10, 11, and 12). According to the presence of the sand injections, we hypothesize that Unit 4a was subjected to pore fluid overpressure, a process known to have a negative on the stability of marine slope sediments (Locat & Lee, 2002). The absence of the MTD in the Western domain might be due to its more remote position from the northern coast of the Dominican Republic, which collided with the Bahamas Carbonate Province during the Late Pliocene. In this perspective, the Western domain is slightly more tectonically stable than the Eastern domain during this period. The eastern domain corresponds to the western offshore extension of the

Septentrional Cordillera (Figure VI.1) and was subjected to intense tectonic activity. The absence of MTD in the western domain can also likely be attributed to the sedimentary flux being less important there, as the sedimentary sources are further away (Figures VI.3 and 14, Cuba, Haiti, Tortue island). Indeed, the greater thickness of Subunit U4b in the Eastern domain would further corroborate higher sedimentation rates, which could have been responsible for important sedimentary loads exceeding sediment resistance. Based on the location of the MTD between Subunits U4a and U4b, a Late Pliocene age can be proposed. Considering that Hispaniola collision with the Bahamas (e.g., Calais et al., 2016) started in the Late Pliocene, it seems reasonable to link the MTD triggering to the combination of tectonics, earthquakes and subsequent liquefaction and post-depositional remobilisation of Unit 4 at that time.

VI.4.3 Wave-like pattern of the Subunit U4b

The topographic lows that formed over the rugged horizon B on the top of the MTD were filled with relatively homogenous sediment of the subunit U4b, displaying reflectors of lower amplitude at the base and higher amplitude at the top (Figures VI.11 and 12).

The subunit U4b covers the entire MTD (Figures VI.10, 11, and 12), and its seismic reflection pattern mirrors the rugosity of horizon B at its top. When the horizon B (top of the MTD) is flatter, the subunit U4b internal reflections exhibit minimal waviness (Figures VI.10, km 6-10, and 12b, km 20-24). Whereas, when the top surface of the MTD is rough, the reflections from the U4b subunit above mimic the crest of horizon B, showing a wavy-like pattern (Figures VI.10 and 12). Different mechanisms could explain the wavy architecture: differential compaction; sliding/creeping and deposition of sediment waves by bottom currents.

Differential compaction during early burial tends to occur in association with variations in lithology, which impose unequal rates of mechanical compaction in strata (Davies, 2005; Herbert, 1993). Differential compaction seems to take place over the more disaggregated (chaotic reflectors) parts of the MTD, i.e., the less cohesive and loosely packed layers experience more pronounced compaction than the relatively solid blocks (less disaggregated layers). This process would, therefore, lead to forced folding of the draping reflectors of the subunit U4b over MTD (Figures VI.8 to 12).

These areas where MTD exhibits chaotic reflectors also appear fluids-saturated with various amplitude anomalies in these locations (Figures VI.10 - inset 3, 11b, and 12 - inset 1). The subunit U4b may act as a seal, preventing fluids from migrating upwards from the MTD. On the other hand, the added weight of the underlying U4b subunit creates an excess fluid pressure, resulting in differential compaction of the MTD. However, the draping seal layers prevent fluids from migrating upwards, keeping them trapped at depth (Figure VI.11b). Nevertheless, the ascent of these fluids exacerbates reflectors folding (Figure VI.11b).

The draping reflectors of Subunit U4b are continuous and have a constant thickness over the MTD top (horizon B, Figures VI.10, 11, and 12). Local depocentres and highs formed on the rough surface of horizon B (Figures VI.10, inset 3, and 12a). The depocentres were filled with sub-horizontal reflections of Subunit U4b, onlapping their inside walls (Figures VI.10 - inset 3 and 11b). Onlapping to concordant reflections of Subunit U4b above Horizon B further suggests that it has “folded” following deposition (Figure VI.10 – inset 3).

The topographic expression of these folds is maintained on the draped reflectors over almost the entire thickness of subunit U4b, sometimes attenuating towards the upper part of the

subunit. Occasionally, the crests and depocenters coincide with the folds on the flanks of the depressions on the seafloor. However, the seafloor depressions are not always linked to subsurface folds, implying that sedimentary and bottom-current processes actively shape the seafloor on the northern Haitian margin. The presence of continuous layers identified on either side of the depressions indicates that erosion processes predominantly shape these seafloor structures (inset in Figure VI.9, between km 112 and 125).

In the seismic profiles where the MTD is not present (Figure VI.13) or its top (Horizon b) is flatter (Figure VI.10, km 5-11), the folding of the reflectors in subunit U4 is interpreted as associated with creeping processes along the slope. Creep is a gravity-driven process, with the updip margins defined by retrogressively formed faults and folds (Lee & Chough, 2001; Li et al., 2016). Subaqueous creep has been observed on steeper slopes ($>3^\circ$), as noted in studies such as Shillington et al. (2012).

Sliding surfaces associated with sub-seafloor crenulations within Subunit U4b (Figure VI.10 inset 2) occur where the slopes exceed 3° (sections A-A', Figure VI.4). These surfaces could be related to growth folds, suggesting that the subunit U4b is also affected by creeping processes that can overwhelm the effects of differential compaction of the MTD. These sliding surfaces do not appear to be linked to the differential compaction of the MTD since these features are observed even in areas where the MTD is not present (as in Figures VI.11 - km 0-2, and 13, inset 1). When these sliding surfaces are present above the MTD, the top of the MTD (Horizon b) is flat (Figure VI.10).

On a large scale, the eastern domain is characterised by a significant U4 sediment thickness (0.75 sec TWTT) and a flat seafloor slope in the open Caicos sub-basin (in contrast to the slope that reverses in the confined North Haitian sub-basin, Figure VI.4 profiles A, B, D). Moreover, in the eastern part of our study area, the base of Unit 4 could act as a décollement level. Undulated sediment features are commonly observed on nearshore bathymetric data as the result of hyperpycnal flows (Lee et al., 2002; Mosher and Thomson, 2002; Urgeles et al., 2007; amongst others) while in deep water, they can also be either induced by deep-water turbiditic systems or by bottom currents (Lee et al., 2002; Rebesco, 2005). On the other hand, when significant discontinuity between seismic reflectors and growth faults is associated, these undulations are interpreted as creeping. The accuracy of the interpretation of undulated sediment features depends mostly on the available data resolution.

Two arguments may support this hypothesis: (a) most of the seismic reflections illustrate individual reflectors as quite continuous and no diffractions are visible on the synform part of the folds, which could indicate a rupture of the reflectors. (b) According to Urgeles et al. (2007) the regularity of the dipping of strata is better explained by sediment waves formed by bottom currents than creep. While the description of the sedimentation of Unit U4 is out of the scope of the present work, we do not rule out the possibility that the wavy architecture results from the interaction between bottom current processes that form sediment waves locally disturbed by creeping and differential compaction processes that would affect post-MTD units. As a result, the analysed landslide strata (MTD), likely dating back to the Late Pliocene, continue to govern part of the contemporary seafloor topography.

VI.5. Tectonic Influences on the Submarine Canyons of the Eastern Domain

VI.5.1 Influence of Deep Faults on Canyon Paths

In the eastern sector, a network of submarine canyons stands out as a striking feature (Figure VI.3). Unlike the western domain, devoid of such canyon incisions, canyon systems developed in the eastern domain, likely by the immediate proximity of the sector with the coasts of northern Haiti and northwestern of the Dominican Republic (Figures VI.2 and 3).

The submarine canyons identified within the eastern domain exhibit geomorphological attributes indicating their control by the regional active tectonics. The canyons are beheaded from the continental drainage system from the Haitian coast by the SOFZ fault trace and are now inactive. However, deviations in the paths of the canyons suggest that their formations were also structurally influenced during the active period (Figure VI.3a).

No geomorphological element (e.g., local bathymetric elevations caused by carbonate banks or seamounts) seems responsible for the canyons' bends. However, at deep, the location of these bends appears to be related to the presence of faults (Figures VI.8 and 12b). The lateral displacement on the canyon path, which causes these deflections, may infer strike-slip fault offsets in a transpressive setting. The shift expression of these faults on the bathymetry is represented by the offset of an inactive canyon (white dots in Figure VI.3a). The canyon was probably used to connect the Hispaniola coast and the Caicos sub-basin. It is now inactive, and a gap has developed in the middle of the canyon where its incision is cut and offset by the presence of the transpressive strike-slip fault that propagates westward and bends the path of Canyon I (Figure VI.3a).

At around 20°0'N, canyons I, II, and III inflexion points also align with the head of the rectilinear slope canyons (Figure VI.3a). It is interesting to note that the rectilinear slope canyon heads stop precisely at the location of the fault (Figure VI.3a). The rectilinear morphology of these slope canyons is probably due to retrogressive headward erosion from the lower to the upper part of the slope (Figure VI.2) (Etienne et al., 2021). The fault may act as a barrier to their progression upstream.

These faults are probably inactive (or much less active than before); they do not have a clear imprint along the seafloor. However, their traces are inferred in the seismic reflection data (Figure VI.8), and by the deflection of canyons, the ancient strike-slip motion along these lateral faults, running parallel to the slope, shifted the flow pathways of the canyons (Figures VI.3a and 8).

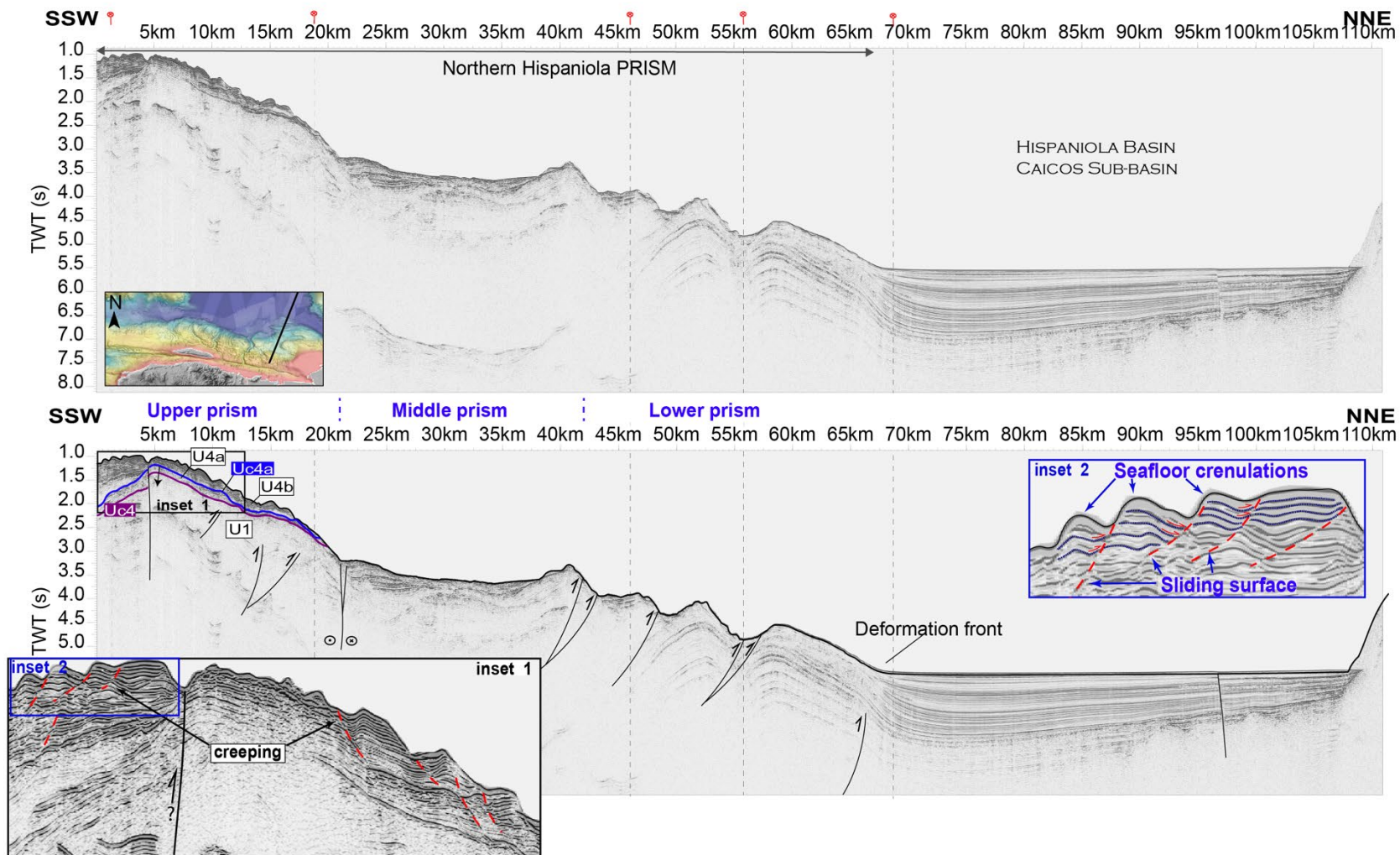


Figure VI.13: Seismic line H12-122a. Uninterpreted seismic line through the Eastern domain showing the offshore North Hispaniola deformed belt. See location in Figure VI.2a. The inset shows a close-up of the easternmost sedimentary cover of the upper prism. Here, the MTD deposit is absent, but sliding surfaces affect unit U4, creating crenulations within this unit and resulting in a very rough seafloor.

VI.5.2 Influence of deformation Front on Canyons morphology

These submarine canyons identified within the Eastern domain have U-shaped profiles and display a convex-up shape (Figure VI.4, inset a).

The rate at which a longitudinal profile becomes flatter downstream is known as its concavity (Zaprowski et al., 2005). Under equilibrium conditions — where erosion balances uplift — concave-up shaped profiles dominate. However, factors like base-level shifts and tectonic uplift can alter this equilibrium, leading to convex profiles (Whipple & Tucker, 1999). Convex profiles are often seen in tectonically active areas where changes in the equilibrium of submarine canyons influence their drainage system dynamics (O'Grady et al., 2000; Seybold et al., 2021; Soutter et al., 2021).

To the north, the activity of the deformation front has contributed to the deform downstream portion of the canyons (Figure VI.3a) and likely influenced the development of the drainage system. Ridges on the canyons' downstream portion indicate that deformation front activity disrupts canyon morphology (Figure VI.4).

The activity along the deformation fronts significantly influences the morphology of submarine slopes and affects the ability of canyons to reach equilibrium (Pettinga & Jobe, 2021). This is revealed by the decreased concavity of submarine canyons formed in forearc basins, which are commonly undergoing active seafloor deformation through folding, faulting, or accretionary prism formation (Pirmez et al., 2000; Soutter et al., 2021). The Sinu accretionary prism, Colombia (Vinnels et al., 2010), and the Cook Strait, New Zealand (Micallef et al., 2014), are examples of these processes, with thrust faulting modifying the profiles of incisional submarine canyons and their channels, causing them to be convex.

The U-shaped canyon axis suggests sediment accumulation, indicating that sediment transport to the deep basin has decreased activity (Shepard, 1981). Ridges formed by the activity in the deformation fronts are a barrier for the canyons to carry sediments to deeper basins. In addition to the fact that the activity of the deformation front reduces the transport capacity of the canyon, there is also the fact that the canyon receives less sediment due to the formation of terraces on the northern side of the SOFZ fault trace (see Figure VI.3a and 4, section h-h'). These terraces might be a result of the incision due to the combined effect of the SOFZ and the active thrusting related to the oblique collision (see next section), subsequently causing an uplift at the canyon's head and likely obstructing the canyon from obtaining sediments from the coasts, as the sediments are trapped in the deep valley shaped by the SOFZ trace.

VI.6 Deformation partitioning and distribution of the morphological features

This study proposes two distinct morpho-structural domains from east to west (Figure VI.14). Between these two domains, an NNE-SSW transition following the aftershocks distribution of the October 6, 2018 event, corresponds to a bathymetric low with landslide scars (Figure VI.3b). It is an extension of the eastern edge of the Great Inagua Bank, serving as a rigid block that swiftly reduces and reverses the northward slope after encountering the deformation front (Figure VI.4 section D-D', Figure VI.2b). It also marks the transition from a further offshore deformation front to a straighter deformation front closer to the margin (Figure

VI.14). Rodriguez-Zurrunero et al. (2020) determined several tectonic domains based on an integrated structural, morphological, seismotectonic, and kinematic study. We propose that our western and eastern domains correspond to the Haitian Strike-slip and the Dominican Republic Oblique Underthrusting domains, respectively (Figure VI.14). The different trends of the SOFZ segments 2-3 and 4-5 (Figure VI.2), the sediment flux intensity, and the Great Inagua Bank indentation could explain the different morphologic and tectonic patterns in the two domains. The nature of the North American plate could play a role in the expression of these two domains. Thus, a continental nature to the west could be proposed with the presence of tilted blocks to the north of Cuba on which the carbonate banks are located (Oliveira de Sá et al. subm) up to the transition zone. And an oceanic nature for the eastern domain, which would allow the plate to undergo subduction as illustrated by Calais et al 2023 (Figure VI.14).

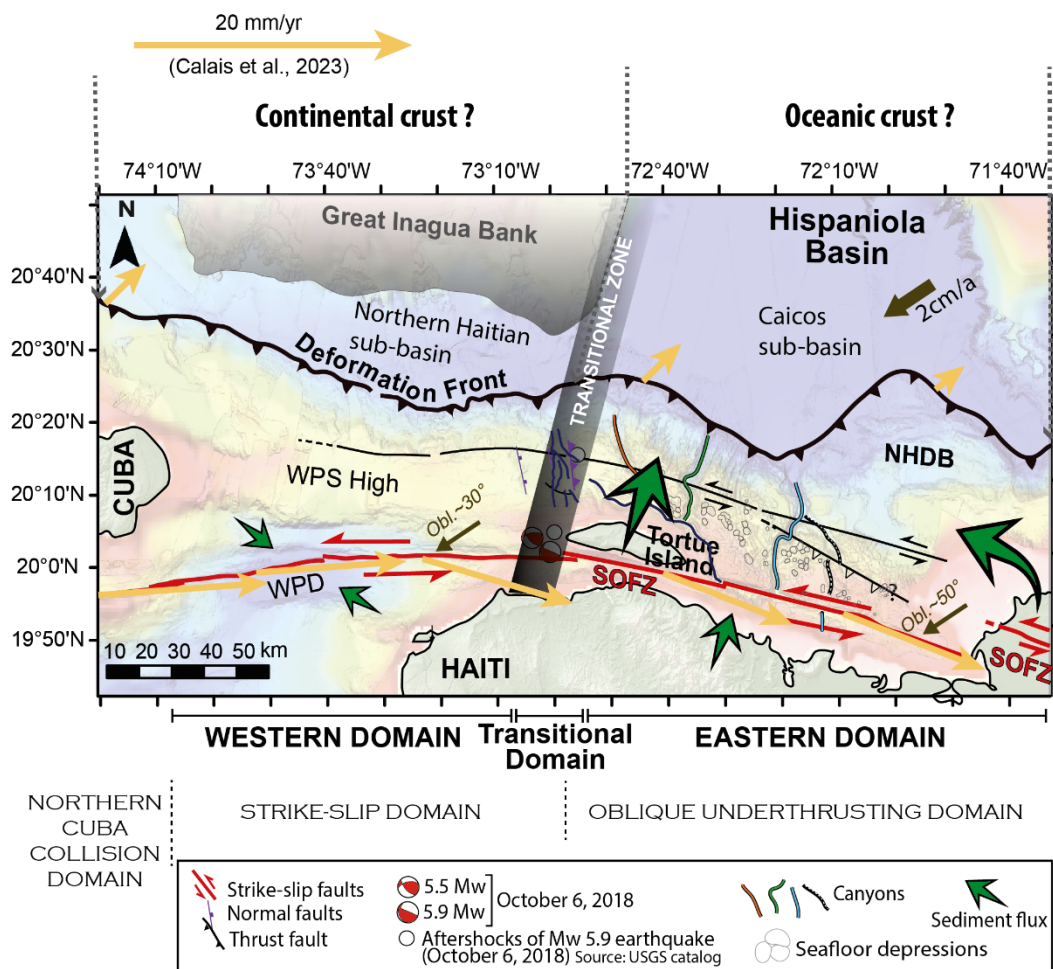


Figure VI.14: Schematic map showing the different characteristics of the western and eastern domains and the proposed nature of the NAM plate. The boundaries of the tectonic domains (strike-slip, oblique, collision) derived from Rodriguez-Zurrunero et al. (2020) are in agreement with our study. The kinematic vectors in yellow are derived from the block model proposed by Calais et al. (2023). WPS: Windward Passage Sill; WPD: Windward Passage Deep.

In the Eastern domain, important sediment flow with the deposition of a fluid-rich layer at the base of unit U4 is likely the origin of instability processes that will later cause differential deformation of this unit. This deformation of unit U4 creates irregularities on the seafloor, which may be indirectly at the origin of the first depressions but are not the direct cause. The direct cause is probably related to sedimentary and erosion processes induced by bottom

currents with the irregular topography of the seabed. The characteristics of the recent sedimentary deposits of this margin, as well as the possible sedimentary processes causing these depressions on the seabed on the northern coast of Haiti, are discussed in Oliveira de Sá et al. (In prep.).

Canyons probably began their incision in continuity with terrestrial rivers. In this case, the presence of a significantly developed canyon system exclusively located in the Eastern domain of the study area is again likely due to its direct proximity to the coasts north of Haiti and the Dominican Republic. In contrast, the Windward Passage over the Western domain is surrounded on each side by two deep basins, at least during the deposition of unit U4.

These canyons have been affected by the regional oblique collision (Figure VI.14). The establishment of strike-slip faults began to affect the course of the canyon's incision, and activity on the deformation front resulted in a progressive uplift of this margin, altering the equilibrium profile of these canyons (Figure VI.4 inset a). Therefore, the onset of the SOFZ-related segments at the canyon heads and the activity at the deformation front appear to have rendered these canyons inactive, as indicated by their convex-up profiles (Figure VI.4).

VI.7. Timing Constraints for the Deformation along the Northern Hispaniola Margin

VI.7.1 From Oligocene to Early Pliocene (Unit 1 to 3; Uc4; onset of U4a)

In the Late Oligocene (~20 Ma), the northern Caribbean Plate boundary shifted south of Cuba towards the Oriente Fault Zone (OFZ) (Figure VI.1b step a), separating Cuba from Hispaniola, which had until then formed a single block (Calais & Mercier De Lépinay, 1991, 1995; Pindell & Draper, 1991). This tectonic shift resulted in the attachment of the Cuban block to the North American Plate (Calais & Mercier de Lépinay, 1992; Mann et al., 1995; Calais & Mercier de Lépinay, 1995; Leroy et al., 2000; Rojas-Agramonte et al., 2008; Wessels, 2019; Oliveira de Sa et al., 2021).

The OFZ spread eastward from the Oligocene to the early Miocene (Figure VI.1b, step a). During this time, the OFZ was in the western continuation of the Northern Hispaniola Fault (NHF in Figure VI.1b, step a) (Dolan et al., 1998; Draper et al., 1994; Erikson et al., 1998; Oliveira de Sá et al., 2021).

The Oligocene-Early Middle Miocene rocks of the Septentrional Cordillera exhibit NE-SW shortening and NW-SE trending folds (Erikson et al., 1998). These characteristics point to a middle Miocene deformation episode, which aligns with the formation of a restraining bend along the northern Hispaniola margin (Figure VI.1b, step a) (De Zoeten and Mann 1991). The ongoing deformation within this restraining bend potentially triggers the folding of the sedimentary units in the study area before the Uc4a unconformity (Figure VI.1b step a). Oliveira de Sá et al. (2021) proposed that thrust faults formed in the Windward Passage during this restraining bend activity in the Early-Middle Miocene (Figures VI.1b step a and 8b). Ongoing compression in the Northern Haitian margin folded Unit 1 and created space to accommodate Unit 3 deposition (Figure VI.5) (Calais & Mercier De Lépinay, 1995; Oliveira de Sá et al., 2021).

This event led to the regional uplift and exposure of the future Septentrional Cordillera, as evidenced by an extensive angular unconformity observed on a regional scale between

middle and upper Miocene up to Pliocene (de Zoeten & Mann, 1991; Erikson et al., 1998; Pindell & Draper, 1991). The erosive phase induced by the subaerial exposure is expressed on our seismic profiles by the Uc4 unconformity (Figures VI.5 to 11). Consequently, erosion would have started during the Middle Miocene, earlier than the Mid-Pliocene age proposed by Oliveira de Sá et al. (2021).

As restraining bends do not efficiently accommodate the regional transcurrent shear of the fault system (Cooke et al., 2013), new strands of the Oriente Fault Zone evolved toward the east to accommodate part of the ongoing strike-slip (dotted red line, Figure VI.1b inset b). The initiation of the lateral fault that displaces the canyon's paths and also the initiation of the Camu fault (CF) (Late Miocene, Early Pliocene) and other fault segments in the Septentrional Cordillera are probably related to this process (Figure VI.1b, steps b and c). The successive southward jumps of these fault segments result in the Septentrional Fault Zone (SFZ) and finally in the SOFZ when the east and west fault systems joined (Figure VI.1b step d).

The Middle Miocene formations observed in the Septentrional Cordillera are characterised by a deepening succession evolution from mixed sandstones and conglomerates in its base (Cercado Formation) to siltstone/mudstone accumulations at its middle (Gurabo Formation) and calcareous siltstone at its top (Mao Formation) corresponding to the Yaque Group (Erikson et al., 1998) (Figure VI.1b steps b and c). These formations are breathy, interrupted by a relatively thin interval of conglomerate and sandstone beds being interpreted as sediment gravity flows. Based on these observations, Erikson (1998) suggests a period of subsidence in which these formations were deposited (deep water deposition) following the uplift period recorded during the Middle Miocene (Figure VI.1b steps a-b). The detrital middle Miocene sediments were mainly derived from the south (probably from the Central Cordillera) with only brief contributions from the Septentrional Cordillera). Erikson (1998) concluded that from the late Miocene time to the Early Pliocene, the ongoing Septentrional fault zone (North Hispaniola area, Figure VI.1b steps b-c) was the locus of large strike-slip but only minor vertical movement.

The inferred offshore fluid-rich layer in the basal part of Subunit U4a is probably the equivalent in age of this coarser Middle Miocene formations on land (Figure VI.1b; step b). The sand was probably transported during turbidite flows and deposited in a channel-levee system (as depicted by its double-wedge shape lateral to the canyons axis, Figure VI.9).

VI.7.2 Pliocene (Further Unit U4a)

The Pliocene's oblique collision of Hispaniola with the Bahama Banks slowed Hispaniola's eastward movement compared to the North American Plate (Calais et al., 2016). Transpressive deformation, caused by oblique collision, likely led to the formation of the SOFZ segments, the growth of the deformation front, and the uplift of the Septentrional Cordillera (Sept. C. in Figure VI.1a and b, step c) (Calais et al., 2016; Escuder-Viruet & Pérez, 2020).

The tectonic activity in the Pliocene significantly affected the northern Haitian margin. With the rise of the Septentrional Cordillera, the sedimentary deposits in the study area become more proximal. In this context of regional uplift, we can infer that the canyons system in the study area developed and increased their incision along the Pliocene due to the upstream uplift gradient.

The submarine canyons formed adjacent to seismically active margins (volcanic or convergent margins) are subject to uplift upstream. This upstream uplift produces more concave-shape canyons (Soutter et al., 2021). The canyons in the study area were probably very erosive during the Pliocene, transporting the sediment from the Septentrional Cordillera to the deep Hispaniola basin (Caicos sub-basin). However, it is known that in convergent margins, upstream uplift is counterbalanced by the downstream uplift regenerated by the activity of thrust fault in the deformation front (Soutter et al., 2021). This process would explain the current convex shape of canyons in the Eastern domain (Figure VI.4).

The activity of the deformation front during the Pliocene triggered the uplift of the northern Haitian margin. In the Western domain, the proximity to the Great Inagua Bank prevents the deformation front from propagating northward (Figure VI.2). That's why the thrust faults are closer in the Western domain, and the wedge is shorter and steeper (Figure VI.6). The linear scarps that form the narrow E-W-oriented channel in the Northern Haitian sub-basin between the Windward Passage Sill and the Great Inagua Bank (Figure VI.3b) show that this oblique collision is the main control of the submarine morphology in the Western domain. The scarps along the entire seabed of the Windward Passage and the presence of the WPS high are also linked to active tectonics (Figures VI.2b, 3b, and 7). As the Eastern domain faces the vast Caicos sub-basin, the deformation front can propagate northward, giving rise to the imbricating anticlinal ridges system of the lower prism with the establishment of well-spaced thrust faults (Figure VI.13) and well-defined ridges on the seabed (Figures VI.2b, 3a and 13). The distinct nature of the crust of the Northern American plate on either side of the transitional zone could be invoked for the distinct morpho-structural features observed in the eastern and western domains.

VI.7.3 From Pliocene to present-day (Unit U4b)

During the Pliocene collision, the major strike-slip motion shifted south to its present location in the Dominican Republic (Calais et al., 2016). (Figure VI.1, step d). At the same time, in the Eastern domain, the initiation and/or reactivation of strike-slip faults begins, as well as compression, offsetting the canyons' course. The fault segments that offset the canyons appear to be the westward extension of the segments of the SOFZ present on land in the Dominican Republic (Figures VI.1a and 3a). These segments were likely formed at the same time as the migration of fault segments of the OFZ from the Windward Passage Basin towards the east, offshore of Haiti (Figure VI.1b, step c).

Progressively, the Oriente fault zone splayed eastward, running across the WPD and into northern Hispaniola to form the SOFZ (Figure VI.1b, steps c-d; Calais & Mercier de Lépinay, 1995; Leroy et al., 2015). Thus, the SOFZ formed in the Late Pliocene when segment 5 started offshore Haiti (Figure VI.1b, step d). The emplacement of the SOFZ established the current Northern Caribbean plate and incorporated part of northern Hispaniola into the North American plate, detaching the canyons in the study area from their continental inputs (Calais et al., 2016; Erikson et al., 1998; Escuder-Viruete & Pérez, 2020; Oliveira de Sá et al 2021).

Despite decreased contractional tectonic activity after the Pliocene, current vertical movements persist in the region (Oliveira de Sa et al., 2021). This is evidenced by Quaternary terraces along the northwestern coastlines of Hispaniola, Tortue Island, and Cuba (Figures VI.3b and 6) (Authemayou et al., 2023; Calais & Mercier De Lépinay, 1992; Sorel et al., 1991). Reverse faults in the Windward Passage Sill and the elevated WPS High also suggest that these

significant vertical movements could influence the northern Haitian margin (Figures VI.2b, 3b, and 7).

VI.8 Conclusion

The tectonic and sedimentary evolution of the Northern Haitian Margin exhibits intricate dynamics from the Oligocene to the Late Pliocene, related to a series of interconnected geological events.

The Late Oligocene was characterised by a shift in the northern Caribbean Plate boundary, which separated the Cuban block from Hispaniola and its consequent attachment to the North American Plate. This tectonic rearrangement resulted in the initiation of the Oriente Fault Zone (OFZ) and its subsequent eastward propagation from the Oligocene to the early Miocene (north of Hispaniola). The initiation of a middle Miocene restraining bend caused the folding and the emersion of the sedimentary formations deposited prior to the Miocene. The same deformation pattern was observed in the whole study area, marked during the final phase of erosion by the emplacement of a significant unconformity (Uc4).

From the late Miocene to the early Pliocene, the area was submerged again during a period of subsidence. The differences between the east and west domains emerge from variable sediment flux and deformation patterns from the late Miocene to the early Pliocene. In the East domain, the occurrence of a Mass Transport Deposit (MTD) is probably at the origin of the differential compaction phenomena occasioning these units' post-depositional remobilisation. This process gives rise to the wave-like pattern of this unit in the east domain, which contrasts the planar arrangement observed in the western domain. The ongoing influence of the ancient MTD, probably of the Late Pliocene age, creates an irregular seafloor, which usually influences sedimentation and erosion processes at the current seafloor.

In the late Pliocene, the oblique collision between Hispaniola and the Carbonate Bahamas Province resulted in a contractional deformation. This deformation governed the initiation of the deformation front, the evolution of the Septentrional Fault Zone, and the uplift of the Septentrional Cordillera. During this time, submarine canyons of the margin underwent morphological changes due to the influence of tectonism in the canyon morphology and sediment transport. During the same period, the OFZ shifted southward, correlating with the emergence of strike-slip faults in the Eastern domain that disrupted the trajectory of canyons.

The geologic evolution of the Northern Haitian Margin attests to the intricate interactions between tectonic mechanisms, sedimentary processes, and distribution of the geomorphological features. From the inception of the OFZ in the Late Oligocene to the emplacement of the SOFZ in the Late Pliocene, the intricate interplay between these factors has profoundly influenced the seafloor of the Northern Haitian coast.

VI.9 References

Authemayou, C., Nuñez, A., Pedroja, K., Peñalver, L., Chauveau, D., Dunán-Avila, P., Martín-Izquierdo, D., de Gelder, G., Husson, L., Castellanos Abella, E., Benítez Frómata, P. de J., & Pastier, A.-M. (2023). Oblique Collision of the Bahamas Platform at the Northern

- Boundary of the Caribbean Plate Recorded by the Late Cenozoic Coastal Terraces of SE Cuba. *Tectonics*, 42(8), e2023TC007806. <https://doi.org/10.1029/2023TC007806>
- Benford, B., DeMets, C., & Calais, É. (2012). GPS estimates of microplate motions, northern Caribbean: Evidence for a Hispaniola microplate and implications for earthquake hazard. *Geophysical Journal International*, 191(2), 481-490. <https://doi.org/10.1111/j.1365-246X.2012.05662.x>
- Calais, É., Freed, A., Mattioli, G., Amelung, F., Jónsson, S., Jansma, P., Hong, S.-H., Dixon, T., Prépetit, C., & Momplaisir, R. (2010). Transpressional rupture of an unmapped fault during the 2010 Haiti earthquake. *Nature Geoscience*, 3(11), Article 11. <https://doi.org/10.1038/ngeo992>
- Calais, E., Gonzales, O., Arango-Arias, E. D., Moreno, B., Clares, R. P., Cutie, M., Diez, E., Montenegro, C., Roche, E. R., Garcia, J., Castellanos, E., & Symithe, S. (2023). Current Deformation Along the Northern Caribbean Plate Boundary from Gns Measurements in Cuba (SSRN Scholarly Paper 4537779). <https://doi.org/10.2139/ssrn.4537779>
- Calais, É., & Mercier De Lépinay, B. (1991). From transtension to transpression along the northern Caribbean plate boundary off Cuba: Implications for the Recent motion of the Caribbean plate. *Tectonophysics*, 186(3), 329-350. [https://doi.org/10.1016/0040-1951\(91\)90367-2](https://doi.org/10.1016/0040-1951(91)90367-2)
- Calais, É., & Mercier De Lépinay, B. (1992). La limite de plaques décrochante Nord Caraïbe en Hispaniola: Évolution paléogéographique et structurale cénozoïque. *Bull. Soc. géol*, 3(163), 309-324.
- Calais, É., & Mercier De Lépinay, B. (1995). Strike-slip tectonic processes in the northern Caribbean between Cuba and Hispaniola (Windward Passage). *Marine Geophysical Researches*, 17(1), 63-95. <https://doi.org/10.1007/BF01268051>
- Calais, É., Symithe, S., Mercier de Lépinay, B., & Prépetit, C. (2016). Plate boundary segmentation in the northeastern Caribbean from geodetic measurements and Neogene geological observations. *Comptes Rendus Geoscience*, 348(1), 42-51. <https://doi.org/10.1016/j.crte.2015.10.007>
- Cotilla-Rodríguez, M. O. (2021). Historia de la sismicidad del segmento Islas Caimán-Cabo Cruz (Cuba), en el marco de la zona de entre placas Norteamérica-Caribe. *Revista Tierra*, 1(1), Article 1. https://revistatierra.unan.edu.ni/index.php/revista_tierra/article/view/25
- Davies, R. J. (2005). Differential compaction and subsidence in sedimentary basins due to silica diagenesis: A case study. *GSA Bulletin*, 117(9-10), 1146-1155. <https://doi.org/10.1130/B25769.1>
- Davies, R. J., Huuse, M., Hirst, P., Cartwright, J., & Yang, Y. (2006). Giant clastic intrusions primed by silica diagenesis. *Geology*, 34(11), 917-920. <https://doi.org/10.1130/G22937A.1>
- de Zoeten, R., & Mann, P. (1991). Structural geology and Cenozoic tectonic history of the central Cordillera Septentrional, Dominican Republic. In *Geological Society of America Special Papers* (Vol. 262, p. 265-280). Geological Society of America. <https://doi.org/10.1130/SPE262-p265>
- de Zoeten, R., & Mann, P. (1999). Chapter 11 Cenozoic el mamey group of northern hispaniola: A sedimentary record of subduction, collisional and strike-slip events within the north America-Caribbean plate boundary zone. In P. Mann (Éd.), *Sedimentary Basins of the World* (Vol. 4, p. 247-286). Elsevier. [https://doi.org/10.1016/S1874-5997\(99\)80045-8](https://doi.org/10.1016/S1874-5997(99)80045-8)
- Dillon, W. P., Austin, J. A., Scanlon, K. M., Terence Edgar, N., & Parson, L. M. (1992). Accretionary margin of north-western Hispaniola: Morphology, structure and

- development of part of the northern Caribbean plate boundary. *Marine and Petroleum Geology*, 9(1), 70-88. [https://doi.org/10.1016/0264-8172\(92\)90005-Y](https://doi.org/10.1016/0264-8172(92)90005-Y)
- Dillon, W. P., Edgar, N. T., Scanlon, K. M., & Coleman, D. F. (1996). A review of the tectonic problems of the strike-slip northern boundary of the Caribbean Plate and examination by GLORIA : Chapter 9. 135-168.
- Dolan, J. F., Mullins, H. T., & Wald, D. J. (1998). Active tectonics of the north-central Caribbean : Oblique collision, strain partitioning, and opposing subducted slabs. In J. F. Dolan & P. Mann, *Active Strike-Slip and Collisional Tectonics of the Northern Caribbean Plate Boundary Zone*. Geological Society of America. <https://doi.org/10.1130/0-8137-2326-4.1>
- Draper, G., Mann, P., & Lewis, J. F. (1994). Hispaniola. In S. K. Donovan & T. A. Jackson, *Caribbean Geology : An Introduction*. University of the West Indies Publishers Association (p. 129-150).
- Emery, K. O. (1980). Continental margins : Classification and petroleum prospects. *Am. Assoc. Pet. Geol. Bull.; (United States)*, 64:3. <https://www.osti.gov/biblio/7048945>
- Erikson, J., Pindell, J., Karner, G., Sonder, L., Fuller, E., & Dent, L. (1998). Neogene Sedimentation and Tectonics in the Cibao Basin and Northern Hispaniola : An Example of Basin Evolution Near A Strike-Slip-Dominated Plate Boundary. *The Journal of Geology*, 106. <https://doi.org/10.1086/516036>
- Escuder-Virueite, J., & Pérez, Y. (2020). Neotectonic structures and stress fields associated with oblique collision and forearc sliver formation in northern Hispaniola : Implications for the seismic hazard assessment. *Tectonophysics*, 784, 228452. <https://doi.org/10.1016/j.tecto.2020.228452>
- Etienne, S., Le Roy, P., Tournadour, E., Roest, W. R., Jorry, S., Collot, J., Patriat, M., Largeau, M. A., Roger, J., Clerc, C., Dechnick, B., Sanborn, K. L., Lepareur, F., Horowitz, J., Webster, J. M., & Gaillot, A. (2021). Large-scale margin collapses along a partly drowned, isolated carbonate platform (Lansdowne Bank, SW Pacific Ocean). *Marine Geology*, 436, 106477. <https://doi.org/10.1016/j.margeo.2021.106477>
- Gay, A., Lopez, M., Cochonat, P., & Sermondadaz, G. (2004). Polygonal faults-furrows system related to early stages of compaction – upper Miocene to recent sediments of the Lower Congo Basin. *Basin Research*, 16(1), 101-116. <https://doi.org/10.1111/j.1365-2117.2003.00224.x>
- Goreau, P. D. (1981). The tectonic evolution of the North Central Caribbean plate margin. Massachusetts Institute of Technology, Dept. of Earth and Planetary Sciences.
- Harris, P. T., & Whiteway, T. (2011). Global distribution of large submarine canyons : Geomorphic differences between active and passive continental margins. *Marine Geology*, 285(1-4), 69-86.
- Herbert, T. D. (1993). Differential compaction in lithified deep-sea sediments is not evidence for “diagenetic unmixing”. *Sedimentary Geology*, 84(1), 115-122. [https://doi.org/10.1016/0037-0738\(93\)90049-B](https://doi.org/10.1016/0037-0738(93)90049-B)
- Hurst, A., Cartwright, J., Huuse, M., Jonk, R., Schwab, A., Duranti, D., & Cronin, B. (2003). Significance of large-scale sand injectites as long-term fluid conduits : Evidence from seismic data. *Geofluids*, 3(4), 263-274. <https://doi.org/10.1046/j.1468-8123.2003.00066.x>
- Huuse, M., Cartwright, J., Hurst, A., & Steinsland, N. (2007). Seismic characterization of large-scale sandstone intrusions. *Sand Injectites: Implications for Hydrocarbon Exploration and Production*, 87, 21-35.
- Iturralde-Vinent, M. A., García-Casco, A., Rojas-Agramonte, Y., Proenza, J. A., Murphy, J. B., & Stern, R. J. (2016). The geology of Cuba : A brief overview and synthesis. *GSA Today*, 4-10. <https://doi.org/10.1130/GSATG296A.1>

- Jackson, C. (2007). The geometry; distribution, and development of clastic injections in slope systems : Seismic examples from the Upper Cretaceous Kyrre formation, Måløy slope, Norwegian margin. *Sand Injectites: Implications for Hydrocarbon Exploration and Production*, 21-35.
- Kane, I. A. (2010). Development and flow structures of sand injectites : The Hind Sandstone Member injectite complex, Carboniferous, UK. *Marine and Petroleum Geology*, 27(6), 1200-1215. <https://doi.org/10.1016/j.marpetgeo.2010.02.009>
- Kane, I. A., & Hodgson, D. M. (2011). Sedimentological criteria to differentiate submarine channel levee subenvironments : Exhumed examples from the Rosario Fm. (Upper Cretaceous) of Baja California, Mexico, and the Fort Brown Fm. (Permian), Karoo Basin, S. Africa. *Marine and Petroleum Geology*, 28(3), 807-823. <https://doi.org/10.1016/j.marpetgeo.2010.05.009>
- Lee, S. H., & Chough, S. K. (2001). High-resolution (2–7 kHz) acoustic and geometric characters of submarine creep deposits in the South Korea Plateau, East Sea. *Sedimentology*, 48(3), 629-644. <https://doi.org/10.1046/j.1365-3091.2001.00383.x>
- Leroy, S. (2012). HAITI-SIS cruise, L'Atalante R/V. <https://doi.org/10.17600/12010070>
- Leroy, S., & Ellouz-Zimmermann, N. (2013). HAITI-SIS2 cruise, L'Atalante R/V. <https://doi.org/10.17600/13010080>
- Leroy, S., Ellouz-Zimmermann, N., Corbeau, J., Rolandone, F., Mercier De Lépinay, B., Meyer, B., Momplaisir, R., Bruña, J.-L. G., Battani, A., Baurion, C., Burov, E., Clouard, V., Deschamps, R., Gorini, C., Hamon, Y., Lafosse, M., Leonel, J., Pourhiet, L. L., Estrada, P. L., ... Muñoz, S. (2015). Segmentation and kinematics of the North America-Caribbean plate boundary offshore Hispaniola. *Terra Nova*, 27(6), 467-478. <https://doi.org/10.1111/ter.12181>
- Li, W., Alves, T. M., Wu, S., Rebesco, M., Zhao, F., Mi, L., & Ma, B. (2016). A giant, submarine creep zone as a precursor of large-scale slope instability offshore the Dongsha Islands (South China Sea). *Earth and Planetary Science Letters*, 451, 272-284. <https://doi.org/10.1016/j.epsl.2016.07.007>
- Locat, J., & Lee, H. J. (2002). Submarine landslides : Advances and challenges. *Canadian Geotechnical Journal*, 39(1), 193-212. <https://doi.org/10.1139/t01-089>
- Lonergan, L., Jamin, N. H., Jackson, C. A.-L., & Johnson, H. D. (2013). U-shaped slope gully systems and sediment waves on the passive margin of Gabon (West Africa). *Marine Geology*, 337, 80-97. <https://doi.org/10.1016/j.margeo.2013.02.001>
- Lonergan, L., Lee, N., Johnson, H. D., Cartwright, J. A., & Jolly, R. J. H. (2000). Remobilization and Injection in Deepwater Depositional Systems : Implications for Reservoir Architecture and Prediction. In P. Weimer (Éd.), *Deep-Water Reservoirs of the World* (Vol. 20, p. 0). SEPM Society for Sedimentary Geology. <https://doi.org/10.5724/gcs.00.15.0515>
- Ma, H.-X., Fan, G.-Z., Shao, D.-L., Ding, L.-B., Sun, H., Zhang, Y., Zhang, Y.-G., & Cronin, B. (2020). Deep-water depositional architecture and sedimentary evolution in the Rakhine Basin, northeast Bay of Bengal. *Petroleum Science*, 17. <https://doi.org/10.1007/s12182-020-00442-0>
- Mann, P., Calais, É., Ruegg, J.-C., DeMets, C., Jansma, P. E., & Mattioli, G. S. (2002). Oblique collision in the northeastern Caribbean from GPS measurements and geological observations. *Tectonics*, 21(6), 7-1-7-26. <https://doi.org/10.1029/2001TC001304>
- Mann, P., Taylor, F. W., Edwards, R. L., & Ku, T.-L. (1995). Actively evolving microplate formation by oblique collision and sideways motion along strike-slip faults : An example from the northeastern Caribbean plate margin. *Tectonophysics*, 246(1), 1-69. [https://doi.org/10.1016/0040-1951\(94\)00268-E](https://doi.org/10.1016/0040-1951(94)00268-E)

- McAdoo, B. G., Pratson, L. F., & Orange, D. L. (2000). Submarine landslide geomorphology, US continental slope. *Marine Geology*, 169(1), 103-136. [https://doi.org/10.1016/S0025-3227\(00\)00050-5](https://doi.org/10.1016/S0025-3227(00)00050-5)
- Micallef, A., Mountjoy, J. J., Barnes, P. M., Canals, M., & Lastras, G. (2014). Geomorphic response of submarine canyons to tectonic activity: Insights from the Cook Strait canyon system, New Zealand. *Geosphere*, 10, 905-929. <https://doi.org/10.1130/GES01040.1>
- Monnier, D., Imbert, P., Gay, A., Mourgues, R., & Lopez, M. (2014). Pliocene sand injectites from a submarine lobe fringe during hydrocarbon migration and salt diapirism: A seismic example from the Lower Congo Basin. *Geofluids*, 14(1), 1-19. <https://doi.org/10.1111/gfl.12057>
- O'Grady, D. B., Syvitski, J. P. M., Pratson, L. F., & Sarg, J. F. (2000). Categorizing the morphologic variability of siliciclastic passive continental margins. *Geology*, 28(3), 207-210. [https://doi.org/10.1130/0091-7613\(2000\)28<207:CTMVOS>2.0.CO;2](https://doi.org/10.1130/0091-7613(2000)28<207:CTMVOS>2.0.CO;2)
- Oliveira de Sá, A., d'Acremont, E., Leroy, S., & Lafuerza, S. (2021). Polyphase Deformation and Strain Migration on the Septentrional-Oriente Fault Zone in the Windward Passage, Northern Caribbean Plate Boundary. *Tectonics*, 40(8), e2021TC006802. <https://doi.org/10.1029/2021TC006802>
- Oliveira de Sá, A., Lafuerza, S., Leroy, S., d'Acremont, E., Ducassou, E., Deschamps, R., Zaragosi, S., Fauquembergue, K., Granja-Buña, J. L., Momplaisir, R., & Boisson, D. (In prep.). Enigmatic deep-water seafloor depressions east of Tortue Island, Northern Haiti margin.
- Oliveira de Sá, A., Leroy, S., d'Acremont, E., Lafuerza, S., Granja Bruña, J. L., Moreno, B., Pico, C., & Letouzey, J. (Subm). The Protracted Evolution of a Plate Boundary: Eastern Cuba Block and Old Bahamas Channel. *Geochemistry, Geophysics, Geosystems*, Submitted.
- Osborne, M. J., & Swarbrick, R. E. (1998). Mechanisms for Generating Overpressure in Sedimentary Basins: A Reevaluation: Reply1. *AAPG Bulletin*, 82(12), 2270-2271. <https://doi.org/10.1306/00AA7F0E-1730-11D7-8645000102C1865D>
- Pettinga, L. A., & Jobe, Z. R. (2021). How submarine channels (re)shape continental margins. *Journal of Sedimentary Research*, 90(11), 1581-1600. <https://doi.org/10.2110/jsr.2020.72>
- Pindell, J. L., & Draper, G. (1991). Stratigraphy and geological history of the Puerto Plata area, northern Dominican Republic. In *Geological Society of America Special Papers* (Vol. 262, p. 97-114). Geological Society of America. <https://doi.org/10.1130/SPE262-p97>
- Pirmez, C., Beaubouef, R. T., Friedmann, S. J., & Mohrig, D. C. (2000). Equilibrium Profile and Baselevel in Submarine Channels: Examples from Late Pleistocene Systems and Implications for the Architecture of Deepwater Reservoirs. In P. Weimer (Ed.), *Deep-Water Reservoirs of the World* (Vol. 20, p. 0). SEPM Society for Sedimentary Geology. <https://doi.org/10.5724/gcs.00.15.0782>
- Rodríguez-Zurrunero, A., Granja-Bruña, J. L., Carbó-Gorosabel, A., Muñoz-Martín, A., Gorosabel-Araus, J. M., Gómez de la Peña, L., Gómez Ballesteros, M., Pazos, A., Catalán, M., Espinosa, S., Druet, M., Llanes, P., & ten Brink, U. (2019). Submarine morpho-structure and active processes along the North American-Caribbean plate boundary (Dominican Republic sector). *Marine Geology*, 407, 121-147. <https://doi.org/10.1016/j.margeo.2018.10.010>
- Rodríguez-Zurrunero, A., Granja-Bruña, J. L., Muñoz-Martín, A., Leroy, S., ten Brink, U., Gorosabel-Araus, J. M., Gómez de la Peña, L., Druet, M., & Carbó-Gorosabel, A. (2020). Along-strike segmentation in the northern Caribbean plate boundary zone

- (Hispaniola sector): Tectonic implications. *Tectonophysics*, 776, 228322. <https://doi.org/10.1016/j.tecto.2020.228322>
- Rojas-Agramonte, Y., Neubauer, F., Garcia-Delgado, D. E., Handler, R., Friedl, G., & Delgado-Damas, R. (2008). Tectonic evolution of the Sierra Maestra Mountains, SE Cuba, during Tertiary times: From arc-continent collision to transform motion. *Journal of South American Earth Sciences*, 26(2), 125-151. <https://doi.org/10.1016/j.jsames.2008.05.005>
- Safronova, P. A., Andreassen, K., Laberg, J. S., & Vorren, T. O. (2012). Development and post-depositional deformation of a Middle Eocene deep-water sandy depositional system in the Sørvestsnaget Basin, SW Barents Sea. *Marine and Petroleum Geology*, 36(1), 83-99. <https://doi.org/10.1016/j.marpetgeo.2012.06.007>
- Saller, A., & Dharmasamadhi, I. (2012). Controls on the development of valleys, canyons, and unconfined channel–levee complexes on the Pleistocene Slope of East Kalimantan, Indonesia. *Marine and Petroleum Geology*, 29. <https://doi.org/10.1016/j.marpetgeo.2011.09.002>
- Seybold, H., Berghuijs, W. R., Prancevic, J. P., & Kirchner, J. W. (2021). Global dominance of tectonics over climate in shaping river longitudinal profiles. *Nature Geoscience*, 14(7), Article 7. <https://doi.org/10.1038/s41561-021-00720-5>
- Shepard, F. P. (1965). Types of Submarine Valleys1: GEOLOGICAL NOTES. *AAPG Bulletin*, 49(3), 304-310. <https://doi.org/10.1306/A663353A-16C0-11D7-8645000102C1865D>
- Shepard, F. P. (1981). Submarine Canyons: Multiple Causes and Long-Time Persistence. *AAPG Bulletin*, 65(6), 1062-1077.
- Shillington, D. J., Seeber, L., Sorlien, C. C., Steckler, M. S., Kurt, H., Dondurur, D., Çifçi, G., İmren, C., Cormier, M.-H., McHugh, C. M. G., Gürçay, S., Poyraz, D., Okay, S., Atgün, O., & Diebold, J. B. (2012). Evidence for widespread creep on the flanks of the Sea of Marmara transform basin from marine geophysical data. *Geology*, 40(5), 439-442. <https://doi.org/10.1130/G32652.1>
- Sorel, D., Purser, B. H., & Senatos, H. (1991). Strike-slip tectonic processes in the northern Caribbean between Cuba and Hispaniola (Windward Passage). *Essai de datation des récifs soulevés d'Haiti par la méthode du forçage climatique orbital*, 313, 1277-1281.
- Soutter, E., Kane, I., Hodgson, D., & Flint, S. (2021). The Concavity of Submarine Canyon Longitudinal Profiles. *Journal of Geophysical Research: Earth Surface*, 126. <https://doi.org/10.1029/2021JF006185>
- Surlyk, F., Noe-Nygaard, N., & Gjelberg, J. (2007). The Upper Jurassic Hareelv Formation of East Greenland: A Giant Sedimentary Injection Complex. In A. Hurst & J. Cartwright (Éds.), *Sand Injectites: Implications for Hydrocarbon Exploration and Production* (Vol. 87, p. 0). American Association of Petroleum Geologists. <https://doi.org/10.1306/1209858M871101>
- Symithe, S., Calais, É., Chabaliér, J. B., Robertson, R., & Higgins, M. (2015). Current block motions and strain accumulation on active faults in the Caribbean. *Journal of Geophysical Research: Solid Earth*, 120(5), 3748-3774. <https://doi.org/10.1002/2014JB011779>
- Vinnels, J. S., Butler, R. W. H., McCaffrey, W. D., & Paton, D. A. (2010). Depositional processes across the Sinú Accretionary Prism, offshore Colombia. *Marine and Petroleum Geology*, 27(4), 794-809. <https://doi.org/10.1016/j.marpetgeo.2009.12.008>
- Wessels, R. J. F. (2019). Chapter 15—Strike-Slip Fault Systems Along the Northern Caribbean Plate Boundary. In J. C. Duarte (Éd.), *Transform Plate Boundaries and Fracture Zones* (p. 375-395). Elsevier. <https://doi.org/10.1016/B978-0-12-812064-4.00015-3>
- Whipple, K. X., & Tucker, G. E. (1999). Dynamics of the stream-power river incision model: Implications for height limits of mountain ranges, landscape response timescales, and

research needs. *Journal of Geophysical Research: Solid Earth*, 104(B8), 17661-17674.
<https://doi.org/10.1029/1999JB900120>

Zaprowski, B. J., Pazzaglia, F. J., & Evenson, E. B. (2005). Climatic influences on profile concavity and river incision. *Journal of Geophysical Research: Earth Surface*, 110(F3).
<https://doi.org/10.1029/2004JF000138>

CHAPITRE VII : Interactions entre les processus tectoniques profonds et processus sédimentaires au large de la côte nord d'Haïti

Ce chapitre correspond à un article en préparation pour soumission à EPSL.

L'analyse tectono-sédimentaire de la région au large de la côte nord d'Haïti a mis en évidence un fond marin marqué par un champ de dépressions s'étendant sur une vaste zone. Suite à ces découvertes, nous avons cherché à comprendre l'origine et la dynamique de ces éléments morphologiques.

Dans cette étude nous détaillons comment les variations structurales et sédimentaires observées d'est en ouest au large de la côte nord d'Haïti influencent la morphologie actuelle du fond marin. De plus, nous explorons l'évolution de cette morphologie en fonction de ses interactions avec le contexte océanographique. Nous avons méthodiquement étudié la morphologie, la formation et l'évolution de ces dépressions sous-marines à l'aide de données bathymétriques haute résolution et de profils sismiques. Ces données ont été enrichies par des analyses sédimentologiques et géochimiques effectuées sur 5 carottes sédimentaires. Ces analyses ont permis de dévoiler les mécanismes morpho-dynamiques et les processus sédimentaires prédominants dans cette région et leur importance comme témoins de l'activité tectonique.

VII. Enigmatic deep-water seafloor depressions east of Tortue Island, Northern Haiti margin

Oliveira de Sá A.¹, Lafuerza S.¹, Leroy S.¹, d'Acremont E.¹, Ducassou E.², Deschamps R.³, Zaragosi S.², Fauquembergue K.², Granja-Buñá J.L.⁴, Momplaisir R.⁵, Boisson D.⁵

1 Sorbonne Université, CNRS, IStEP, Institut des Sciences de la Terre de Paris, France

2 Environnements et Paléoenvironnements Océaniques et Continentaux (EPOC), Univ. Bordeaux, CNRS, Bordeaux INP, EPOC, UMR 5805, F-33600 Pessac, France

3 IPFEN, Rueil Malmaison, France

4 Universidad Complutense, Madrid, Spain

5 Université d'Etat d'Haïti, Port-au-Prince, Haïti

Abstract

A widespread area of seafloor depressions - circular, arcuate to elongated-shaped - has been found along the Northern Haitian coast, in water depths between 600 and 2000 m. Characterized by wavelengths spanning several hundred meters and heights of tens of meters, these depressions are linked with a series of narrow ridges boasting varied morphologies. Our analysis integrating multichannel seismic reflection, high-resolution bathymetry data, and sedimentological and geochemical evaluations of surface sediment cores indicate that along-slope bottom currents influence the sedimentary processes in the study area. The analyzed sediment cores show sedimentary deposits as hemipelagites, silty and sandy contourites, fine-grained turbidites and reworked sand layers, implying sedimentation in a contourite drift

system. This is further corroborated by seismic reflection data depicting wavy reflectors and aggradational stacking features typical of contourite drifts. Seafloor depressions are likely erosional features formed on the top of a contourite drift formed by interacting bottom currents with irregular seafloor morphology. The equilibrium seafloor was initially disturbed by mass-wasting events. Subsequently, the quasi-steady flow of along-slope bottom currents influenced sedimentary distribution and control the morphology of the seafloor depressions by constant reshaping through erosion on their flanks. The resulting rough seafloor could have facilitated the destabilization of bottom currents and the development of erosive eddies responsible for the current morphology of the seafloor depressions. This study highlights the interplay between sedimentary processes (accumulation and compaction) and bottom currents, showing how their combined effect influences slope sedimentation and seafloor geomorphology, forming unique erosional features.

VII.1. Introduction

Seafloor depressions are common features found in various marine environments, exhibiting diameters that span from hundreds of meters to several kilometers (Betzler et al., 2014; Cartigny et al., 2011; Hovland et al., 1984; Warnke et al., 2023). A number of geological processes can be attributed to the formation of these seabed features, however determining the specific mechanisms involved in their formation can be challenging due to the high variability of these occurrences.

The formation of circular seafloor depressions is generally attributed to the vertical migration of fluids or gas, i.e., pockmarks (Hovland, 1981; Hovland et al., 2002; Loncke, 2004). In the absence of direct evidence of fluid migration, such as the presence of gas-charged sediments or fluid pipes, other alternative mechanisms are suggested to explain the formation of seafloor depressions. These include tectonic or diagenetic faulting (Gay et al., 2004, 2017), carbonate dissolution (Kan et al., 2015), salt tectonics (Geletti et al., 2008), and local turbulence-induced erosion (Hillman et al., 2018; Wenau et al., 2021).

Regardless of their initial formation mechanisms, seafloor depressions are influenced by continuous sedimentary processes, frequently driven by ocean bottom currents found along continental slopes (de Castro et al., 2020; Hernández-Molina et al., 2009; Rebesco et al., 2014). Turbidity currents (downslope) and contour currents (along slope) play a significant role in maintaining and reshaping these features, particularly in energetic oceanographic environments (García et al., 2016; Heinio & Davies, 2009; Waghorn et al., 2018; Warnke et al., 2023). The interaction of bottom currents and seafloor depressions has been proven via numerical models and tank experiments (Hammer et al., 2009; Pau et al., 2014). The stability of downslope and along-slope currents can be significantly compromised if the seafloor morphology is rough (Serra et al., 2005; Waghorn et al., 2018). This flow-induced particle generates crescent or elongated sedimentary features (Cukur et al., 2019; García et al., 2016; Hammer et al., 2009; Heinio & Davies, 2009; Pau et al., 2014; Sun et al., 2016; Wenau et al., 2021).

During the HAITI-SIS 1-2 cruises in 2012-2013, extensive seabed depressions with elongated shapes, ranging from 1 to 5 km in width, were discovered to dominate slope along the Northern Haitian coast (Figures VII. 1 to 3). This study aims to comprehensively investigate the geomorphology, formation, and evolution of the seafloor depressions by utilizing high-resolution bathymetric and backscatter data, seismic reflection profiles, and sediment core

samples. The specific objectives of this study include (1) characterizing the morphology and the internal structure of the seafloor depressions, (2) analyzing the distribution of sediment along the slope, (3) evaluating the active processes that shape the geomorphology of these depressions, and (4) identifying potential mechanisms responsible for their formation.

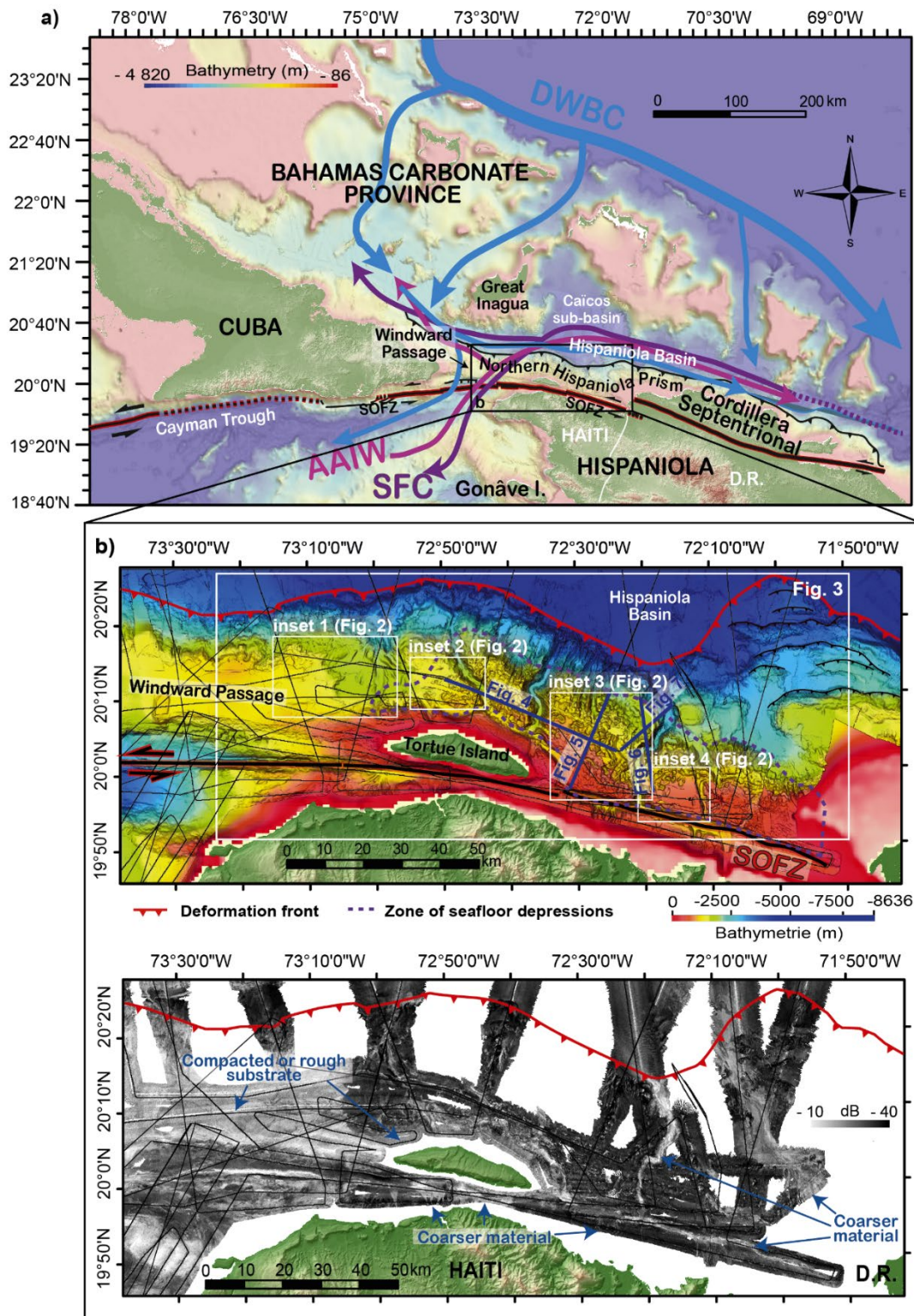


Figure VII. 1. Study area situated along the northern margin of Haiti. (a) Overview map. DWBC: Deep Western Boundary Current; AAIW: Antarctic Intermediate Water; SFC: Surface and thermocline waters; SOFZ: Septentrional-Oriente Fault Zone; D.R.: Dominican Republic. (b) Detailed view of the

study area showing bathymetry (top) and backscatter (bottom) maps. Black lines represent seismic profiles, with bold black lines indicating the seismic profiles used in this paper. Processed multibeam bathymetry data from HAITISIS 1-2 and NORCARIBE cruises are superimposed on the regional GEBCO grid bathymetry.

VII.2. Geological and oceanographic settings

VII.2.1 Geological Setting

The study area is located in the Northern Haitian Margin (or Northern Hispaniola Deformed Belt, e.g. Rodriguez-Zurrunero et al., 2019, 2020 and therein references), which includes the northern slope of Haiti and the Dominican Republic (Figure VII. 1). The region of the North Haitian Margin is occupied by the Northern Hispaniola Prism (Figure VII. 2a), which is considered as an accretionary prism (Oliveira de Sá et al., In Prep.). The Northern Hispaniola Prism was formed by the oblique convergence and collision/underthrusting between the Hispaniola (Caribbean plate) and the Bahamas Banks (North American plate) (e.g., Erikson et al., 1998; Calais et al., 2016). In the scientific literature, there is a general agreement that the collision started in Eocene times, but recent studies in northern Dominican Republic suggest Pliocene ages (Escuder-Viruete and Pérez, 2020; Escuder et al., 2020).

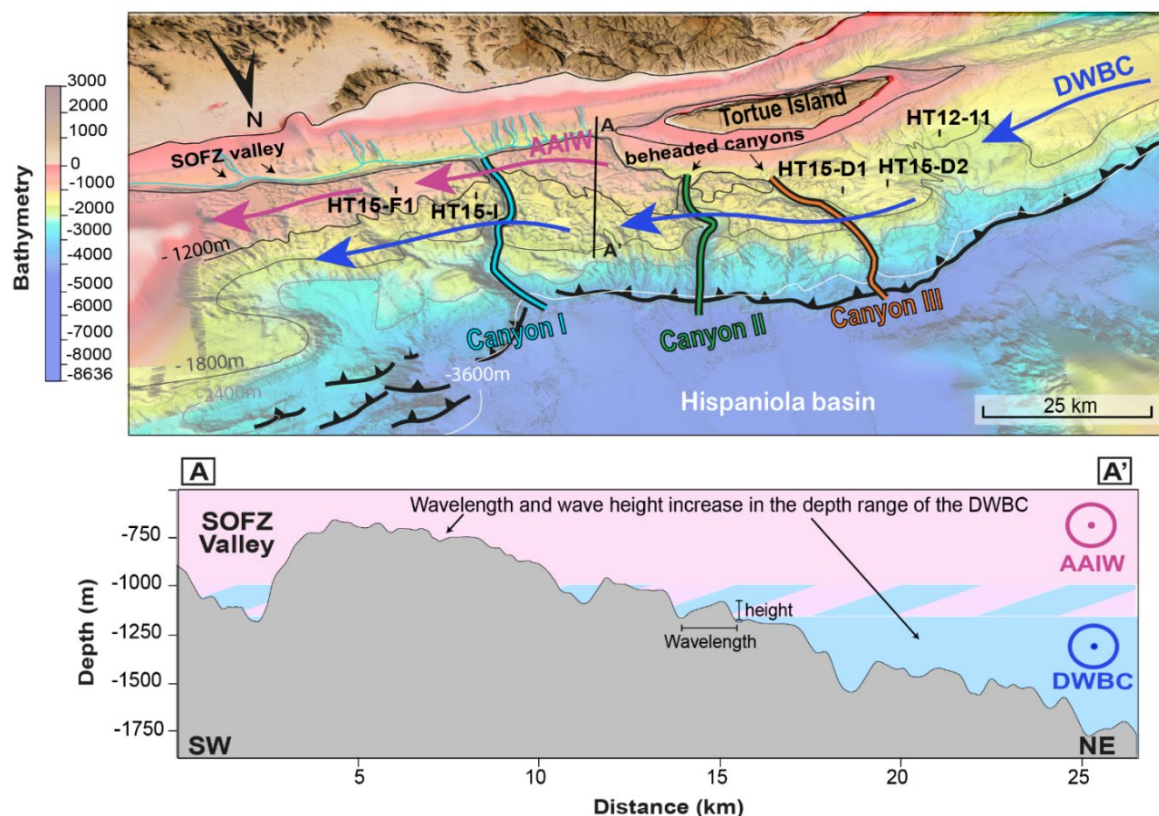


Figure VII. 2. 3D representation of the bathymetric extent of the study area from the NE illustrating the distribution of modern-day near-bottom water masses. The dominant flow directions of bottom currents are depicted by colored arrows, adapted from Johns (2006). Bathymetric profile A-A' illustrating the seafloor depressions zone, with emphasis on the increasing wavelength and wave height of the depressions downslope. For clarity, only approximate positions of water mass interfaces are indicated. AAIW: Antarctic Intermediate Water; DWBC: Deep Western Boundary Current.

This collision led to the reconfiguration of the preexisting plate boundary, altering the ancient boundary located further to the north (Calais et al., 2016). This process led to the uplift of the Septentrional Cordillera (Figure VII. 1a) and the initiation of several strike-slip faults that gradually migrated southward until the establishment of the current active segments of the Septentrional Orient Fault Zone (SOFZ) (Calais and Mercier de Lépinay, 1992; Erikson et al., 1998; Leroy et al., 2015; Oliveira de Sá et al., 2021). These processes were responsible for a major paleogeographic reorganization in the area (Erikson et al., 1998; Escuder-Viruete et al., 2020). With the initiation of the SOFZ, the current Northern boundary of the Caribbean plate, the Cordillera Septentrional (northern Dominican Republic, Figure VII. 1a), was transferred to the North-American plate, and the northern Hispaniola region reached its current distribution (Calais et al., 2016; Calais & Mercier De Lépinay, 1995; Erikson et al., 1998; Escuder-Viruete & Pérez, 2020; Leroy et al., 2015; Rodríguez-Zurrunero et al., 2019, 2020).

Table 1. Summary of locations, water depths (m), core lengths (m), and target feature of the sediment cores retrieved from the study area.

| Core | Latitude | Longitude | Water depth (m) | Length (m) | Target feature |
|---------|--------------|--------------|-----------------|------------|---------------------------------------------------|
| HT15-F1 | N 19° 56,868 | W 72° 12,782 | 981 | 4,76 | Zone not affected by seafloor depressions |
| HT15-I | N 20° 00,134 | W 72° 18,604 | 1146 | 3,15 | In the wall of a seafloor depression |
| HT15-D1 | N 20° 12,387 | W 72° 47,741 | 1598 | 3,78 | Inside a seafloor depression |
| HT15-D2 | N 20° 13,499 | W 72° 51,550 | 1534 | 4,8 | Adjacent to seafloor depression zone |
| HT12-11 | N 20° 10,843 | W 73° 01,240 | 1700 | 2,98 | Outside the zone affected by seafloor depressions |

VII.2.2 Oceanographic Setting

No recent oceanographic or palaeoceanographic studies undertaken in the eastern part of the Northern Haitian Margin are available. Consequently, its current regime and water masses distribution in depth are poorly known. However, valuable information on local current flow can be inferred from volume transport and flow variability data at Windward Passage and the surrounding region (Figure VII. 1a; west of the study area)(Johns, 2006; Mulder et al., 2019).

The flow through Windward Passage displays a relatively consistent vertical structure, with a net inflow to the Caribbean Sea typically observed above approximately 600 meters, a net outflow between approximately 700-1200 meters, and a deep inflow near the bottom (Johns, 2006). Surface and thermocline waters (SFC) typically enter the study area from the east, along the Dominican Republic coast, and primarily flow into the Caribbean Sea through the Windward Passage (Figure VII. 1a). The net transport of Antarctic Intermediate Water (AAIW) is exported from the Caribbean Sea, with similar amounts flowing west and east to either side of Great Inagua (Figure VII. 1a).

Atlantic waters flow just above the deepest part of the Windward Passage (>1200 m in depth) (Figure VII. 1a). The deep inflow in the study area comes northward from a branch of the Deep Western Boundary Current (DWBC, see Figure VII. 1a). This branch splits off from the main path of the DWBC on the northern side of the Bahamas and passes through deep passages in the central Bahamas (Figure VII. 1a) (Johns, 2006). Nearly half of the total DWBC, associated with waters formed in the Labrador Sea, are diverted through these passages. This diversion creates a deep jet that flows southeastward along the coasts of Cuba and Hispaniola, on the southern coast of the Bahamas (Figures VII. 1a and 2) (Johns, 2006). The deep flow is persistent, typically exhibiting 20-40 cm/s speeds in the Windward Passage (Johns, 2006).

The vertical stratification of the water column and flow directions in the study area are determined based on measurements taken in the Windward Passage, as shown in Figure VII. 2. The AAIW is distributed between 600 and 1200 m with its interface to the DWBC located at ~1200 m water depth in the study area (as depicted in the A-A' section of Figure VII. 2) (T. N. Lee et al., 1990; Mulder et al., 2019).

VII.3. Data and Methodology

The database made available for the present study includes a geophysical dataset and a collection of five surficial sediment cores. The available geophysical database, including multibeam bathymetry, and seismic reflection data was collected during HAITISIS 1-2 cruises (2012-2013; <https://doi.org/10.17600/12010070>; <https://doi.org/10.17600/13010080>) onboard the R/V L'Atalante from the *Flotte Océanographique Française* (Leroy, 2012; Leroy & Ellouz-Zimmermann, 2013). Seafloor backscatter data were acquired simultaneously during the cruises. Seismic reflection data are recorded using a source comprising two GI air guns (2.46 L, 300 in3) and a streamer with 24 traces (600 m long) operated at c.a 9.7 knots (fast and light seismic system). The multichannel seismic reflection data were processed using classical steps, including CDP gathering (fold 6), binning at 25 m, detailed velocity analysis, stack, and post-stack time migration. All the seismic reflection profiles presented are time-migrated with Seismic Unix®.

The five piston cores were collected in the study area during the HAITISIS 1 cruise in 2012 (Core HT12-11) and during the Caracalhis - Haïti-BGF cruise in 2015 (Cores HT15-D1, HT15-D2, HT15-F1, and HT15-I1) ([10.17600/15006900](https://doi.org/10.17600/15006900); Ellouz-Zimmermann and Beaufort, 2015) (Table 1; Figures VII. 2 and 3). The other three sediment cores collected during the Caracalhis - Haïti-BGF cruise (HT15-C1, HT15-D0, HT15-E1) were unavailable for the present study. The sediment cores were recovered using a Kullenberg piston corer (Kullenberg, 1947).

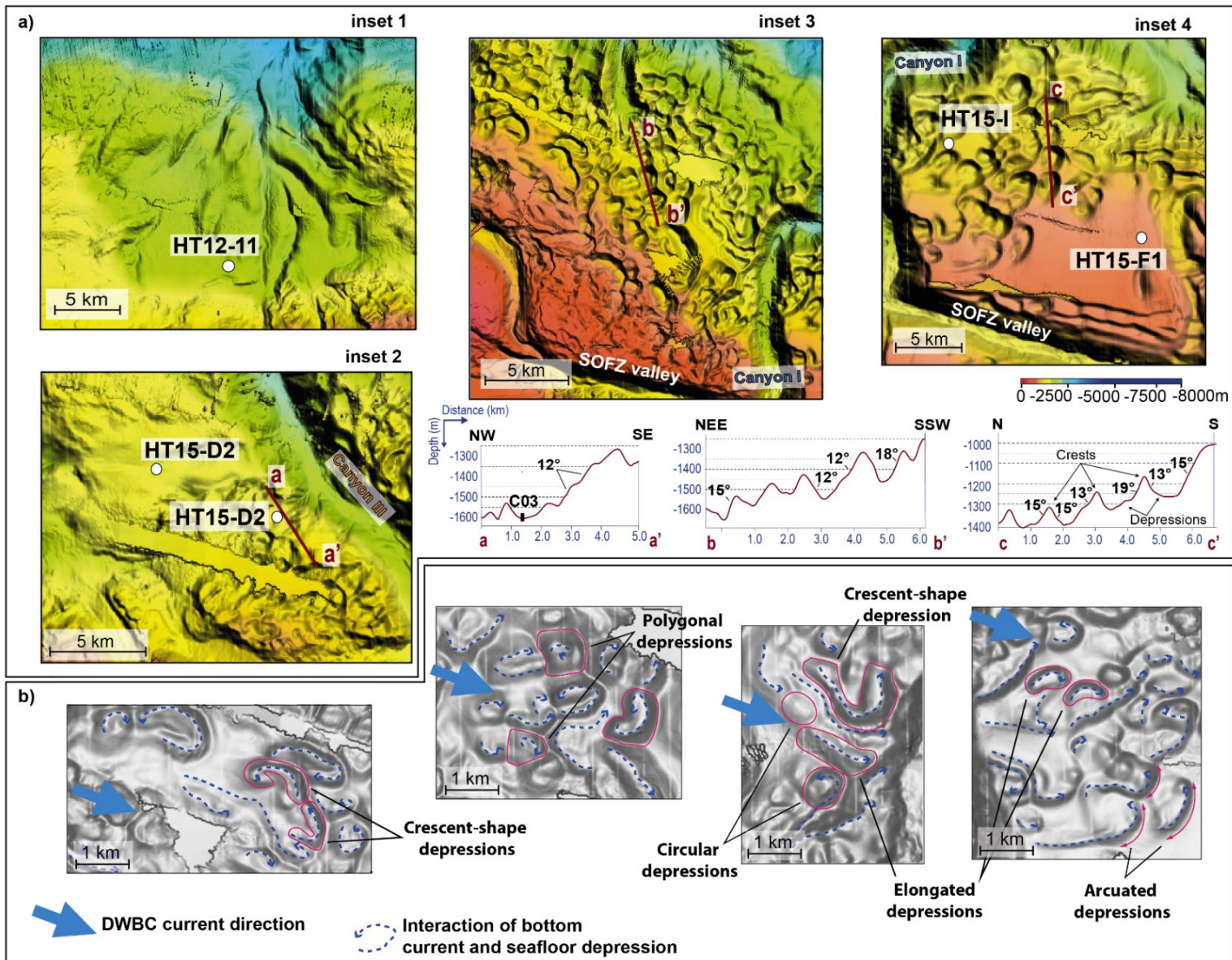


Figure VII. 3. Insets of bathymetry maps highlighting the location of the sediment cores used inside and outside the seabed depressions discovered. The locations of the insets are indicated on the bathymetric map in Figure VII. 1b. Bathymetric profiles depict the geometries of the seafloor depressions, with circular to sub-circular, elongated to polygonal, with ridges roughly aligned NW-SE between canyons II, I (inset 3), and arcuate morphologies with ridges aligned mostly N-S east of canyon I.

VII.3.1 Geophysical data

Multibeam data was gridded with a spacing of 50 m. Moreover, multibeam bathymetric data collected during the NORCARIBE geophysical cruise in November–December 2013 aboard the Spanish R/V Sarmiento de Gamboa is used to fill the gaps in our data coverage in deeper waters (Rodríguez-Zurrunero et al., 2019, 2020). The gridded bathymetry data was augmented with the GEBCO Digital Atlas (https://www.gebco.net/data_and_products/gebco_digital_atlas/) with an 800 m resolution to provide almost complete area coverage (Figure VII. 1a).

From the bathymetric dataset acquired, the backscatter of the seafloor, whose variability mainly depends on the lithology, water content, and microtopography of the sea bottom, has also been used (Lamarche et al., 2011).

Seismic reflection data are recorded using a source comprising two GI air guns (2.46 L, 300 in³) and a streamer with 24 channels (600 m-long) operated at c.a 9.7 knots (fast and light seismic system). The multichannel seismic reflection data were processed using classical steps, including CDP gathering (6-fold), binning at 25 m, detailed velocity analysis, stack, and post-stack time migration. All the seismic reflection profiles were time-migrated. The Kingdom™ IHS Suite©, Global Mapper©, and ArcGIS© software were used for data interpretation and mapping.

VII.3.2 Sedimentological data

A set of two sediment cores (HT15-I and HT15-F1) was obtained in the eastern part of the area presenting the seafloor depressions. Another set of two cores (HT15-D1 and HT15-D2) was collected from inside and adjacent to seafloor depressions, respectively, on the western part of the area (Figures VII. 2 and 3). One core (HT12-11) was obtained from the adjacent area where the seafloor depressions are absent.

These five coring locations stored at the laboratory EPOC of the University of Bordeaux (France) were primarily analyzed to determine sedimentary processes within and outside seafloor depressions. Core sample recovery at the five sites ranged from 2.98 to 4.8 m in length (Table 1). All cores were split lengthwise and photographed using a line scan camera at EPOC.

Grain-size measurements were taken at discrete depths along the core were performed using a laser particle size analyzer MALVERN Mastersizer hydro2000G. The GRADISTAT 9.1 program was used for grain-size statistical analysis. Statistics are calculated using Folk and Ward (1957) Method (μm scale): mean, standard-deviation, skewness, kurtosis. Furthermore, thin sections were performed on specific cores HT15-F1, HT15-D1, and HT15-D2 for a detailed description of microfacies and small-scale textural properties. Thin sections were carried out for some core intervals to describe micro-scale sedimentary structures.

VII.3.3. Geochemical data

Continuous geochemical data along cores were acquired on a cm-scale with an AVAATECH XRF core scanner at EPOC using the 10 and 30 kV instrumental settings. Because the sediment matrix is characterized by variable water content and grain size distributions, the XRF scanner only provides a semi-quantitative measurement; spurious

variations can occur due to changes, e.g., in water content. Two elemental ratios have been used for identifying sedimentary sources and environmental conditions: detrital versus carbonate sedimentary input from the Ti/Ca and Zr/Al ratio as a proxy for bottom currents (Alonso et al., 2021; Bahr et al., 2014; de Castro et al., 2020, 2021). The relative contents of these elements were measured on split core sediment sections at 1 cm intervals.

VII.4 Results

VII.4.1 Seafloor geomorphology

The investigated seabed lies at about 600 m water depth at the shelf edge, dropping to more than 4000 m toward the deep Caïcos Sub-basin (Hispaniola Basin, in Figures VII. 1b and 2). The SOFZ trends almost E-W as it runs offshore along the upper insular slope of northern Haiti margin, forming a linear east-west oriented valley (Figures VII. 1b and 2) (Leroy et al., 2015). North of the SOFZ valley, the seabed morphology displays noticeable several features. These include large-scale seafloor depressions, and south-north running canyons (Figures VII. 2 and 3). These morphologies are notably absent in the Windward Passage area west of Tortue Island (Figure VII. 1b) and eastward along the Dominican margin (Rodriguez-Zurrunero et al., 2019, 2020).

VII.4.1.1 Depressions

The most striking features are a closely packed set of alternating depressional ponds and raised ridges (Figure VII. 3a). They appear in depths ranging from 600 to 2000 m (Figure VII. 2). These structures are km-scale features that occur only in the north and eastern part of Tortue Island, covering an area of ca 2224 km² (Figures VII. 1b and 3). To the west of Tortue Island, the zone of seafloor depressions abruptly passes over to the undisturbed seabed Windward Passage (Figure VII. 1b).

The average diameter of these structures is around 2 km, and the average area is 1.4 km². The shapes vary from circular to elongated, or more polygonal (pentagonal and hexagonal shapes) and crescent-shaped, usually asymmetrical (Figure VII. 3b).

The narrow-raised ridges that define individual walls of the depressions have a complex morphological pattern, from linear, arcuate to polygonal to irregular with steep flanks (slopes from 5° to approximately 22°, Figure VII. 3a). The ridges of these depressions are less distinct in the depth range of 600 and 1200 meters (Figure VII. 2), and the wavelength and wave height of the crests are more discernible at a depth from 1200 m (Figure VII. 2, profile A-A').

Ridges with arcuate shapes seem to be roughly aligned (Figures VII. 3a and b): For the slope sector between Canyon I and II, ridges follow a W-E direction (in particular the longest ones) and a N-S direction east of Canyon I (Figure VII. 3a, inset 3). Depressions east of Canyon I also appear controlled by an N-S direction (Figure VII. 3a, inset 4). This alignment is sometimes accompanied by a step-like slope profile (Figure VII. 3a, profiles b-b' and c-c').

VII.4.1.2 Backscatter

Although the morphological complexity of the study area is well expressed in the bathymetry (Figures VII. 1b and 3), the backscatter imagery provides complementary detailed information about seafloor features and substrates (Figure VII. 1b).

Backscatter values are dependent on the amplitude (dB) of the reflected signal, resulting from the physical characteristics of the sediment (composition, texture) as well as the local bathymetry of the seafloor. The seafloor in the north and eastern part of Tortue Island has homogeneous weak backscatter values (dark grey), whereas it is medium to strong along the canyon's flanks and the SOFZ valley (medium to light grey) (Figure VII. 1c). A region of strong to very strong backscatter values extends westward of Tortue Island, along the Windward Passage (light grey) (Figure VII. 1b).

The backscatter dependence on the microtopography offers a valuable method for distinguishing bedform (Fonseca et al., 2009; Lamarche et al., 2011). Even though bathymetry reveals a seafloor shaped by multiple ridges that delineate depressions, backscatter provides us with very few aspects of this topography. Instead, the seafloor characterized by these bedforms predominantly displays a homogeneous, low-reflectivity signature interspersed with isolated, high-reflectivity points, as indicated in Figure VII. 1c. This observation suggests that the backscatter reflectivity across this area is controlled by sediment type rather than by incidence angle along the crests of these features. Only a few highly reflective points can be seen in the backscatter on the area affected by the depressions.

Backscatter values from the seafloor can indicate sediment lithology and consolidation, which depend on factors like porosity and water content (Goff et al., 2000). Although interpreting these values can be complex and often necessitates calibration and correlation with other data, such as core samples, they provide insights into seafloor characteristics and underlying sediments. Also, backscatter intensity was positively correlated with coarse fractions and inversely correlated with finer fractions of the sediment composition (De Falco et al., 2010; Goff et al., 2000; Huang et al., 2018).

High backscatter values indicate possibly the presence of relatively coarser material along the canyon's axes and the SOFZ valley (Figure VII. 1c). High backscatter values in the Windward Passage area and along the Tortue Island slope would suggest a more compacted substrate or a rougher. By contrast, the zone of seafloor depressions (Figure VII. 1b) does not exhibit a significant contrasting backscatter change, suggesting that finer fractions of the sediment characterize the substrate of this area. However, the few highly reflective points along this area affected by the depressions are probably related to a local accumulation of coarser material.

Based on these observations, we can infer that the coarse material captured by the canyons and SOFZ valley seems to come from the easternmost area of the study region, the western offshore region of the Septentrional Cordillera in the Dominican Republic where discharges the 300 km-long Yaque del Norte river (Figure VII. 1a). This coarser detrital input inferred from high backscatter values would be catch and carried westward through the SOFZ valley where they probably mix with coarse coastal sediment from Haitian rivers. Part of this coarser material seems also to be channelized in Canyon I (Figure VII. 1c).

VII.4.2. Seismic facies

The sedimentary succession affected by seafloor depressions has a thickness of about 1.2 s TWT, corresponding to Unit 4 as identified by Oliveira de Sá et al. (2021). To maintain consistency and uniformity, we employed the naming convention used by the authors in their examination of this seismic unit in the study area.

Unit 4 has been divided into two subunits from bottom to top: U4a and U4b (Figures VII. 4 to 7). Nearly parallel reflectors characterize subunit U4a, while subunit U4b shows a seismic signature characterized by complex wave-like seismic reflections (Figure VII. 4). Contrary to the subunit U4a, which presents high amplitudes at this bottom and moderate amplitude in its upper part (inset in Figure VII. 6, km 0-4), the amplitude of the reflectors within subunit U4b is higher at the top of the unit, transitioning to lower amplitude reflectors at its base (inset in Figure VII. 4). The seafloor depressions affect the upper succession of subunit U4b (Figures VII. 4 to 7).

Chaotic facies between units U4a and U4b are interpreted as a Mass Transport Deposit (MTD) (inset in Figure VII. 5). The lower part of this MTD is marked by Horizon A (Dotted orange line), and its upper part by Horizon B (Dotted green line) (Figures VII. 4 to 6). Horizon B is overlapped by the basal reflectors of the subunit U4b, forming a very undulated contact (inset Figure VII. 5).

The topographic imprint of Horizon B is preserved across much of the thickness of subunit U4b, as depicted by the gray arrows in the inset in Figures VII. 5 and 7. However, it can attenuate towards its upper portion. Continuous layers truncated on either side of the depressions indicate that erosion processes predominantly shape these seafloor structures (inset in Figure VII. 4).

Failure surfaces (Figure VII. 5, km 8-13) and amplitude anomalies (Figure VII. 6b) also induce the reflectors' folding, thereby influencing the seafloor morphology. Amplitude anomalies are found above the MTD, accentuating the folding of the overburden reflections locally (Figure VII. 6b). These amplitude anomalies would infer the presence of fluid accumulations (Figure VII. 6b).

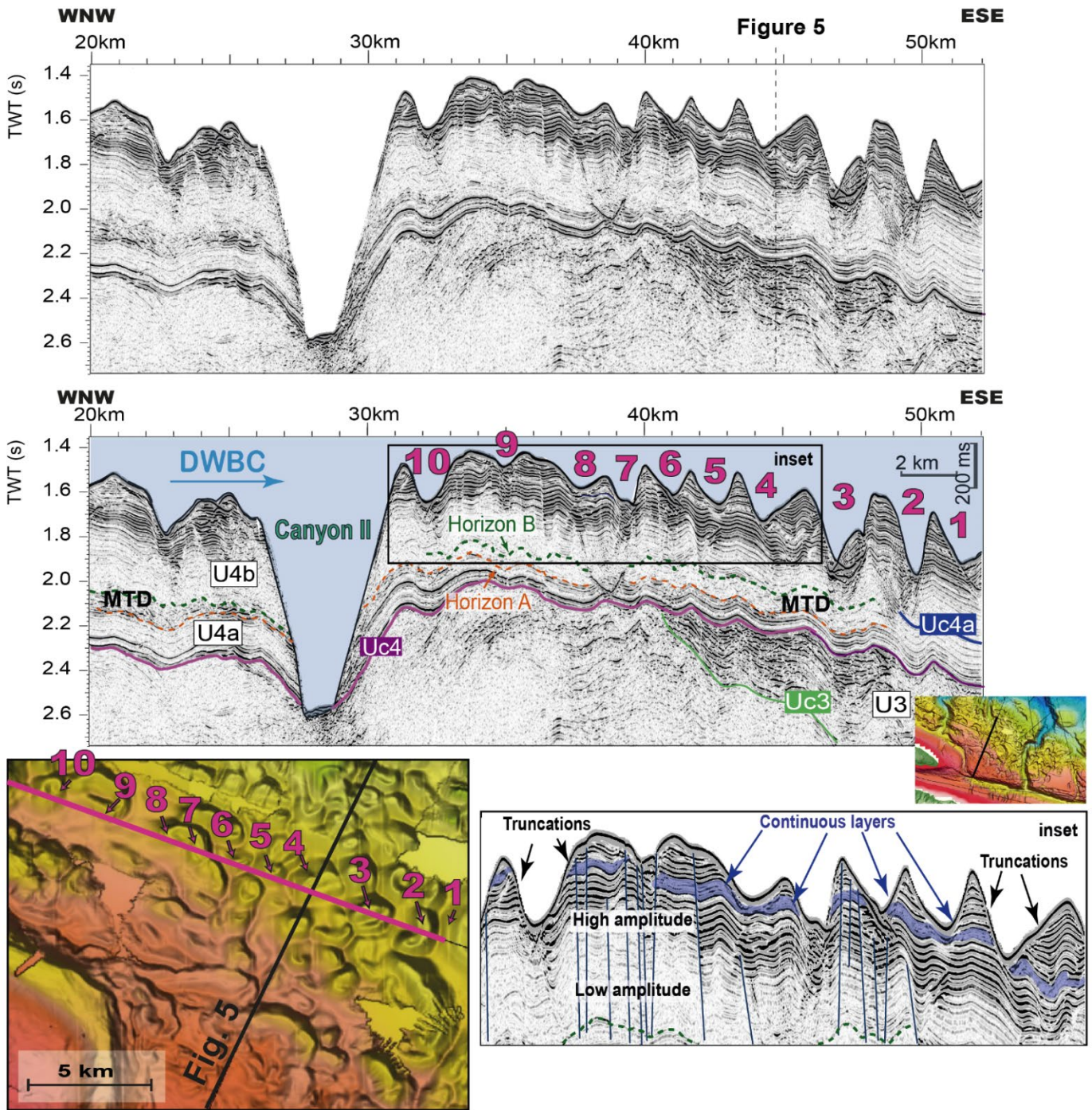


Figure VII. 4. At the top, the uninterpreted WNW-ESE trending seismic line shows Unit 4 affected by seafloor depressions. Refer to Figure VII. 1b for location. Below, the interpreted seismic line is displayed. The approximate position of Deep Western Boundary Current (DWBC) are indicated. MTD: Mass Transport Deposit. The inset with the zoom on the bathymetric map (on the right side) shows the morphology of the depressions intersected by the seismic lines on the seafloor. The seabed depressions are numbered and subsequently pinpointed on the interpreted seismic profile. The inset shows the subseafloor expression of depressions showing continuous wavy geometry and the presence of vertical discontinuities (faults).

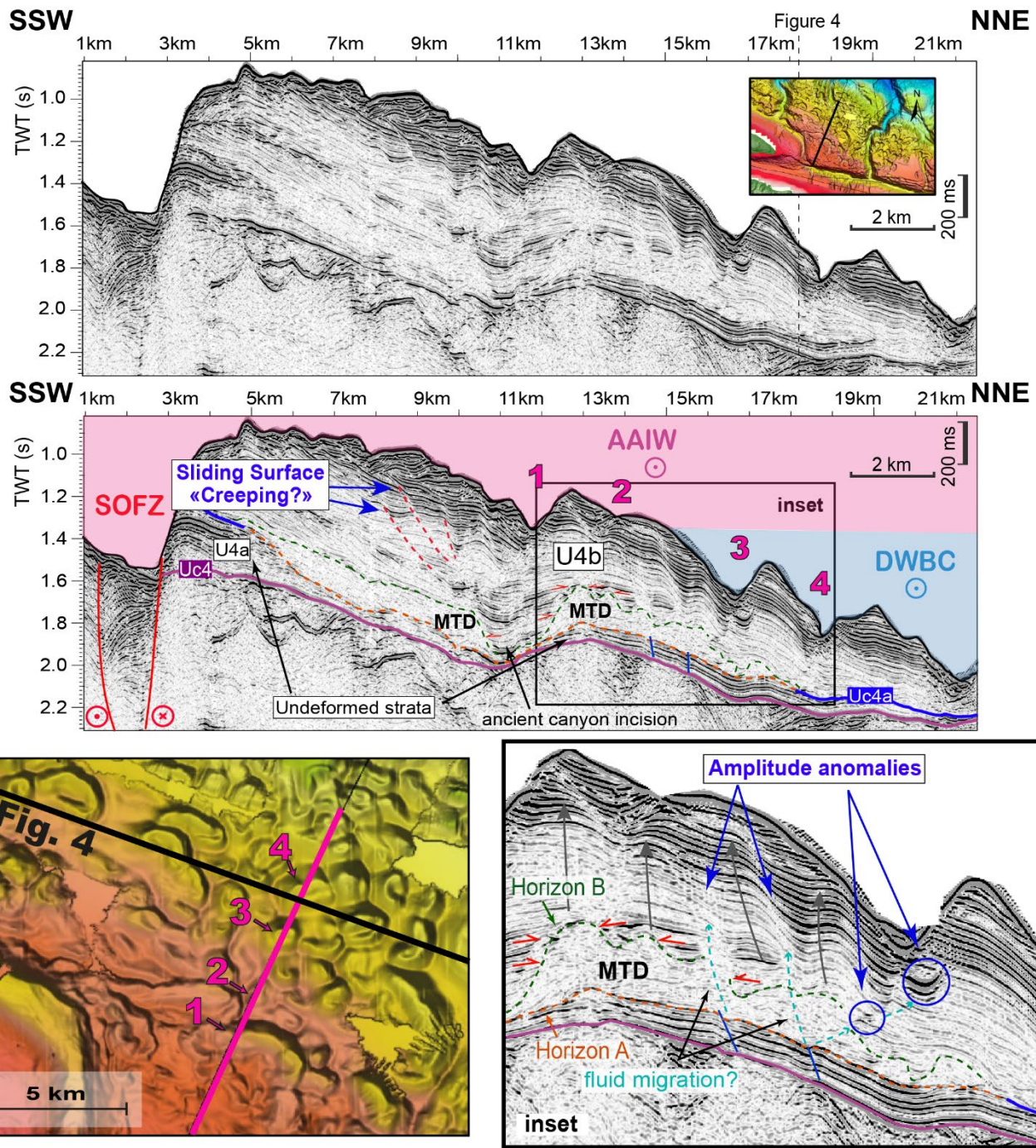


Figure VII. 5. a) At the top, the uninterpreted SSW-NNE trending seismic line shows Unit 4 affected by seafloor depressions. Refer to Figure VII. 1b for location. Below, the interpreted seismic line is displayed. The approximate positions of water mass interfaces are indicated. AAIW: Antarctic Intermediate Water; DWBC: Deep Western Boundary Current. Inset: Close-up on the distal part of the MTD, which appears more chaotic. The reflectors of the U4b unit onlap the MTD and seem to be "whitened" by potential fluids migrating upwards from the MTD. These fluid exits are inferred by the local amplitude loss of the U4b unit reflectors in contact with this MTD. Grey-coloured arrows indicate that the reflectors of unit U4b mimic the reliefs of Horizon B. The inset with the zoom on the bathymetric map (on the right side) shows the morphology of the depressions intersected by the seismic lines on the seafloor. The seabed depressions are numbered and subsequently pinpointed on the interpreted seismic profile.

VII.4.3. Sediment facies

Grain size analyses of the investigated sediment cores (Figure VII. 8) have allowed us to identify five sedimentary facies, labeled as F1 through F5. Their characteristics are summarized in Table 2. Grain size distributions are interpreted in volume (%) of particle diameter (μm). For a comprehensive understanding of the sedimentation, the "first mode" of each sample's frequency curve is established by associating it with the highest percentage fraction (cf. Table 2 for grain size values of first mode). Statistical parameters, namely sorting, skewness, and kurtosis, have been compared to the calculated modes of grain sizes for improved facies classification (Table 2).

Moreover, continuous core logs, including visual descriptions (LOG in Figure VII. 8), abundance of bioturbation, core photographs, and XRF measurements (Figure VII. 10), have allowed us to corroborate consistency between identified facies and sediment changes. Additionally, Ti/Ca and Zr/Al ratios derived from XRF measurements were appropriate for facies discrimination. Micro-texture descriptions were possible for available thin sections (F1, F2, F4, and F5, Figure VII. 9), which constitutes valuable information illustrating the contact between coarse particles (i.e., bioclasts and detrital grains) with fine-grained particles (i.e., matrix).

VII.4.3.1 Facies F1

This facies consists of poorly sorted, bioturbated sandy silts (the color code used in Figure VII. 5 for this type is dark green), with a bimodal distribution in cores HT12-11 and HT15-D2 and a third mode in cores HT15-D1, HT15-I, HT15-F1, due to a higher content in the sandy fraction towards the eastern cores (including foraminifera shells) (Figure VII. 8). Locally, F1 presents normal and inverse grading (e.g., the interval between 100 and 200 cm in core HT15-D2). The thin section illustrates the trimodal character and the intermingled alternance of matrix-supported and grain-supported textures (Figure VII. 9). Mud clasts may be present (Figure VII. 9). First mode ranges between 3-20 μm (Table 2). Except for core HT15-F1, facies F1 are prevalent in nearly all the studied cores, particularly in HT15-D2 and HT12-11 (Figure VII. 8). Ti/Ca and Zr/Al ratios present similar trends and similar values measured in F2 (Figure VII. 10). This facies is interpreted as a **silty contourite**, according to Stow and Smillie (2020) and Stow et al. (2023).

VII.4.3.2 Facies F2

F2 presents a unimodal distribution of moderate to poorly sorted silts with fine to fine sands (light green color code). While the first mode of this facies is similar to F1 (3-20 μm for F1 and 3-17 μm for F2), F2 distinguishes from F1 with better sorting, symmetrical skewness, and higher bioturbation degree (vertically and horizontally). We observed a homogeneous sediment mostly made of a very fine silty matrix from thin sections interspersed with isolated foraminifera shells. F2 is the predominant facies in HT15-F1 (Figure VII. 8).

The top part (10-20 cm) of the five cores investigated, except HT15-D1, are constituted by the unimodal fine-grained facies F2. Ti/Ca ratios are higher in HT15-F1 (>0.04) compared to HT12-11 (<0.03) (Figure VII. 10). Sediments with similar grain size distributions and kurtosis character (mesokurtic to platikurtic) have been interpreted as **hemipelagites** (Castro et al., 2020; Castro et al., 2021).

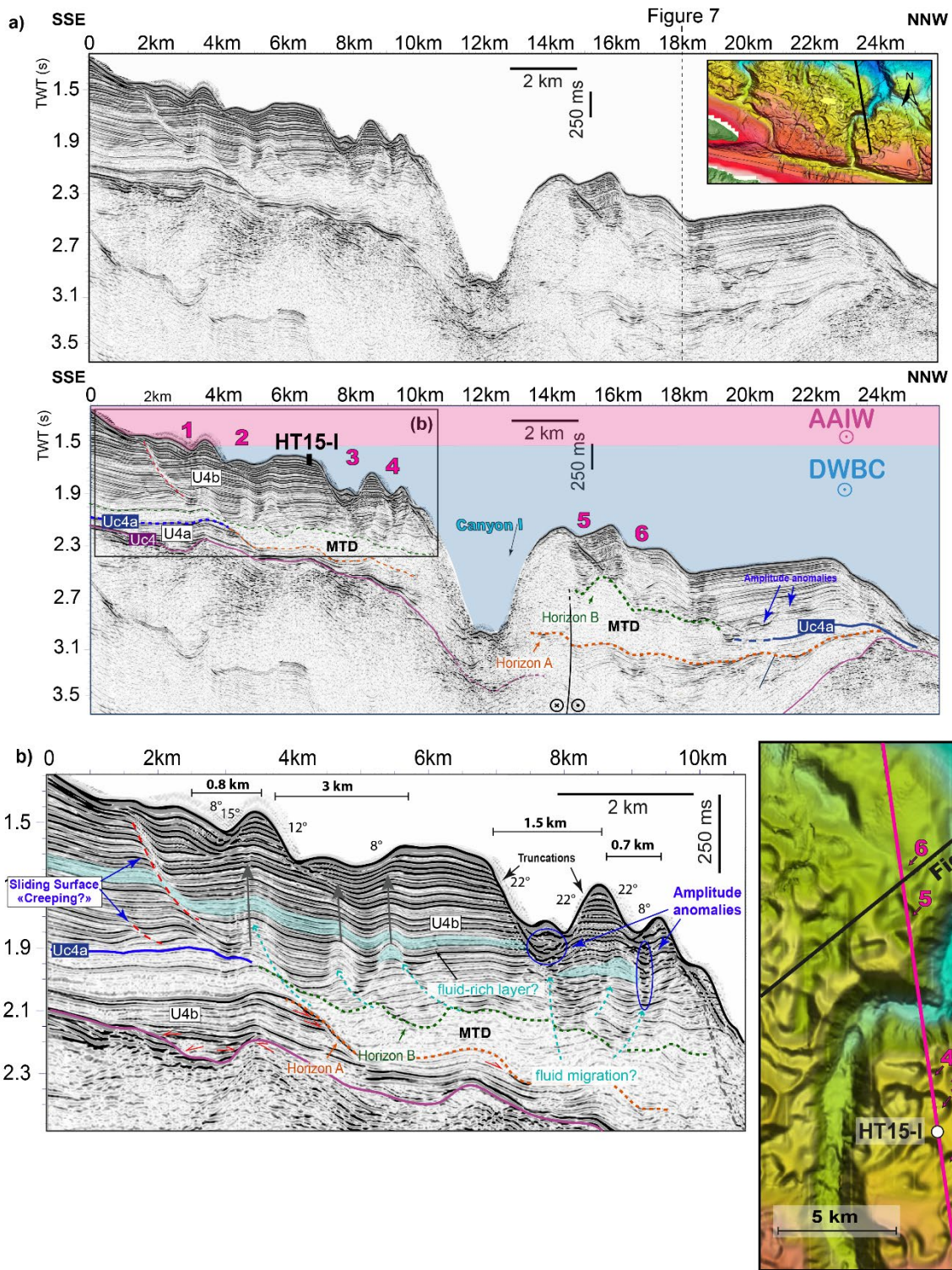


Figure VII. 6 : a) At the top, the uninterpreted SSE-NNW trending seismic line shows Unit 4 affected by seafloor depressions. Refer to Figure VII. 1b for location. Below, the interpreted seismic line is displayed. The approximate positions of water mass interfaces are indicated. AAIW: Antarctic Intermediate Water; DWBC: Deep Western Boundary Current. b) A detailed view of Unit U4 reveals the MTD continuous with sub-unit U4a. Amplitude anomalies can be observed at the MTD's top, suggesting upward fluid migration.

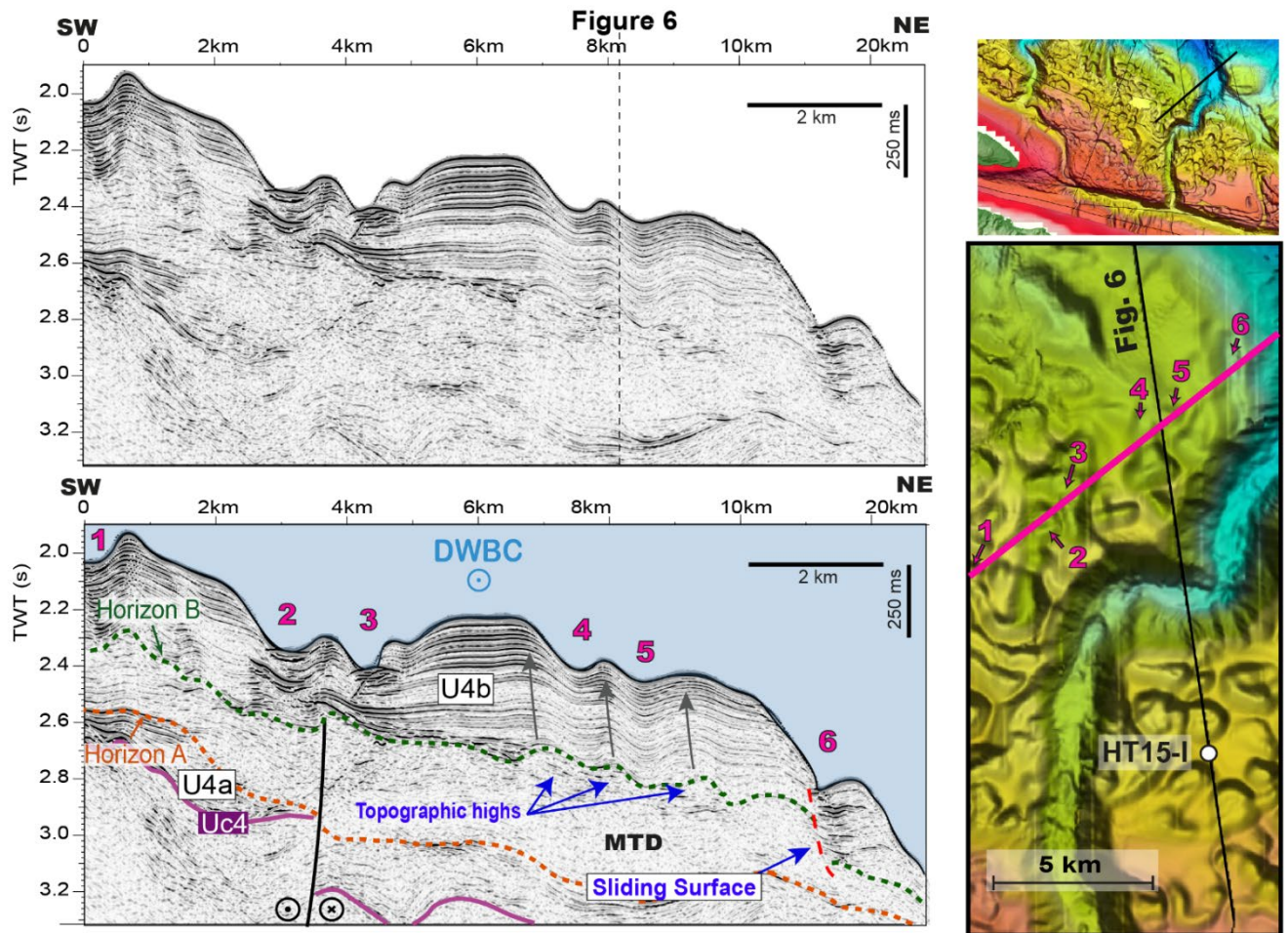


Figure VII. 7. Uninterpreted SW-NE trending seismic line on top showing Unit 4 impacted by depressions on the seafloor. See location in Figure VII. 1b. At the bottom, the interpreted seismic line particularly displays the wavy geometry of horizon B, which defines the top of the MTD.

VII.4.3.3 Facies F3

This facies presents a bimodal distribution of very poorly sorted homogeneous silty clays (color code light pink, Table 2 and Figure VII. 8). Its first mode ranges between 8-72 μm , mostly platykurtic. It is characterized by relatively high Ti/Ca (>0.03) compared to the other facies identified. Zr/Al ratios are <1 (Figure VII. 10). F3 is exclusively found in HT15-F1 and HT15-I, constituting nearly 75% of the latter. The bioturbation within F3 is minimal (Figure VII. 8). F3 encompasses three main facies: homogeneous mud, mottled silt and mud, and sand and silt, arranged in an acyclic bi-gradational sequence that first coarsens upward, then fines upward in some core intervals (94-183 cm bsf). The presence of bi-gradational sequences, as in Stow and Smillie (2020) and Stow et al. (2023) brings us to interpret these facies as a **sandy contourite** (Gonthier et al. 1984; Martín-Chivelet et al., 2008; Mccave, 2008; Rebesco et al., 2014).

VII.4.3.4 Facies F4

F4 presents a trimodal distribution with poorly sorted silty sands reworked that can present normal grading, with a first mode between 60-177.5 μm . Bi-gradational sequences are present in core HT12-D2 (86.5-212.6, 249-336, 392.5-436.5 cm bsf) and in core HT15-F1 (403.2-443.9 cm bsf) (Figure VII. 8). It shows a bimodal distribution: first mode is made of fine-grained sands. F4 presents numerous detrital and carbonate fragments and broken neritic fragments. Bioturbation is generally rare in F4. Cross bedding observed visually is well preserved in F4 intervals at core site HT12-11. Micro-structure reveals mostly grain-supported texture and low content of fine-grained matrix (Figure VII. 9). Ti/Ca and Zr/Al ratios are variable: Ti/Ca are generally <0.3 towards the east but higher in the east (HT15-F1) (Figure VII. 10). At site, HT15-D2, closer to Canyon III (Figure VII. 2), intervals of **F4** are thicker and include several normal graded intervals interpreted as **fine-grained turbidites**, according to Stow and Smillie (2020). No sorting is recognizable similarly to commonly observed in contourites facies (de Castro et al., 2020).

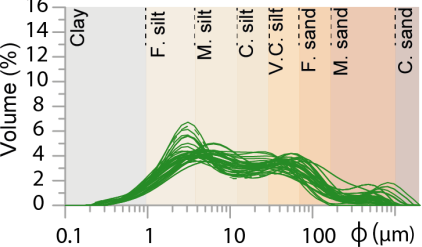
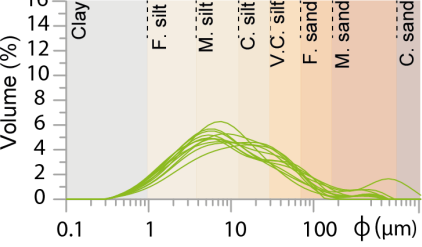
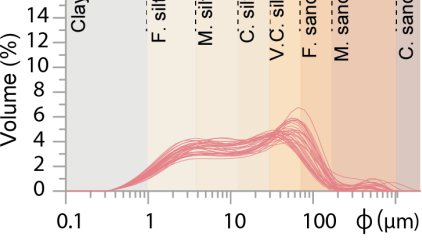
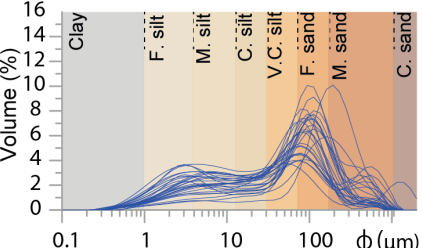
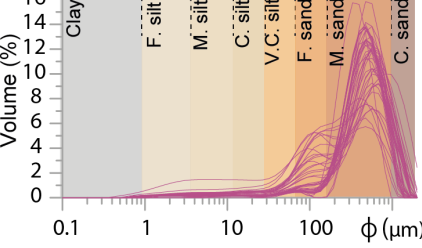
VII.4.3.5 Facies F5

Sediments in F5 is mostly unimodal, poorly to moderately sorted massive medium sands to coarse and very coarse sands, with first mode between 212-1533 μm . Several damaged bioclastic fragments have been observed. The thin section performed on core HT15-D1 illustrates the bioclastic nature of F5 and the total absence of matrix or fines in both cores (Figure VII. 9). The microstructure observed is grain-supported with very little fine-grained matrix (Figure VII. 9). F5 is constituted by a very low Ti/Ca ratio and a high Zr/Al (>1), which is particularly high in core HT15-D1, where Zr/Al exceeds largely 10 (Figure VII. 10). The massive F5 succession in HT15-D1 show reversely- and normally-graded trends (Figure VII. 8).

Based on the coarse character and unimodal distribution and sorting, facies F5 could be interpreted as a coarse-grained turbidite. However, the lack of a fine-grained matrix in both cores (HT15-D2 and HT15-D1) could point to the reworking (winnowing) of sand sheet deposits. Based on this, and in agreement with the contourite facies model of Stow and Smillie (2020), this facies could correspond to a **bioclastic sandy contourite** composed of sand condensation layers (Miramontes et al., 2021).

Bioclastic sand contourites are typically found in high-energy environments, where bottom currents remove fine-grained sediments and favor the concentration of sand (sediment winnowing). Strong currents can also rework sediments, transporting sediments and forming accumulations enriched in foraminifera, classified as sandy condensation layers (Miramontes et al., 2021). Massive deposits of sand condensation layers, closely resembling the Facies F5 found in cores HT15-D1 and HT15-D2, have been described on the lower slope north of the Mozambique Ridge. These deposits comprise bioclastic sand, with 80% of the particles larger than 100 μm (Babonneau et al., 2018; Miramontes et al., 2021). This classification also aligns with that of Castro et al. (2020), in which bioclastic sandy contourites are composed of winnowed bioclasts that display reverse and standard grading patterns.

Table 2. Sediment facies classification according to grain-size distributions.

| Faciès | Grain-size density curves | Grain size parameters | Facies Description |
|-----------|-------------------------------------------------------------------------------------|-----------------------------------------------------------------------------------------------------------------------------------------------------------------------------------------------------------------------------------------------------------------------|----------------------------------------------------------------------------------------------------------------------------------------------------------------------------------------------------------------------------------------------------------------------------------------------------------------------------------------------------------------------------------------------------------------------------------------------------------------------------------------------------------|
| F1 |  | <p>Sand: 32,8% Silt: 57,3% Clay: 9,9%</p> <p>Sorting: Very Poorly sorted to Poorly sorted</p> <p>Skewness: Symmetrical to very fine skewed</p> <p>Kurtosis: Mesokurtic to Platykurtic</p> <p>Mode: Trimodal</p> <p>(2.8 µm < First mode < 20.4 µm)</p> | <ul style="list-style-type: none"> • Mostly bioturbated • Reworked deposits • Clay and silty clay interrupted by coarsening up and fining up sandy intervals • Forams, pteropods and bioclasts • Detrital grains <p style="text-align: right;">Silt contourite mixed with silty turbidites</p> |
| F2 |  | <p>Sand: 15,5% Silt: 74,1% Clay: 10,4%</p> <p>Sorting: Poorly sorted to Very Poorly sorted</p> <p>Skewness: Mostly Symmetrical</p> <p>Kurtosis: Mesokurtic to Platykurtic</p> <p>Mode: Mostly Unimodal</p> <p>(2.82 µm < First mode < 17.07 µm)</p> | <ul style="list-style-type: none"> • Vertically and Horizontally bioturbated • Fining up levels • Foram-rich with <i>Orbulina</i>, pteropods, and bioclasts • Detrital grains <p style="text-align: right;">Hemipelagite</p> |
| F3 |  | <p>Sand: 20,1% Silt: 69,8% Clay: 10,0%</p> <p>Sorting: Very Poorly sorted</p> <p>Skewness: Symmetrical to fine skewed</p> <p>Kurtosis: Mostly Platykurtic</p> <p>Mode: Bimodal</p> <p>(8.3 µm < First mode < 72.02 µm)</p> | <ul style="list-style-type: none"> • Scarce bioturbation <p style="text-align: right;">Sandy to silt contourite</p> |
| F4 |  | <p>Sand: 38,9% Silt: 51,5% Clay: 9,5%</p> <p>Sorting: Poorly sorted to Very Poorly sorted</p> <p>Skewness: Very fine to fine skewed</p> <p>Kurtosis: Leptokurtic to Platykurtic</p> <p>Mode: Bimodal</p> <p>(60.16 µm < First mode < 177.5 µm)</p> | <ul style="list-style-type: none"> • Silty-clay intervals locally bioturbated • Reworked deposits • Coarsening up intervals • Some alternations of fine up levels • Foram-rich (<i>Orbulina</i> rich), pteropods, and bioclasts • Detrital grains • Reworked deposits, numerous detrital and carbonate fragments, broken neritic organisms (<i>Peneroplis</i> spp.) <p style="text-align: right;">Fine grained turbidate</p> |
| F5 |  | <p>Sand: 81,1% Silt: 16,1% Clay: 2,8%</p> <p>Sorting: Poorly to Moderately sorted</p> <p>Skewness: Fine skewed</p> <p>Kurtosis: Leptokurtic</p> <p>Mode: Mostly Unimodal</p> <p>(211.9 µm < First mode < 1533.1 µm)</p> | <ul style="list-style-type: none"> • Massif medium to coarsed sand intervals • Reworked deposits • Numerous detrital and carbonate fragments, broken neritic organisms (<i>Peneroplis</i> spp.). Damaged fragments of <i>G. Menardi</i>, fragments of pink corals, planktonic forams, benthic forams, clasts of red algae, and pteropods. <p style="text-align: right;">Bioclastic Sandy contourite</p> |

VII.5. Discussion

VII.5.1 Synthesis and interpretation of the main sedimentary facies

The hydrodynamic conditions within the water column govern the transport of sedimentary material through the ocean floor. Consequently, an increase in transported and deposited material size generally implies an increase in the flow speed and turbulence (Hjulström, 1949).

The distribution of facies varies laterally according to the coring location. Towards the west, at site HT12-11 and HT15-D2, F1 and F4 are abundant and F3 absent, while towards the east, in cores HT15-I and HT15-F1, F1 is absent and F3 is present (east of Canyon I, in cores HT15-I and HT15-F1, Figure VII. 2). Facies F5 is observed filling a seafloor depression in HT15-D1 (Figure VII. 3, inset 2) and less represented in a 20 cm-thick interval in core HT15-D2 (212.6-248.9 cm bsf, Figure VII. 8).

The proportions of silt and sand exhibit notable variations across distinct facies, while the concentration of clay displays no significant fluctuations (Table 2). Facies with higher sand content (F1, F4 and F5), predominate towards the west (HT15-D1, HT15-D2, and HT12-11, e.g. Table 2 and Figure VII. 8). While facies with lower sand content and predominantly finer fractions characterize the HT15-I and HT15-F1 cores (Table 2 and Figure VII. 8). These differences could indicate a greater hydrodynamic activity towards the west and in the depths from the cores were sampled.

Cores HT15-D1, HT15-D2, and HT12-11 were collected from bathymetric depths dominated by the Deep Western Boundary Current (DWBC) flow. Conversely, the HT15-F1 core was acquired from depths predominantly influenced by the Antarctic Intermediate Water (AAIW) flow. The HT15-I core is positioned between the depth ranges influenced by the DWBC and AAIW currents (refer to Figure VII. 2).

Although current velocity data are lacking in the Northern Haitian Margin, comparative analysis with measurements from the Windward Passage (Figure VII. 1) and north Atlantic flow trends enables us to infer that the Deep Western Boundary Current (DWBC) exhibits greater flow velocities than the Antarctic Intermediate Water (AAIW). Specifically, velocities for the DWBC range from 20 to 40 cm/s (Johns, 2006), contrasting sharply with the AAIW's 1 to 4 cm/s (Fu et al., 2019; van der Boog et al., 2022). This significant disparity in velocities directly influences the sediment deposition patterns within the water column. Fine-grained sediments, including clay and silt, are more likely to remain suspended at greater depths within the DWBC.

In contrast, the AAIW domain facilitates gravitational settling of these finer sediment fractions within the water column. The sedimentary succession underscores this, as evidenced by the predominance of hemipelagic deposits (Facies F2) rich in planktonic foraminifera, pteropods, and detrital grains in core HT15-F1. Core HT15-I predominantly features fine contourite deposits (Facies F3) with limited bioturbation, further supporting the notion that sedimentary characteristics are intimately linked to the prevailing current velocities.

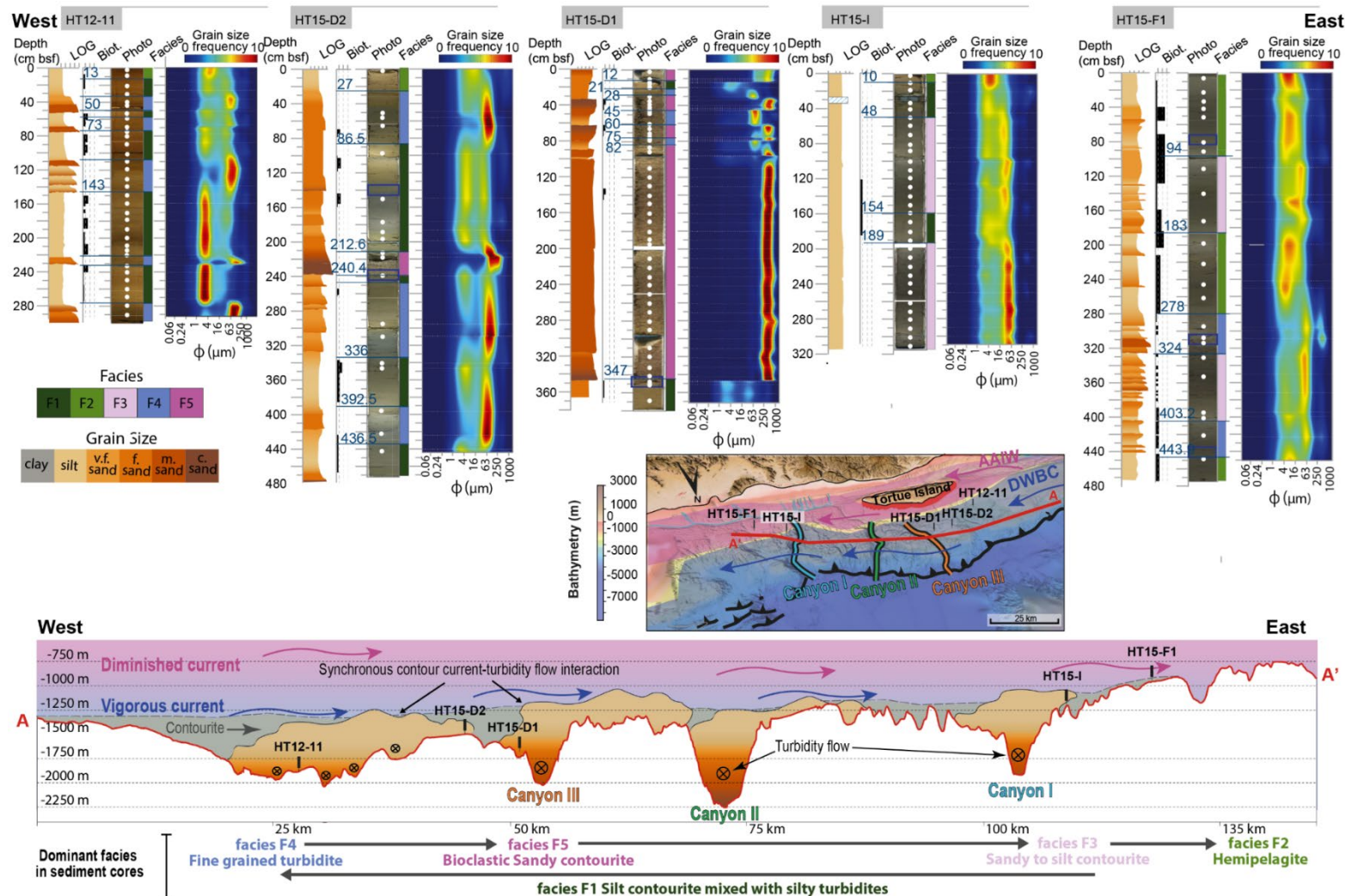


Figure VII. 8. W-E correlation panel of sedimentary facies illustrating the vertical and lateral variation. Variations of grain size are shown as frequency plots of the volume for each size. White dots indicate location of samples for grain size analyses. Blue rectangles show thin sections of Figure VII. 9. Synthetic schemas in the bottom represent the lateral facies distribution along the Northern Haitian Margin according to the interaction of contour currents (grey colour) and turbiditic flows.

Finer-grained deposits are notably scarce in the bioclastic contourite (HT15-D1) (Figure VII. 9). This can be attributed to reworking of these deposits a significant amount of fine-grained particles being winnowed by the bottom current and subsequently redistributed towards the southwest direction by the Deep Western Boundary Current (DWBC) (Figures VII. 1a and 2). This observation is supported by the grain-size data in Figure VII. 9, which reveals that the sandy sediments within the bioclastic turbidite have very low clay and silt contents. In contrast, in the adjacent HT15-D2, these fractions are more common.

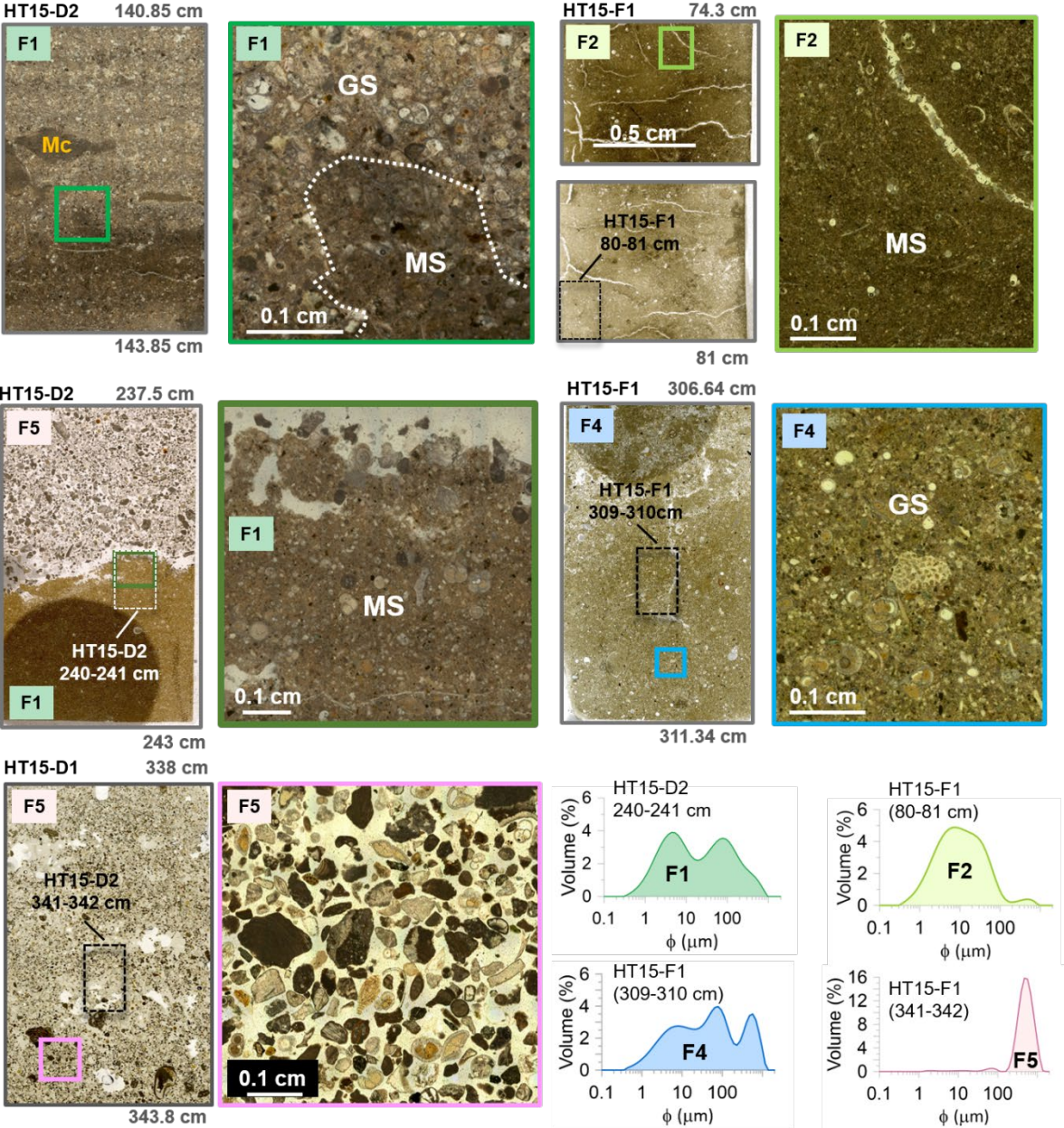


Figure VII. 9. Micro-structure of sediment facies F1, F2, F4 and F5 observed on selected thin sections. For core HT15-D1, two zooms corresponding to different sampling depths are given. GS, grain-supported; MS, matrix supported; Mc, mud clast. When available, location of samples dedicated to grain size analyses are indicated and corresponding grain size distributions given in plots at the right bottom.

The similarity in the grain-size distribution between cores HT12-11 and HT15-D2 (in close geographical proximity, Figure VII. 2) is indicative of their shared influences. These cores

exhibit elevated proportions of sandy fractions (F1) and display evidence of intermittent fine-grained deep-sea turbiditic events (F4) (Figure VII. 8). Such characteristics suggest that these deposits are shaped by enhanced flow dynamics of the DWBC and local turbidity currents, potentially originating from proximal submarine canyons. In contrast, the prevalence of very coarse sediment throughout HT15-D1, only partially registered in the adjacent HT15-D2 core, suggests a localized acceleration of sediment-carrying flows within the depressions. Intermittent currents with higher velocities play a role in the deposition of bioclasts sandy contourites (F5) by facilitating enhanced lateral transport (de Castro et al., 2020).

The alternation of fine contourites and hemipelagic deposits observed in core HT15-F1 is interpreted as indicative of fluctuations in bottom current velocity, in accordance with established literature (Hüneke & Stow, 2008; Wynn & Stow, 2002). Similar sedimentary patterns are noted in other cores from the region; for instance, transitions from fine silt to silty sand (Interbeds of F1 and F3 in HT15-I) or from silty sand to sand (Interbeds of F1 and F4 in both HT15-D2 and HT15-D1) also signal enhanced bottom current activity. These observations are also reflected by the Ti/Ca and Zr/Al ratios. F5 shows high Zr/Al and low Ti/Ca ratios, signs of strong bottom current activity and substantial bioclastic input. The sandier deposits (F1, F4) match increases in Zr/Al (Figure VII. 10), which also suggests the influence of a strong bottom current.

Intercalations of hemipelagites, silty contourites, fine-grained sandy contourites, bottom current reworked sands, and fine-grained turbidite deposits are typical contourite drifts (Figure VII. 8) (de Castro et al., 2021). The current sedimentation along the Northern Haitian coast is characterized by a widespread contourite drift system (de Castro et al., 2020; Miramontes et al., 2021).

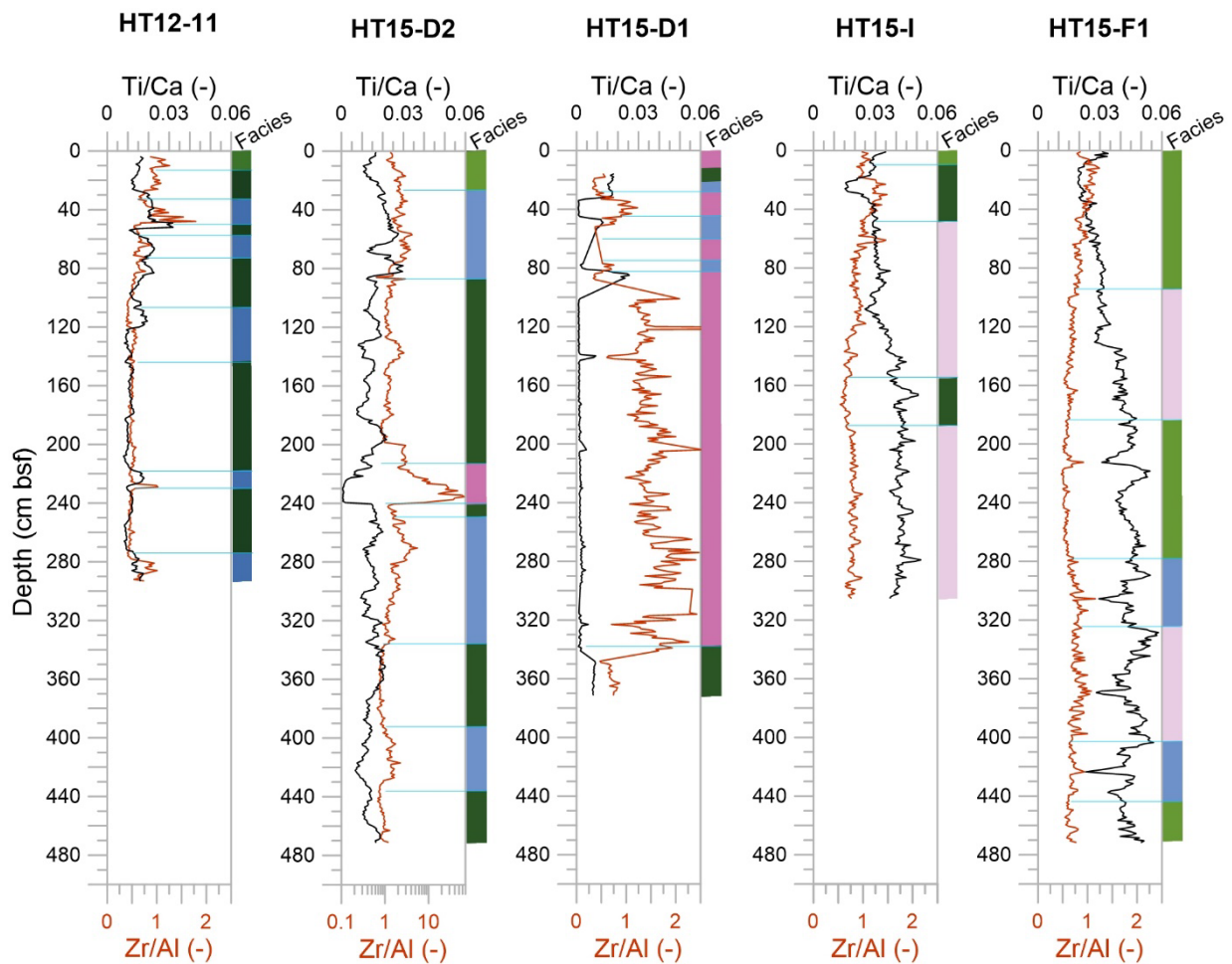


Figure VII. 10. Ti/Ca and Zr/Al ratios obtained from XRF measurements correlated with facies associations by core.

VII.5.2 Possible Origins of the seafloor depressions

Analogous seafloor depressions with similar geomorphological characteristics were previously described in various settings worldwide and have been attributed to a range of geologic processes. Features related to focused fluid escape (e.g., pockmarks) can develop as clustered circular depressions (Howarth & Alves, 2016; Moss & Cartwright, 2010), and karst formations associated with the dissolution and collapse of carbonate strata can show closely spaced circular to polygonal shapes (Ahlborn et al., 2014; Kan et al., 2015; Zeng et al., 2011). Soft sediment bulk contraction accompanied by diagenetic processes (Morley et al., 2017; Niyazi et al., 2020), dewatering (Bertoni et al., 2020), mudstone dolomitization (Riera et al., 2019), or a combination of these mechanisms can give rise to hexagonal-shaped polygonal features. Erosional features within contourite depositional systems formed by bottom currents can also display sub-circular to elongated depressional morphologies (García et al., 2009, 2016; Hernández-Molina et al., 2009; Miramontes et al., 2021; Rebesco et al., 2014; Tallobre, Loncke, Uusõue, et al., 2016; Warnke et al., 2023). In the following section, we highlighted possible hypotheses for forming these features in the study area by comparing them with similar published examples.

VII.5.2.1 Pockmarks

Clustered circular depressions can form due to focused fluid escape, where sediment collapses due to the volume change caused by fluid release (Howarth & Alves, 2016; Judd & Hovland, 2007; Moss & Cartwright, 2010). In this case, the seafloor depressions in the study area would be interpreted as pockmarks formed through the venting of fluids (Judd & Hovland, 2007). In typical 2D seismic data, fluid expulsion features are recognized by acoustic anomalies from signal loss or weakness. These features are often associated with faults or fractures that act as conduits for gas and other fluids (Zhang et al., 2014).

The closely spaced small-scale faults that deform Unit 4, rooted in depth (Figure VII. 4), would act as a conduit to the fluid rising. However, these faults are only observed in specific locations and do not appear directly connected to the depressions on the seafloor (inset in Figure VII. 4).

The anomalies in amplitude visible in the inset in Figure VII. 5 and in Figure VII. 6b, which indicate the presence of fluids in the sedimentary layers, do not extend upward and do not seem to be correlated with the positioning of the depressions along this seismic profile. In specific locations, however, these fluids appear to migrate upward, forming conduits that display amplitude anomalies at the base of certain depressions (Figure VII. 6, km 7-9). Such phenomena are observed only in a limited number of depressions, suggesting that fluid escape is not the predominant, nor the exclusive, mechanism responsible for the formation of these features.

VII.5.2.2 Submarine karstification

Karst formations associated with the dissolution and collapse of carbonate rocks, can also give rise to closely spaced circular to polygonal shapes (Ahlborn et al., 2014; Kan et al., 2015; Zeng et al., 2011). Submarine karst landscapes have been observed at different depths on platforms and continental margins (Kan et al., 2015; Zeng et al., 2011). Haiti's tropical climate favors the dissolution of carbonates, facilitating karstification (Gilli, 2011). Limestone formations in Haiti are predominantly fractured, resulting in karsts and sinkholes in onland formations (Héraud-Piña, 1996).

Karsts can develop either by epigenetic (relatively superficial) or hypogenic (deep) processes. Epigenetic karstification is linked mainly with meteoric flow systems on exposed bedrock (Klimchouk, 2017). Epigenetic processes can also affect marine successions when sea-level changes cause subaerial exposure, allowing meteoric groundwater infiltration (Kan et al., 2015). However, karst features in deeper waters need an alternative interpretation. Hypogenic karst development is commonly associated with ascending fluids of different natures (Klimchouk, 2017). Mixtures between the ascending fluids and seawater may promote the dissolution of limestones (Gilli, 2011). Hypogenic karsts may occur in the seafloor at varying depths (ranging from the shallow subsurface to a hundred meters), especially in regions of active plate boundaries (Betzler et al., 2014; Kan et al., 2015; Klimchouk, 2017).

Cormier et al. (2010) previously reported similar seafloor depressions off the coast of Port-au-Prince (Southwest Haiti), measuring 1-2 km in diameter and ~ 80 m in depth, which were interpreted as a karst landscape developed during previous ice maximums and

subsequently flooded. Although the shape and size of these structures are similar to those found in the study area, it is challenging to explain the emergence of the seafloor to create these depressions by subsequent flooding.

The subunit U4a is assigned to have a Late Miocene-Early Pliocene age, and the U4b subunit is thought to have a Late Pliocene age to the present day (Oliveira de Sá et al., 2021). The northern coast of Hispaniola are characterized by a regional uplift since the Late Pliocene (Díaz de Neira et al., 2017; Escuder-Viruete et al., 2020; Escuder-Viruete & Pérez, 2020), associated with its collision with the Bahamas (Calais et al., 2016). In this case, no significant subsidence episode recorded in the northern Haitian margin from the uppermost Pliocene to the present would explain the flooding of the seafloor depressions to their current water depths (from 900m to 4000m, as shown in Figure VII. 2). Moreover, the presence of the MTD at the base of subunit U4b, coupled with the turbidite deposits (Facies F4) within the unit, suggests that Unit 4 was most likely deposited in a deep-water environment.

In the absence of a period of subsidence that could explain sub-aerial exposure of the margin, the hypogenic karstification hypothesis could be plausible. Therefore, the sediments in Unit 4 are probably not carbonates. However, in this scenario, subsurface fluids may flow through fractures or faults and interact with seawater, leading to a dissolution process as they mix. However, the hypothesis of upward fluids has already been set aside in the previous section due to the scarce fluid migration conduits directly related to the depressions in the seismic profiles. Furthermore, in most of the cores, the nature of the sediments is not predominantly carbonated, making it difficult to justify the formation of these depressions exclusively by dissolution processes. Moreover, karstic conduits are not visible on the seismic data what would exclude dissolution as a potential process behind the investigated structures.

VII.5.2.3 Differential compaction and post-MTD sediment distribution

Another possibility is that the seafloor morphology north of Haiti could be strictly associated with deep processes. According to Oliveira de Sá et al. (In Prep.), the wave-like pattern of the subunit U4b in the eastern domain is primarily attributed to post-MTD emplacement differential compaction (Figure VII. 7). The authors interpreted this MTD to result from the catastrophic failure of the subunit U4a, potentially caused by liquefaction or strain softening. The undulated morphology on the Top of this MTD (Horizon B, inset in Figure VII. 5) would influence the current seafloor morphology (Figure VII. 7).

Differential compaction during early burial (between 0.6-0.8s TWTT, i.e. 400-500 m thick) can locally generate depressions and short wavelengths, influencing the seafloor morphology. Variations in seafloor topography associated with near-seafloor differential compaction of MTDs were already described in the different settings, as in the deep-water Tarfaya-Agadir Basin (Offshore Morocco, e.g. Lee et al., 2004), in the continental slope of the Espirito Santos (Brazil, e.g. Alves, 2010; Ward et al., 2018), and in the passive transform margin of French Guiana (Demerara Plateau, e.g. Tallobre et al., 2016a). Furthermore, Wenau et al. (2021) reports in the Namibian continental margin seafloor depressions exhibiting morphology akin to those outlined in this study. Notably, the author proposes that these seafloor depressions also linked to mass wasting events.

The seismic profiles demonstrate that the draped reflectors within subunit U4b preserve the topographic features of the underlying Mass Transport Deposits (MTD) (Figures VII. 4 to

7). These draped reflectors occasionally align with the crests of the seafloor depressions (Figure VII. 7). In addition, truncations of the reflectors on the flanks of the depressions strongly suggest that it has been subjected to distinct erosion and post-deposition processes leading to its actual morphology (inset in Figure VII. 4).

VII.5.2.4 Erosional features related to irregular seafloor in a contouritic system

According to the seismic criteria for identifying contouritic features (i.e., deposits linked to along-slope bottom currents; cf. Rebesco and Stow, 2001; Rebesco and Camerlenghi, 2008 and Rebesco et al., 2014), the characteristics of the subunit U4b could be interpreted as a contourite. More precisely, its geometry with "a variable degree of mounding and somewhat evident elongation" (as in Figure VII. 7) and stacked to the margin with continuous internal reflections (inset in Figure VII. 4), slightly convergent, low- to high seismic amplitude with an aggradational stacking pattern, would suggest the presence of a contourite.

Slope topography, gravity flows, and bottom currents are additional factors that can influence sedimentation, consequently impacting the generation of seabed deposits and giving rise to distinctive bedforms (Howlett et al., 2019; Fuhrmann et al., 2022; Warnke et al., 2023, Heiniö and Davies, 2009; Sun et al., 2017; Wenau et al., 2022; Garcia et al., 2016). The initial seafloor topography inherited from the topographic expression of the MTD in the subsurface would explain why the contourite drift (U4) developed the enigmatic depressions along the seafloor (Figure VII. 3).

Various studies have extensively discussed the formation of seafloor depressions through the interaction between stable bottom currents and seafloor topography (e.g., Nakajima and Satoh, 2001; Wynn and Stow, 2002; Cattaneo et al., 2004). In the South China Sea, this interaction has been observed to give rise to intricate seafloor depressions characterized by various shapes ranging from circular to irregular, as documented by Sun et al. (2017).

The interaction between bottom currents and an irregular, laterally varying seafloor can bifurcate the flow into multiple cores and branches (i.e., eddies, e.g., Stow et al., 2019). According to Bursik and Woods (2000), this leads to flow deceleration upstream and subsequent acceleration on the locally steepened downstream side of an obstacle. This phenomenon has been observed in the Gulf of Cadiz, where the Mediterranean water outflow from Gibraltar splits into several branches responsible for forming eddies (Serra et al., 2005).

Irregularities along the seafloor and the presence of the SOFZ valley, the Tortue channel, and canyons I to III may favor the splitting of water masses flows and lead to increasing vorticity. Based on the works of Serra et al. (2005) and Stow et al. (2019), we infer that along-slope currents, with an east direction associated with the AAIW and DWBC, are affected by eddies formation. This ongoing process leads to the reshaping of the seafloor topography and would explain the development of seafloor depressions by erosional and depositional processes close to each other (Rebesco et al., 2014). In addition, the arcuate morphology of the ridges surrounding these depressions, as observed in the bathymetric data, suggests a perpendicular asymmetry in the depressions relative to the direction of the current (Figure VII. 3b).

In this case, the seafloor depressions in the study area would be interpreted as contouritic erosional features on a contourite depositional system dominated by erosion and non-deposition (de Castro et al., 2020; Rebesco et al., 2014). Erosional features such as furrows, scours, abraded surfaces, or channels can be formed on top of large-scale contourite features in high-

energy areas, where strong bottom currents either erode the slope or prevent sediment deposition (Miramontes et al., 2021). The lack of deposits within the seafloor depressions and the erosion of its steep truncated flanks would be attributed to perennial ocean currents' constant remobilization of sediments.

Another observation that supports this hypothesis is that a bioclastic sand contourite (F5) without mud fraction within a depression (HT15-D1) may indicate an acceleration of the DWBC within the depressions in which the mud is vanished by the DWBC. Lateral confinement causes increased flow runout length, promoting the development of deposits with a high proportion of bottom current reworked sands. This mechanism leads to elongated and crescent-shape seafloor depressions and the creation of arcuated rides perpendicular to the bottom current direction (Figure VII. 3b).

However, contrary to what might be expected, we do not attribute the observed seabed roughness between 600m and 1200m (inset 3 in Figure VII. 3) to hydrodynamic activities associated with the AAIW (Profile A-A' in Figure VII. 2). The relatively low flow speeds of this current and the prevalence of finer sediment deposits in cores extracted from this depth range do not support the idea that significant hydrodynamic forces are at play. Instead, the seafloor morphology at these depths appears to result from deeper subsurface processes. Mass Transport Deposits (MTDs) are often absent in the southern regions near the coasts and within this specific 600m to 1200m depth range. Thus, the observed seabed features cannot be attributed to irregularities at the top of MTDs or strong bottom currents.

Failure surfaces affecting the subunit U4b suggest that creeping processes are also affecting this subunit (Figures VII. 5 and 6). These creeping are unrelated to the presence of MTDs at greater depths (Figure VII. 5, km 7 – 10). The seafloor morphology within the 600m to 1200m depth range, influenced by the Antarctic Intermediate Water (AAIW) (Figure VII. 2), should, therefore, be more closely linked to these deeper creeping processes rather than surface hydrodynamic forces.

VII.5.3 A model for the formation of the seafloor depressions along the northern Haitian coast

The influence of bottom currents on the distribution of deposits (discussed in section 5.1.), along with the erosional features observed on the flanks of the depressions (inset in Figure VII. 4) and the presence of sand condensation layers indicative of strong hydrodynamic forces within these depressions, collectively support the hypothesis that these depressions are erosive contouritic features formed along an irregular seafloor morphology shaped by deeper subsurface processes. Thus, we propose the following model to explain the establishment of these depressions on the current seabed:

As presented in Oliveira de Sa et al. (2021) and reviewed in (Oliveira de Sá et al., In Prep.), the subunit U4a is deposited above the unconformity Uc4 in a deep sedimentary environment (Figure VII. 11, a and b). This deposition occurred during a period of subsidence that came after a long period of emergence of sedimentary formations to the north of Hispaniola during the Miocene, which initially caused the unconformity Uc4 (see tectonic setting proposed for the study area in Oliveira de Sá et al., In Prep.)

During the late Pliocene, tectonic instability related to the onset of the collision between the island of Hispaniola and the Bahamas resulted in a catastrophic failure of the subunit U4a,

which led to the deposition of MTD (Mass Transport Deposits) along the lateral continuity of this subunit (Figure VII. 11c).

The added weight of the underlying U4b subunit creates an excess fluid pressure, resulting in differential compaction of the MTD, which is the post-depositional deformation of the reflections within subunit U4b. This process modifies the internal architecture of these units, creating topographic highs on the seafloor (Figure VII. 11d).

These sedimentary highs appear at the origin of hydraulic disturbances, forming eddies that generate subcircular and elongated erosional depressions (Figure VII. 11d). However, amplitude anomalies shows that fluids from depth are rising locally along pathways (Figure VII. 6b). The release of these fluids can lead to the collapse of sediment layers. In this case, some of these depressions could be regarded as elongated by deep currents, as observed on the Norwegian margin (Bøe et al., 1998) and in the Demerara Plateau (Tallobre, Loncke, Bassetti, et al., 2016).

In addition, deep processes gravity-driven process (creeping) seems to overwhelm the effects of differential compaction of the MTD and the erosional processes induced by the bottom currents, creating a complex seafloor morphology (Figure VII. 11e).

These instances suggest that the interaction between gravity flows, bottom currents, and surface topography, in conjunction with deep subsurface processes, reshapes the seafloor topography and influences sedimentation and erosion. This complex interplay results in an extensive zone of seafloor depressions along the northern Haiti margin.

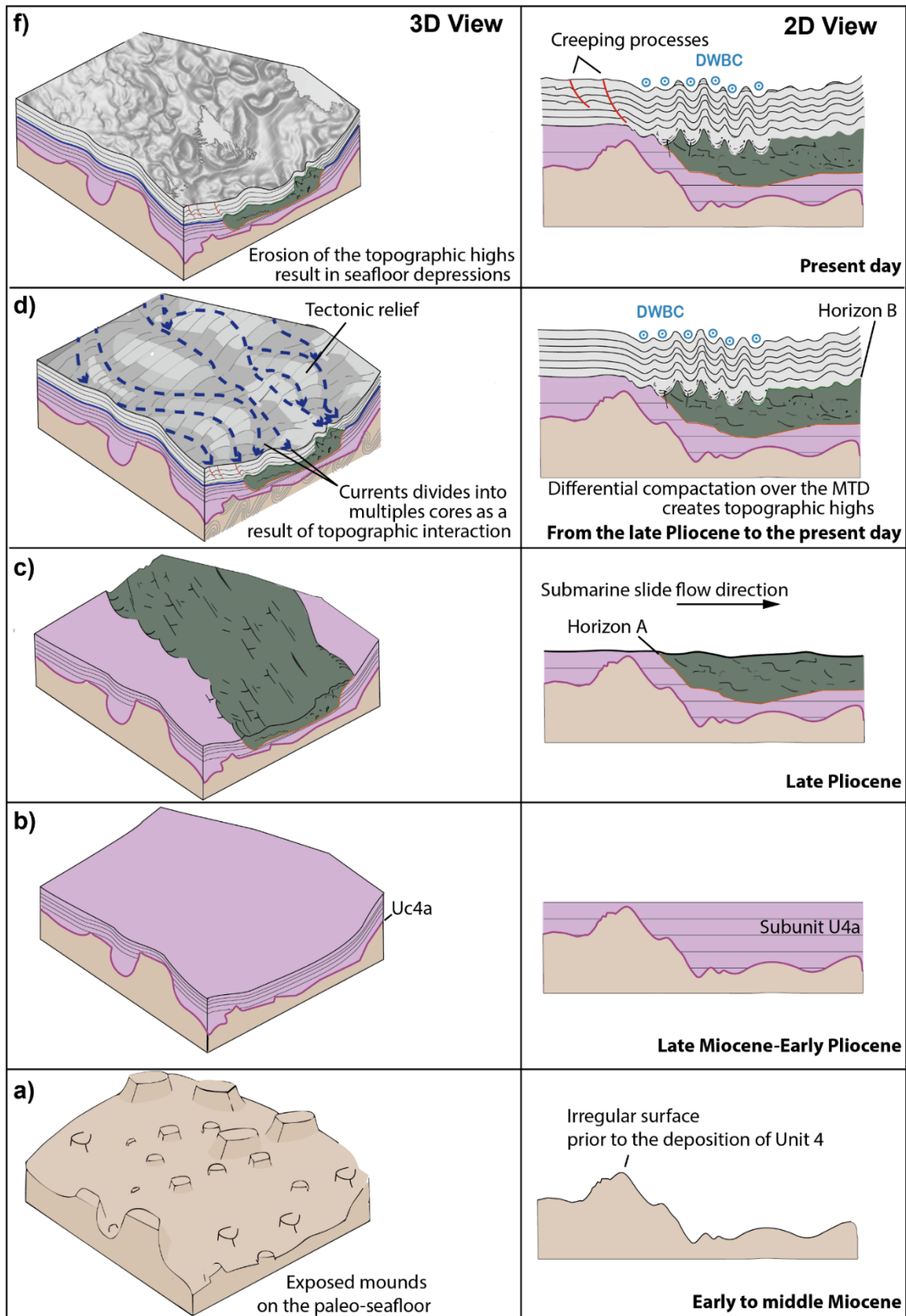


Figure VII. 11. Schematic model/illustration based on the results of this study, showing the possible successive interactions between the deposition of the subunit U4a (a and b), its subsequent catastrophic failure at the origin of a MTD (c), and its influence in the overlain layers of the Subunit U4b (d), which in turn influences the present-day seafloor morphology (e). This schematic model does not take into account the paleoslopes, and the Early to Middle Miocene erosion surface has been flattened.

VII.6 Conclusion

We have shown evidence in this study that seafloor depressions along the Northern Haiti margin are mainly formed through the interaction of bottom currents with an irregular seafloor morphology induced by the differential compaction of a underlying mass transport deposit (MTD). The interaction of quasi-steady bottom currents with irregular seafloor possibly creates eddies that erode and reshape these seafloor irregularities, modifying their morphology and giving rise to elongated and arcuated seafloor depressions limited by very irregular and meandering ridges on the flanks. However, in this complex system, some depressions appear to be formed by fluid escape processes, and the bottom roughness also appears to be enhanced by local creeping processes.

Sedimentological and geochemical analyses on the surface cores allowed the identification of distinct sedimentary deposits, including hemipelagites, silty contourites, sandy contourites, fine-grained turbidites, and reworked sand condensation layers. These findings imply the prevalence of sedimentation within a contourite drift system. This dominant sedimentation pattern characterizes the sedimentary system along the slope of the Northern Haitian coast. The alternation between these deposits and the grain-size variations all over the sedimentary cores analyzed are likely related to variability bottom current velocity, which modifies the sediment distribution by directly interacting with the flow.

The recent establishment of a contourite drift along the Northern Haiti margin raises other unresolved questions. This system might result from increased current velocities in the Quaternary. In this case, the strong seafloor reshaping by bottom currents discussed in this study may be a self-amplifying phenomenon stemming from heightened current velocities.

VII.7 References

- Ahlborn, M., Stemmerik, L., & Kalstø, T.-K. (2014). 3D seismic analysis of karstified interbedded carbonates and evaporites, Lower Permian Gipsdalen Group, Loppa High, southwestern Barents Sea. *Marine and Petroleum Geology*, 56, 16-33. <https://doi.org/10.1016/j.marpetgeo.2014.02.015>
- Alonso, B., Juan, C., Ercilla, G., Cacho, I., López-González, N., Rodríguez-Tovar, F. J., Dorador, J., Francés, G., Casas, D., Vadorpe, T., & Vázquez, J. T. (2021). Paleoceanographic and paleoclimatic variability in the Western Mediterranean during the last 25 cal. Kyr BP. New insights from contourite drifts. *Marine Geology*, 437, 106488. <https://doi.org/10.1016/j.margeo.2021.106488>
- Alves, T. M. (2010). 3D Seismic examples of differential compaction in mass-transport deposits and their effect on post-failure strata. *Marine Geology*, 271(3), 212-224. <https://doi.org/10.1016/j.margeo.2010.02.014>
- Babonneau, F., Thalmann, P., & Vielle, M. (2018). Defining deep decarbonization pathways for Switzerland: An economic evaluation. *Climate Policy*, 18(1), 1-13. <https://doi.org/10.1080/14693062.2016.1227952>
- Bahr, A., Jiménez-Espejo, F. J., Kolasinac, N., Grunert, P., Hernández-Molina, F. J., Röhl, U., Voelker, A. H. L., Escutia, C., Stow, D. A. V., Hodell, D., & Alvarez-Zarikian, C. A. (2014). Deciphering bottom current velocity and paleoclimate signals from contourite deposits in the Gulf of Cádiz during the last 140 kyr: An inorganic geochemical approach. *Geochemistry, Geophysics, Geosystems*, 15(8), 3145-3160. <https://doi.org/10.1002/2014GC005356>
- Bertoni, C., Lofi, J., Micallef, A., & Moe, H. (2020). Seismic Reflection Methods in Offshore Groundwater Research. *Geosciences*, 10, 299. <https://doi.org/10.3390/geosciences10080299>
- Betzler, C., Lindhorst, S., Eberli, G., Lüdmann, T., Moebius, J., Ludwig, J., Schutter, I., Wunsch, M., Reijmer, J., & Huebscher, C. (2014). Periplatform drift: The combined result of contour current and off-bank transport along carbonate platforms. *Geology*. <https://doi.org/10.1130/G35900.1>
- Bøe, R., Rise, L., & Ottesen, D. (1998). Elongate depressions on the southern slope of the Norwegian Trench (Skagerrak): Morphology and evolution. *Marine Geology*, 146(1), 191-203. [https://doi.org/10.1016/S0025-3227\(97\)00133-3](https://doi.org/10.1016/S0025-3227(97)00133-3)
- Bursik, M. I., & Woods, A. W. (2000). The Effects of Topography on Sedimentation from Particle-Laden Turbulent Density Currents. *Journal of Sedimentary Research*, 70(1), 53-63. <https://doi.org/10.1306/2DC408FE-0E47-11D7-8643000102C1865D>
- Calais, É., & Mercier De Lépinay, B. (1992). La limite de plaques décrochante Nord Caraïbe en Hispaniola: Évolution paléogéographique et structurale cénozoïque. *Bull. Soc. géol.*, 3(163), 309-324.
- Calais, É., & Mercier De Lépinay, B. (1995). Strike-slip tectonic processes in the northern Caribbean between Cuba and Hispaniola (Windward Passage). *Marine Geophysical Researches*, 17(1), 63-95. <https://doi.org/10.1007/BF01268051>
- Calais, É., Smithe, S., Mercier de Lépinay, B., & Prépetit, C. (2016). Plate boundary segmentation in the northeastern Caribbean from geodetic measurements and Neogene geological observations. *Comptes Rendus Geoscience*, 348(1), 42-51. <https://doi.org/10.1016/j.crte.2015.10.007>
- Cartigny, M. J. B., Postma, G., van den Berg, J. H., & Mastbergen, D. R. (2011). A comparative study of sediment waves and cyclic steps based on geometries, internal structures and

- numerical modeling. *Marine Geology*, 280(1), 40-56.
<https://doi.org/10.1016/j.margeo.2010.11.006>
- Cattaneo, A., Correggiari, A., Marsset, T., Thomas, Y., Marsset, B., & Trincardi, F. (2004). Seafloor undulation pattern on the Adriatic shelf and comparison to deep-water sediment waves. *Marine Geology*, 213, 121-148.
<https://doi.org/10.1016/j.margeo.2004.10.004>
- Cormier, M., Mchugh, C., Gulick, S., Braudy, N., Davis, M., Diebold, J., Dieudonné, N., Douilly, R., Hornbach, M., Johnson, H., Mishkin, K., Seeber, L., Sorlien, C., Steckler, M., Symithe, S., & Templeton, J. (2010). Vertical Deformation of Late Quaternary Features Across Port-au-Prince Bay, Haiti. AGU Fall Meeting Abstracts, 0005.
- Cukur, D., Kong, G.-S., Chun, J.-H., Kang, M.-H., Um, I.-K., Kwon, T., Johnson, S. Y., & Kim, K.-O. (2019). Morphology and genesis of giant seafloor depressions on the southeastern continental shelf of the Korean Peninsula. *Marine Geology*, 415, 105966.
<https://doi.org/10.1016/j.margeo.2019.105966>
- De Falco, G., Tonielli, R., Di Martino, G., Innangi, S., Simeone, S., & Michael Parnum, I. (2010). Relationships between multibeam backscatter, sediment grain size and *Posidonia oceanica* seagrass distribution. *Continental Shelf Research*, 30(18), 1941-1950. <https://doi.org/10.1016/j.csr.2010.09.006>
- de Castro, S., Hernández-Molina, F. J., de Weger, W., Jiménez-Espejo, F. J., Rodríguez-Tovar, F. J., Mena, A., Llave, E., & Sierro, F. J. (2021). Contourite characterization and its discrimination from other deep-water deposits in the Gulf of Cadiz contourite depositional system. *Sedimentology*, 68(3), 987-1027.
<https://doi.org/10.1111/sed.12813>
- de Castro, S., Hernández-Molina, F. J., Rodríguez-Tovar, F. J., Llave, E., Ng, Z. L., Nishida, N., & Mena, A. (2020). Contourites and bottom current reworked sands: Bed facies model and implications. *Marine Geology*, 428, 106267.
<https://doi.org/10.1016/j.margeo.2020.106267>
- Díaz de Neira, J. A., Braga, J., Perez Cerdan, F., & Lopera, E. (2017). Marine terraces of the Promontorio de Cabrera (Pleistocene, northern Dominican Republic). *BOLETÍN GEOLÓGICO Y MINERO*, 128, 657-674.
<https://doi.org/10.21701/bolgeomin.128.3.007>
- Erikson, J., Pindell, J., Karner, G., Sonder, L., Fuller, E., & Dent, L. (1998). Neogene Sedimentation and Tectonics in the Cibao Basin and Northern Hispaniola: An Example of Basin Evolution Near A Strike-Slip-Dominated Plate Boundary. *The Journal of Geology*, 106. <https://doi.org/10.1086/516036>
- Escuder-Virujete, J., Beranoaguirre, A., Valverde-Vaquero, P., & McDermott, F. (2020). Quaternary deformation and uplift of coral reef terraces produced by oblique subduction and underthrusting of the Bahama Platform below the northern Hispaniola forearc. *Tectonophysics*, 796, 228631. <https://doi.org/10.1016/j.tecto.2020.228631>
- Escuder-Virujete, J., Fernández, F. J., Valera, F. P., & Medialdea, A. (2023). Present-Day Caribbean-North American Oblique Convergence Through the Ocoa-Bonao-La Guacara Fault Zone, Southern Central Hispaniola: A Transition Zone Between Oceanic Subduction and Arc-Oceanic Plateau Collision. *Tectonics*, 42(4), e2022TC007618.
<https://doi.org/10.1029/2022TC007618>
- Escuder-Virujete, J., & Pérez, Y. (2020). Neotectonic structures and stress fields associated with oblique collision and forearc sliver formation in northern Hispaniola: Implications for the seismic hazard assessment. *Tectonophysics*, 784, 228452.
<https://doi.org/10.1016/j.tecto.2020.228452>
- Folk, R. L., & Ward, W. C. (1957). Brazos River Bar: A Study in the Significance of Grain Size Parameters. *Journal of Sedimentary Research*, 27(1).

- Fonseca, L., Brown, C., Calder, B., Mayer, L., & Rzhanov, Y. (2009). Angular range analysis of acoustic themes from Stanton Banks Ireland : A link between visual interpretation and multibeam echosounder angular signatures. *Applied Acoustics*, 70(10), 1298-1304. <https://doi.org/10.1016/j.apacoust.2008.09.008>
- Fu, Y., Wang, C., Brandt, P., & Greatbatch, R. J. (2019). Interannual Variability of Antarctic Intermediate Water in the Tropical North Atlantic. *Journal of Geophysical Research: Oceans*, 124(6), 4044-4057. <https://doi.org/10.1029/2018JC014878>
- Fuhrmann, A., Kane, I. A., Schomacker, E., Clare, M. A., & Pontén, A. (2022). Bottom Current Modification of Turbidite Lobe Complexes. *Frontiers in Earth Science*, 9.
- García, M., Hernández-Molina, F. J., Alonso, B., Vázquez, J. T., Ercilla, G., Llave, E., & Casas, D. (2016). Erosive sub-circular depressions on the Guadalquivir Bank (Gulf of Cadiz) : Interaction between bottom current, mass-wasting and tectonic processes. *Marine Geology*, 378, 5-19. <https://doi.org/10.1016/j.margeo.2015.10.004>
- García, M., Hernández-Molina, F. J., Llave, E., Stow, D. A. V., León, R., Fernández-Puga, M. C., Diaz del Río, V., & Somoza, L. (2009). Contourite erosive features caused by the Mediterranean Outflow Water in the Gulf of Cadiz : Quaternary tectonic and oceanographic implications. *Marine Geology*, 257(1), 24-40. <https://doi.org/10.1016/j.margeo.2008.10.009>
- Gay, A., Lépinay, B. M. de, Ratzov, G., Lebrun, J.-F., & Lallemand, S. (2017, octobre 10). Seafloor giant polygons associated with underlying polygonal faults in the Caribbean Sea, west of Grenada Basin. *International Meeting of Sedimentologists 2017*, Toulouse, France.
- Gay, A., Lopez, M., Cochonat, P., & Sermondadaz, G. (2004). Polygonal faults-furrows system related to early stages of compaction – upper Miocene to recent sediments of the Lower Congo Basin. *Basin Research*, 16(1), 101-116. <https://doi.org/10.1111/j.1365-2117.2003.00224.x>
- Geletti, R., Ben, A., Busetti, M., Ramella, R., & Volpi, V. (2008). Gas seeps linked to salt structures in the Central Adriatic Sea. *Basin Research*, 20, 473-487. <https://doi.org/10.1111/j.1365-2117.2008.00373.x>
- Gilli, E. (2011). *Karstologie : Karsts, grottes et sources*. Dunod.
- Goff, J. A., Olson, H. C., & Duncan, C. S. (2000). Correlation of side-scan backscatter intensity with grain-size distribution of shelf sediments, New Jersey margin. *Geo-Marine Letters*, 20(1), 43-49. <https://doi.org/10.1007/s003670000032>
- Gonthier, E. G., Faugères, J.-C., & Stow, D. A. V. (1984). Contourite facies of the Faro Drift, Gulf of Cadiz. *Geological Society of London Special Publications*, 15, 275-292. <https://doi.org/10.1144/GSL.SP.1984.015.01.18>
- Hammer, Ø., Webb, K. E., & Depreiter, D. (2009). Numerical simulation of upwelling currents in pockmarks, and data from the Inner Oslofjord, Norway. *Geo-Marine Letters*, 29, 269-275. <https://doi.org/10.1007/s00367-009-0140-z>
- Heinio, P., & Davies, R. (2009). Trails of depressions and sediment waves along submarine channels on the continental margin of Espirito Santo Basin, Brazil. *Geological Society of America Bulletin - GEOL SOC AMER BULL*, 121, 698-711. <https://doi.org/10.1130/B26190.1>
- Héraud-Piña, M.-A. (1996). Le karst du Yucatan : Pays des Mayas. In *Le karst du Yucatan : Pays des Mayas*. Presses Universitaires de Bordeaux. <http://books.openedition.org/pub/1527>
- Hernández-Molina, F., Paterlini, C., Violante, R., Marshall, P., Isasi, M., Somoza, L., & Rebesco, M. (2009). Contourite depositional system on the Argentine Slope : An exceptional record of the influence of Antarctic water masses. *Geology*, 37, 507-510. <https://doi.org/10.1130/G25578A.1>

- Hillman, J., Klaucke, I., Pecher, I., Gorman, A., Schneider von Deimling, J., & Bialas, J. (2018). The influence of submarine currents associated with the Subtropical Front upon seafloor depression morphologies on the eastern passive margin of South Island, New Zealand. *New Zealand Journal of Geology and Geophysics*, 61, 1-14. <https://doi.org/10.1080/00288306.2018.1434801>
- Hjulström, F. (1949). Climatic Changes and River Patterns. *Geografiska Annaler*, 31(1-4), 83-89. <https://doi.org/10.1080/20014422.1949.11880795>
- Hovland, M. (1981). Characteristics of pockmarks in the Norwegian Trench. *Marine Geology*, 39(1), 103-117. [https://doi.org/10.1016/0025-3227\(81\)90030-X](https://doi.org/10.1016/0025-3227(81)90030-X)
- Hovland, M., Gardner, J., & Judd, A. (2002). The significance of pockmarks to understanding fluid flow processes and geohazards. *Geofluids*, 2, 127-136. <https://doi.org/10.1046/j.1468-8123.2002.00028.x>
- Hovland, M., Judd, A. G., & King, L. H. (1984). Characteristic features of pockmarks on the North Sea Floor and Scotian Shelf. *Sedimentology*, 31(4), 471-480. <https://doi.org/10.1111/j.1365-3091.1984.tb01813.x>
- Howarth, V., & Alves, T. M. (2016). Fluid flow through carbonate platforms as evidence for deep-seated reservoirs in Northwest Australia. *Marine Geology*, 380, 17-43. <https://doi.org/10.1016/j.margeo.2016.06.011>
- Howlett, D., Ge, Z., Nemec, W., Gawthorpe, R., Rotevatn, A., & Jackson, C. (2019). Response of unconfined turbidity current to deep-water fold and thrust belt topography: Orthogonal incidence on solitary and segmented folds. *Sedimentology*, 66. <https://doi.org/10.1111/sed.12602>
- Huang, Z., Siwabessy, J., Cheng, H., & Nichol, S. (2018). Using Multibeam Backscatter Data to Investigate Sediment-Acoustic Relationships. *Journal of Geophysical Research: Oceans*, 123(7), 4649-4665. <https://doi.org/10.1029/2017JC013638>
- Hüneke, H., & Stow, D. (2008). Chapter 17 Identification of Ancient Contourites : Problems and Palaeoceanographic Significance. In *Developments in Sedimentology* (Vol. 60, p. 323-344). [https://doi.org/10.1016/S0070-4571\(08\)10017-6](https://doi.org/10.1016/S0070-4571(08)10017-6)
- Johns, W. E. (2006). Dynamics of Boundary Currents and Marginal Seas : Windward Passage Experiment (N0014-03-1-0319; p. 6). University of Miami.
- Judd, A., & Hovland, M. (2007). *Seabed Fluid Flow : The Impact on Geology, Biology and the Marine Environment*.
- Kan, H., Urata, K., Nagao, M., Hori, N., Fujita, K., Yokoyama, Y., Nakashima, Y., Ohashi, T., Goto, K., & Suzuki, A. (2015). Submerged karst landforms observed by multibeam bathymetric survey in Nagura Bay, Ishigaki Island, southwestern Japan. *Geomorphology*, 229, 112-124. <https://doi.org/10.1016/j.geomorph.2014.07.032>
- Klimchouk, A. (2017). Types and Settings of Hypogene Karst. https://doi.org/10.1007/978-3-319-53348-3_1
- Kullenberg, B. (1947). The Piston Core Sampler. *Svenska Hydrografiska Biologiska Rommissionens skrifter, Tredje Serien : Hydrografi, Band 1, Hafte. 2*, 1-46.
- Lamarche, G., Lurton, X., Verdier, A.-L., & Augustin, J. (2011). Quantitative characterisation of seafloor substrate and bedforms using advanced processing of multibeam backscatter—Application to Cook Strait, New Zealand. *Continental Shelf Research*, 31. <https://doi.org/10.1016/j.csr.2010.06.001>
- Lee, C., Nott, J., Keller, F., & Parrish, A. (2004). Seismic Expression of Cenozoic Mass Transport Complexes, Deepwater Tarfaya-Agadir Basin, Offshore Morocco. *Proceedings of the Annual Offshore Technology Conference*. <https://doi.org/10.4043/16741-MS>
- Lee, T. N., Johns, W., Zantopp, R., & Schott, F. (1990). Western Boundary Current Structure and Variability East of Abaco, Bahamas at 26.5°N. *Journal of Physical Oceanography*,

- 20(3), 446-466. [https://doi.org/10.1175/1520-0485\(1990\)020<0446:WBCSAV>2.0.CO;2](https://doi.org/10.1175/1520-0485(1990)020<0446:WBCSAV>2.0.CO;2)
- Leroy, S. (2012). HAITI-SIS cruise, L'Atalante R/V. <https://doi.org/10.17600/12010070>
- Leroy, S., & Ellouz-Zimmermann, N. (2013). HAITI-SIS2 cruise, L'Atalante R/V. <https://doi.org/10.17600/13010080>
- Leroy, S., Ellouz-Zimmermann, N., Corbeau, J., Rolandone, F., Mercier De Lépinay, B., Meyer, B., Momplaisir, R., Bruña, J.-L. G., Battani, A., Baurion, C., Burov, E., Clouard, V., Deschamps, R., Gorini, C., Hamon, Y., Lafosse, M., Leonel, J., Pourhiet, L. L., Estrada, P. L., ... Muñoz, S. (2015). Segmentation and kinematics of the North America-Caribbean plate boundary offshore Hispaniola. *Terra Nova*, 27(6), 467-478. <https://doi.org/10.1111/ter.12181>
- Loncke, L. (2004). Mud volcanoes, gas chimneys, pockmarks and mounds in the Nile deep-sea fan (Eastern Mediterranean): Geophysical evidences. *Marine and Petroleum Geology - MAR PETROL GEOL*, 21. [https://doi.org/10.1016/S0264-8172\(04\)00036-4](https://doi.org/10.1016/S0264-8172(04)00036-4)
- Martín-Chivelet, J., Fregenal-Martínez, M. A., & Chacón, B. (2008). Chapter 10 Traction Structures in Contourites. In M. Rebesco & A. Camerlenghi (Éds.), *Developments in Sedimentology* (Vol. 60, p. 157-182). Elsevier. [https://doi.org/10.1016/S0070-4571\(08\)10010-3](https://doi.org/10.1016/S0070-4571(08)10010-3)
- Mccave, I. (2008). Chapter 8 Size Sorting During Transport and Deposition of Fine Sediments. Sortable Silt and Flow Speed. *Developments in Sedimentology*, 60. [https://doi.org/10.1016/S0070-4571\(08\)10008-5](https://doi.org/10.1016/S0070-4571(08)10008-5)
- Miramontes, E., Thiéblemont, A., Babonneau, N., Penven, P., Raison, F., Droz, L., Jorry, S., Fierens, R., Counts, J., Wilckens, H., Cattaneo, A., & Gwenaél, J. (2021). Contourite and mixed turbidite-contourite systems in the Mozambique Channel (SW Indian Ocean): Link between geometry, sediment characteristics and modelled bottom currents. *Marine Geology*, 437, 106502. <https://doi.org/10.1016/j.margeo.2021.106502>
- Morley, C. K., Maczak, A., Rungprom, T., Ghosh, J., Cartwright, J. A., Bertoni, C., & Panpichityota, N. (2017). New style of honeycomb structures revealed on 3D seismic data indicate widespread diagenesis offshore Great South Basin, New Zealand. *Marine and Petroleum Geology*, 86, 140-154. <https://doi.org/10.1016/j.marpetgeo.2017.05.035>
- Moss, J. L., & Cartwright, J. (2010). 3D seismic expression of km-scale fluid escape pipes from offshore Namibia. *Basin Research*, 22(4), 481-501. <https://doi.org/10.1111/j.1365-2117.2010.00461.x>
- Mulder, T., Gillet, H., Hanquiez, V., Reijmer, J. J. G., Droxler, A. W., Recouvreur, A., Fabregas, N., Cavailhes, T., Fauquembergue, K., Blank, D. G., Guiastrennec, L., Seibert, C., Bashah, S., Bujan, S., Ducassou, E., Principaud, M., Conesa, G., Le Goff, J., Ragusa, J., ... Borgomano, J. (2019). Into the deep: A coarse-grained carbonate turbidite valley and canyon in ultra-deep carbonate setting. *Marine Geology*, 407, 316-333. <https://doi.org/10.1016/j.margeo.2018.11.003>
- Nakajima, T., & Satoh, M. (2001). The formation of large mudwaves by turbidity currents on the levees of the Toyama deep-sea channel, Japan Sea. *Sedimentology*, 48, 435-463. <https://doi.org/10.1046/j.1365-3091.2001.00373.x>
- Niyazi, Y., Warne, M., & Ierodiaconou, D. (2020). Hectometer-scale, shallow buried honeycomb-like structures on the continental shelf of the Otway Basin, southeastern Australia. *Interpretation*, 8(4), SR65-SR81. <https://doi.org/10.1190/INT-2020-0039.1>
- Oliveira de Sá, A., d'Acremont, E., Leroy, S., & Lafuerza, S. (2021). Polyphase Deformation and Strain Migration on the Septentrional-Oriente Fault Zone in the Windward Passage, Northern Caribbean Plate Boundary. *Tectonics*, 40(8), e2021TC006802. <https://doi.org/10.1029/2021TC006802>

- Oliveira de Sá, A., Leroy, S., d'Acremont, E., Lafuerza, S., Boisson, D., Watremez, L., & Moreno, B. (In Prep.). Dynamic Evolution of the Northern Caribbean Plate Boundary : Impact on Seabed and Tectonics from Miocene to Present.
- Pau, M., Gisler, G., & Hammer, Ø. (2014). Experimental investigation of the hydrodynamics in pockmarks using particle tracking velocimetry. *Geo-Marine Letters*, 34(1), 11-19. <https://doi.org/10.1007/s00367-013-0348-9>
- Rebesco, M., Hernández-Molina, F., Rooij, D., & Wåhlin, A. (2014). Contourites and associated sediments controlled by deep-water circulation processes : State-of-the-art and future Considerations. *Marine Geology*, 352. <https://doi.org/10.1016/j.margeo.2014.03.011>
- Riera, R., Bourget, J., Paumard, V., Wilson, M. E. J., Shragge, J., George, A. D., Borgomano, J., & Wilson, T. (2019). Discovery of a 400 km² honeycomb structure mimicking a regional unconformity on three-dimensional seismic data. *Geology*, 47(12), 1181-1184. <https://doi.org/10.1130/G46484.1>
- Rodríguez-Zurrunero, A., Granja-Bruña, J. L., Carbó-Gorosabel, A., Muñoz-Martín, A., Gorosabel-Araus, J. M., Gómez de la Peña, L., Gómez Ballesteros, M., Pazos, A., Catalán, M., Espinosa, S., Druet, M., Llanes, P., & ten Brink, U. (2019). Submarine morpho-structure and active processes along the North American-Caribbean plate boundary (Dominican Republic sector). *Marine Geology*, 407, 121-147. <https://doi.org/10.1016/j.margeo.2018.10.010>
- Rodríguez-Zurrunero, A., Granja-Bruña, J. L., Muñoz-Martín, A., Leroy, S., ten Brink, U., Gorosabel-Araus, J. M., Gómez de la Peña, L., Druet, M., & Carbó-Gorosabel, A. (2020). Along-strike segmentation in the northern Caribbean plate boundary zone (Hispaniola sector): Tectonic implications. *Tectonophysics*, 776, 228322. <https://doi.org/10.1016/j.tecto.2020.228322>
- Serra, N., Ambar, I., & Käse, R. H. (2005). Observations and numerical modelling of the Mediterranean outflow splitting and eddy generation. *Deep Sea Research Part II: Topical Studies in Oceanography*, 52(3), 383-408. <https://doi.org/10.1016/j.dsr2.2004.05.025>
- Stow, D., Smillie, Z., Pan, J., & Esentia, I. (2019). Deep-Sea Contourites : Sediments and Cycles. In J. K. Cochran, H. J. Bokuniewicz, & P. L. Yager (Éds.), *Encyclopedia of Ocean Sciences (Third Edition)* (p. 111-120). Academic Press. <https://doi.org/10.1016/B978-0-12-409548-9.10879-6>
- Sun, Q., Cartwright, J., Lüdmann, T., Wu, S., & Yao, G. (2016). Three-dimensional seismic characterization of a complex sediment drift in the South China Sea : Evidence for unsteady flow regime. *Sedimentology*, 64. <https://doi.org/10.1111/sed.12330>
- Tallobre, C., Loncke, L., Bassetti, M.-A., Giresse, P., Bayon, G., Buscail, R., de Madron, X. D., Bourrin, F., Vanhaesebroucke, M., & Sotin, C. (2016). Description of a contourite depositional system on the Demerara Plateau : Results from geophysical data and sediment cores. *Marine Geology*, 378, 56-73. <https://doi.org/10.1016/j.margeo.2016.01.003>
- Tallobre, C., Loncke, L., Uusõue, M., Marsset, T., Droz, L., Bassetti, M., Bayon, G., & IGUANES, l'équipe. (2016, octobre 24). Caractérisation d'un système de dépôt contouritique sur le Plateau marginal de Demerara à partir de la cartographie des échofaciès Chirp.
- van der Boog, C., Dijkstra, H., Pietrzak, J., & Katsman, C. (2022). Spatial Variations of Antarctic Intermediate Water in the Caribbean Sea Due To Vertical Mixing Along Its Path. *Geophysical Research Letters*, 49. <https://doi.org/10.1029/2021GL095977>
- Waghorn, K., Pecher, I., Strachan, L., Crutchley, G., Bialas, J., Coffin, R., Davy, B., Koch, S., Kroeger, K. F., Papenberg, C., Rose, P., & Sarkar, S. (2018). Paleo-Fluid Expulsion

- Influencing Contouritic Drift Formation on the Chatham Rise, New Zealand. *Basin Research*, 30(1), Article 1. <https://doi.org/10.1111/bre.12237>
- Ward, N. I. P., Alves, T. M., & Blenkinsop, T. G. (2018). Submarine sediment routing over a blocky mass-transport deposit in the Espírito Santo Basin, SE Brazil. *Basin Research*, 30(4), 816-834. <https://doi.org/10.1111/bre.12282>
- Warnke, F., Schwenk, T., Miramontes, E., Spiess, V., Wenau, S., Bozzano, G., Baques, M., & Kasten, S. (2023). Evolution of complex giant seafloor depressions at the northern Argentine continental margin (SW Atlantic Ocean) under the influence of a dynamic bottom current regime. *Frontiers in Earth Science*, 11, 1117013. <https://doi.org/10.3389/feart.2023.1117013>
- Wenau, S., Spiess, V., & Zabel, M. (2021). Giant Seafloor Depressions Caused by Slope Failures and Bottom Currents on the Namibia Continental Margin. *Geochemistry, Geophysics, Geosystems*, 22. <https://doi.org/10.1029/2020GC009548>
- Wynn, R. B., & Stow, D. A. V. (2002). Classification and characterisation of deep-water sediment waves. *Marine Geology*, 192(1), 7-22. [https://doi.org/10.1016/S0025-3227\(02\)00547-9](https://doi.org/10.1016/S0025-3227(02)00547-9)
- Zeng, H., Loucks, R., Janson, X., Wang, G., Xia, Y., Yuan, B., & Xu, L. (2011). Three-dimensional seismic geomorphology and analysis of the Ordovician paleokarst drainage system in the central Tabei Uplift, northern Tarim Basin, western China. *AAPG Bulletin*, 95, 2061-2083. <https://doi.org/10.1306/03111110136>
- Zhang, Z., McConnell, D., & Yao, Q. (2014). Seismic amplitudes and attenuations of gas hydratebearing sediments in fractured and sand reservoirs. *Fugro GeoConsulting*. <https://www.osti.gov/biblio/1434050>

-
-
-
-
-
-
-
-
-
-

QUATRIÈME PARTIE

— *Conclusions et Perspectives* —

CHAPITRE VIII : Conclusions et Perspectives

VIII.1. Conclusions

L'analyse conjointe de l'ensemble des données et des travaux antérieurs nous permet de répondre à certaines questions et d'aboutir aux résultats détaillés ci-après.

Quelles sont les implications géodynamiques de nos résultats sur le fonctionnement dans le temps de la frontière Nord de la plaque Caraïbe ? Quel est le calendrier de la migration de ces différents segments actifs ?

La déformation observée sur les unités sédimentaires au nord de Cuba révèle une histoire tectonique complexe (Figures VIII.1 et VIII.2). Cette histoire est marquée par des événements géodynamiques majeurs liés à la mise en place de la région des Caraïbes pendant le Cénozoïque, notamment le rifting de la Pangée et la subduction de la plaque océanique Proto-Caribéenne (Figure VIII.2). Une découverte significative de notre étude concerne la nature du socle au large de Cuba, que l'on associe aux bancs carbonatés des Bahamas. Nous avons mis en évidence que ces bancs carbonatés se sont formés au sommet de blocs basculés lors du rifting de la Pangée. Cette conclusion répond à un débat longtemps en cours, en affirmant que le socle des Bahamas, au large de Cuba Oriental, est constitué de croûte amincie plutôt que de croûte océanique normale ou épaissie par des matériaux volcaniques. Les mécanismes au foyer des séismes observés dans l'Old Bahamas Channel (Braunmiller et al., 2017) montrent un plan de faille normale orienté NE-SW, de même orientation que les failles normales qui décalent les blocs basculés que nous avons décrits (chapitre IV).

Nos observations révèlent également que le positionnement de la limite nord de la plaque Caraïbe pendant l'Éocène moyen est guidé par la réactivation de failles jurassiques préexistantes. La prolongation en mer de la faille de Cauto-Nipe est probablement liée à l'abandon de l'ancienne faille transformante située au nord de Cuba (Cuba Fracture Zone, Figure VIII.2), qui est devenue une barrière crustale lors de la collision entre le bloc Est de Cuba et la plaque nord-américaine. La faible déformation observée dans les unités sismiques plus récentes indique une phase tectonique moins active, corroborée par des observations terrestres qui montre à son tour l'abandon de la faille de Cauto-Nipe en faveur de la mise en place du système de faille Septentrional-Orientale (SOFZ) (Figure VIII.3).

L'analyse des données sismiques au nord du bloc de Cuba oriental a permis de dévoiler l'évolution tectonique précoce de la marge nord de la plaque Proto-Caraïbe, influencée par la phase orogénique et la phase post-orogénique pendant laquelle Cuba a été progressivement transféré sur la plaque Nord-Américaine (Figures VIII.2 et 3).

La poursuite de notre interprétation des lignes sismiques dans le détroit du Passage du Vent révèle que la sédimentation dans ce détroit s'est probablement déroulée initialement dans un cadre paléogéographique commun avec le Bloc de Cuba Oriental, jusqu'à l'installation de la zone de faille d'Orientale (OFZ ; Figure VIII.3). L'émergence du champ de contraintes décrochantes lié à l'initiation de l'OFZ est caractérisée par un bref épisode transtensionnel, qui a engendré l'ouverture du bassin du Passage du Vent, provoquant ainsi la séparation des blocs

de Cuba Oriental et d'Hispaniola (entre la fin de l'Oligocène-Début du Miocène, Figures VIII.2 et 3).

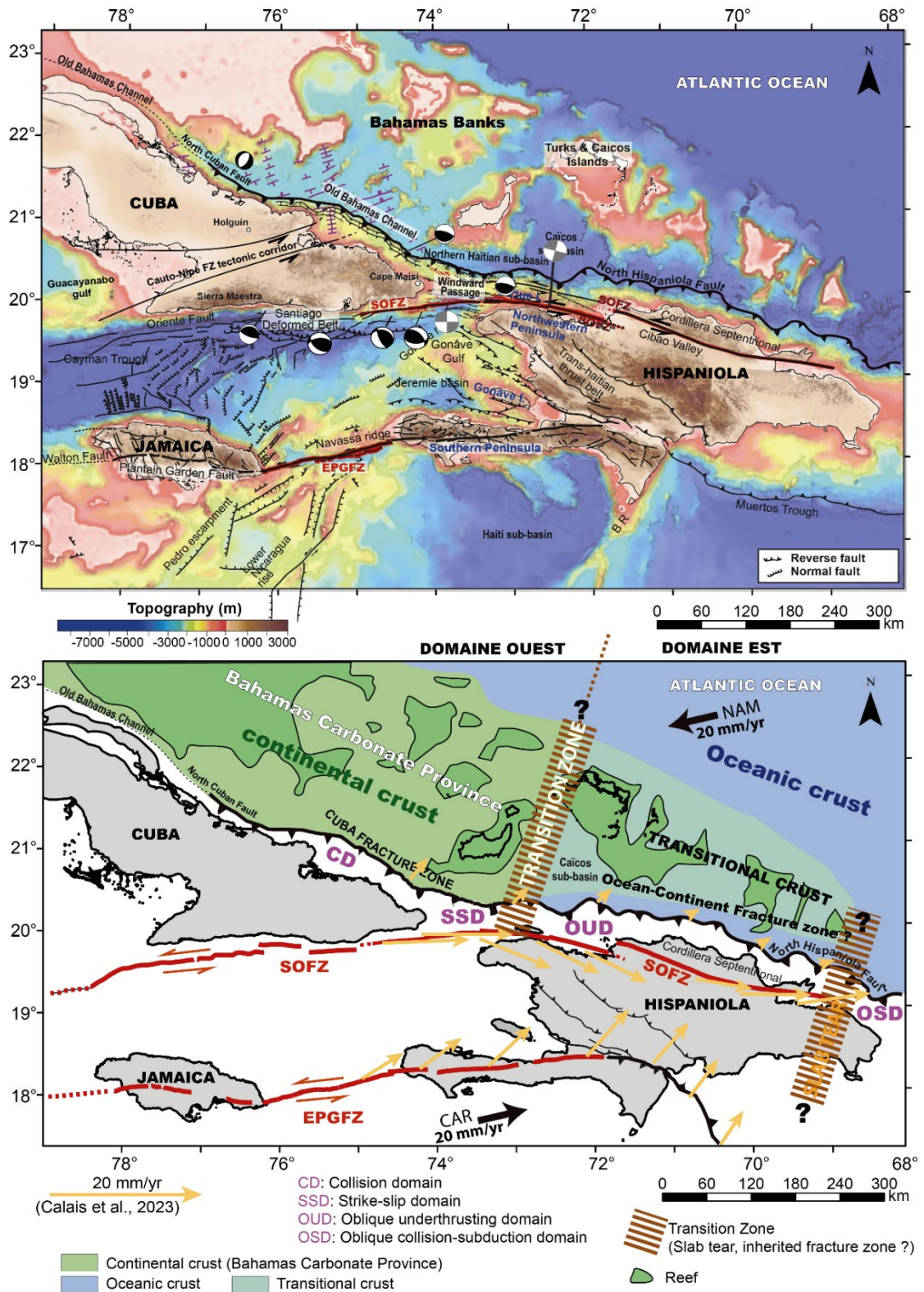


Figure VIII.1. En haut : Carte bathymétrique et topographique générale de la zone d'étude avec les principaux traits structuraux et mécanismes au foyer (Source : Calais et al., 2023) NHF : North Hispaniola fault = front de déformation Hispaniola ; SOFZ : Système de failles Septentrionale-Orientale; EPGFZ : Zone de Faille Enriquillo-Plantain . En bas : Schéma synthétique illustrant les hypothèses sur les différents domaines de croûtes. Les

vecteurs cinématiques en jaune sont tirés du modèle de blocs proposés par Calais et al. (2023). Les domaines tectoniques sont ceux de Rodriguez-Zurrenero et al. 2020. NAM: plaque Nord Amérique; CAR: plaque Caraïbe.

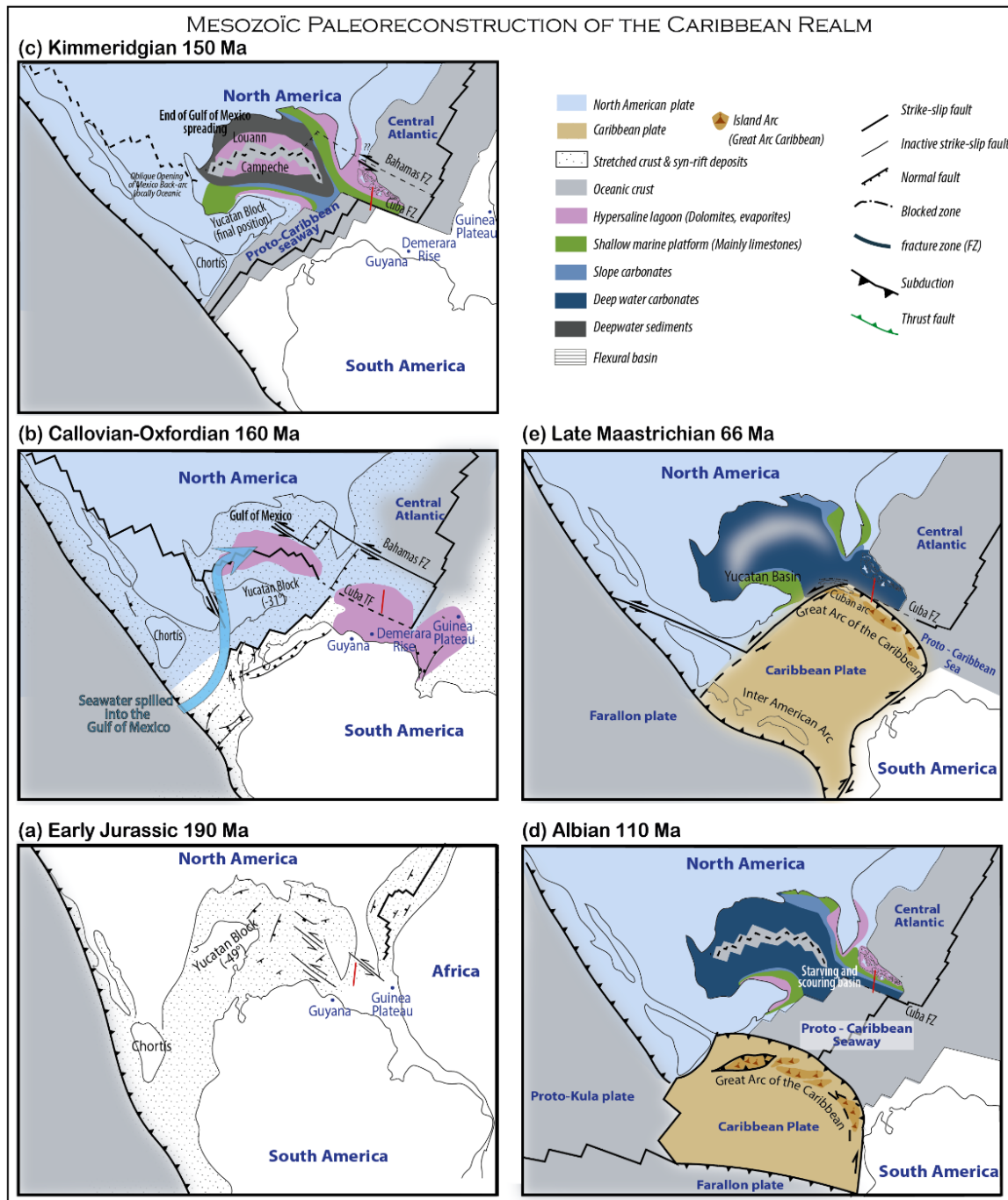


Figure VIII.2. Reconstitutions paléogéodynamiques mésozoïques de la région des Caraïbes. Dépôts sédimentaires associés du Jurassique inférieur au Crétacé supérieur.

Un fait majeur ressortant de cette étude sur le Passage du Vent est la mise en évidence d'un décalage latéral d'environ 80 km de la couverture sédimentaire du bassin du Passage du Vent, de part et d'autre des segments de failles décrochantes sénestres. Cette observation nous a permis d'estimer l'âge de la formation des segments de l'OFZ dans le bassin à $\sim 5.4 \pm 0.2$ Ma, plaçant ainsi cet événement au Pliocène. Cet événement est contemporain du début de la collision de l'île d'Hispaniola avec la province Carbonatée des Bahamas.

Ainsi, il est probable que la OFZ se soit étendue vers l'est, au large du bloc d'Hispaniola, depuis sa formation initiale jusqu'à sa collision avec les Bahamas pendant le Pliocène. Cette collision a entraîné une réorganisation paléogéographique majeure, déjà décrite par divers auteurs sur les affleurements à Hispaniola (Calais & Mercier De Lépinay, 1992; de Zoeten & Mann, 1999; Erikson et al., 1998; Pindell & Draper, 1991). En mer, cette réorganisation est marquée par l'initiation de nouveaux segments de l'OFZ plus au sud de Cuba Oriental, à travers le bassin du Passage du Vent, puis le long de la côte nord d'Haïti (Figure VIII.3). Ces segments finalement s'intègrent au système de faille Septentrional situé dans la vallée du Cibao, au nord de la République Dominicaine (SFZ ; Figure VIII.3). Cela marque l'émergence au Pliocène supérieur -Pleistocène du Système de failles décrochantes Septentrional-Oriente (SOFZ). La frontière de plaque actuelle entre la plaque Caraïbe et la plaque Amérique du Nord se répartit entre ce système décrochant (SOFZ) et le front de déformation Hispaniola (NHF; Figure VIII-1).

Pour résumé, nous avons mis en évidence que le passage du vent a subi une déformation polyphasée avec au moins 4 événements tectoniques liés à la collision oblique entre la plaque caraïbe et les bancs de Bahamas. Le premier événement tectonique dans la région correspond à la période de collision entre l'arc cubain et l'arc hispanique avec la Province Carbonatée des Bahamas, au cours de laquelle la couverture sédimentaire de l'ancien bassin d'avant-arc a été progressivement soulevée, ce qui a entraîné la formation de bassins de type "piggyback" le long d'une marge syn-collisionnelle. Le deuxième événement tectonique correspond à une période de transition entre des mouvements principalement en convergence et en coulissement. Cette période est marquée par une importante réorganisation paléogéographique qui correspond à un bref événement en transtension qui a entraîné l'ouverture du bassin du Passage du Vent pendant l'initiation de l'OFZ et la dislocation consécutive des blocs de Cuba et d'Hispaniola. Les deux derniers événements sont caractérisés par une déformation en compression, puis par la déformation en transpression actuelle.

CENOZOÏC PALEORECONSTRUCTION OF THE NORTHERN CARIBBEAN PLATE BOUNDARY

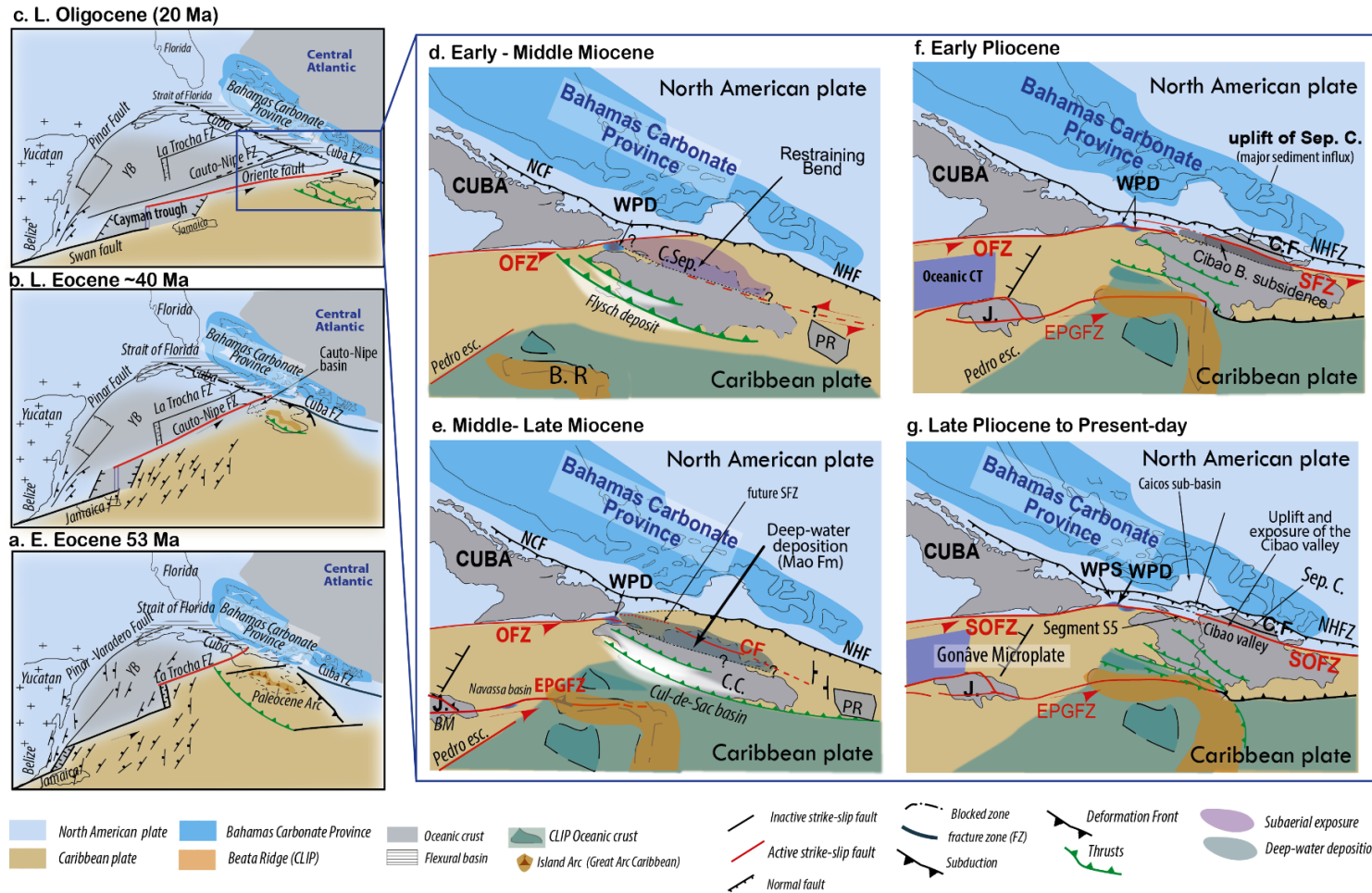


Figure VIII.3. Paléo-reconstruction/Cadre tectonique de la limite nord de la plaque caraïbe du Miocène inférieur au Pliocène supérieur, modifié d'après Leroy et al. (2000), Calais et al 2016 et Oliveira de Sa et al. (2021). B.R : ride de Beata ; Pedro Esc. : escarpement de Pedro ; NHF : faille nord d'Hispaniola ; NCF : faille nord de Cuba ; BM : Blue Mountains ; J. Jamaïque ; C. Sept. : cordillère septentrionale ; PR : Porto Rico EPGFZ : zone de faille Enriquillo-Plantain-Garden ; OFZ : zone de faille Oriente ; CF : faille Camu ; SFZ : zone de faille Septentrionale ; SOFZ : zone de faille Septentrionale Oriente ; WPD : Windward Passage Deep ; WPS : Windward Passage Sill.

Quels sont les conséquences de cette migration et ses implications sur les éléments morphologiques du fond marin ? Existe-t-il un lien entre les processus tectoniques profonds et l'actuel morphologie du fond marin ? Quels types de sédimentation et de systèmes sédimentaires sont-ils associés à ce système de faille ?

La migration diachrone de la déformation de l'ouest vers l'est est apparemment associée à une instabilité tectonique. Cette dernière est mise en évidence dans les séries sédimentaires par la mise en place de *Mass Transport Deposits* (MTDs), comme observé dans notre étude des séquences sédimentaires au nord de Cuba. Ces MTDs indiquent probablement une activité tectonique accrue lors de la collision et de la migration de cette limite de plaques. La chronologie de cette collision est clairement illustrée par les MTDs : la collision semble être plus ancienne à l'ouest du bloc oriental de Cuba, où les MTDs sont enregistrés au sommet de l'unité C (Paléocène supérieur, Figure VII.2). Vers l'est, les manifestations de cette collision deviennent progressivement plus récentes, avec des MTDs présents au sommet de l'unité D, à la base de l'unité E (Éocène supérieur, Figure VII.2) et au sein de l'unité U4 (Figure VII.2) au nord d'Haïti. Nos résultats montrent que la chronologie estimée pour la formation de ces MTDs coïncide avec celle de la collision entre la bordure nord de la plaque Caraïbe et la province carbonatée des Bahamas. La tectonique active lors de la collision diachrone se traduit par le déclenchement de ces MTDs.

La mise en place du MTD au large de la côte nord d'Haïti est aussi accompagnée par la mise en place des failles décrochantes pendant la migration vers le sud de l'ancienne limite de plaque. L'activité de ces failles décrochantes exerce un contrôle structural décalant les cours des canyons sous-marins. Avec l'émergence de la SOFZ le long de la côte Nord d'Haïti, il y a environ 2 Ma (segment 5; Figure VIII.2), les canyons sous-marins ont progressivement été coupés de l'apport continental. De plus, le soulèvement induit par l'activité des failles inverses, associé au front de déformation créé par la collision pliocène, a perturbé le profil de stabilité de ces canyons, conduisant à leur inactivation progressive et à des géométries complexes de décalages (Figures VI.3 et 4, chapitre VI).

Notre étude des unités sédimentaires le long de la côte Nord d'Haïti, montre clairement la variabilité d'Ouest en Est de la déformation de l'unité U4 (Pliocène supérieur, Figure VII.2). Cette variabilité semble être étroitement liée à la différence d'épaisseur sédimentaire et à la présence du MTD en profondeur uniquement dans le domaine Est au front des côtes d'Haïti. Comme nous l'avons discuté dans nos deux derniers articles (Chapitres VI et VII), ce dépôt semble influencer la déformation de cette unité récente, engendrant une morphologie de fonds marins irrégulière. Cette topographie complexe est remodelée par les courants de fonds qui sont à l'origine de la sédimentation de type contouritique et turbiditiques et de la diversité de structures érosives/dépositionnelles observées. Ces phénomènes donnent naissance aux dépressions observées sur le fond marin au Nord d'Haïti (Figure VII. 3, chapitre VII). Ces observations ont été complétées par des analyses sédimentologiques et géochimiques effectuées sur des carottes sédimentaires. Ces analyses mettent en évidence des dépôts sédimentaires spécifiques, dominés par une sédimentation typique d'un système de dépôt contouritique.

Sur quelles structures sont accommodées la composante compressive de la déformation et quelle sédimentation y est associée ?

Notre étude a aussi démontré que la composante compressive de la déformation le long de la Frontière Nord de la plaque Caraïbe est toujours active. Et, même si Cuba reste relativement bien fixée à la Plaque Nord-Américaine actuellement, certaines failles inverses près de la côte nord du bloc de Cuba oriental déforment les unités sismiques récentes, suggérant une activité tectonique localisée au front de déformation, en accord avec l'étude récente de Calais et al. (2023) dans la région de Cuba. Cette observation est renforcée par des séismes récents localisés le long de la faille du nord de Cuba (Figure VIII.1) (Calais et al., 2023). Cette structure majeure, auparavant peu documentée, a été mise en évidence grâce à nos profils sismiques et semble active le long du bloc de Cuba oriental jusqu'à la latitude de -77° (Figure VIII.1).

Dans le domaine occidental, près de Cuba, toute l'ancienne croûte océanique de la proto-Caraïbe semble avoir été subductée. La zone de fracture de Cuba (Cuba Fracture Zone) pourrait se situer directement sur le front de déformation, en juxtaposition avec la province carbonatée des Bahamas (Figure IV. 12. Chapitre IV) formant le front de déformation. Ainsi, la relique Jurassique de limite de plaques entre la plaque Amérique du Nord et Sud (et les croûtes océaniques de la Proto-Caraïbe et de l'Atlantique Central) aurait été responsable au Crétacé, de l'obduction de la croûte océanique à Cuba (limite entre les plaques Caraïbe et Nord Amérique) (Figure VIII.2).

Dans le domaine oriental, la déformation compressive se concentre sur le Prisme Nord Hispaniola, dont nous avons détaillé sa morphologie dans le chapitre VI. Dans ce domaine, nous sommes confrontés à une incertitude. Existe-t-il un slab sous l'île d'Hispaniola (Figure VIII.1) ? Si ce slab est connu à l'est d'Hispaniola, il n'est pas évident dans la partie ouest (e.g. Zurrunero et al 2020 ; Calais et al 2023).

S'agit-il d'une relique du slab de la proto-Caraïbe ou de la lithosphère océanique de la plaque NAM ? L'hypothèse de la croûte océanique de l'Atlantique central nous semble la plus probable. Nous proposons qu'une zone de fracture pourrait séparer la croûte océanique de l'Atlantique central à proximité du front de déformation (dans le sous-bassin Caicos) de la croûte continentale amincie située plus au Nord et sur laquelle repose les bancs de Bahamas à l'est du banc d'Inagua (Figure VIII.1). Ainsi, pour le moment, le terme "croûte transitionnelle" semble approprié (Figure VIII.1).

Y a-t-il une zone d'accommodation entre ces deux types distincts de lithosphère ? Cette accommodation pourrait-elle être superficielle (au niveau crustal) ou plus profonde (lithosphérique tel que "slab tear") ? À l'ouest, nous avons les Bahamas en collision, tandis qu'à l'est se situe une zone de lithosphère océanique et transitionnelle (Figure VIII.1). Les épencentres des séismes (profondeurs 10 à 25km ; source USGS) liés à la crise sismique de 2018 s'alignent sur la zone proposée de transition de direction NE-SW à l'ouest de la tortue, de plus nous avons identifié une dépression sur cette même zone de transition que nous avons associée à des failles (Chapitre VI). Ces observations sont en faveur d'une d'accommodation de la déformation dans cette zone au moins à l'échelle crustale.

Plus à l'est, vers Porto Rico, la lithosphère océanique est en subduction, et une déchirure du slab (ou "slab tear") est proposée pour accommoder le changement de type de lithosphère en subduction entre le domaine de Porto Rico (lithosphère océanique) et notre domaine Est, où une lithosphère transitionnelle semble avoir du mal à subduire.

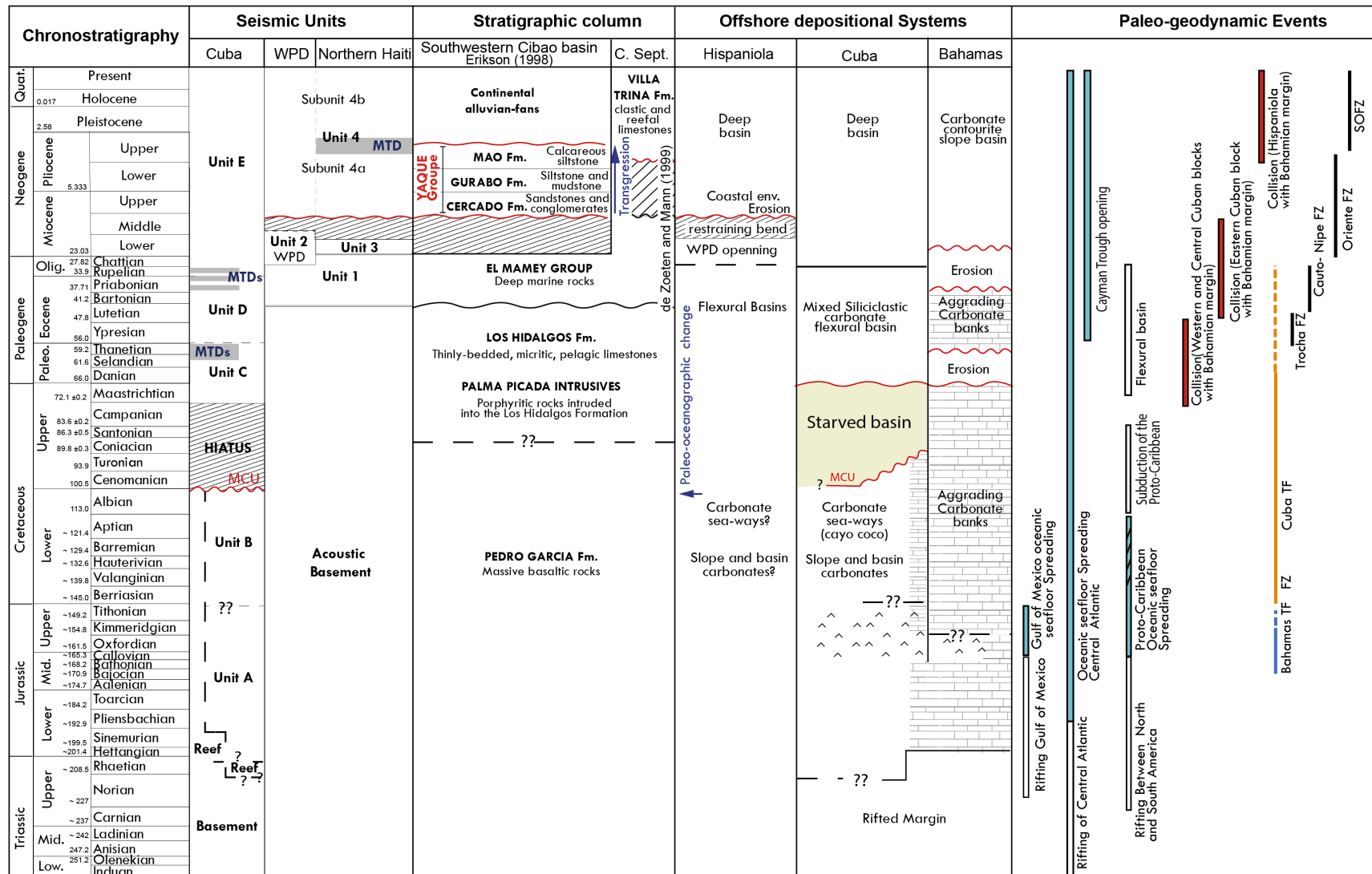


Figure VIII.4. Synthèse sismo-stratigraphique de la région orientale Cuba-Bahamas et Ouest Hispaniola, basée sur le levé sismique Haïti-Sis 2 et les puits publiés. Elle permet de corréler les systèmes de dépôt, les phases tectoniques et les événements paléogéodynamiques dans la région.

Les domaines tectoniques de Rodriguez-Zurrunero (CD, SSD, etc.) et les vecteurs du modèle de blocs de Calais et al 2023a) semblent coïncider avec les domaines que nous avons identifiés (Figure VIII.1). La zone de transition marque un changement de régime tectonique, passant d'un décrochement à une tectonique en oblique/transpression (ou "oblique underthrusting domain"). En allant vers Cuba, la collision est effective.

Une meilleure intégration des données géologiques, géophysiques et tectoniques est toujours nécessaire à plus grande échelle pour mieux comprendre les déformations, les systèmes sédimentaires, la cinématique et les interactions lithosphériques dans cette partie des Caraïbes.

Pour conclure, les trois objectifs majeurs de cette thèse étaient les suivants :

- 1) identifier les phases de déformation qui affectent la couverture sédimentaire en mer, leur style structural, leur impact régional et leur évolution ;
- 2) contraindre l'histoire de la déformation de la limite nord de la plaque Caraïbe dans son ensemble, en prenant en compte le domaine insulaire et ;
- 3) caractériser l'interaction entre la dynamique sédimentaire et la déformation en reliant la tectonique régionale et les processus sédimentaires actifs.

La corrélation des événements tectoniques et stratigraphiques a pu être établie entre les différents domaines marins et à terre (insulaire). Elle révèle que les principales phases de déformation observées à terre sont observées dans les unités sédimentaires en mer, au large de la côte nord de Cuba Oriental jusqu'à la région au large de la côte nord haïtienne. Ainsi, nous avons pu répondre aux deux premiers objectifs fixés. Quant au troisième objectif, nos études des séries sédimentaires au large de la côte nord d'Hispaniola ont démontré que l'évolution géologique de ces séries met en évidence les interactions complexes entre les phénomènes tectoniques et les processus sédimentaires. Ces interactions jouent un rôle prépondérant dans la configuration actuelle de cette région et dans la distribution des éléments géomorphologiques du fond marin, éclairant ainsi l'interrelation entre la dynamique sédimentaire, la déformation, et la tectonique régionale.

VIII.2. Les perspectives

Cette recherche a significativement contribué à notre compréhension de l'évolution de la limite actuelle au nord de la plaque Caraïbe. Néanmoins, certains points non résolus concernant la dynamique de cette frontière de plaques et l'évolution des systèmes sédimentaires associées nécessitent une attention approfondie dans les travaux futurs.

1. Selon nos observations, la province carbonatée des Bahamas, au large de Cuba, semblent organisée sur des blocs basculés d'une croûte continentale amincie de l'Atlantique central.

Toutefois, le sont-ils plus à l'est ? Les Bancs des Bahamas reposent-ils également sur une croûte de même nature ? Une zone d'accommodation, qu'elle soit superficielle (au niveau crustal) ou plus profonde (au niveau lithosphérique, telle qu'un « slab tear »), pourrait-elle se situer entre les deux types de lithosphère ? D'un côté, à l'ouest, nous avons la province carbonatée avec une croûte continentale riftée en collision, et de l'autre, à l'est, une lithosphère de nature différente, plutôt océanique. La présence d'une zone de transition clairement identifiée dans notre étude à l'ouest de l'île de la Tortue a soulevé ces questions. Cependant, la présence éventuelle d'un panneau plongeant sous

Hispaniola reste une énigme. Il serait intéressant d'entreprendre des acquisitions de sismique réfraction, tant terrestres que maritimes. L'analyse de ces données de sismique grand-angle au large de l'île d'Hispaniola et de Cuba permettrait l'élaboration de modèles tomographiques qui pourraient fournir des informations sur la structure sismique des plaques en convergence et leur géométrie. De plus, ils offriraient des informations sur la nature et la structure profonde de la lithosphère, et permettraient de déterminer la présence ou l'absence d'un panneau plongeant sous l'île d'Hispaniola, qui pourrait être un vestige de l'océan proto-caraïbe. Une telle découverte aurait des implications sur notre compréhension de la déformation actuelle, de la distribution de la sismicité et soulignerait le rôle de la structure crustale dans la dynamique de cette collision oblique.

2. Les séismes le long de cette frontière de plaques sont majoritairement dans le domaine marin, d'où la nécessité d'étudier les caractéristiques des fonds marins pour une meilleure compréhension de ces phénomènes. Malgré les avancées remarquables dans l'exploration des grandes failles terrestres, notamment après le séisme de 2010 en Haïti et la mise en place du réseau GPS sur Hispaniola et Cuba, les failles sous-marines n'ont pas bénéficié d'une attention équivalente. Dans les perspectives de travaux futurs, l'adoption d'instruments spécifiquement conçus pour mesurer la sismicité sur le fond sous-marin, comme les sismomètres fond de mer (OBS, pour l'acronyme anglais "ocean-bottom seismometer"), est importante. Ceci permettrait non seulement de mesurer la sismicité, mais aussi de comprendre comment la sismicité se propage dans la couverture sédimentaire et comment celle-ci réagit à cette déformation. D'autre part, il faut pouvoir réaliser des prélèvements d'échantillons sous la surface du fond océanique, ce qui implique des forages océaniques profonds, absents dans la région. Ce travail de recherche et d'exploration est essentiel pour mieux comprendre et prévoir les séismes le long de cette frontière de plaques et, en fin de compte, pour renforcer la sécurité des populations vivant dans ces régions exposées aux aléas.
3. Au cours de notre recherche, nous avons apporté de nombreuses réponses concernant les processus sédimentaires actifs au large de la côte nord d'Haïti. Toutefois, plusieurs carottes sédimentaires recueillies lors des missions HAITISIS 1 et BGF restent à étudier. L'analyse de ces échantillons pourrait nous éclairer davantage sur les processus sédimentaires et nous offrir une caractérisation plus précise des conditions environnementales en mer autour d'Haïti. Il serait donc judicieux d'examiner minutieusement ces carottes pour qu'elles viennent compléter et enrichir nos conclusions relatives au système sédimentaire contouritique identifié au large du nord d'Haïti. En outre, une étude micropaléontologique approfondie de ces échantillons serait précieuse pour raffiner le contexte chrono-stratigraphique et affiner la connaissance du contexte paléo-environnemental de cette région maritime. Dans une optique idéale, la collecte de nouvelles carottes sédimentaires à des emplacements stratégiques, tels qu'au centre des dépressions et sur les sommets des rides qui l'entourent, pourrait perfectionner notre compréhension des mécanismes de formation de ces structures.

REFERENCES BIBLIOGRAPHIQUES

- Acton, G., Galbrun, B., & King, J. (2000). Paleolatitude of the Caribbean Plate since the Late Cretaceous. *Proceedings of the Ocean Drilling Program: Scientific Results*, 165, 149-173. <https://doi.org/10.2973/odp.proc.sr.165.001.2000>
- Alvarado, G. E., Denyer, P., & Sinton, C. W. (1997). The 89 Ma Tortugal komatiitic suite, Costa Rica : Implications for a common geological origin of the Caribbean and Eastern Pacific region from a mantle plume. *Geology*, 25(5), 439-442. [https://doi.org/10.1130/0091-7613\(1997\)025<0439:TMTKSC>2.3.CO;2](https://doi.org/10.1130/0091-7613(1997)025<0439:TMTKSC>2.3.CO;2)
- Anselmetti, F. S., Eberli, G. P., & Ding, Z.-D. (2000). From the Great Bahama Bank into the Straits of Florida : A margin architecture controlled by sea-level fluctuations and ocean currents. *GSA Bulletin*, 112(6), 829-844. [https://doi.org/10.1130/0016-7606\(2000\)112<829:FTGBBI>2.0.CO;2](https://doi.org/10.1130/0016-7606(2000)112<829:FTGBBI>2.0.CO;2)
- Augustin, J. M., Le Suave, R., Lurton, X., Voisset, M., Dugelay, S., & Satra, C. (1996). Contribution of the multibeam acoustic imagery to the exploration of the sea-bottom. *Marine Geophysical Researches*, 18(2), 459-486. <https://doi.org/10.1007/BF00286090>
- Authemayou, C., Nuñez, A., Pedoja, K., Peñalver, L., Chauveau, D., Dunán-Avila, P., Martin-Izquierdo, D., de Gelder, G., Husson, L., Castellanos Abella, E., Benítez Frómata, P. de J., & Pastier, A.-M. (2023). Oblique Collision of the Bahamas Platform at the Northern Boundary of the Caribbean Plate Recorded by the Late Cenozoic Coastal Terraces of SE Cuba. *Tectonics*, 42(8), e2023TC007806. <https://doi.org/10.1029/2023TC007806>
- Bader, R., Gerard, R., Benson, W., Bolli, H., Hay, W., Rothwell, W., Ruef, M., Riedel, W., & Sayles, F. (1970). Deep Sea Drilling Project Leg 4—1. Introduction (p. 3-15). <https://doi.org/10.2973/dsdp.proc.4.101.1970>
- Ball, M. (1967). Tectonic control of the configuration of the Bahama Banks : Gulf Coast. *Association of Geological Transactions*, 17, 265-267.
- Benford, B., DeMets, C., & Calais, É. (2012). GPS estimates of microplate motions, northern Caribbean : Evidence for a Hispaniola microplate and implications for earthquake hazard. *Geophysical Journal International*, 191(2), 481-490. <https://doi.org/10.1111/j.1365-246X.2012.05662.x>
- Bird, D., Hall, S., Burke, K., Casey, J., & Sawyer, D. (2007). Early Central Atlantic Ocean seafloor spreading history. *Geosphere*, 3. <https://doi.org/10.1130/GES00047.1>
- Boschman, L. M., van Hinsbergen, D. J. J., Torsvik, T. H., Spakman, W., & Pindell, J. L. (2014). Kinematic reconstruction of the Caribbean region since the Early Jurassic. *Earth-Science Reviews*, 138, 102-136. <https://doi.org/10.1016/j.earscirev.2014.08.007>
- Bouysse, P., Garcia-Reyes, A., Lépinay, B. M. de, Ellouz-Zimmermann, N., & Pubellier, M. (2020). Structural Map of the Caribbean, scale 1:4M. <https://cnrs.hal.science/hal-03080774>
- Bowland, C. L., & Rosencrantz, E. (1988). Upper crustal structure of the western Colombian Basin, Caribbean Sea. *GSA Bulletin*, 100(4), 534-546. [https://doi.org/10.1130/0016-7606\(1988\)100<0534:UCSOTW>2.3.CO;2](https://doi.org/10.1130/0016-7606(1988)100<0534:UCSOTW>2.3.CO;2)
- Brandes, C., & Winsemann, J. (2018). From incipient island arc to doubly-vergent orogen : A review of geodynamic models and sedimentary basin-fills of southern Central America. *Island Arc*, 27. <https://doi.org/10.1111/iar.12255>
- Braunmiller, J., Thompson, G., & McNutt, S. R. (2017). The January 2014 Northern Cuba Earthquake Sequence—Unusual Location and Unexpected Source Mechanism Variability. 2017, S53B-0709.
- Bryant, W. R., Meyerhoff, A. A., Brown, N. K., Jr., Furrer, M. A., Pyle, T. E., & Antoine, J. W. (1969). Escarpments, Reef Trends, and Diapiric Structures, Eastern Gulf of

- Mexico1. *AAPG Bulletin*, 53(12), 2506-2542. <https://doi.org/10.1306/5D25C971-16C1-11D7-8645000102C1865D>
- Burke, K. (1988). Tectonic Evolution of the Caribbean. *Annual Review of Earth and Planetary Sciences*, 16(1), 201-230. <https://doi.org/10.1146/annurev.earth.16.050188.001221>
- Burke, K., Cooper, C., Dewey, J. F., Mann, P., & Pindell, J. L. (1984). Caribbean tectonics and relative plate motions. 162, 31-64. <https://doi.org/10.1130/MEM162-p31>
- Burke, K., Fox, P. J., & Şengör, A. M. C. (1978). Buoyant ocean floor and the evolution of the Caribbean. *Journal of Geophysical Research: Solid Earth*, 83(B8), 3949-3954. <https://doi.org/10.1029/JB083iB08p03949>
- Calais, É., Gonzales, O., Arango-Arias, E. D., Moreno, B., Clares, R. P., Cutie, M., Diez, E., Montenegro, C., Roche, E. R., Garcia, J., Castellanos, E., & Symithe, S. (2023). Current Deformation Along the Northern Caribbean Plate Boundary from Gns Measurements in Cuba (SSRN Scholarly Paper 4537779). <https://doi.org/10.2139/ssrn.4537779>
- Calais, É., & Mercier De Lépinay, B. (1991). From transtension to transpression along the northern Caribbean plate boundary off Cuba : Implications for the Recent motion of the Caribbean plate. *Tectonophysics*, 186(3), 329-350. [https://doi.org/10.1016/0040-1951\(91\)90367-2](https://doi.org/10.1016/0040-1951(91)90367-2)
- Calais, É., & Mercier De Lépinay, B. (1992). La limite de plaques décrochante Nord Caraïbe en Hispaniola : Évolution paléogéographique et structurale cénozoïque. *Bull. Soc. géol.*, 3(163), 309-324.
- Calais, É., & Mercier De Lépinay, B. (1995). Strike-slip tectonic processes in the northern Caribbean between Cuba and Hispaniola (Windward Passage). *Marine Geophysical Researches*, 17(1), 63-95. <https://doi.org/10.1007/BF01268051>
- Calais, E., Symithe, S., & de Lépinay, B. (2022). Strain Partitioning within the Caribbean–North America Transform Plate Boundary in Southern Haiti, Tectonic and Hazard Implications. *Bulletin of the Seismological Society of America*, 113. <https://doi.org/10.1785/0120220121>
- Calais, É., Symithe, S., Mercier de Lépinay, B., & Prépetit, C. (2016). Plate boundary segmentation in the northeastern Caribbean from geodetic measurements and Neogene geological observations. *Comptes Rendus Geoscience*, 348(1), 42-51. <https://doi.org/10.1016/j.crte.2015.10.007>
- Corbeau, J., Rolandone, F., Leroy, S., Meyer, B., Mercier De Lépinay, B., Ellouz-Zimmermann, N., & Momplaisir, R. (2016). How transpressive is the northern Caribbean plate boundary? *Tectonics*, 35(4), 1032-1046. <https://doi.org/10.1002/2015TC003996>
- Cotilla-Rodríguez, M. O. (2021). Historia de la sismicidad del segmento Islas Caimán-Cabo Cruz (Cuba), en el marco de la zona de entre placas Norteamérica-Caribe. *Revista Tierra*, 1(1), Article 1. https://revistatierra.unan.edu.ni/index.php/revista_tierra/article/view/25
- Cruz-Orosa, I., Sàbat, F., Ramos, E., Rivero, L., & Vázquez-Taset, Y. M. (2012). Structural evolution of the La Trocha fault zone : Oblique collision and strike-slip basins in the Cuban Orogen. *Tectonics*, 31(5). <https://doi.org/10.1029/2011TC003045>
- De Zoeten, R., & Mann, P. (1991). Structural geology and Cenozoic tectonic history of the central Cordillera Septentrional, Dominican Republic (Vol. 262, p. 265-279). <https://doi.org/10.1130/SPE262-p265>
- Demets, C. (1992). Oblique convergence and deformation along the Kuril and Japan Trenches. <https://doi.org/10.1029/92JB01306>
- DeMets, C., Jansma, P. E., Mattioli, G. S., Dixon, T. H., Farina, F., Bilham, R., Calais, É., & Mann, P. (2000). GPS geodetic constraints on Caribbean-North America Plate Motion. *Geophysical Research Letters*, 27(3), 437-440. <https://doi.org/10.1029/1999GL005436>

- Denyer, P., Baumgartner, P. O., & Gazel, E. (2006). Characterization and tectonic implications of Mesozoic-Cenozoic oceanic assemblages of Costa Rica and Western Panama. *Journal of South American Earth Sciences*, 28(4), 219-236. <https://doi.org/10.1344/105.000000367>
- Denyer, P., & Gazel, E. (2009). The Costa Rican Jurassic to Miocene oceanic complexes : Origin, tectonics and relations. *Journal of South American Earth Sciences*, 28(4), 429-442. <https://doi.org/10.1016/j.jsames.2009.04.010>
- Desreumaux, C. (1987). Contribution à l'étude géologique des régions centrales et méridionales d'Haïti (Grandes Antilles) du Crétacé à l'Actuel [Ph.D. Thesis, Univ.].
- de Zoeten, R., & Mann, P. (1991). Structural geology and Cenozoic tectonic history of the central Cordillera Septentrional, Dominican Republic. In *Geological Society of America Special Papers* (Vol. 262, p. 265-280). Geological Society of America. <https://doi.org/10.1130/SPE262-p265>
- de Zoeten, R., & Mann, P. (1999). Chapter 11 Cenozoic el mamey group of northern hispaniola : A sedimentary record of subduction, collisional and strike-slip events within the north America-Caribbean plate boundary zone. In P. Mann (Éd.), *Sedimentary Basins of the World* (Vol. 4, p. 247-286). Elsevier. [https://doi.org/10.1016/S1874-5997\(99\)80045-8](https://doi.org/10.1016/S1874-5997(99)80045-8)
- Diebold, J., Driscoll, N., & EW-9501 Science Team. (1999). Chapter 19 New insights on the formation of the caribbean basalt province revealed by multichannel seismic images of volcanic structures in the Venezuelan basin. In P. Mann (Éd.), *Sedimentary Basins of the World* (Vol. 4, p. 561-589). Elsevier. [https://doi.org/10.1016/S1874-5997\(99\)80053-7](https://doi.org/10.1016/S1874-5997(99)80053-7)
- Diebold, J., Stoffa, P., Buhl, P., & Truchan, M. (1981). Venezuela Basin crustal structure. *Journal of Geophysical Research*, 86, 7901-7923. <https://doi.org/10.1029/JB086iB09p07901>
- Dietz, R. S. (1973). Morphologic fits of North America/Africa and Gondwana : A review. In Tarling, D. H., Runcorn, S. K, eds., *Implications of Continental Drift to the Earth Sciences* : Academic Press (p. 1865-1872).
- Dietz, R. S., Holden, J. C., & Sproll, W. P. (1970). Geotectonic Evolution and Subsidence of Bahama Platform | *GSA Bulletin* | GeoScienceWorld. Geological Society of America Bulletin, 81, 1915-1928.
- Dolan, J. F., Mullins, H. T., & Wald, D. J. (1998). Active tectonics of the north-central Caribbean : Oblique collision, strain partitioning, and opposing subducted slabs. In J. F. Dolan & P. Mann, *Active Strike-Slip and Collisional Tectonics of the Northern Caribbean Plate Boundary Zone*. Geological Society of America. <https://doi.org/10.1130/0-8137-2326-4.1>
- Drake, C. L., Heirtzler, J., & Hirshman, J. (1963). Magnetic Anomalies off Eastern North America. *Journal of Geophysical Research* (1896-1977), 68(18), 5259-5275. <https://doi.org/10.1029/j.2156-2202.1963.tb00004.x>
- Dubreuilh, P. (1982). Contribution à l'étude du bassin Néogène du Plateau Central d'Haïti [Sc.D. Thesis, Univ.]. Bordeaux I.
- Duncan, R. A., & Hargraves, R. B. (1984). Plate tectonic evolution of the Caribbean region in the mantle reference frame. In *Geological Society of America Memoirs* (Vol. 162, p. 81-94). Geological Society of America. <https://doi.org/10.1130/MEM162-p81>
- Eberli, G. P., & Ginsburg, R. N. (1987). Segmentation and coalescence of Cenozoic carbonate platforms, northwestern Great Bahama Bank. *Geology*, 15(1), 75-79. [https://doi.org/10.1130/0091-7613\(1987\)15<75:SACOCC>2.0.CO;2](https://doi.org/10.1130/0091-7613(1987)15<75:SACOCC>2.0.CO;2)
- Echevarria-Rodriguez, G., Hernandez-Perez, G., Lopez-Quintero, J. O., Lopez-Rivera, J. G., Rodriguez-Hernandez, R., Sanchez-Arango, J. R., Socorro-Trujillo, R., Tenreyro-Perez, R., & Yparraguirre-Pena, J. L. (1991). Oil and Gas Exploration in Cuba. *Journal of*

- Petroleum Geology, 14(2), 259-274. <https://doi.org/10.1111/j.1747-5457.1991.tb00311.x>
- Edgar, N. T., Saunders, J. B., & et al. (1973). Initial Reports of the Deep Sea Drilling Project, 15. 15. <https://doi.org/10.2973/dsdp.proc.15.1973>
- Ellouz-Zimmermann, N., & Beaufort, L. (2015). CARACALHIS / HAÏTI-BGF cruise, RV L'Atalante. <https://doi.org/10.17600/15006900>
- Erikson, J., Pindell, J., Karner, G., Sonder, L., Fuller, E., & Dent, L. (1998). Neogene Sedimentation and Tectonics in the Cibao Basin and Northern Hispaniola : An Example of Basin Evolution Near A Strike-Slip-Dominated Plate Boundary. *The Journal of Geology*, 106. <https://doi.org/10.1086/516036>
- ¿Es activa la falla Cauto-Nipe? (2021). Geoscience, La Habana, Cuba.
- Escuder-Virueite, J., Fernández, F. J., Valera, F. P., & Medialdea, A. (2023). Present-Day Caribbean-North American Oblique Convergence Through the Ocoa-Bonao-La Guacara Fault Zone, Southern Central Hispaniola : A Transition Zone Between Oceanic Subduction and Arc-Oceanic Plateau Collision. *Tectonics*, 42(4), e2022TC007618. <https://doi.org/10.1029/2022TC007618>
- Escuder-Virueite, J., & Pérez, Y. (2020). Neotectonic structures and stress fields associated with oblique collision and forearc sliver formation in northern Hispaniola : Implications for the seismic hazard assessment. *Tectonophysics*, 784, 228452. <https://doi.org/10.1016/j.tecto.2020.228452>
- Escuder-Virueite, J., Suárez-Rodríguez, A., Gabites, J., & Pérez-Estaún, A. (2015). The Imbert Formation of northern Hispaniola : A tectono-sedimentary record of arc-continent collision and ophiolite emplacement in the northern Caribbean subduction-accretionary prism. *Solid Earth Discussions*, 7(2), 1827-1876. <https://doi.org/10.5194/sed-7-1827-2015>
- Escuder-Virueite, J., Valverde-Vaquero, P., Rojas-Agramonte, Y., Gabites, J., Castillo-Carrión, M., & Pérez-Estaún, A. (2013). Timing of deformational events in the Río San Juan complex : Implications for the tectonic controls on the exhumation of high-P rocks in the northern Caribbean subduction-accretionary prism. *Lithos*, 177, 416-435. <https://doi.org/10.1016/j.lithos.2013.07.006>
- Escuder-Virueite, J., Valverde-Vaquero, P., Rojas-Agramonte, Y., Jabites, J., & Pérez-Estaún, A. (2013). From intra-oceanic subduction to arc accretion and arc-continent collision : Insights from the structural evolution of the Río San Juan metamorphic complex, northern Hispaniola. *Journal of Structural Geology*, 46, 34-56. <https://doi.org/10.1016/j.jsg.2012.10.008>
- Field, R. M. & Collaborators. (1931). Geology of the Bahamas. *GSA Bulletin*, 42(3), 759-784. <https://doi.org/10.1130/GSAB-42-759>
- Frisch, W., Meschede, M., & Sick, M. (1992). Origin of the Central American ophiolites : Evidence from paleomagnetic results. *Geological Society of America Bulletin*, 104(10), 1301-1314. [https://doi.org/10.1130/0016-7606\(1992\)104<1301:OOTCAO>2.3.CO;2](https://doi.org/10.1130/0016-7606(1992)104<1301:OOTCAO>2.3.CO;2)
- Furrázola-Bermúdez, G. (1964). *Geología de Cuba*. Editorial Nacional de Cuba.
- García Pelaez, J. A., Alvarez, L., Peruzza, L., & Rebez, A. (2003). Seismic Hazard Maps for Cuba and Surrounding Areas. *Bulletin of the Seismological Society of America*, 93, 2563-2590. <https://doi.org/10.1785/0120020144>
- García-Casco, A., Iturralde-Vinent, M. A., & Pindell, J. (2008). Latest Cretaceous Collision/Accretion between the Caribbean Plate and Caribbeana : Origin of Metamorphic Terranes in the Greater Antilles. *International Geology Review*, 50(9), 781-809. <https://doi.org/10.2747/0020-6814.50.9.781>

- García-Reyes, A., & Dymant, J. (2021). Structure, age, and origin of the Caribbean Plate unraveled. *Earth and Planetary Science Letters*, 571, 117100. <https://doi.org/10.1016/j.epsl.2021.117100>
- Garroq, C., Lallemand, S., Marcaillou, B., Lebrun, J.-F., Padron, C., Klingelhoefer, F., Laigle, M., Münch, P., Gay, A., Schenini, L., Beslier, M.-O., Cornée, J.-J., Mercier de Lépinay, B., Quillévéré, F., BouDagher-Fadel, M., & Team, the G. cruise. (2021). Genetic Relations Between the Aves Ridge and the Grenada Back-Arc Basin, East Caribbean Sea. *Journal of Geophysical Research: Solid Earth*, 126(2), e2020JB020466. <https://doi.org/10.1029/2020JB020466>
- Gaumet, F., Letouzey, J., & Sanchez, J. R. (2004). Paleogeographic Evolution of the Southeastern Region of the Gulf of Mexico (NW Cuba – Deep Waters). AAPG International Conference, Cancun, Mexico. https://www.searchanddiscovery.com/pdfz/documents/abstracts/2004intl_cancun/extended/A90219.pdf.html
- Gazel, E., Flores, K., & Carr, M. (2021). Architectural and Tectonic Control on the Segmentation of the Central American Volcanic Arc. *Annual Review of Earth and Planetary Sciences*, 49. <https://doi.org/10.1146/annurev-earth-082420-055108>
- Geldmacher, J., Hanan, B. B., Blichert-Toft, J., Harpp, K., Hoernle, K., Hauff, F., Werner, R., & Kerr, A. C. (2003). Hafnium isotopic variations in volcanic rocks from the Caribbean Large Igneous Province and Galápagos hot spot tracks. *Geochemistry, Geophysics, Geosystems*, 4(7). <https://doi.org/10.1029/2002GC000477>
- Geldmacher, J., Hoernle, K., van den Bogaard, P., Hauff, F., & Klügel, A. (2008). Age and Geochemistry of the Central American Forearc Basement (DSDP Leg 67 and 84): Insights into Mesozoic Arc Volcanism and Seamount Accretion on the Fringe of the Caribbean LIP. *Journal of Petrology*, 49, 1781-1815. <https://doi.org/10.1093/petrology/egn046>
- Ghosh, N., Hall, S. A., & Casey, J. F. (1984). Seafloor spreading magnetic anomalies in the Venezuelan Basin. In W. E. Bonini, R. B. Hargraves, & R. Shagam (Éds.), *The Caribbean-South American Plate Boundary and Regional Tectonics* (Vol. 162, p. 0). Geological Society of America. <https://doi.org/10.1130/MEM162-p65>
- Gordon, M. B., Mann, P., Cáceres, D., & Flores, R. (1997). Cenozoic tectonic history of the North America-Caribbean plate boundary zone in western Cuba. *Journal of Geophysical Research: Solid Earth*, 102(B5), 10055-10082. <https://doi.org/10.1029/96JB03177>
- Gorney, D., Escalona, A., Mann, P., Magnani, M. B., & BOLIVAR Study Group. (2007). Chronology of Cenozoic tectonic events in western Venezuela and the Leeward Antilles based on integration of offshore seismic reflection data and on-land geology. *AAPG Bulletin*, 91(5), 653-684. <https://doi.org/10.1306/11280606002>
- Guevara, N., García-Reyes, A., & Arnaiz-Rodríguez, M. (2013). Magnetic anomalies in the Eastern Caribbean. *International Journal of Earth Sciences*, 102, 591-506. <https://doi.org/10.1007/s00531-012-0828-6>
- Hauff, F., Hoernle, K., Van den Bogaard, P., Guillermo, A., & Garbe-Schönberg, D. (2000). Age and geochemistry of basaltic complexes in Western Costa Rica : Contributions to the geotectonic evolution of Central America. *Geochemistry Geophysics Geosystems - GEOCHEM GEOPHYS GEOSYST*, 1. <https://doi.org/10.1029/1999GC000020>
- Hayman, N. W., Grindlay, N. R., Perfit, M. R., Mann, P., Leroy, S., & Mercier de Lépinay, B. (2011). Oceanic core complex development at the ultraslow spreading Mid-Cayman Spreading Center. *Geochemistry, Geophysics, Geosystems*, 12(3). <https://doi.org/10.1029/2010GC003240>

- Helsley, C. E., & Steiner, M. B. (1968). Evidence for long intervals of normal polarity during the cretaceous period. *Earth and Planetary Science Letters*, 5, 325-332. [https://doi.org/10.1016/S0012-821X\(68\)80060-3](https://doi.org/10.1016/S0012-821X(68)80060-3)
- Hoernle, K., Van den Bogaard, P., Werner, R., Lissinna, B., Hauff, F., Guillermo, A., & Garbe-Schönberg, D. (2002). Missing history (16-71 Ma) of the Galapagos hotspot: Implications for the tectonic and biological evolution of the Americas. *Geology*, 30. [https://doi.org/10.1130/0091-7613\(2002\)030<0795:MHMOTG>2.0.CO;2](https://doi.org/10.1130/0091-7613(2002)030<0795:MHMOTG>2.0.CO;2)
- Iturralde-Vinent, M. A. (1994). Cuban Geology : A New Plate-Tectonic Synthesis. *Journal of Petroleum Geology*, 17(1), 39-69. <https://doi.org/10.1111/j.1747-5457.1994.tb00113.x>
- Iturralde-Vinent, M. A. (2003). Ensayo sobre la paleogeografía del Cuaternario de Cuba. 74.
- Iturralde-Vinent, M. A. (1998). Sinopsis de la Constitución Geológica de Cuba. /paper/Sinopsis-de-la-Constituci%C3%B3n-Geol%C3%B3gica-de-Cuba-Vinent/d0d19ca942426b21834e5fb0eaf2eee94ded3fe4
- Iturralde-Vinent, M. A., & Gahagan, L. (2002). (PDF) Late Eocene to Middle Miocene tectonic evolution of the Caribbean : Some principles and their implications for plate tectonic modeling. ResearchGate. https://www.researchgate.net/publication/260512455_Late_Eocene_to_Middle_Miocene_tectonic_evolution_of_the_Caribbean_Some_principles_and_their_implications_for_plate_tectonic_modeling
- Iturralde-Vinent, M. A., García-Casco, A., Rojas-Agramonte, Y., Proenza, J. A., Murphy, J. B., & Stern, R. J. (2016). The geology of Cuba : A brief overview and synthesis. *GSA Today*, 4-10. <https://doi.org/10.1130/GSATG296A.1>
- Iturralde-Vinent, M., & Macphee, R. (1999). Paleogeography of the Caribbean Region : Implications for Cenozoic biogeography. *Bulletin of the American Museum of Natural History*, 238, 1-95.
- Iturralde-Vinent, M., Otero, C., Garcia-Casco, A., & van Hinsbergen, D. (2008). Paleogene Foredeep Basin Deposits of North-Central Cuba : A Record of Arc-Continent Collision between the Caribbean and North American Plates. *International Geology Review*, 50. <https://doi.org/10.2747/0020-6814.50.10.863>
- James, K. (2009). In situ origin of the Caribbean : Discussion of data. Geological Society, London, Special Publications, 328, 77-125. <https://doi.org/10.1144/SP328.3>
- Jany, I., Scanlon, K. M., & Mauffret, A. (1990). Geological interpretation of combined Seabeam, Gloria and seismic data from Anegada Passage (Virgin Islands, north Caribbean). *Marine Geophysical Researches*, 12(3), 173-196. <https://doi.org/10.1007/BF02266712>
- Kearey, P., Brooks, M., & Hill, I. (1984). An introduction to geophysical exploration. <https://www.semanticscholar.org/paper/An-introduction-to-geophysical-exploration-Kearey-Brooks/c0689fe151243c166bf27436501a266eb5074ab8>
- Kerr, A. C., Iturralde-Vinent, M. A., Saunders, A. D., Babbs, T. L., & Tarney, J. (1999). A new plate tectonic model of the Caribbean : Implications from a geochemical reconnaissance of Cuban Mesozoic volcanic rocks. *Geological Society of America Bulletin*, 111, 1581. [https://doi.org/10.1130/0016-7606\(1999\)111<1581:ANPTMO>2.3.CO;2](https://doi.org/10.1130/0016-7606(1999)111<1581:ANPTMO>2.3.CO;2)
- Kerr, A. C., Tarney, J., Marriner, G. F., Klaver, G. T., Saunders, A. D., & Thirlwall, M. F. (1996). The geochemistry and petrogenesis of the late-Cretaceous picrites and basalts of Curacao, Netherlands Antilles : A remnant of an oceanic plateau. *Contributions to Mineralogy and Petrology*, 124(1), 29-43.
- Kerr, A. C., Tarney, J., Marriner, G. F., Nivia, A., Klaver, G. T., & Saunders, A. D. (1996). The geochemistry and tectonic setting of late Cretaceous Caribbean and Colombian volcanism. *Journal of South American Earth Sciences*, 9(1-2), 111.

- Kerr, A., White, R., Thompson, P., Tarney, J., & Saunders, A. (2003). No Oceanic Plateau - No Caribbean Plate? The Seminal Role of an Oceanic Plateau in Caribbean Plate Evolution. In AAPG Mem. (Vol. 79, p. 126-168). <https://doi.org/10.1306/M79877C6>
- Khudoley, K. M. (1967). Principal Features of Cuban Geology. AAPG Bulletin, 51. <https://doi.org/10.1306/5D25C0BF-16C1-11D7-8645000102C1865D>
- Klitgord, K. D., Popenoe, P., & Schouten, H. (1984). Florida: A Jurassic transform plate boundary. *Journal of Geophysical Research: Solid Earth*, 89(B9), 7753-7772. <https://doi.org/10.1029/JB089iB09p07753>
- Kroehler, M., Escalona, A., & Christeson, G. (2011). Late Cretaceous-Miocene diachronous onset of back thrusting along the South Caribbean deformed belt and its importance for understanding processes of arc collision and crustal growth. *Tectonics*, 30. <https://doi.org/10.1029/2011TC002918>
- Laó-Dávila, D. A. (2014). Collisional zones in Puerto Rico and the northern Caribbean. *Journal of South American Earth Sciences*, 54, 1-19. <https://doi.org/10.1016/j.jsames.2014.04.009>
- Lapierre, H., Bosch, D., Dupuis, V., Polvé, M., Maury, R. C., Hernandez, J., Monié, P., Yeghicheyan, D., Jaillard, E., Tardy, M., De Lépinay, B. M., Mamberti, M., Desmet, A., Keller, F., & Sénebier, F. (2000). Multiple plume events in the genesis of the peri-Caribbean Cretaceous oceanic plateau province. *Journal of Geophysical Research: Solid Earth*, 105(B4), 8403-8421. <https://doi.org/10.1029/1998JB900091>
- Leroy, S. (2012). HAITI-SIS cruise, L'Atalante R/V. <https://doi.org/10.17600/12010070>
- Leroy, S., & Ellouz-Zimmermann, N. (2013). HAITI-SIS2 cruise, L'Atalante R/V. <https://doi.org/10.17600/13010080>
- Leroy, S., Ellouz-Zimmermann, N., Corbeau, J., Rolandone, F., Mercier De Lépinay, B., Meyer, B., Momplaisir, R., Bruña, J.-L. G., Battani, A., Baurion, C., Burov, E., Clouard, V., Deschamps, R., Gorini, C., Hamon, Y., Lafosse, M., Leonel, J., Pourhiet, L. L., Estrada, P. L., ... Muñoz, S. (2015). Segmentation and kinematics of the North America-Caribbean plate boundary offshore Hispaniola. *Terra Nova*, 27(6), 467-478. <https://doi.org/10.1111/ter.12181>
- Leroy, S., Mauffret, A., Patriat, P., & Mercier de Lépinay, B. (2000). An alternative interpretation of the Cayman trough evolution from a reidentification of magnetic anomalies. *Geophysical Journal International*, 141(3), 539-557. <https://doi.org/10.1046/j.1365-246x.2000.00059.x>
- Leroy, S., Mercier De Lépinay, B., Mauffret, A., & Pubellier, M. (1996). Structural and Tectonic Evolution of the Eastern Cayman Trough (Caribbean Sea) From Seismic Reflection Data. <https://doi.org/10.1306/64ED8796-1724-11D7-8645000102C1865D>
- Macdonald, R., Hawkesworth, C., & Heath, E. (2000). The Lesser Antilles volcanic chain: A study in arc magmatism. *Earth-science Reviews - EARTH-SCI REV*, 49, 1-76. [https://doi.org/10.1016/S0012-8252\(99\)00069-0](https://doi.org/10.1016/S0012-8252(99)00069-0)
- Malfait, B. T., & Dinkelman, M. G. (1972). Circum-Caribbean Tectonic and Igneous Activity and the Evolution of the Caribbean Plate. *GSA Bulletin*, 83(2), 251-272. [https://doi.org/10.1130/0016-7606\(1972\)83\[251:CTAIAA\]2.0.CO;2](https://doi.org/10.1130/0016-7606(1972)83[251:CTAIAA]2.0.CO;2)
- Manaker, D. M., Calais, E., Freed, A. M., Ali, S. T., Przybylski, P., Mattioli, G., Jansma, P., Prépetit, C., & De Chabaliér, J. B. (2008). Interseismic Plate coupling and strain partitioning in the Northeastern Caribbean. *Geophysical Journal International*, 174(3), 889-903. <https://doi.org/10.1111/j.1365-246X.2008.03819.x>
- Mann, P. (1997). Model for the formation of large, transtensional basins in zones of tectonic escape. *Geology*, 25(3), 211-214. [https://doi.org/10.1130/0091-7613\(1997\)025<0211:MFTFOL>2.3.CO;2](https://doi.org/10.1130/0091-7613(1997)025<0211:MFTFOL>2.3.CO;2)

- Mann, P. (1999). Caribbean sedimentary basins : Preface. In P. Mann (Éd.), *Sedimentary Basins of the World* (Vol. 4, p. XV-XX). Elsevier. [https://doi.org/10.1016/S1874-5997\(99\)80032-X](https://doi.org/10.1016/S1874-5997(99)80032-X)
- Mann, P. (2007). Global catalogue, classification and tectonic origins of restraining- and releasing bends on active and ancient strike-slip fault systems. *Geological Society, London, Special Publications*, 290(1), 13-142. <https://doi.org/10.1144/SP290.2>
- Mann, P. (2021). Gulf of Mexico, Central America, and the Caribbean. 47-67. <https://doi.org/10.1016/B978-0-08-102908-4.00118-1>
- Mann, P., Calais, É., Ruegg, J.-C., DeMets, C., Jansma, P. E., & Mattioli, G. S. (2002a). Oblique collision in the northeastern Caribbean from GPS measurements and geological observations. *Tectonics*, 21(6), 7-1-7-26. <https://doi.org/10.1029/2001TC001304>
- Mann, P., Calais, É., Ruegg, J.-C., DeMets, C., Jansma, P. E., & Mattioli, G. S. (2002b). Oblique collision in the northeastern Caribbean from GPS measurements and geological observations. *Tectonics*, 21(6), 7-1-7-26. <https://doi.org/10.1029/2001TC001304>
- Mann, P., Gahagan, L., & Rogers, R. (2006). Overview of Plate tectonic history and its unsolved tectonic problem. In *Spec. Pap. Geol. Soc. Am.* (Vol. 428, p. 205-241). <https://doi.org/10.1201/9780203947043.ch8>
- Mann, P., McLaughlin, P. P., & Cooper, C. (1991). Geology of the Azua and Enriquillo basins, Dominican Republic; 2, Structure and tectonics. In *Geological Society of America Special Papers* (Vol. 262, p. 367-390). Geological Society of America. <https://doi.org/10.1130/SPE262-p367>
- Mann, P., Taylor, F. W., Edwards, R. L., & Ku, T.-L. (1995). Actively evolving microplate formation by oblique collision and sideways motion along strike-slip faults : An example from the northeastern Caribbean plate margin. *Tectonophysics*, 246(1), 1-69. [https://doi.org/10.1016/0040-1951\(94\)00268-E](https://doi.org/10.1016/0040-1951(94)00268-E)
- Masaferro, J. L., & Eberli, G. P. (1999). Chapter 7 Jurassic-cenozoic structural evolution of the southern great Bahama bank. In P. Mann (Éd.), *Sedimentary Basins of the World* (Vol. 4, p. 167-193). Elsevier. [https://doi.org/10.1016/S1874-5997\(99\)80041-0](https://doi.org/10.1016/S1874-5997(99)80041-0)
- Mattinson, J., Pessagno, E., Montgomery, H., & Hopson, C. (2008). Late Jurassic age of oceanic basement at La Désirade Island, Lesser Antilles arc. *Ophiolites, Arcs, and Batholiths: A Tribute to Cliff Hopson*, 438, 175-190. [https://doi.org/10.1130/2008.2438\(06\)](https://doi.org/10.1130/2008.2438(06))
- Mattson, P. H. (1972). Plate Tectonics in the Caribbean. *Nature*, 235(5334), Article 5334. <https://doi.org/10.1038/235155a0>
- Mauffret, A., & Leroy, S. (1997). Seismic stratigraphy and structure of the Caribbean igneous province. *Tectonophysics*, 283(1), 61-104. [https://doi.org/10.1016/S0040-1951\(97\)00103-0](https://doi.org/10.1016/S0040-1951(97)00103-0)
- Mauffret, A., & Leroy, S. (1999a). Chapter 21 Neogene intraplate deformation of the caribbean plate at the beata ridge. In P. Mann (Éd.), *Sedimentary Basins of the World* (Vol. 4, p. 627-669). Elsevier. [https://doi.org/10.1016/S1874-5997\(99\)80055-0](https://doi.org/10.1016/S1874-5997(99)80055-0)
- Mauffret, A., & Leroy, S. (1999b). Chapter 21 Neogene intraplate deformation of the caribbean plate at the beata ridge. [https://doi.org/10.1016/S1874-5997\(99\)80055-0](https://doi.org/10.1016/S1874-5997(99)80055-0)
- Melekhova, E., Schlaphorst, D., Blundy, J., Kendall, J.-M., Connolly, C., McCarthy, A., & Arculus, R. (2019). Lateral variation in crustal structure along the Lesser Antilles arc from petrology of crustal xenoliths and seismic receiver functions. *Earth and Planetary Science Letters*, 516, 12-24. <https://doi.org/10.1016/j.epsl.2019.03.030>
- Meschede, M. (1998). The impossible Galapagos connection : Geometric constraints for a near-American origin of the Caribbean plate. *Geologische Rundschau*, 87(2), 200. <https://doi.org/10.1007/s005310050202>

- Meschede, M., & Frisch, W. (1998). A plate-tectonic model for the Mesozoic and Early Cenozoic history of the Caribbean plate. *Tectonophysics*, 296(3), 269-291. [https://doi.org/10.1016/S0040-1951\(98\)00157-7](https://doi.org/10.1016/S0040-1951(98)00157-7)
- Meyerhoff, A. A., & Hatten, C. W. (1968). Diapiric Structures in Central Cuba. In J. Braunstein & G. D. O'Brien (Éds.), *Diapirism and Diapirs : A symposium* (Vol. 8, p. 0). American Association of Petroleum Geologists. <https://doi.org/10.1306/M8361C21>
- Meyerhoff, A. A., & Hatten, C. W. (1974). Bahamas Salient of North America. In C. A. Burk & C. L. Drake (Éds.), *The Geology of Continental Margins* (p. 429-446). Springer. https://doi.org/10.1007/978-3-662-01141-6_31
- Molnar, P., & Sykes, L. R. (1969). Tectonics of the Caribbean and Middle America Regions from Focal Mechanisms and Seismicity. *Geological Society of America Bulletin*, 80(9), 1639. [https://doi.org/10.1130/0016-7606\(1969\)80\[1639:TOTCAM\]2.0.CO;2](https://doi.org/10.1130/0016-7606(1969)80[1639:TOTCAM]2.0.CO;2)
- Montes, C., Rodriguez-Corcho, A. F., Bayona, G., Hoyos, N., Zapata, S., & Cardona, A. (2019). Continental margin response to multiple arc-continent collisions : The northern Andes-Caribbean margin. *Earth-Science Reviews*, 198, 102903. <https://doi.org/10.1016/j.earscirev.2019.102903>
- Montgomery, H., & Kerr, A. (2009). Rethinking the Origins of the Red Chert at La Désirade, French West Indies. In *Geological Society, London, Special Publications* (Vol. 328, p. 455-466). <https://doi.org/10.1144/SP328.18>
- Montgomery, H., Pessagno Jr., E. A., Lewis, J. F., & Schellekens, J. (1994). Paleogeography of Jurassic fragments in the Caribbean. *Tectonics*, 13(3), 725-732. <https://doi.org/10.1029/94TC00455>
- Montheil, L. (2023, février 14). Reconstruction cinématique et paléomagnétisme des Petites et Grandes Antilles depuis l'Eocène : Un nouveau regard sur la déformation intraplaque, l'activité magmatique et la paléogéographie du Nord-Est de la plaque Caraïbe. <http://www.theses.fr>. <http://www.theses.fr/s226240>
- Moretti, I., Tenreyro, R., Linares, E., López, J., Letouzey, J., Magnier, C., Gaumet, F., Lecomte, J. C., Lopez, J. O., & Zimine, S. (2003). Petroleum System of the Cuban Northwest Offshore Zone. Undefined. </paper/Petroleum-System-of-the-Cuban-Northwest-Offshore-Moretti-Tenreyro/6cd3cb5fc85186e5ea46c9d990cf2f769477d0fa>
- Muhs, D. R., Schweig, E. S., Simmons, K. R., & Halley, R. B. (2017). Late Quaternary uplift along the North America-Caribbean plate boundary : Evidence from the sea level record of Guantanamo Bay, Cuba. *Quaternary Science Reviews*, 178, 54-76. <https://doi.org/10.1016/j.quascirev.2017.10.024>
- Mullins, H. T., & Lynts, G. W. (1977). Origin of the northwestern Bahama Platform : Review and reinterpretation. *GSA Bulletin*, 88(10), 1447-1461. [https://doi.org/10.1130/0016-7606\(1977\)88<1447:OOTNBP>2.0.CO;2](https://doi.org/10.1130/0016-7606(1977)88<1447:OOTNBP>2.0.CO;2)
- Newell, N. D. (1955). Bahamian platforms. In Poldervaart, A., ed., *Crust of the Earth*. Geological Society of America Special Paper, 62, 303-315.
- Padron, C., Klingelhoefer, F., Marcaillou, B., Lebrun, J.-F., Lallemand, S., Garrocq, C., Laigle, M., Roest, W. R., Beslier, M.-O., Schenini, L., Graindorge, D., Gay, A., Audemard, F., Münch, P., & Team, the G. C. (2021). Deep Structure of the Grenada Basin From Wide-Angle Seismic, Bathymetric and Gravity Data. *Journal of Geophysical Research: Solid Earth*, 126(2), e2020JB020472. <https://doi.org/10.1029/2020JB020472>
- Pardo, G. (2009). Overview. In G. Pardo (Éd.), *The Geology of Cuba* (p. 1-47). The American Association of Petroleum Geologists. <https://doi.org/10.1306/13141059St583328>
- Peñalver, L., Pedoja, K., Martin-Izquierdo, D., Authemayou, C., Nuñez, A., Chauveau, D., de Gelder, G., Davilan, P., & Husson, L. (2021). The Cuban staircase sequences of coral reef and marine terraces : A forgotten masterpiece of the Caribbean geodynamical puzzle. *Marine Geology*, 440, 106575. <https://doi.org/10.1016/j.margeo.2021.106575>

- Pindell, J., & Kennan, L. (2001). Kinematic Evolution of the Gulf of Mexico and Caribbean. In R. H. Fillon, N. C. Rosen, P. Weimer, A. Lowrie, H. Pettingill, R. L. Phair, H. H. Roberts, & H. H. van Hooft (Éds.), *Petroleum Systems of Deep-Water Basins—Global and Gulf of Mexico Experience* (Vol. 21, p. 0). SEPM Society for Sedimentary Geology. <https://doi.org/10.5724/gcs.01.21.0193>
- Pindell, J., & Kennan, L. (2009). Tectonic evolution of the Gulf of Mexico, Caribbean and northern South America in the mantle reference frame : An update. *Geological Society, London, Special Publications*, 328, 1-55. <https://doi.org/10.1144/SP328.1>
- Pindell, J., Kennan, L., Maresch, W. V., Stanek, K.-P., Draper, G., & Higgs, R. (2005). Plate-kinematics and crustal dynamics of circum-Caribbean arc-continent interactions : Tectonic controls on basin development in Proto-Caribbean margins. In H. G. A. Lallemand & V. B. Sisson, *Caribbean-South American plate interactions, Venezuela*. Geological Society of America. <https://doi.org/10.1130/0-8137-2394-9.7>
- Pindell, J., Kennan, L., Stanek, K., Maresch, W., & Draper, G. (2006a). Foundations of Gulf of Mexico and Caribbean evolution : Eight controversies resolved. *Geologica acta: an international earth science journal*, 4(1-2), 303-341.
- Pindell, J., Kennan, L., Stanek, K. P., Maresch, W., & Draper, G. (2006b). Foundations of Gulf of Mexico and Caribbean evolution : Eight controversies resolved. ., 303-341. <https://doi.org/10.1344/105.000000371>
- Pindell, J. L., & Barrett, S. F. (1991). Geological evolution of the Caribbean region; A plate-tectonic perspective. In G. Dengo & J. E. Case (Éds.), *The Caribbean Region: Vol. H* (p. 0). Geological Society of America. <https://doi.org/10.1130/DNAG-GNA-H.405>
- Pindell, J. L., Cande, S. C., Pitman, W. C., Rowley, D. B., Dewey, J. F., Labrecque, J., & Haxby, W. (1988). A plate-kinematic framework for models of Caribbean evolution. *Tectonophysics*, 155(1), 121-138. [https://doi.org/10.1016/0040-1951\(88\)90262-4](https://doi.org/10.1016/0040-1951(88)90262-4)
- Pindell, J. L., & Draper, G. (1991). Stratigraphy and geological history of the Puerto Plata area, northern Dominican Republic. In *Geological Society of America Special Papers* (Vol. 262, p. 97-114). Geological Society of America. <https://doi.org/10.1130/SPE262-p97>
- Pindell, J. L., Maresch, W. V., Martens, U., & Stanek, K. P. (2012). The Greater Antillean Arc : Early Cretaceous origin and proposed relationship to Central American subduction mélanges: implications for models of Caribbean evolution. <https://doi.org/10.1080/00206814.2010.510008>
- Prentice, C. S., Mann, P., Taylor, F. W., Burr, G., & Valastro, S. (1993). Paleoseismicity of the North American-Caribbean plate boundary (Septentrional fault), Dominican Republic. *Geology*, 21(1), 49-52. [https://doi.org/10.1130/0091-7613\(1993\)021<0049:POTNAC>2.3.CO;2](https://doi.org/10.1130/0091-7613(1993)021<0049:POTNAC>2.3.CO;2)
- Principaud, M. (2015). Morphologie, architecture et dynamique sédimentaire d'une pente carbonatée moderne : Le Great Bahama Bank (Bahamas) [These de doctorat, Bordeaux]. <http://www.theses.fr/2015BORD0301>
- Pubellier, M., Mauffret, A., Leroy, S., Vila, J. M., & Amilcar, H. (2000). Plate boundary readjustment in oblique convergence : Example of the Neogene of Hispaniola, Greater Antilles. *Tectonics*, 19(4), 630-648. <https://doi.org/10.1029/2000TC900007>
- Révillon, S., Hallot, E., Arndt, N. T., Chauvel, C., & Duncan, R. A. (2000). A Complex History for the Caribbean Plateau : Petrology, Geochemistry, and Geochronology of the Beata Ridge, South Hispaniola. *The Journal of Geology*, 108(6), 641-661. <https://doi.org/10.1086/317953>
- Rodríguez-Zurrunero, A., Granja-Bruña, J. L., Carbó-Gorosabel, A., Muñoz-Martín, A., Gorosabel-Araus, J. M., Gómez de la Peña, L., Gómez Ballesteros, M., Pazos, A., Catalán, M., Espinosa, S., Druet, M., Llanes, P., & ten Brink, U. (2019). Submarine morpho-structure and active processes along the North American-Caribbean plate

- boundary (Dominican Republic sector). *Marine Geology*, 407, 121-147. <https://doi.org/10.1016/j.margeo.2018.10.010>
- Rodríguez-Zurrunero, A., Granja-Bruña, J. L., Muñoz-Martín, A., Leroy, S., ten Brink, U., Gorosabel-Araus, J. M., Gómez de la Peña, L., Druet, M., & Carbó-Gorosabel, A. (2020). Along-strike segmentation in the northern Caribbean plate boundary zone (Hispaniola sector): Tectonic implications. *Tectonophysics*, 776, 228322. <https://doi.org/10.1016/j.tecto.2020.228322>
- Rojas-Agramonte, Y., Neubauer, F., Garcia-Delgado, D. E., Handler, R., Friedl, G., & Delgado-Damas, R. (2008). Tectonic evolution of the Sierra Maestra Mountains, SE Cuba, during Tertiary times: From arc-continent collision to transform motion. *Journal of South American Earth Sciences*, 26(2), 125-151. <https://doi.org/10.1016/j.jsames.2008.05.005>
- Rojas-Agramonte, Y., Neubauer, F., Handler, R., Garcia-Delgado, D. E., Friedl, G., & Delgado-Damas, R. (2005). Variation of palaeostress patterns along the Oriente transform wrench corridor, Cuba: Significance for Neogene–Quaternary tectonics of the Caribbean realm. *Tectonophysics*, 396(3), 161-180. <https://doi.org/10.1016/j.tecto.2004.11.006>
- Rosencrantz, E., Ross, M. I., & Sclater, J. G. (1988). Age and spreading history of the Cayman Trough as determined from depth, heat flow, and magnetic anomalies. *Journal of Geophysical Research: Solid Earth*, 93(B3), 2141-2157. <https://doi.org/10.1029/JB093iB03p02141>
- Ross, M., & Scotese, C. (1988). A hierarchical tectonic model of the Gulf of Mexico and Caribbean Region. *Tectonophysics*, 155, 139-168. [https://doi.org/10.1016/0040-1951\(88\)90263-6](https://doi.org/10.1016/0040-1951(88)90263-6)
- Saura, E., Vergés, J., Brown, D., Lukito, P., Soriano, Sofía, Torrecusa, S., García, R., Sánchez, J. R., Sosa, C., & Tenreyro, R. (2008). Structural and tectonic evolution of western Cuba fold and thrust belt. *Tectonics*, 27, TC4002. <https://doi.org/10.1029/2007TC002237>
- Schlager, W., & Ginsburg, R. N. (1981). Bahama carbonate platforms—The deep and the past. *Marine Geology*, 44(1-2), 1-24. [https://doi.org/10.1016/0025-3227\(81\)90111-0](https://doi.org/10.1016/0025-3227(81)90111-0)
- Sinton, C. W., Duncan, R. A., Storey, M., Lewis, J., & Estrada, J. J. (1998). An oceanic flood basalt province within the Caribbean plate. *Earth and Planetary Science Letters*, 155(3), 221-235. [https://doi.org/10.1016/S0012-821X\(97\)00214-8](https://doi.org/10.1016/S0012-821X(97)00214-8)
- Sorel, D., Purser, B. H., & Senatos, H. (1991). Strike-slip tectonic processes in the northern Caribbean between Cuba and Hispaniola (Windward Passage). *Essai de datation des récifs soulevés d'Haiti par la méthode du forçage climatique orbital*, 313, 1277-1281.
- Symithe, S., Calais, É., Chabalier, J. B., Robertson, R., & Higgins, M. (2015). Current block motions and strain accumulation on active faults in the Caribbean. *Journal of Geophysical Research: Solid Earth*, 120(5), 3748-3774. <https://doi.org/10.1002/2014JB011779>
- Tadapansawut, T., Okuwaki, R., Yagi, Y., & Yamashita, S. (2021). Rupture Process of the 2020 Caribbean Earthquake Along the Oriente Transform Fault, Involving Supershear Rupture and Geometric Complexity of Fault. *Geophysical Research Letters*, 48(1), e2020GL090899. <https://doi.org/10.1029/2020GL090899>
- ten Brink, U. S., Bakun, W. H., & Flores, C. H. (2011). Historical perspective on seismic hazard to Hispaniola and the northeast Caribbean region. *Journal of Geophysical Research: Solid Earth*, 116(B12). <https://doi.org/10.1029/2011JB008497>
- Uchupi, E., Milliman, J. D., Luyendyk, B. P., Bowin, C. O., & Emery, K. O. (1971). Structure and Origin of Southeastern Bahamas. *AAPG Bulletin*, 55(5), 687-704. <https://doi.org/10.1306/819A3C56-16C5-11D7-8645000102C1865D>

- Unterseh, S. (1999). Cartographie et caractérisation du fond marin par sondeur multifaisceaux [These de doctorat, Vandoeuvre-les-Nancy, INPL]. <https://www.theses.fr/1999INPL081N>
- van der Lelij, R., Spikings, R. A., Kerr, A. C., Kounov, A., Cosca, M., Chew, D., & Villagomez, D. (2010). Thermochronology and tectonics of the Leeward Antilles : Evolution of the southern Caribbean Plate boundary zone. *Tectonics*, 29(6). <https://doi.org/10.1029/2009TC002654>
- van Benthem, S., Govers, R., & Wortel, R. (2014). What drives microplate motion and deformation in the northeastern Caribbean plate boundary region? *Tectonics*, 33(5), 850-873. <https://doi.org/10.1002/2013TC003402>
- van Gestel, J.-P., Mann, P., Dolan, J. F., & Grindlay, N. R. (1998). Structure and tectonics of the upper Cenozoic Puerto Rico-Virgin Islands carbonate platform as determined from seismic reflection studies. *Journal of Geophysical Research: Solid Earth*, 103(B12), 30505-30530. <https://doi.org/10.1029/98JB02341>
- Walker, L., Mylroie, J., Walker, A., & Mylroie, J. (2008). The caves of Abaco Island, Bahamas : Keys to geologic timelines. *Journal of Cave and Karst Studies*, 70.
- Wessels, R. J. F. (2019). Chapter 15—Strike-Slip Fault Systems Along the Northern Caribbean Plate Boundary. In J. C. Duarte (Éd.), *Transform Plate Boundaries and Fracture Zones* (p. 375-395). Elsevier. <https://doi.org/10.1016/B978-0-12-812064-4.00015-3>
- Zoeten, R. (1991). Structural geology and Cenozoic tectonic history of the central Cordillera Septentrional, Dominican Republic (Vol. 262, p. 265-279). <https://doi.org/10.1130/SPE262-p265>